The magma source(s) and Ni-PGE potential of the Ventersdorp large igneous province

Khulekani B. Khumalo

A thesis submitted to the Faculty of Science, University of the Witwatersrand in fulfilment of the requirements for the degree of

Doctor of Philosophy

School of Geosciences

University of the Witwatersrand

May 2023

Johannesburg, South Africa

Declaration

I declare that this thesis is my own work except where otherwise stated. It is hereby submitted for the degree of Doctor of Philosophy at the University of the Witwatersrand, South Africa. This work has not been submitted for any degree or examination in any other university.

Khulekani Brillient Khumalo

May 31, 2023

Johannesburg, South Africa

Abstract

This thesis investigates the magmas source(s) of the Ventersdorp Supergroup on the Kaapvaal Craton in South Africa. The investigation is addressed in three interlinked geochemical studies using new radiogenic Sr-Nd-Hf isotopes, stable in-situ oxygen isotopes, multiple sulphur isotopes, and platinum group elements (PGE), in combination with new trace element analysis and new in-situ major element analysis. The Ventersdorp Supergroup is a Neoarchean sequence comprising volcanic and sedimentary rocks that have been metamorphosed to greenschist facies. Little is known and agreed about the source(s) of the magmas and the petrogenesis of the Ventersdorp Supergroup.

The basal group, the Klipriviersberg Group, comprises flood basalts with komatiites of the Westonaria Formation at its base. The whole-rock Sr-Nd-Hf isotopes of the Westonaria komatiites and the in-situ oxygen isotope compositions of fresh clinopyroxene in the komatiites are investigated. Komatiites are high-magnesian magmas that are mainly restricted to the Archean, reflecting the hotter mantle of the Archean that was dominated by mantle plumes. The komatiite investigation shows that the Westonaria komatiites were sourced from a depleted sublithospheric mantle and that the magmas experienced insignificant crustal contamination. This is supported by the mantle compositions of the freshly preserved clinopyroxene grains.

The radiogenic isotope compositions of the flood basalts of the Klipriviersberg Group, together with the felsic lavas of the Platberg Group (medial group) and the lavas of the Pniel Group (uppermost group) show that the Ventersdorp Supergroup comprises three large igneous provinces (LIPs) that include the Klipriviersberg LIP, Platberg silicic LIP, and the Allanridge LIP. This isotope study contributes to the current redefinition of the Ventersdorp Supergroup from being one magmatic event to three magmatic events over 70 million years. The study also emphasises the effects of alteration and metamorphism on the Rb-Sr isotope system and the significance of the robust Lu-Hf isotope system.

The Ni-PGE potential of the Ventersdorp Supergroup is also investigated by analysis of the PGE contents and multiple sulphur isotope composition of the Klipriviersberg LIP mafic-ultramafic lavas. The Klipriviersberg LIP has low PGE contents and has mass-independent

sulphur isotope signatures that are readily explained by the sulphide minerals that are associated with secondary features such as veins and amygdales. The investigation shows that the depleted sublithospheric mantle source of the Klipriviersberg LIP was poor in PGE.

This study demonstrates the importance and value of multi-sourced data when dealing with altered geological samples.

Acknowledgements

Firstly, I would like to thank Prof. Lewis Ashwal for introducing me to this research and for the initial data and sample collection. I thank my supervisors, Prof. Lewis Ashwal and Dr Ben Hayes, for their guidance and support throughout the research.

This research work was supported by the Harry Oppenheimer Fellowship Award granted to Prof. Lewis Ashwal and research funds from the DSI-NRF Centre of Excellence (CoE) for Integrated Mineral and Energy Resource Analysis (DSI-NRF CIMERA). Opinions expressed and conclusions arrived at, are those of the author(s) and are not necessarily to be attributed to the CoE.

To the members of the Wits LIPs research team; I am grateful for the weekly meetings that were insightful for this research. I am grateful to the laboratory technicians at the University of the Witwatersrand. I am grateful to Linda Iaccheri (isotope analyses), Caiphas Majola, Sam Tshabalala, Louis Mudalahothe (thin section preparation), Marlin Patchappa and his team (trace element analysis), Nonkuselo Madlakana (TIMA), Sarah Glynn (SIMS) and Alexander Ziegler (EPMA). To Henriette Ueckermann (University of Johannesburg), I am thankful for the isotope analyses.

I would like to thank Themba Khumalo (father), Thembalethu Khumalo (brother), Tennyson Ndlovu (brother) and Andile Mazibuko (brother) for their patience and support. I am grateful to my grandfather (Erick Ndlovu) for introducing me to nature and taking me on his adventurous hikes. I enjoyed the hikes and the work we did together in the field.

To Goitseone Mogale (partner), I thank you for your unlimited support throughout the whole period of this research.

Finally, I dedicate this work to the family members I have lost during my research. To Paletah Ndlovu (grandmother) and Kholwani Khumalo (brother), you played a part in my Ph.D. journey. I also dedicate this work to my late mother, Nomalanga Ndlovu.

Table of Contents

List of Figures

List of Tables

List of Appendices Figures and Tables

Chapter 1: Introduction

1.1 Large igneous provinces

Large igneous provinces (LIPs) are large volumes of intraplate magmatism emplaced in a short period as continental flood basalts (CFBs: e.g., Karoo LIP), mafic-ultramafic layered intrusions (e.g., Bushveld LIP), oceanic flood basalts (OFBs: e.g., Ontong Java Plateau), sill complexes (e.g., Midland Valley) and associated dyke swarms (Coffin & Eldholm, 1994; Raymond & Murchison, 1991; Taylor, 2006; Ernst, 2014; Ballmer et al., 2015). The provinces have been linked to continental break-ups, mass extinctions, changes in climate, regional uplifts and ore deposits, making them useful for the reconstruction of supercontinents and exploration of resources (Jerram & Widdowson, 2005; Saunders et al., 2007; Schulz et al., 2010; Bryan & Ferrari, 2013; Ernst & Jowitt, 2013; Wang et al., 2014; Ballmer et al., 2015). Felsic magmatism, carbonatites, nephelinites, lamprophyres, lamproites, and kimberlites are also commonly associated with LIPs (Ernst & Bell, 2009; Ernst, 2013; Torsvik et al., 2014). Ernst (2014) discriminated LIPs from non-LIP events based on their (i) volume, (ii) areal extent, (iii) duration of magmatism, (iv) nature of magmatism, and (v) tectonic setting. The first two mentioned criteria (i and ii) have been set to a minimum of 0.1 million km^3 and 0.1 million km^2 in order to meet the definition of a LIP. The next two criteria (iii and iv) require the determination of precise ages in order to understand the age and rate of magmatic emplacement, with most LIPs being emplaced in less than 10 million years and a few rare cases of up to 50 million years.

The link of LIP events to mass extinctions and climatic changes is well established using dates and changes observed in atmospheric and oceanic chemistry (Jerram and Widdowson, 2005; Ballmer et al., 2015). LIP events release a huge amount of volatiles into the atmosphere and oceans with implications that extend to evolutionary patterns. Mass extinctions that are well connected to LIP events are: (i) The Cretaceous extinction linked to the ca. 65 Ma Deccan Traps, (ii) The Triassic extinction linked to the ca. 200 Ma Central Atlantic Magmatic Province (CAMP), (iii) The Permian extinction linked to ca. 250 Ma Siberian Traps, and (iv) The Guadalupian extinction linked to ca. 258 Ma Emeshian magmatism (Ballmer et al., 2015).

The enormous amount of energy and ore metals brought by magmatism of LIPs can form eitherprimary or secondary ore deposits. The deposits related to LIP events can be (i) hosted

by the LIPs (orthomagmatic), (ii) concentrated by LIPs acting as the drivers of hydrothermal systems or they can be the sources of the metals or they can form structural barriers where metals collect and form ore deposits, and (iii) the ore deposits can be the weathering products of LIPs (Ernst & Jowitt, 2013). Knowledge of how ore deposits are linked to LIPs has crucial implications on exploring for deposits (Schulz et al., 2010). Different types of deposits are related to different settings or parts of LIPs,for example, high magnesian Ni-Cu-2 type deposits (nickel-copper-PGE deposit type related to flood basalt magmatism) are linked to feeder dykes and sills (Ernst & Jowitt, 2013). Reconstruction of previously connected crustal blocks that are mineralized is another way of exploring for ore deposits using LIPs (Ernst & Jowitt, 2013). Ore deposits studies have shown a temporal and spatial linkage between LIPs and kimberlites (diamonds), carbonatites (Nb-Ta-REE-P), Ni-Cu-PGE, Fe-Ti-V and Cr deposits (Naldrett et al., 1992; Schulz et al., 2010; Torsvik et al., 2010; Dobretsov et al., 2012; Ernst & Jowitt, 2013). The majority of mineralization is in the vicinity of the plume centre, which is related to the high-temperature centres and greater magma volumes where there are higher chances of sulphur saturation (Naldrett et al., 1992). The heat brought by LIPs drives the mobilization of metals within LIPs or host rocks to form ore deposits (e.g., copper and gold).

Various sources of large igneous provinces have been proposed, and these include a sub-lithospheric mantle plume (Morgan, 1971; White, 1997; Ashwal, 2017; Sharkov et al., 2017), a sub-continental lithospheric mantle (SCLM: Jourdan et al., 2007; Yu et al., 2017), volumetrically small regions with “enriched” compositions in the SCLM (Ashwal, 2017); and finally, the convecting asthenospheric mantle (Neumann et al., 2011).

The mantle plume origin of LIPs has been overwhelmingly proposed (for the Ventersdorp Supergroup: Hatton, 1995; White, 1997; Eriksson et al., 2002; van der Westhuizen et al., 2006; Klausen et al., 2010; Altermann & Lenhardt, 2012). At least 228 large magmatic events, ranging from ca. 3.5 Ga to today have been linked to mantle plumes (Ernst & Buchan, 2001). The proposed mechanisms for melt production from the plumes are decompression melting by lithospheric thinning of the ascending plume material and/ or by heating without thinning of the lithosphere (White, 1997). Klausen et al. (2010) suggest the Ventersdorp plume centre to have been located beneath the current eastern limb of the Bushveld Complex; White (1997) suggests that the source region was located in the rifted lithosphere beneath present Mozambique. A superplume event at 2.7 Ga was proposed for the Vaalbara supercraton, a

craton made up of the Kaapvaal Craton of South Africa and the Pilbara Craton of Australia (Eriksson et al., 2002).

In 1971, W. J. Morgan introduced the concept of the plume to explain magmatism within oceanic and continental plates. Predictions and observations of the plume model have since been developed and these are mentioned in the following statements. Firstly, the mantle plumes originate from a thermal boundary layer (e.g., core-mantle boundary- CMB and mantle transition zone) or from instabilities and compositional heterogeneities within the mantle (Davies and Bunge, 2006; Torsvik et al., 2008, 2010). Tomographic studies of the mantle have imaged plumes rooted at different depths of the mantle (e.g., Montelli et al., 2004; Zhao, 2004). The mantle plumes are made up of a large head that will form LIPs, followed by a thin tail that can be linked to tracks of volcanoes. Therefore, some LIPs are related to time-progressive volcanoes, for example, the Columbia River Flood Basalt and the Snake River Plain volcanoes (Ernst & Buchan, 2001; Davies & Bunge, 2006; Foulger, 2010; Ballmer et al., 2015). In addition, the plume heads flatten to at least 2000 km in diameter and the temperature excess should decrease from the plume centre (Campbell, 2005). The flood volcanism of mantle plumes follows a transient or permanent domal uplift of 0.5 km to 1 km at the centre (Ernst & Buchan, 2001; Campbell, 2005; Jerram & Widdowson, 2005) and this can be identified by drainage patterns – radiating pattern at the uplift dome and break of radiating pattern at the boundary of the uplifted region. The mantle plume head and the tail erupt high-temperature/ high-magnesian lavas in the early stages of flood volcanism, mostly near the centre of the plume head (Ernst & Buchan, 2001; Campbell, 2005). The plume flood volcanism is associated with temporal and spatial change related to the structure of the mantle plume. Campbell (2005) also highlights an expected distinct chemistry of plume-related magmas from other basalts, and giant radiating dyke swarms (e.g., for the Ventersdorp Supergroup: Olsson et al., 2010; Klausen et al., 2010). Two thermochemical large low shear-wave velocity provinces (LLSVPs) at the CMB - African and Pacific LLSVPs - have been detected and proposed to have plume generation zones (PGZs) at their margins on which reconstructed LIPs erupted directly above them (Torsvik et al., 2010, 2014; Davies et al., 2015; Ballmer et al., 2015). Intraplate magmas have distinct geochemical signatures that have been attributed to multiple distinct mantle reservoirs sampled by ascending plumes (Lohmann et al., 2009). To establish mantle plumes as the source of the LIPs, the unique

composition of the plumes and deep Earth must be known, together with an understanding of the interaction between plumes and the heterogeneous mantle. This has been investigated by Cagney et al. (2015), Hawkesworth and Scherstén (2007), and Hastie et al. (2016), who concluded that plumes either sample different sources of varying composition or originate from isolated poorly mixed sources.

The SCLM is considered a significant upper mantle geochemical reservoir and one of the proposed source regions for many types of intrusive and extrusive intraplate magmatism (Hawkesworth et al., 1984, 1990; Greenough & McDivitt, 2017). In general, Archean SCLMs are thought to be relatively buoyant and stable relative to the asthenospheric mantle, due to the extraction of mafic and ultramafic melts from mantle peridotites that left it depleted in basaltic components (e.g., Al, Ca, Na, Ti and Fe), (O'Reilly et al., 2001; Tang et al., 2013). It has also been suggested that the isolation of the SCLM from the convecting asthenospheric mantle, its buoyancy and its refractory nature make it unsusceptible to partial melting (O'Reilly et al., 2001). Recent studies of xenoliths suggest an evolution of the SCLM through refertilization by upwelling fertile asthenosphere (O'Reilly et al., 2001; Tang et al., 2013; Greenough & McDivitt, 2017). Evidence presented for the refertilization includes: the compositional change of mantle xenoliths becoming less depleted from the Archean to Phanerozoic; the lowered Re-Os model ages; and the sections of the Kaapvaal SCLM that show fertilization by metasomatism. Ashwal (2021) argues against large-scale chemical fertilization of the Kaapvaal SCLM, which would be required if it was the sole source of the LIPs. Such refertilization would increase its bulk density as this would crystallize as eclogite, therefore, disturbing its long-term stability and buoyancy reflected by the high elevations of southern Africa. Another argument against the refertilization of the Kaapvaal SCLM is the long-term survival of the lithospheric diamonds since the Archean, indicating that their SCLM host was not subjected to repeated LIP-melt producing events (Ashwal, 2017). Some of the oldest mineral inclusions in the Kaapvaal diamonds date between 3.3 and 3.5 Ga, suggesting that isolation from the hot convecting mantle by incorporation into the SCLM had already occurred before those ages (Shirey & Richardson, 2011; Smart et al., 2016).

Despite the strict physical criteria set for LIPs, these magmatic bodies do not have a unique geochemical signature, however, most CFBs and OFBs are generally geochemically characterized due to their distinct crustal contaminants. A LIP system will also exhibit

geochemical variations (mostly trace element geochemistry) between different components (Ernst, 2014). Major- and trace-element chemistry, isotopes, melting points and seismic scattering show the heterogeneity of the upper mantle (Jahn et al., 1980; Anderson, 2007; Iwamori & Nakamura, 2014). The asthenosphere heterogeneity is seen in the varying chemistry of magmas (Anderson, 2007). The fertility, productivity and heterogeneity of the mantle are due to plate tectonics recycling fertile and enriched material, igneous processes internal to the mantle, and delamination of the lower continental crust. It has been suggested that the melting of large volumes of the mantle can homogenize basalts that come from the heterogeneous mantle (Anderson, 2007). More up-to-date information on LIPs is available on www.largeigneousprovinces.org, a website gathering LIP data and focussing on their temporal and spatial distributions, interplanetary LIPs and the origin of LIPs.

1.2 The scope of the study

This study forms part of research that investigates the magmatism of four overlapping large igneous provinces in southern Africa. These are the Ventersdorp Supergroup (ca. 2.7 Ga, ~0.7 million km^3), the Bushveld layered Intrusion (ca. 2.1 Ga, ~1.5 million km^3), the Umkondo LIP (ca. 1.1 Ga, ~2 million km^3) and the Karoo LIP (ca. 0.2 Ga, ~3 million km^3) (Ashwal, 2021).

The previous section unveils the complexity of large igneous provinces as there are many aspects that are currently debated and investigated to better understand the magmatism of enormous volumes of magma. In this study, I focus on the radiogenic Sr-Nd-Hf, stable O-S isotope and platinum group element compositions of the Ventersdorp Supergroup to better understand the:

- Regions in the Earth that partially melted to produce huge volumes of magma
- Source of the heat
- Transportation of the magma to the surface
- Extent of interaction between the magma and crustal components
- Interrelation of the associated mineral deposits

The approach taken to understand the above-mentioned aspects is as follows:

- The altered rocks of the Ventersdorp Supergroup were explored petrographically using optical microscopes (Olympus BX41 and BX53), scanning electron microscope

(TIMA: Tescan Integrated Mineral Analyzer), and electron probe micro-analyzer (EPMA) to understand the textures and mineral chemistry from available rock samples.

- Solution-based inductively coupled mass spectrometry (ICP-MS) was used to analyse the trace element compositions of bulk rock powders.
- The bulk rock, combined Sr-Nd-Hf analysis using isotope dilution multi-collector inductively coupled mass spectrometry (ID-MC-ICP-MS) was applied because of the different behaviour of the isotope systems and their different degrees of resistance to metamorphism and alteration.
- In-situ analysis of stable oxygen isotopes of fresh clinopyroxene using Secondary Ion Mass Spectrometry (SIMS) technique (a high-precision in-situ isotope analysis technique) was explored for primary signatures and to assess the effects of contamination and alteration in addition to the Sr-Nd-Hf isotope analysis.
- Nickel-sulphur fire assay Te co-precipitation was used to determine and characterize the platinum group elements of the mafic-ultramafic lavas. This technique factors and reduces the nugget effects, therefore, yielding accurate measurements.
- Bulk rock sulphur isotopes were determined to assess crustal contamination of the magmas and the role of crustal contamination on the PGE concentrations of the Klipriviersberg lavas, as well as the effects of the mass-independent fractionated sulphur.

1.3 Thesis structure

This thesis is presented in seven chapters that include three manuscripts for publication that are at different stages of preparation. Chapter 1 (this chapter) introduces the topic of large igneous provinces and outlines the scope of the study and the approach taken to achieve the aims of the study. Chapter 2 provides the geological background of the Ventersdorp Supergroup and synthesises the literature from previous researchers. Chapter 3 describes the methods used in this study to achieve the aims. Chapter 4 presents new whole rock Sr-Nd-Hf and trace element data as well as oxygen isotope data of clinopyroxene in the Westonaria komatiites with detailed implications for the magma source of the Westonaria magmas.

Chapter 4 was submitted to Earth and Planetary Science Letters (EPSL) and is currently in revision in line with the review comments. Chapter 5 presents new whole rock Sr-Nd-Hf isotope and trace element data from the Ventersdorp Supergroup. The new isotopic data have implications for the magma sources and the contamination of the Ventersdorp LIPs, and the petrogenesis of the Ventersdorp LIPs. Chapter 5 is to be submitted to the South African Journal of Geology. Chapter 6 presents new PGE and multiple sulphur isotopic data of the mafic-ultramafic Klipriviersberg LIP with implications for the PGE nature of the mantle source and potential PGE mineralization. Chapter 6 is in preparation for submission to a journal yet to be decided. Chapter 7 integrates the findings of Chapters 4, 5 and 6 to provide an overview of the research results and conclusions on the magmatism of the Ventersdorp LIPs. The detailed geological background and methodology sections have been excluded from the manuscript chapters to avoid the repetition of Chapters 2 and 3.

Chapter 2: Geological Background

2.1 Ventersdorp Supergroup

The Neoarchean Ventersdorp Supergroup constitutes the bimodal volcano-sedimentary sequence (~5100 m thick) on the Kaapvaal Craton, Fig. 2.1 (Crow & Condie, 1988; van der Westhuizen et al., 2006; de Kock et al., 2012; Cornell et al., 2017; Altermann & Lenhardt, 2012; Meintjes & van der Westhuizen, 2018). The initial lavas of the Ventersdorp Supergroup unconformably overlie the Witwatersrand Supergroup in the West Rand and Central Rand areas; the Transvaal Supergroup in turn unconformably overlies the Ventersdorp Supergroup (Fig. 2.1: van der Westhuizen et al., 2006; Cornell et al., 2017; Gumsley et al., 2020). Ventersdorp lavas flowed beyond the Witwatersrand basin area, as there are lavas in the Alberton Formation that overlie Archean basement, exposed in a NE-SW trending elliptical area of ~450 000 km^2 extending for ~800 km in length and ~550 km in width (Crow & Condie, 1988; White, 1997; van der Westhuizen et al., 1991; Meintjes & van der Westhuizen, 2018). Most of the succession of the Supergroup is exposed in the Bothaville region, (Fig. 2.1: Winter, 1976). The Supergroup is divided into the basal Klipriviersberg Group, medial Platberg Group and the upper Pniel Group, formerly known as Pniel Sequence (Fig. 2.2: van der Westhuizen et al., 1991). The sedimentary package of the Supergroup is both siliciclastic and carbonate. Detailed descriptions of the Ventersdorp Supergroup exposed in the type locality, Bothaville area, are provided in Winter (1976).

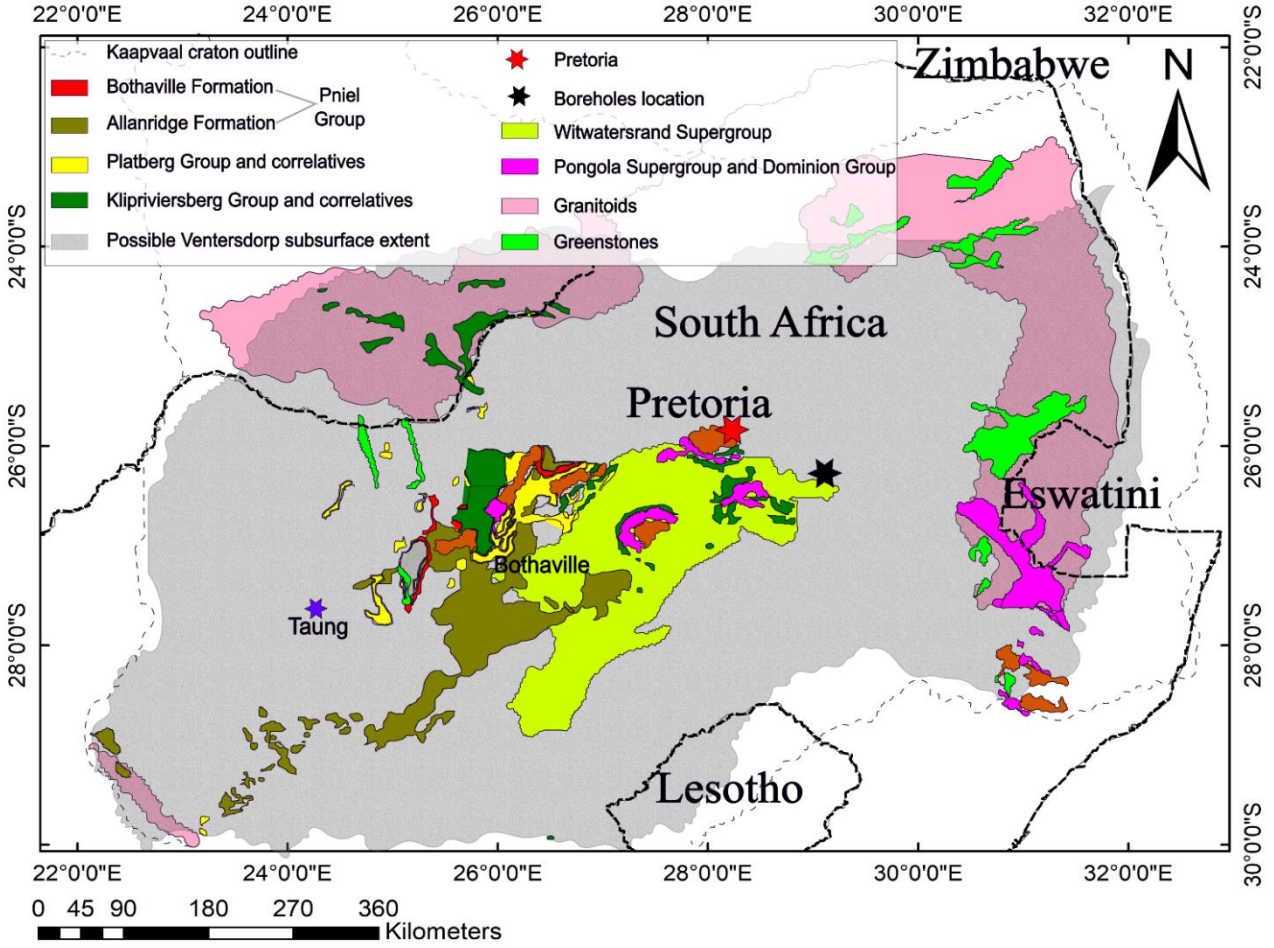

Figure 2. 1 Distribution map of the Ventersdorp LIP and its correlatives, modified after Gumsley et al. (2017). Sequences that are older than the Ventersdorp LIP are also shown. The map shows the area of surface exposure of the LIP. The possible subsurface extent (grey area) is based on borehole data and maps in Crow and Condie (1988) and Gumsley et al. (2017).

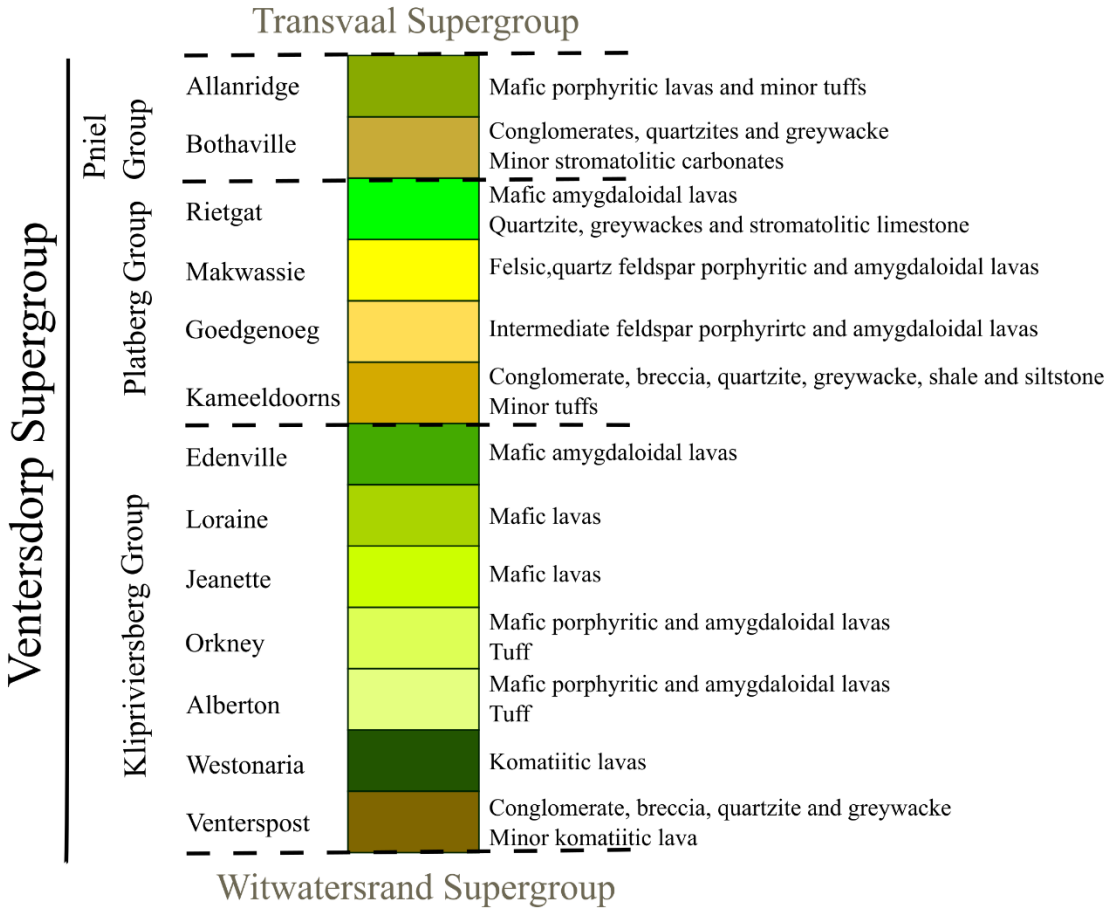

Figure 2. 2 General lithostratigraphic column of the Ventersdorp Supergroup, showing its groups and formations, with typical lithologies that are characteristic of the formations.

2.2 Klipriviersberg Group

The Klipriviersberg Group is the basal flood basalt sequence covering an area of ~30 000 km^2 and consisting of mafic to ultramafic lavas that make up a third to a half of the Supergroup's lavas (Crow & Condie, 1988; van der Westhuizen et al., 1991; White, 1997; Gumsley et al., 2020). The basalts are tholeiitic with a mild calc-alkaline affinity (Crow & Condie, 1988; van der Westhuizen et al., 2006). The Klipriviersberg Group is subdivided into the Venterspost, Westonaria, Alberton, Orkney, Jeanette and Loraine-Edenville Formations. The Formations that form the basal contact of the Klipriviersberg Group vary with locality across the basin, possibly due to the uneven topography of the basin. The Venterspost Formation is not

commonly included in the stratigraphic column of the Ventersdorp Supergroup by other researchers, although it is considered in this study.

2.2.1 Venterspost Formation

The Venterspost Formation, mostly known as Ventersdorp Contact Reef (VCR), forms the lowermost unit of the Klipriviersberg Group, and it comprises immature conglomerates (van der Wetshuizen et al., 2006). Reddy and Germs (1994) provided a detailed description of the stratigraphy and facies of the Formation using pebble size, packing, thicknesses and depositional environments, identifying unconformity-bounded units. In localities where the VCR forms the basal unit of the Klipriviersberg Group, it unconformably overlies the Witwatersrand Supergroup with its lower contact on erosional surfaces, and gravel beds on terraces and palaeolows (Reddy & Germs, 1994; van der Westhuizen et al., 2006; Manzi et al., 2013). Units I, II and III were identified by Reddy and Germs (1994) consisting of unconformity-bounded cycles and subcycles. Unit I is referred to as 'Grey Quartzite' cycle and is characterized by green, black and grey quartzite for Cycles 1, 2 and 3, respectively. The cycles comprise subcycles with basal lag conglomerates with black and white vein quartz pebbles. Unit II, also known as 'Black Sandstone', has at least four unconformity-bounded cycles. The lower cycles contain black and white vein quartz pebbles, with the lowermost cycle consisting of quartzite, chert and shale pebbles, and the overlying cycles being more mature and having whiter vein quartz pebbles (Reddy & Germs, 1994). The upper cycles contain green quartzite with inter-reef lavas of Westonaria Formation varying in thicknesses; the uppermost cycles have oligomictic basal conglomerates with white and black vein quartz pebbles (Reddy & Germs, 1994). According to Reddy and Germs (1994), there are black, tuffaceous, quartzitic sandstones with chemical signatures similar to the overlying Westonaria lavas. Barton et al. (1990) dated the Venterspost Formation to be 2780 ± 5 Ma using U-Pb zircon, similar to the 2787 ± 2 date reported by Gumsley et al. (2020) using U-Pb zircon. Deposition of the VCR was gradually terminated by the eruption of komatiitic lavas of the Westonaria Formation that flowed along VCR channels (van der Westhuizen et al., 2006).

2.2.2 Westonaria Formation

The Westonaria Formation consists of fine-grained ultramafic lavas with komatiitic compositions (average MgO = 22 wt. %; Myers et al., 1987) that are well preserved in the deepest parts of the basin (Winter, 1976; Crow & Condie, 1988; van der Westhuizen et al., 2006). The lavas have higher TiO_2 contents (average of 1.06 wt. %) than typical komatiitic lavas with less than 1 wt. % (Crow & Condie, 1988; Eriksson et al., 2002; van der Westhuizen et al., 2006). Wyatt (1976) documented the geology and geochemistry of the Meredale Member volcanic rocks in the Westonaria Formation and described them as a series of alternating light and dark weathered horizons with sharp contacts and/ or textural changes. The low-grade metamorphism of the magnesian minerals formed the extensive talcose character of the units (van der Westhuizen et al., 2006). The overlying Formations (Alberton, Orkney, Jeanette and Loraine-Edenville) gradually become primitive upwards, with higher Mg numbers, higher Ni contents, and lower incompatible element contents (Crow & Condie, 1988; Eriksson et al., 2002; Gumsley et al., 2020).

2.2.3 Alberton, Orkney and Jeanette Formations

The Alberton Formation is subdivided into basaltic lower and upper Alberton Formations. The lower Formation consists of a basal porphyritic unit (plagioclase phenocrysts up to 5 mm in length) that is referred to as the Lower Porphyritic Marker and is overlain by a non-porphyritic unit (Wyatt, 1976; Reddy & Germs, 1994; van der Westhuizen et al., 1991, 2006). The Upper Alberton Formation is grey-green with amygdaloidal (quartz and chalcedony amygdales) lava flows that are coarser-grained than the Lower Alberton Formation, which has finer-grained lava flows overlying the Lower Porphyritic Marker (Wyatt, 1976; van der Westhuizen et al., 2006). Marsh et al. (1992) reported similarities between the Alberton Formation and the overlying Orkney Formation lavas in terms of their major element composition. The evolved basalts of Alberton Formation are slightly enriched in P_2O_5, Zr and Cr, and slightly depleted in V and Co, as well as slightly enriched and depleted in light rare earth elements (LREE) and heavy rare earth elements (HREE), respectively (Marsh et al., 1992). Both the Alberton and Orkney Formations have lower Mg# (0.42 – 0.53) and higher Zr contents (90 – 137) relative to the overlying Loraine-Edenville lavas (Marsh et al., 1992). The Orkney Formation consists of alternating amygdaloidal and massive flows and has brecciated lava flows similar to the Alberton Formation (Wyatt, 1976; van der Westhuizen et al., 2006). The evolved basalts (MgO

< 6 wt. %)- slightly less evolved than Alberton lavas - are enriched in Zr, Y, Nb, P_2O_5 and TiO_2. Zr is positively correlated with Ti, P, V and other incompatible elements (Marsh et al., 1992). The Formation is marked by the Lower Purple Marker made up of purple bands in a grey-green aphanitic lava groundmass (van der Westhuizen et al., 2006). The Jeanette Formation consists of mafic lava flows with thick flow-topped breccias that are thought to represent a'a lava flows (van der Westhuizen et al., 1991, 2006).

2.2.4 Loraine-Edenville Formations

The Loraine-Edenville Formations consist of both porphyritic and non-porphyritic lavas with amygdales bounded by alteration zones (van der Westhuizen et al., 2006). Loraine-Edenville Formations are mainly basaltic in composition (Mg# = 0.47 – 0.75); the Loraine Formation contains light variolites and spherulites within dark groundmass; and the Edenville Formation has distinctive amygdales of green chalcedony and milky quartz (Winter, 1976; Crow & Condie, 1988; van der Westhuizen et al., 1991; Marsh et al., 1992). Marsh et al. (1992) reported a variation in composition from picritic (MgO > 15 wt. %) to basaltic (MgO < 6 wt. %) with an increase in the content of immobile incompatible elements in the less primitive basalts.

2.3 Platberg Group

The Platberg Group is a volcano-sedimentary sequence made up of four formations that show variations in thicknesses across the basin. The bimodal lavas (mafic and felsic) and sediments (clastic and chemical) of the Platberg Group are bounded by an unconformity at the lower contact with the Klipriviersberg Group (Crow & Condie, 1988; van der Westhuizen et al., 2006). The lowermost Kameeldoorns Formation is overlain by the Goedgenoeg Formation, which in turn is overlain by the Makwassie Formation, and capped by the uppermost Rietgat Formation (Crow & Condie, 1988; van der Westhuizen et al., 1991, 2006; Eriksson et al., 2002). The lava compositions range from the basaltic Rietgat Formation to the rhyolitic Goedgenoeg Formation and Makwassie Formation (Meintjes & van der Westhuizen, 2018).

2.3.1 Kameeldoorns Formation

The Kameeldoorns Formation is the basal succession of the Platberg Group that consists of sediments that grade towards an inferred depocentre into arkose, siltstones and carbonates, with mafic tuff and lava (MgO = 3 wt. %) interbedded in the clastic material (Crow & Condie, 1988; Grobler et al., 1989; van der Westhuizen et al., 1991). The textures and composition of the basal sediments (enriched in Fe_2O_3, TiO_2 and MgO) show similarity with the volcanic breccias and lavas of the Klipriviersberg Group. They are depleted in large ion lithophile elements (LILE) when compared to the upper continental crust (UCC) and post Archean average shale (PAAS); they have similar high field strength element (HFSE) concentrations to those of UCC and PAAS, as well as similar REE patterns to PAAS. The quartz-bearing lithoclasts (average size of ~200 µm) have three distinct textural characteristics that include (1) rounded mafic lava fragments, (2) dark green-brown lava fragments, and (3) elongated pyroclastic clasts (Schneiderhan et al., 2011). The Formation has a thickness ranging from a minimum of ~555 m to a maximum of ~1798 m around the type locality, the Bothaville area (Winter, 1976). Winter (1976) documented massive boulder conglomerates adjacent to major faults. Several sedimentary structures have been observed across the elongate lenticular layout of the Formation: raindrop imprints, desiccation cracks, cross- and graded-bedding (Eriksson et al., 2002; van der Westhuizen et al., 2006; Altermann & Lenhardt, 2012). The occurrence of arkose changes from minor at the base to dominating in the upper section of the succession; chert and dolomites mainly occur in the deeper parts of the basin (van der Westhuizen et al., 2006).

2.3.2 Goedgenoeg Formation

The Goedgenoeg Formation conformably overlies the Kameeldoorns Formation through a gradational contact formed by interbedding of lavas and the Kameeldoorns sediments (van der Westhuizen et al., 2006). The Formation consists of low-Zr (upper Goedgenoeg) and high-Zr (lower Goedgenoeg) dacitic feldspar porphyries with minor non-porphyritic lavas that dominate the upper section of the Goedgenoeg succession (Eriksson et al., 2002; van der Westhuizen et al., 2006). The lower section of the Formation comprises non-porphyritic lavas of mafic-andesitic composition, overlain by dacitic porphyritic lavas (Meintjes & van der Westhuizen, 2018). Crow and Condie (1988) reported the Goedgenoeg Formation to be compositionally similar to some of the lava flows of the uppermost Rietgat Formation. The

lower volcanic rocks are restricted to the deepest parts of the basin and also consist of amygdaloidal flow bases and tops, and are brecciated in many instances (Meintjes & van der Westhuizen, 2018). Meintjes and van der Westhuizen (2018) report inclusions of granite, quartzite, and amygdaloidal mafic lava.

2.3.3 Makwassie Formation

The Makwassie Formation consists of felsic porphyritic lavas (quartz/ feldspar phenocrysts) with thin tuffaceous units and minor interbedded mafic lava flows (van der Westhuizen et al., 1991, 2006; Meintjes & van der Westhuizen, 2018). The Formation extends up to 2 km in thickness and the underlying unit of the Makwassie Formation varies in thickness across the basin. At some localities, it overlies the Goedgenoeg lavas and elsewhere it overlies Kameeldoorns sediments (Eriksson et al., 2002; van der Westhuizen et al., 2006; Cornell et al., 2017). Meintjes and van der Westhuizen (2018) report breccias, reworked volcanic rocks, conglomerates, tuffs and shales at the Makwassie-Goedgenoeg contact. The quartz and feldspar porphyries in this Formation are reported to be lighter coloured than other porphyries of Ventersdorp Supergroup, and phenocrysts increase in size up the Makwassie succession to the flow tops that consist of amygdales and breccias (van der Westhuizen et al., 2006; Meintjes & van der Westhuizen, 2018). The feldspar phenocrysts (plagioclase and alkali-feldspar) display mantling, zoning, sieve textures, fracturing and inclusions of heavy accessory minerals (Fe – Ti oxides, apatite, spinel, sphene and zircon). The quartz porphyries are divided into dacitic lower and rhyolitic (low-Zr and high-Zr) upper porphyries (Meintjes & van der Westhuizen, 2018). Armstrong et al. (1991) dated the Makwassie Formation to be 2709 ± 4 Ma using U-Pb zircon (by SHRIMP), however, recent studies using more developed analytical practices date the Formation to be older than 2720 ± 2 Ma (Poujol et al., 2005; de Kock et al., 2012; Cornell et al., 2017). White (1997) pointed out the similarity of Makwassie rhyolitic volcanism to the Karoo rhyolitic volcanism in Lebombo, attributing the volcanism to crustal melting during the latter stages of flood basalt volcanism.

2.3.4 Rietgat Formation

The uppermost Formation of the Platberg Group, the Rietgat Formation, consists of clastic and chemical sediments, and mafic-to-dacitic lavas and tuffs. The lavas are porphyritic (mostly

plagioclase phenocrysts up to 3 mm) and are characterized by intergranular textures (Winter, 1976; van der Westhuizen et al., 1991). The thickness of the Formation ranges from a minimum of ~927 m to a maximum of ~1319 m around the type locality, the Bothaville area (Winter, 1976). The volcanic rocks have amygdaloidal flow tops and sedimentary rocks include siltstones, arkosic sandstones, gritstones and stromatolitic cherty limestones (van der Westhuizen et al., 1991; Eriksson et al., 2002). The sedimentary units are similar to those of the Kameeldoorns Formation, although the units are thinner (Winter, 1976). Van der Westhuizen et al. (2006) suggested that the presence of stromatolitic cherty limestones indicates a decrease in volcanic activity towards the end of the deposition of the Platberg Group in the graben basins.

2.4 Pniel Group

There is a time break between the Pniel Group and the Platberg Group that forms the Pniel unconformity. The sequence consists of the Bothaville Formation at the base that is overlain by the Allanridge Formation (Winter, 1976; Crow & Condie, 1988; van der Westhuizen et al., 1991).

2.4.1 Bothaville Formation

The Bothaville Formation unconformably overlies the Platberg Group and has more mature cyclic sediments than the underlying sediments (Crow & Condie, 1988; van der Westhuizen et al., 1991, 2006). The quartz grains (average size of ~400 µm) become more rounded up sequence (Schneiderhan et al., 2011). The Formation has basal conglomerate (well-rounded pebbles and boulders of vein quartz, quartzite, granite, banded iron formation, chert, tuff, lava and quartz porphyry) that grades into sandstone, shales and limestones up sequence (Crow & Condie, 1988; van der Westhuizen et al., 2006). The sediments are more depleted in large-ion lithophile elements (LILE) than the Kameeldoorns Formation when compared with upper continental crust (UCC) and Post Archean Australian Shale (PAAS), but have similar rare earth element (REE) concentrations to those of Archean upper crust (Schneiderhan et al., 2011).

2.4.2 Allanridge Formation

There is a conformable relationship between the Allanridge and Bothaville Formations in the deeper parts of the basin (Crow & Condie, 1988). The Allanridge Formation contains localized, rare basal komatiitic lava flows, pillow basalts, and a less mafic top (van der Westhuizen et al., 2006). Most of the sequence contains fine- to medium-grained amygdaloidal and porphyritic (acicular feldspar phenocrysts) andesitic lavas, and pyroclastic rocks (Crow & Condie, 1988; Eriksson et al., 2002; van der Westhuizen et al., 2006; Altermann & Lenhardt, 2012). The mafic lavas are similar to those of the Klipriviersberg Group both chemically and petrographically (Schneiderhan et al., 2011). Crow and Condie (1988) reported altered and relict plagioclase phenocrysts, altered glass, clinopyroxene pseudomorphs (replaced by actinolite-chlorite-epidote) and relict clinopyroxene. Using age constraints, geochemistry and palaeomagnetism, the Allanridge Formation lavas have been linked to the ca. 2.65 Ga east- to southeast-trending Rykoppies dyke swarm located in the Archean basement in the eastern Kaapvaal Craton (Olsson et al., 2010; Klausen et al., 2010; Altermann & Lenhardt, 2012).

2.5 Ventersdorp geochronology

The Neoarchean Ventersdorp volcano-sedimentary sequence has been considered as one magmatic and sedimentary event since the late 1800s (Wyley, 1859; Stow, 1874; Hatch; 1903). The view of the Ventersdorp Large Igneous Province (VLIP) as a single event was based on the age dating of amygdaloidal and porphyritic volcanic rocks of the Klipriviersberg Group (2714 ± 8 Ma) and quartz feldspar porphyritic volcanic rocks of the Platberg Group (2709 ± 4 Ma) using zircon ion microprobe U-Pb studies by Armstrong et al. (1991). However, the lavas have been re-dated (using ID-TIMS, LA-ICP-MS and SHRIMP) to be around 2780 Ma for the Klipriviersberg Group and around 2720 Ma for the Platberg Group, specific dates are provided in Table A1.1 (Poujol et al., 2005; de Kock et al., 2012; Cornell et al., 2017; Stamsnijder, 2017; Gumsley et al., 2020). The more recent dates suggest that the Platberg Group is much younger than the Klipriviersberg Group and this invokes the reconsideration of the Ventersdorp Supergroup as a single LIP. This has important implications for understanding the petrogenesis of the Ventersdorp Supergroup, the deposition of the Witwatersrand and Transvaal Supergroups, as well as the evolution of the Kaapvaal Craton.

Stamsnijder (2017) dated baddeleyite grains from two mafic feeder sills of the Klipriviersberg Group to be 2787 ± 2 Ma using isotope dilution thermal ionization mass spectrometry (ID-

TIMS) and laser ablation inductively coupled plasma mass spectrometry (LA-ICP-MS). The dates of Stamsnijder (2017) are different from the widely cited dates of Armstrong et al. (1991) by ~ 73 million years. The dates reported in Gumsley et al. (2020) are in agreement with dates reported in earlier research that are different from those reported in Armstrong et al. (1991) (Barton et al, 1990; Wingate, 1998; Poujol et al., 2005; de Kock et al., 2012; Cornell et al., 2017). The Klipriviersberg and Platberg dates of Armstrong et al. (1991) have been attributed to samples that had up to 15 % of common lead (Pb) and lead loss yielding minimum ages (Cornell et al., 2017), and therefore must be treated with caution. Recent geochronological studies date the Makwassie Formation of the Platberg Group (previously dated at 2709 ± 4 Ma) to be around 2720 Ma (Poujol et al., 2005; de Kock et al., 2012; Cornell et al., 2017). The Allanridge Formation of the Pniel Group has been linked to ca. 2.65 Ga dolerite dykes (Olsson et al., 2010, 2011; Klausen et al., 2010; Altermann & Lenhardt, 2012). Numerous geochemical and geochronology studies have been done on dykes and sills associated with the Ventersdorp lavas occurring on the Kaapvaal Craton (Harris & Watkins, 1990; McCarthy et al., 1990; Meier et al., 2009; Olsson et al., 2010, 2011; Klausen et al., 2010; Gumsley et al., 2020). The studies successfully linked the intrusions to the Ventersdorp Supergroup using structures, geochemistry and geochronology. Olsson et al. (2010) dated east-west trending mafic dykes of the Rykoppies Dyke Swarm in the eastern Kaapvaal Craton using U-Pb dating of baddeleyite by ID-TIMS. They showed that the dykes date between 2.70 Ga and 2.66 Ga, and together with Klausen et al. (2010), they linked the dykes to the lavas of the Allanridge Formation. Stamsnijder (2017) performed U-Pb geochronology on baddeleyite from dolerite sills in the Witwatersrand sediments a few kilometres from Edenville and Steynsrus towns, using ID-TIMS and LA-ICP-MS. The baddeleyite grains yielded upper intercepts of 2787 ± 2 Ma and 2789 ± 4 Ma and links the mafic sills to basal units of Ventersdorp LIP, the Klipriviersberg lavas. Stamsnijder (2017) further re-evaluated the date published in Armstrong et al. (1991) using a 1.1 Ga lower intercept that yielded upper intercept dates of 2809 ± 45 Ma and 2807 ± 48 Ma for the Alberton Formation. These geochronological studies on the intrusions not only aided in constraining the duration of Ventersdorp magmatic event(s) (2.78 Ga – 2.66 Ga) but also connected the Ventersdorp Supergroup type sequence to correlatives on the Kaapvaal Craton. This also improved the understanding of the plumbing system of Ventersdorp Supergroup.

2.6 Correlatives

The Kaapvaal Craton is made up of the Witwatersrand, Kimberley, and Pietersburg blocks that amalgamated around 3.1 Ga, and this is where the Ventersdorp Supergroup crops out (de Kock et al., 2012). Petrographic and petrological information on the Ventersdorp Groups and sequences comes from the drillcores into the Witwatersrand Supergroup that intersected the Ventersdorp Groups during the exploration for gold, making the Witwatersrand basin the type locality of Ventersdorp Supergroup, specifically the Bothaville region (Winter, 1976; Cornell et al., 2017). There are equivalents of the Groups across the Kaapvaal Craton and on the Pilbara Craton in Australia that crop out poorly due to the extensive coverage of the Transvaal Supergroup and Karoo Supergroup, as well as isolated grabens of the Platberg on different blocks (Grobler et al., 1989; van der Westhuizen et al., 2006; Altermann & Lenhardt, 2012; de Kock et al., 2012; Cornell et al., 2017; Gumsley et al., 2020). See Table A1.2 for the correlatives of the Ventersdorp Supergroup.

2.6.1 Correlatives on the Kaapvaal Craton

The extent of the Ventersdorp Supergroup on the Kaapvaal Craton has been documented in detail in a bid to reconcile the 2.7 Ga volcano-sedimentary sequences outside the type locality to the Ventersdorp Supergroup using thorough descriptions, geochemical analysis and dating of the lithologies.

2.6.1.1 Klipriviersberg correlatives

The Klipriviersberg Group is the basal group of the Ventersdorp Supergroup, defined on the Witwatersrand block, and has been correlated to the volcanic rocks at the triple junction of the three crustal blocks of the Kaapvaal Craton situated along the border between Botswana and South Africa. The volcanic rocks in the Derdepoort, Kanye and Lobatse areas date at 2780 ± 5 Ma, which are similar to the dates published by Gumsley et al. (2020) and Barton et al. (1990) for the Klipriviersberg Group volcanic rocks. Tyler (1979) documented volcanics in the Tshwene-Tshwene and Derdepoort belts and correlated them to the type-locality volcanic rocks.

2.6.1.2 Platberg correlatives

The Sodium Group is in the southwestern portion of the Kaapvaal Craton – in the Kimberley block - cropping out in the T'Kuip Hills between Prieska and Britstown (Grobler et al., 1989; Altermann & Lenhardt, 2012). This Group, famous for well-preserved raindrop imprints, is correlated with the Platberg Group on the Witwatersrand block (Altermann & Lenhardt, 2012). The Sodium Group unconformably rests on the basement granite and comprises the basal Ongers River Formation, the medial T'Kuip Formation that is overlain by the Omdraaivlei Formation (Grobler et al., 1989). The Ongers River Formation is ~ 500 m thick and it consists of lenticular beds that laterally vary in thickness (Altermann & Lenhardt, 2012). The Ongers River Formation fines upwards, and this is recognizable by the decrease in the size of the clasts and concomitant thickening of fine-grained beds of sandstone and tuffaceous shales. The basal units contain mafic tuff lenses and matrix-supported granitic boulders (derived from the basement) with diameters of up to 1.4 m (Grobler et al., 1989). Altermann and Lenhardt (2012) document lenses of mafic lava, quartz porphyry and limestone in the upper part, and published a preliminary date of 2739 ± 39 Ma using zircon from lava and tuff beds. The Ongers Formation, with its bimodal grain size and composition, is correlated with the Kameeldoorns Formation. Conformably overlying the Ongers River Formation is the T'Kuip Formation which has been correlated with the Makwassie Formation. The ~ 350 km thick T'Kuip Formation also overlies the basement granites. The exposure of the Formation is very limited and mainly consists of quartz and feldspar porphyry with the minor occurrence of tuff and arkose sandstones (Altermann & Lenhardt, 2012). The base and tops of the flows are characterized by quartz and calcite amygdales. The base of the quartz porphyry shows extreme alteration with banding and round clasts. Accessory minerals reported by Grobler et al. (1989) are apatite, zircon and titanite. The uppermost unit of the Sodium Group is the Omdraaivlei Formation with the lower contact between the T'Kuip quartz porphyry and a mafic lava flow. The Formation is correlated with the Rietgat Formation of the type area, Bothaville region (Grobler et al., 1989). The basal lava flows are overlain by interbedded lavas and sediments. The lava flows contain amygdales composed of quartz, chert, chalcedony, chlorite or calcite. Detailed descriptions of the Sodium Group are included in Altermann and Lenhardt (2012) and Grobler et al. (1989).

Northwest of Vryburg in the Northern Cape Province, there is the Zoetlief Group. The Zoetlief Group is also a correlative to the Platberg Group, and it comprises a volcano-sedimentary

sequence. The lithostratigraphy of the Group is summarized in Walraven et al. (1991). The basal unit is the Oasis Formation, which correlates to the Kameeldoorns Formation. Both Formations consist of conglomerate, arkose sandstones, quartzite, shale and slate. The Oasis Formation is overlain by the Kareefontein Formation, a correlative of the Makwassie Formation that consists of quartz porphyry, rhyolite and trachyte. The uppermost unit, the Vogelvei Formation, is correlated with the Rietgat Formation, comprises tuff, breccia, and limestone, and chert with andesitic and trachytic lavas. Walraven et al. (1991) used the similarities in the lithologies and disturbances in Rb-Sr, Pb-Pb and Sm-Nd isotopic compositions (open system behaviour possibly related to tectonism) to support the correlation of the Zoetlief Group and Platberg Group and they suggested that the two successions have similar ages and that they have a similar geological history. Zircon analysed by Pb evaporation technique by Walraven et al. (1991) from the Kareefontein Formation of the Zoetlief Group was dated 2714 ± 3 Ma. This was subsequently revised to 2718 ± 6 Ma by Cornell et al. (2017) and is within the range of the newly accepted dates.

The Hartswater Group is another correlative of the Platberg Group on the Kimberley block, and it extensively crops out in the Taung area and along the Orange River between Douglas and Hopetown (de Kock et al., 2012). The Hartswater Group comprises the basal Mohle Formation and upper Phokwane Formation and they are correlated with the Kameeldoornss Formation and Rietgat Formation respectively. No correlations between the Makwassie and Goedgenoeg Formations have been reported in the area. The Mohle Formation consists of upward-fining, repetitive sequences from a basal conglomerate of granite and quartz clasts, gritstone, arkose, greywacke, shale and tuff with stromatolitic limestone (de Kock et al., 2012). The Formation was dated to be 2733 ± 3.4 Ma. Conformably overlying the Mohle Formation is the 2724 ± 5.8 Ma Phokwane Formation, a correlative to the Rietgat Formation, comprising quartz-feldspar porphyry and mafic lavas. The porphyry flows show banding and chloritization. De Kock et al. (2012) reports basal agglomerate made up of porphyry fragments supported by a groundmass of quartz, feldspar, chlorite and sericite. Polymitic breccia forms the top of the Phokwane Formation, with localized stromatolitic limestones.

2.6.2 Correlatives on the Pilbara Craton

Multiple supercraton or supercontinental models have been proposed using both paleomagnetic and geochronological constraints, as well as lithostratigraphic and geochemistry correlations. Supercratonic configurations that have been proposed include Vaalbara, which comprises the Kaapvaal, Pilbara and Grunehogna cratons (de Kock et al., 2009); Superia made up of Superior, Wyoming, Hearne and Kola-Karelia cratons (Ernst & Bleeker, 2010); Sclavia composed of Dharwar and Slave cratons (French & Heamann, 2010); and Zimgarn composed of Zimbabwe and Yilgarn cratons (Smirnov et al., 2013). The following section focuses on the Vaalbara supercraton and provides descriptions of the geological similarities that have been used as evidence to argue that the Kaapvaal and Pilbara Cratons were once adjoined.

The occurrence of the 2.7 Ga Ventersdorp volcano-sedimentary succession on the Kaapvaal Craton in South Africa has been extended to the Pilbara Craton in Australia. The 2.7 Ga Fortescue Group on the Pilbara Craton has been correlated to the Ventersdorp Supergroup, Table A1.3 (Trendall, 1968; Button, 1979; Grobler et al., 1989; Nelson et al., 1992; Wingate, 1999; Blake et al., 2004; de Kock et al., 2012). The similarities in the ages, lithostratigraphy and chemostratigraphy across the two different cratons have given rise to the actively debated concept of the supercraton 'Vaalbara'. Various supercraton models that reconstruct the configuration of the cratons (i.e., Cheney fit, de Kock fit and Zegers fit) have been proposed in order to try to fit various structural elements and lithologies found on both cratons. The Transvaal Supergroup overlying the Ventersdorp Supergroup on the Kaapvaal Craton is also correlated with the Hammersley Group on the Pilbara Craton, lending further support to the notion that the Kaapvaal Craton was once adjoined to the Pilbara Craton. In addition, the quartz porphyries of the Kylena and Maddina basalts (2724 – 2721 Ma) on the Pilbara Craton might be related to the Platberg Group quartz porphyries based on their ages (e.g., Gumsley et al., 2020).

2.7 Tectonic setting of the Ventersdorp Supergroup

The Klipriviersberg and Platberg Groups, as well as the Pniel Group, may represent different tectonic settings during the deposition of the lavas and sediments of the Ventersdorp Supergroup. The extensive volcanism of the Klipriviersberg Group lavas is related to extension and rifting across the Kaapvaal craton (Burke et al., 1985; Whitelaw, 1988; van der

Westhuizen et al., 1991; Zeh et al., 2009). It has been suggested that the Klipriviersberg Group lavas were extruded on the foreland basin that resulted from the collision of the Kaapvaal and Zimbabwe cratons (Burke et al., 1985; Grobler et al., 1989; Altermann & Lenhardt, 2012). However, the age of the Limpopo orogeny is still actively debated and does not support this model, as the ages show that the collision of the two cratons is much younger than the Ventersdorp Supergroup (Altermann & Lenhardt, 2012). Alternative models have been proposed, and these include rifting induced by: (1) a mantle plume; or (2) an upwelling asthenosphere beneath the Kaapvaal Craton (van der Westhuizen et al., 1991; Altermann & Lenhardt, 2012). The topographic undulations of the lowermost unit, the Venterpost Formation, reflect a compressional tectonic regime characterized by regional transpression and extensional block faulting that began during the Central Rand (van der Westhuizen et al., 1991; Altermann & Lenhardt, 2012). Graben basins were already developing during the deposition of the Venterspost Formation (Altermann & Lenhardt, 2012). Eriksson et al. (2002) and van der Westhuizen et al. (1991) proposed the mantle plume and the upwelling asthenosphere models, respectively. They proposed a craton uplift by mantle and upwelling asthenosphere that led to the erosion of the Witwatersrand Supergroup sequence, extensional rifting, and development of graben and half-graben basins.

Development of rift-induced isolated graben and half-graben basins dominated the Witwatersrand basin. The rifting mobilised the magmas in sub-chambers, which had evolved to dacitic and rhyolitic composition by assimilation of Kaapvaal crustal material, to deposit the Goedgenoeg and Makwassie Formations (Meintjes & van der Westhuizen, 2018). Horst blocks of different lithologies provided the Platberg Group sediments that were deposited in the basins. Reactivation of faults continued throughout the Platberg Group times resulting in further erosion and sedimentation indicated by near vertical contacts between the sediments and horst blocks (e.g., Ongers River Formation) sediments and granitoids of the Sodium Group (Grobler et al., 1989; Altermann & Lenhardt, 2012). The faulting diminished towards the end of the Platberg deposition as indicated by coarse, immature sediments at the base and finer, mature sediments at the top of the Rietgat Formation (Burke et al., 1985).

The Pniel Group is thought to reflect subsidence and extensional forces that formed the basins of the Bothaville and Allanridge Formations, and the deposition of the lavas and sediments. Altermann and Lenhardt (2012) suggested that the thermal subsidence was a result of the

mantle plume subsiding. The mature sediments of the Bothaville Formation reflect remobilised sediments indicating that the faulting had ceased, and the horst blocks were covered by older Formations, contributing little or no material to the Bothaville Formation.

Chapter 3: Methodology

3.1 Sample Selection

The samples analysed in this study were selected from a suite of powders and drillcore material collected from the borehole core stored in the School of Geosciences at the University of the Witwatersrand (Wits) (Table A2.1). The major element data were compiled from the existing data in theses, published articles and the GEOROC database (https://georoc.eu). The pre-existing major element data were used to select the samples for this study, with those that have low loss on ignition (LOI) values prioritized for isotopic work. This was done to avoid samples with high volatile content, as these are very likely to be highly altered. Thin sections were prepared for the selected samples from available drillcore material. Drillcore samples that were used for geochemical analyses were pulverized and subsequently milled using a tungsten carbide mill into a whole-rock powder in the Earth Lab facilities at the Wits. The mill was cleaned between samples by milling quartz grains and rinsing with water and wiping with acetone to avoid cross contamination. The crusher and the mill have potential of contaminating the samples by introducing new tungsten and cobalt to the samples causing interference with hafnium, however, no interference was detected during the analysis of the samples. The machines were cleaned with care to avoid introduction of these metals into the samples.

3.2 Petrographic analysis

The thin sections made from the available drillcore were analysed using optical microscopes (Olympus BX41 and BX53) for mineral identification and texture analysis. Due to the altered nature of the samples, mineral identification and element maps of the thin sections were quantified using the energy-dispersive X-ray spectroscopy (EDS) using the VEGA-3 scanning electron microscope instrument and the VEGA-3 X64 TESCAN TIMA 1.7.0 software at the Wits Automated Mineralogy Laboratory (WAMLAB) at the University of the Witwatersrand. Liberation analysis was performed at varying resolutions (up to 2 µm per pixel) at a 15 mm working distance. The machine was set to 25 kV accelerating voltage, 17.68 nA of specimen beam current and 43 µA emission current.

3.3 Geochemistry

3.3.1 Trace elements

Trace element concentrations were determined using a Thermo Scientific iCAP RQ ICP-MS at the Earth Laboratory at the University of the Witwatersrand. In brief, 50 mg of sample powder was digested in Ultra High Purity 2:1 HF:HNO_3 and placed on a hotplate at 70°C in order to evaporate, and subsequently taken up in HF:HNO_3, capped and placed on the hotplate at 70°C for 72 hours. The sample solutions were diluted to 50 ml with 5% HNO_3 for measurement by ICP-MS (inductively coupled mass spectrometry). Internal Standards and Certified Reference Materials were monitored throughout the analyses and the results are shown in Table 3.1 and Fig. 3.1.

Table 3. 1 Concentrations of Certified Reference Materials analysed along trace element analysis.

	BCR2			**BHV02**		
ppm	Measured	Recommended	Error (%)	Measured	Recommended	Error (%)
Li	10.25	9.90	3.56	4.85	5.00	-3.00
P	1564.11	1571.00	-0.44	1183.57	1178.00	0.47
Sc	32.54	32.00	1.67	30.51	31.00	-1.57
Ti	12895.56	13005.00	-0.84	15766.01	15621.00	0.93
V	409.64	414.00	-1.05	332.75	329.00	1.14
Cr	15.73	17.00	-7.45	280.12	285.00	-1.71
Co	37.60	35.80	5.02	44.88	47.00	-4.51
Ni	11.93	12.70	-6.07	114.34	112.00	2.09
Cu	19.67	19.40	1.37	140.17	142.00	-1.29
Zn	144.13	147.00	-1.95	109.23	107.00	2.09
Ga	22.47	22.70	-1.00	21.22	21.00	1.07
Rb	50.08	49.00	2.21	9.89	10.10	-2.08
Sr	337.52	321.00	5.15	364.67	382.00	-4.54
Y	31.16	31.00	0.52	22.89	23.00	-0.47
Zr	183.89	194.00	-5.21	169.32	160.00	5.82
Nb	11.90	12.80	-7.02	17.75	16.40	8.21
Sn	3.01	2.10	43.48	2.07	2.70	-23.26
Sb	0.46	0.62	-26.13	0.16	0.16	0.00
Cs	1.23	1.17	5.21	0.11	0.11	-4.55
Ba	628.84	641.00	-1.90	131.26	128.70	1.99
La	25.21	24.50	2.90	15.17	15.60	-2.74
Ce	51.24	50.50	1.46	36.48	37.00	-1.41
Pr	6.37	6.30	1.08	4.95	5.00	-1.06
Nd	27.68	27.00	2.51	23.43	24.00	-2.39
Sm	6.32	6.30	0.29	5.78	5.80	-0.28
Eu	1.93	1.91	1.15	1.98	2.00	-1.15
Gd	6.52	6.50	0.31	5.88	5.90	-0.31
Tb	0.97	0.95	1.89	0.84	0.86	-1.86
Dy	5.97	6.00	-0.55	4.93	4.90	0.57
Ho	1.21	1.20	0.50	0.91	0.91	-0.44
Er	3.31	3.30	0.21	2.30	2.30	-0.22
Tm	0.47	0.46	1.52	0.30	0.30	-1.33
Yb	3.28	3.20	2.53	1.97	2.02	-2.43
Lu	0.47	0.47	-0.43	0.26	0.26	0.38
Hf	4.82	5.00	-3.62	4.26	4.10	3.90
Ta	0.71	0.78	-9.10	1.05	0.94	11.38
W	0.48	0.44	9.77	0.25	0.27	-8.15
Tl	0.30	0.30	0.00	0.02	0.06	-67.24
Pb	9.43	10.90	-13.50	1.66	1.40	18.50
Th	5.67	5.50	3.09	1.15	1.18	-2.88
U	1.75	1.73	0.92	0.44	0.44	-0.91

BCR2 = Columbia River Basalt, BHVO2 = Hawaiian Basalt

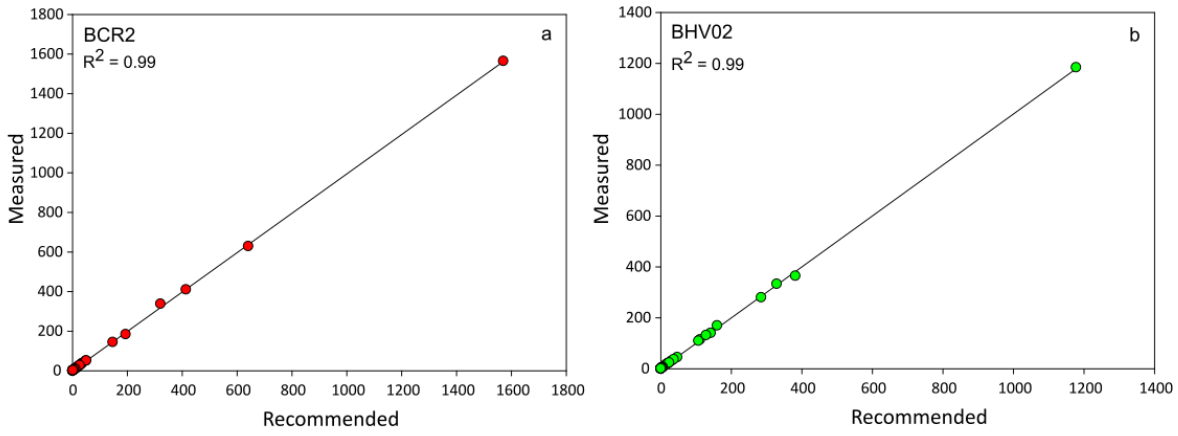

Figure 3. 1 Plot of quality assurance and quality control (QAQC) for the Certified Reference Materials used for trace element analysis.

3.3.2 Sr-Nd-Hf isotopes

The samples were prepared for chemical purification of Lu, Hf, Rb, Sr, Sm and Nd and isotopic analyses in the Wits Isotope Geosciences Laboratory (WIGL) at the University of the Witwatersrand. The sample powders were spiked with mixed ^{176}Lu-^{180}Hf, ^{149}Sm-^{150}Nd and ^{87}Rb-^{86}Sr tracers and dissolved in HF-HNO_3 in PFA beakers on the hotplate at 110°C for 5 days. The mass of each sample and the spikes varied depending on the concentrations of Sr, Hf and Nd in each sample. Samples were processed in batches of 8, which included 7 unknown (Westonaria) samples and either a Certified Reference Material (BHVO2, BCR2) or a Total Procedural Blank. After sample digestion, the chemical purification of the elements was obtained by a 3-stage chromatography method set up and calibrated in the WIGL and it is described in detail in Table 3.2. Lutetium and Hf were separated from the matrix using a 1 ml Ln-Spec 100 – 150 µm particle size resin bed, following an elution scheme modified from Münker et al. (2001). The bulk of LREE, Rb and Sr were separated on PFA columns with a 2 ml resin bed of BioRad AG 50W-X8, 200-400 mesh. The separation of Nd from Sm was performed on PFA columns using a 1 ml Ln-Spec resin bed as a cation exchange medium. The International Certified Reference Materials (BHVO2 or BCR2) and Total Procedure Blanks (TPB) were processed and analysed as unknown samples so to monitor and validate the reliability and reproducibility of the isotope dilution schemes of the laboratory as well as to monitor the precision and accuracy of the mass spectrometer (Fig. 3.2 and Tables A2.2, A2.3 and A2.4). All isotopic measurements were performed in low-resolution mode on a Nu Instruments Plasma II MC-ICP-MS (Nu Instrument, Wrexham) housed at Spectrum (University

of Johannesburg). Overall the sessions, JMC-475 ($^{176}Hf/^{177}Hf$ = 0.28216; Weis et al., 2007) yielded an average $^{176}Hf/^{177}Hf$ of 0.28214 ± 0.00003 (2σ: n = 78), JNdi ($^{143}Nd/^{144}Nd$ = 0.51212; Tanaka et al., 2000) yielded an average $^{143}Nd/^{144}Nd$ of 0.51212 ± 0.00001 (2σ: n = 107) and International Sr (SRM 987: $^{87}Sr/^{86}Sr$ = 0.71024) yielded an average $^{87}Sr/^{86}Sr$ of 0.71025 ± 0.00002 (2σ: n = 131).The ε_{Nd} was calculated using λ values of Begemann et al. (2001) (λ = 6.54 x 10^{-12} yr^{-1}) and present-day CHUR of Wasserburg et al. (1981) ($^{143}Nd/^{144}Nd$ = 0.51264; $^{147}Sm/^{144}Nd$ = 0.1967). The ε_{Hf} was calculated using λ values of Söderlund et al. (2004) (λ = 1.867 x 10^{-11} yr^{-1}) and present-day CHUR of Bouvier et al. (2008) ($^{176}Hf/^{177}Hf$=0.28279 ± 1; $^{176}Lu/^{177}Hf$ = 0.0336). See equations (1) to (5) for the calculations.

$$\left(\frac{^{87}Sr}{^{86}Sr}\right)_{(t)} = \left(\frac{^{87}Sr}{^{86}Sr}\right)_{(now)} - \left(\frac{^{87}Rb}{^{86}Sr}\right)_{(now)} (e^{\lambda t} - 1) \quad (1)$$

$$\left(\frac{^{143}Nd}{^{144}Nd}\right)_{(t)} = \left(\frac{^{143}Nd}{^{144}Nd}\right)_{(now)} - \left(\frac{^{147}Sm}{^{144}Nd}\right)_{(now)} (e^{\lambda t} - 1) \quad (2)$$

$$\left(\frac{^{176}Hf}{^{177}Hf}\right)_{(t)} = \left(\frac{^{176}Hf}{^{177}Hf}\right)_{(now)} - \left(\frac{^{176}Lu}{^{177}Hf}\right)_{(now)} (e^{\lambda t} - 1) \quad (3)$$

$$\varepsilon_{Nd(t)} = \left[\frac{\left(\frac{^{143}Nd}{^{144}Nd}\right)_{Sample(t)}}{\left(\frac{^{143}Nd}{^{144}Nd}\right)_{CHUR(t)}} - 1\right] \times 10^4 \quad (4)$$

$$\varepsilon_{Hf(t)} = \left[\frac{\left(\frac{^{176}Hf}{^{177}Hf}\right)_{Sample(t)}}{\left(\frac{^{176}Hf}{^{177}Hf}\right)_{CHUR(t)}} - 1\right] \times 10^4 \quad (5)$$

Table 3. 2 Three-column chromatography schemes for purification of Lu, Hf, Rb, Sr, Sm and Nd

Step	Solvent	Volume (mL)
	Column I: Lu and Hf purification	
Pre-conditioning	6 mol l^{-} HCl	5
Conditioning	2 mol l^{-} HCl	2 (x 3)
Sample loading	2 mol l^{-} HCl	5
Matrix elution	2 mol l^{-} HCl	5
Yb elution	2.5 mol l^{-} HCl	5
HREE elution	6 mol l^{-} HCl	5
Post-Lu clean up	6 mol l^{-} HCl	5
HCl removal	Milli-Q H_2O	2 (x 2)
Ti elution	3 mol l^{-} HNO_3-3% H_2O_2	3 (x 5)
H_2O_2 wash off	0.1 mol l^{-} HNO_3	2
Zr elution	6 mol l^{-} HCl – 0.06 mol l^{-} HF	10 (x 3)
Zr – Ti clean up	6 mol l^{-} HCl – 0.2 mol l^{-} HF	2
Hf elution	6 mol l HCl – 0.2 mol l^{-} HF	10
Wash	6 M HCl	10
	2 M HF	10
	6 M HCl	10
	Column II: Rb and Sr purification	
Conditioning	1.5 mol l^{-} HCl	2 (x 3)
Sample loading	1.5 mol l^{-} HCl	1
Rinse	1.5 mol l^{-} HCl	1 (x 2)
Matrix elution	1.5 mol l^{-} HCl	4
Rb elution	1.5 mol l^{-} HCl	4
Ca clean up	1.5 mol l^{-} HCl	10
Sr elution	1.5 mol l^{-} HCl	15
HREE elution	6 mol l^{-} HCl	2
LREE elution	6 mol l^{-} HCl	7
Wash	6 mol l^{-} HCl	10 (x 3)
	Column III: Sm and Nd purification	
Conditioning	0.2 mol l^{-} HCl	2 (x 3)
Load sample	0.2 mol l^{-} HCl	0.3
Rinse	0.2 mol l^{-} HCl	0.4 (x 2)
La – Ce elution	0.2 mol l^{-} HCl	8
Nd elution	0.2 mol l^{-} HCl	10
Clean up	0.4 mol l^{-} HCl	3
Sm elution	0.4 mol l^{-} HCl	6
Wash	6 mol l^{-} HCl	10 (x 3)

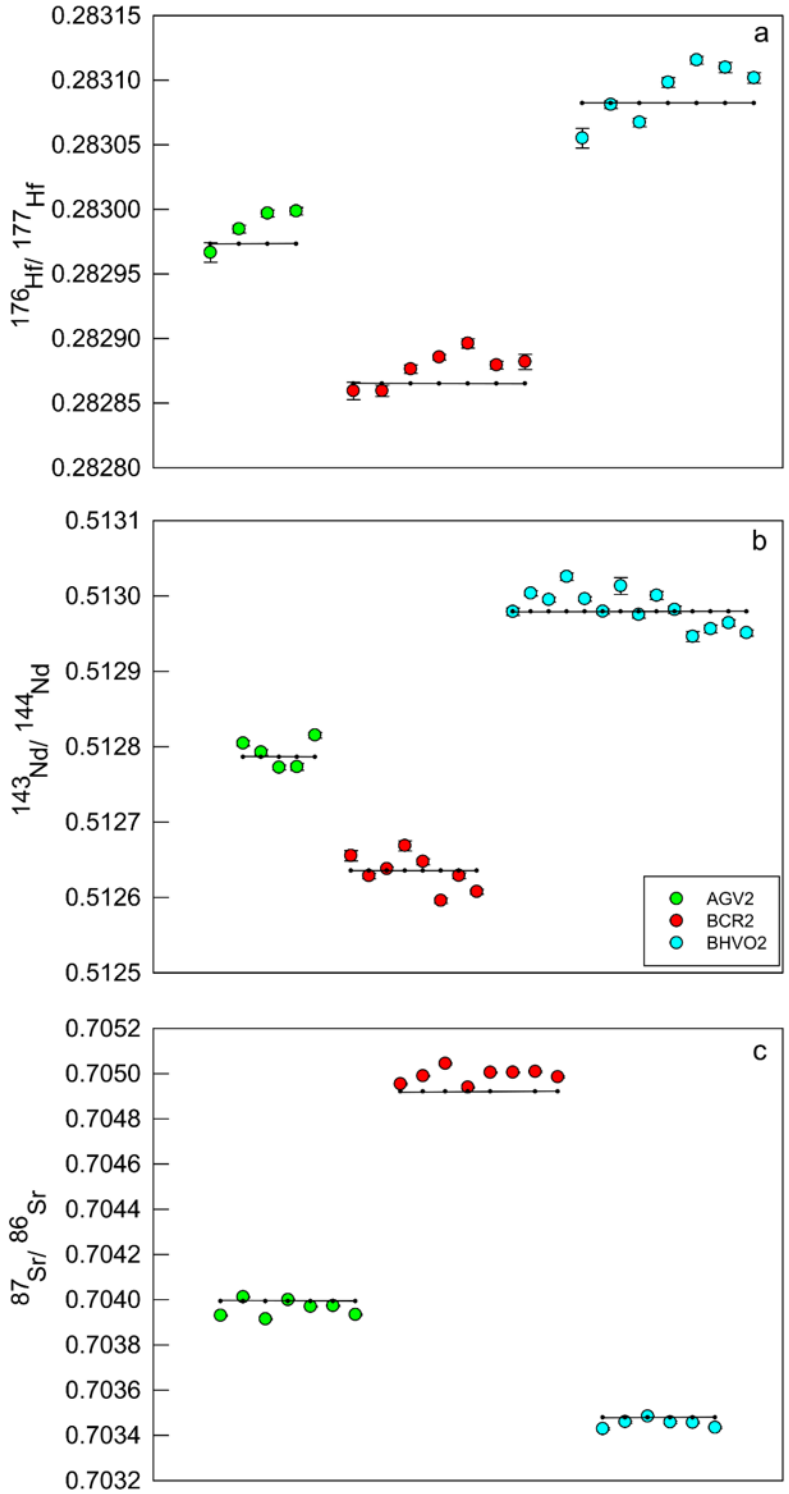

Figure 3. 2 Isotopic compositions of Certified Reference Materials that were digested analysed along with our samples. The black lines are the accepted values of the CRMs. The one standard error bars, showing the repeatability of the measurements, are smaller than the symbols where they are not visible.

3.3.3 Platinum group elements

The platinum-group elements (PGE) and gold (Au) were determined at the Université du Quebec à Chicoutimi (UQAC) using the nickel-sulphur fire assay (NiS-FA) technique, followed by $SnCl_2.2H_2O$-Te co-precipitation described in Savard et al. (2010). The technique takes into account and reduces the effect of nuggets, therefore, yielding accurate measurements. Sample powders of 15 g were mixed with 10 g sodium carbonate, 15 g sodium tetraborate, 5 g silica, 5 g nickel and 3 g sulphur to produce NiS beads that were subsequently mixed with an additional 15 g sodium tetraborate. The mixtures were put in a muffle furnace at 1050 °C for 90 min, followed by dissolution in 12 mol l^- HCl for 24 hr in PFA jars in a vented oven at 110 °C. The dissolved beads were then mixed with 4 g of stannous chloride dehydrate-($SnCl_2.2H_2O$). The mixtures were then placed in the oven for 24 hr and then cooled. The product was collected in a cellulose membrane filter, then rinsed with 1 mol l^- HCl and dissolved in 2 mL HCl and 2 mL HNO_3 in sealed PFA jars on a hot plate for 12 hr at 120 °C, converting the samples to acid solutions. The solutions were then diluted with 18.2 MΩ/cm de-ionised water to measure the PGE and Au using inductively coupled plasma mass spectrometry (ICP-MS). Certified reference materials (CRM) were measured to validate the digestion NiS-FA digestion method. The CRM results are shown in Table 3.3.

Table 3. 3 PGE and Au concentrations for Certified Reference Materials

ppb	101 Ru	103 Rh	105 Pd	189 Os	191 Ir	195 Pt	197 Au
OKUM	3.93	1.55	11.11	0.99	0.87	10.55	0.85
Working OKUM (OGS)	4.25 ± 0.30	1.40 ± 0.13	11.7 ± 0.5	nd	0.99 ± 0.07	11.0 ± 0.6	1.49 ± 0.16
LK-NIP-1	0.45	1.05	17.17	0.12	0.17	12.48	3.92
Working LK-NIP-1 (GEO LABS)	0.44	0.90	17.96	nd	0.19	13.43	4.63
KPT	16.57	19.24	105.87	4.49	5.57	95.70	*128.28
Working KPT	17.3 ± 2.0	17.1 ± 1.1	122.0 ± 17.0	2.8 ± 0.6	6.8 ± 1.5	97.4 ± 20.1	41.1 ± 21.3
LDI-1	0.31	0.89	727.42	0.54	0.07	103.66	85.41
Provisional Composition LDI-1	0.32	0.70	834.00	Nd	0.08	98.20	83.90
LOD	0.12	0.08	0.47	0.07	0.03	0.08	0.48

*It has been shown with several analyzes that KPT sometimes has a nugget effect. OKUM = Komatiite, LK-NIP-1 = Nipigon Diabase dolerite, KPT = Quartz diorite and LD1-1 = Lac-des-Îles, Pd deposit. The second rows labelled 'Working…' have the values analysed in this study.

3.3.4 Sulphur isotopes

The whole rock analysis for multiple sulphur isotope compositions was conducted at the University of Maryland, following the procedure described in Magalhaes et al. (2018). To extract sulphur from the sulphide and disulphide phases, the sample powders were put in heated Cr(II) solution in 5 M HCl in a boiling flask. The sulphur was released in a form of hydrogen sulphide (H_2S) carried by nitrogen and then trapped in 0.3 M $AgNO_3$, producing silver sulphide (Ag_2S). After storing the silver sulphide for 7 days, the samples were washed using Milli-Q water and 1 M NH_4OH and dried up at 50 °C. The dried samples were then sealed in aluminium foil capsules and put in heated Ni vessels in which fluorine gas was introduced and left overnight to produce SF_6. The SF_6 samples were then purified using cryogenic separation, passivation and gas-chromatography, and then subsequently frozen in preparation for mass spectrometer analysis. The extraction and fluorination results are shown in Tables A2.5 and A2.6. Table 3.4 shows the results of five extractions of in-house pyrite standard were conducted with three measurements of each show the reproducibility of the measurements. The isotope analysis was done using a Thermo-Finnigan MAT253 gas source mass spectrometer using the Vienna-Canyon Diablo Troilite (VCDT) standard.

Table 3. 4 Sulphur composition results of an in-house pyrite standard for reproducibility

Name	δ34S cdt (‰)	Δ33S cdt (‰)	Δ36S cdt (‰)
AB 20-08 1	-2.39	-0.007	-0.098
AB 20-08 1	-2.39	-0.008	-0.090
AB 20-08 1	-2.38	-0.022	-0.108
SD	0	0.01	0.01
AB 21-08 4	-3.16	-0.019	-0.144
AB 21-08 4	-3.17	-0.016	-0.029
AB 21-08 4	-3.16	-0.028	-0.130
SD	0	0.01	0.05
AB 22-08 3	-2.50	-0.017	-0.179
AB 22-08 3	-2.49	-0.015	-0.120
AB 22-08 3	-2.49	-0.015	-0.120
SD	0.01	0	0.03
Ag2S CM	-2.94	-0.033	0.059
Ag2S CM	-2.94	-0.032	-0.021
Ag2S CM	-2.94	-0.035	0.064
SD	0	0	0.04
Ag2S 8-26 CM	-2.76	-0.020	-0.115
Ag2S 8-26 CM	-2.76	-0.013	-0.062
Ag2S 8-26 CM	-2.76	-0.011	-0.121
SD	0	0	0.03

3.3.5 Oxygen isotopes

The in-situ oxygen isotope analysis of the clinopyroxene grains in the Westonaria Formation was carried out at the Potsdam-Deutsches GeoForschungsZentrum (GFZ) using Secondary Ion Mass Spectrometer (SIMS). Round sample mounts were prepared, and all analyses were done away from edges and cracks. NIST610 glass was also analysed to evaluate the data and the time dependent drift. The NIST610 yielded an analytical repeatability of 0.12 ‰. The measured $^{18}O/^{16}O$ ratios of the samples were normalised to the reference materials and corrected for instrument mass fractionation (IMF) using the mean IMF (1.00284) of the clinopyroxene reference materials The absolute zero-point of the Vienna Standard Mean Ocean Water (VSMOW) $^{18}O/^{16}O$ used for $\delta^{18}O$ calculations is 0.00200520 from Baertschi (1976). Calibration results using reference materials are shown in Table 3.5.

Table 3. 5 Oxygen isotope composition of reference materials used for calibration in SIMS measurements.

NIST 610			
$\delta^{18}O$ VSMOW	10.91	± 0.09	Kasemann et al. (2001)
Zero-point VSMOW	0.0020052	± 0.45	Baertschi (1976)
Absolute	0.002027077		
	Dates		
	22nd	23rd	24th
$^{18}O/^{16}O$ Average	0.002025224	0.002024895	0.002024965
$^{18}O/^{16}O$ SD	3.32686E-07	3.09294E-07	1.69592E-07
$^{18}O/^{16}O$ Repeatability (‰)	0.164271266	0.152745811	0.083750628
N	16	4	7
IMF (measured/true)	0.999085915	0.998923541	0.998958156
OPX 31			
$\delta^{18}O$ VSMOW	5.54		Tang et al. (2019)
Zero-point VSMOW	0.0020052	± 0.45	Baertschi (1976)
Absolute	0.002016309		
	Dates		
	22nd	23rd	24th
$^{18}O/^{16}O$ Average	0.002016779	0.002016112	0.002016096
$^{18}O/^{16}O$ SD	2.63458E-07	2.5136E-07	1.69468E-07
$^{18}O/^{16}O$ Repeatability (‰)	0.130633188	0.124675579	0.084057552
N	8	5	9
IMF (measured/true)	1.000233008	0.99990259	0.999894402
OPX 06			
$\delta^{18}O$ VSMOW	5.75		Tang et al. (2019)
Zero-point VSMOW	0.0020052	± 0.45	Baertschi (1976)
Absolute	0.00201673		
	Dates		
	22nd	23rd	24th
$^{18}O/^{16}O$ Average	0.002017148	0.002016097	0.002016318
$^{18}O/^{16}O$ SD	3.74667E-07	1.91836E-07	1.66574E-07
$^{18}O/^{16}O$ Repeatability (‰)	0.185740985	0.095152173	0.082612733
N	8	5	8
IMF (measured/true)	1.00020744	0.999685977	0.999795573
CPX 29			
$\delta^{18}O$ VSMOW	5.45		Tang et al. (2019)
Zero-point VSMOW	0.0020052	± 0.45	Baertschi (1976)
Absolute	0.002016128		
	Dates		
	22nd	23rd	24th
$^{18}O/^{16}O$ Average	0.002022023	0.002021382	0.002021487
$^{18}O/^{16}O$ SD	1.8143E-07	3.3569E-07	2.65776E-07
$^{18}O/^{16}O$ Repeatability (‰)	0.089726864	0.166069313	0.13147548
N	7	6	8
IMF (measured/true)	1.002923894	1.002605899	1.002657834
CPX 31			
$\delta^{18}O$ VSMOW	5.19		Tang et al. (2019)
Zero-point VSMOW	0.0020052	± 0.45	Baertschi (1976)
Absolute	0.002015607		
	Dates		
	22nd	23rd	24th
$^{18}O/^{16}O$ Average	0.00202178	0.002020985	0.002021061
$^{18}O/^{16}O$ SD	1.92034E-07	3.60383E-07	2.39468E-07
$^{18}O/^{16}O$ Repeatability (‰)	0.094982565	0.178320664	0.11848631
N	6	5	8
IMF (measured/true)	1.003062607	1.002668086	1.002705767

Chapter 4: Nd-Hf-O isotope evidence of a sublithospheric mantle source for the Neoarchean Westonaria komatiites

Khulekani B. Khumalo, Lewis D. Ashwal, Ben Hayes & Linda M. Iaccheri

The manuscript was submitted to the Earth and Planetary Science Letters (EPSL) and is currently being revised.

Contributions:

Khulekani Khumalo: Conceptualised the study; wrote the manuscript; conducted the Sr-Nd-Hf isotope dilution and mass spectrometry analyses; and conducted the petrographic analysis.

Lewis Ashwal: Conceptualised the study; Compiled literature data; and reviewed the manuscript drafts.

Ben Hayes: Conceptualised the study; reviewed and edited manuscript drafts.

Linda Iaccheri: Supervised the isotope dilution laboratory work; and reviewed manuscript drafts.

Sarah Glynn: Supervised the oxygen isotope analysis.

Siphesihle Mnqayi: Conducted the oxygen isotope analysis for her honours project.

Please note that the detailed geological background and methodology sections have been excluded from this manuscript chapter and are presented in Chapters 2 and 3.

The manuscript was reviewed (without the oxygen isotope data analysis) by two reviewers for the Earth and Planetary Science Letters (EPSL) and rejected based on the alteration nature of the lavas with the assumption that the Nd-Hf isotopes are meaningless for the magma source composition.

We have revised the manuscript in accordance with the reviewer's comments and supplemented the Sr-Nd-Hf data with in-situ oxygen isotopes of freshly preserved clinopyroxene. The oxygen isotope study was undertaken by Siphesihle Mnqayi for her Honours project under the supervision of Mr Khulekani Khumalo, Prof. Lewis Ashwal and Dr Sarah Glynn. The new oxygen isotope compositions of the clinopyroxene grains in the lavas show the mantle origin of the Westonaria komatiites and support the minimal crustal contamination of the magmas.

4.1 Introduction

Komatiites are high-magnesian (>18% MgO) lavas that are almost entirely restricted to the Archean with the exception of the minor Tertiary-aged Gorgona komatiites (Arndt et al., 2008). This temporal restriction may be related to the secular cooling of the mantle and so komatiites may record the thermal and chemical evolution of the Archean mantle (e.g., Blichert-Toft & Puchtel, 2010; Blichert-Toft et al., 2015; Barnes & Arndt, 2019). Large degrees of partial melting of the mantle, along with elevated temperatures above those of the ambient mantle are necessary to produce komatiitic liquids, and such conditions are generally attributed to melting in a mantle plume (e.g., Barnes & Arndt, 2019). The decrease in the occurrence of komatiites after the end of Archean, as well as their decreasing MgO contents with time, indicates a change in mantle dynamics, such as changes in the rate and style of recycling of crustal material into the mantle. Geochemical studies of komatiites can therefore provide important insights into the thermal and chemical evolution of the mantle and mantle plumes (Arndt et al., 2008; Mole et al., 2014; Barnes & Arndt, 2019; Boyet et al., 2021; Puchtel et al., 2022) in the Archean as well as insights into the process of cratonatisation.

Komatiite types include Al-depleted (Barberton-type), Al-undepleted (Munro-type), Al-enriched (Commondale-type) and Ti-enriched (Karasjok-type) (see summary in Barnes & Arndt, 2019). These different types have been explained by the depth (or pressure) of melting and by the presence or absence of garnet in their mantle sources (Ohtani et al., 1989; Barnes & Arndt, 2019). Komatiites typically have SiO_2 and Al_2O_3 contents of <52% and <5%, respectively, TiO_2 contents of <1%, and flat rare earth element profiles (perhaps with a slight depletion in light rare earth elements). There are also komatiites that contain greater amounts of SiO_2 (>53%) and Al_2O_3 (10-17%), lesser amounts of TiO_2 (<1.2%), and which are enriched in light rare earth elements. These are the so-called 'siliceous high magnesian basalts' (SHMB: Barnes & Arndt, 2019). The origin of SHMB has been explained by extensive (up to 30%) crustal contamination of a primary komatiite magma (e.g., Sensarma et al., 2002; Barnes & Arndt, 2019).

In this study, we report new high-precision Sr-Nd-Hf isotopes and trace elements for komatiite lavas that are preserved in the Westonaria Formation at the base of the Neoarchean Ventersdorp Supergroup on the Kaapvaal craton in South Africa. We also report

oxygen isotope compositions of the fresh clinopyroxene grains that are well preserved in the Westonaria komatiites. We use the Nd-Hf-O isotopes and the trace element data, to constrain the mantle sources of the Westonaria komatiites and the role of crustal contamination in their petrogenesis. Multiple isotope studies of komatiites show no correlation of komatiite types and isotopic compositions (Arndt et al., 2008). A recent komatiite review in Puchtel et al. (2022) demonstrates that komatiites sampled isotopic and chemical heterogeneities of the mantle. There are variations in initial ratios of radiogenic isotope systems that point to a heterogeneous source, especially for the Cretaceous Gorgona Island komatiites as well as Precambrian komatiites, however, this can be a result of contamination and secondary processes (Arndt et al., 2008).

4.2 Regional Geology

The Ventersdorp Supergroup is one of the least deformed Neoarchean low-grade metamorphosed supracrustal sequences in the world and it is located on the Kaapvaal craton in South Africa (Van der Westhuizen et al., 1991). The Ventersdorp Supergroup is subdivided into the Klipriviersberg, Platberg, and Pniel Groups with each containing lava sequences. Previously, these lava sequences have been referred to as the 'Ventersdorp Large Igneous Province' (LIP); however, recent age data has indicated that there are disparate magmatic events in the Ventersdorp Supergroup. The Klipriviersberg LIP has been shown to have been deposited between 2791 and 2779 Ma and the Allanridge LIP to be deposited between 2701 and 2683 Ma. The bimodal volcanics of the Platberg Group is considered to mark the onset of the Allanridge LIP (Gumsley et al., 2020). The Westonaria Formation occurs at the base of the Klipriviersberg Group and it unconformably overlies supracrustal rocks of the Mesoarchean Witwatersrand Supergroup (2.8 to 3.0 Ga in age) in the West Rand and Central Rand areas of the Kaapvaal Craton (Fig. 4.1: van der Westhuizen et al., 1991). It is at least 50 m in thickness and consists of intercalated fine-grained komatiites and komatiitic basalts and clastic rocks (Winter, 1976; Crow & Condie, 1988; van der Westhuizen et al., 1991). The Klipriviersberg Group is further subdivided into the Alberton, Orkney, Jeanette, and Lorraine-Edenville Formations. Komatiitic basalts and basalts are present in some of these other formations. We report here a new trace element and isotopic dataset for the komatiites of the Westonaria

Formation. The isotopic geochemistry of the rest of the Klipriviersberg Group and the overlying Platberg-Pniel Groups will be considered in a companion paper (Chapter 5).

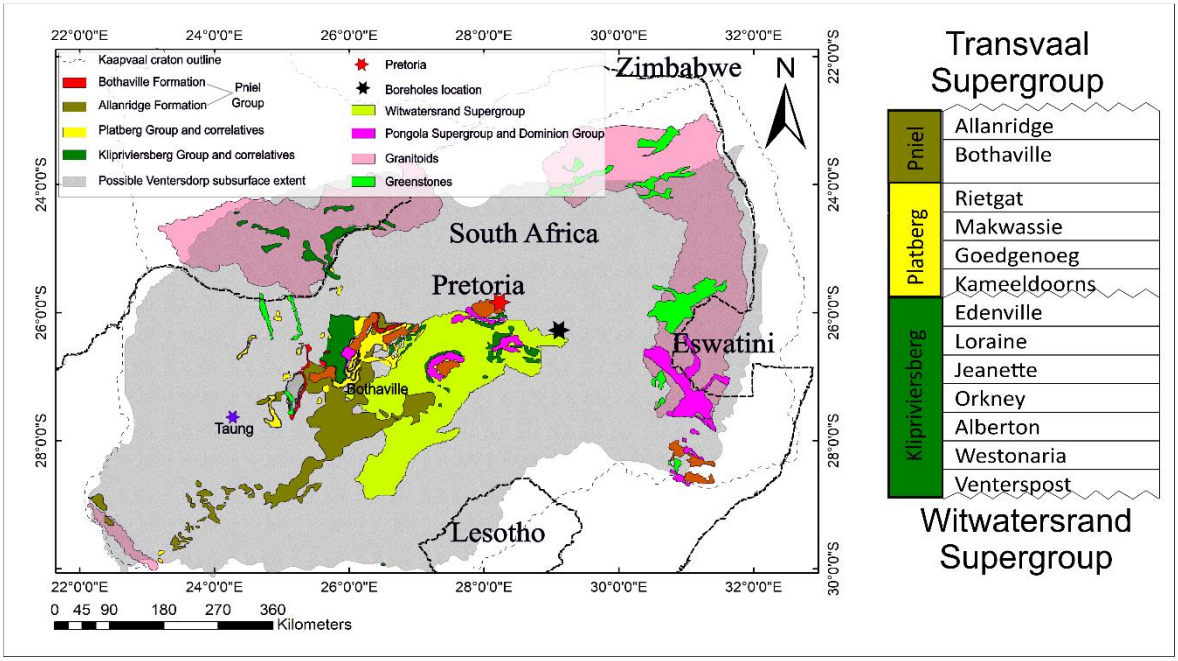

Figure 4. 1 Distribution map of the Ventersdorp LIP and its correlatives, modified after Gumsley et al. (2017). Sequences that are older than the Ventersdorp LIP are also shown. The map shows the area of surface exposure of the LIP. Possible subsurface extent (grey area) is based on borehole data and maps in Crow and Condie (1988) and Gumsley et al. (2017).

4.3 Samples

Fifteen whole rock samples of powders and drillcore material collected from five drillcores (E0, E1, E3, E4 and E5) were analysed in this study. The samples were stored at the school of Geosciences at the University of the Witwatersrand, for which only major and limited trace element data were previously reported in Myers et al. (1990). The drillcores are from the east of Johannesburg around the town of Secunda (Fig. 4.1 and Fig. 4.2). Samples with the lowest loss on ignition values were selected for trace element and isotope analyses. About 50 % of the analysed samples are from drillcore E5 shown in Figure 4.3.

Figure 4. 2 Google Earth image showing the locations of the drillcores used in this study. The drillcores were collected and stored at the University of the Witwatersrand, Johannesburg.

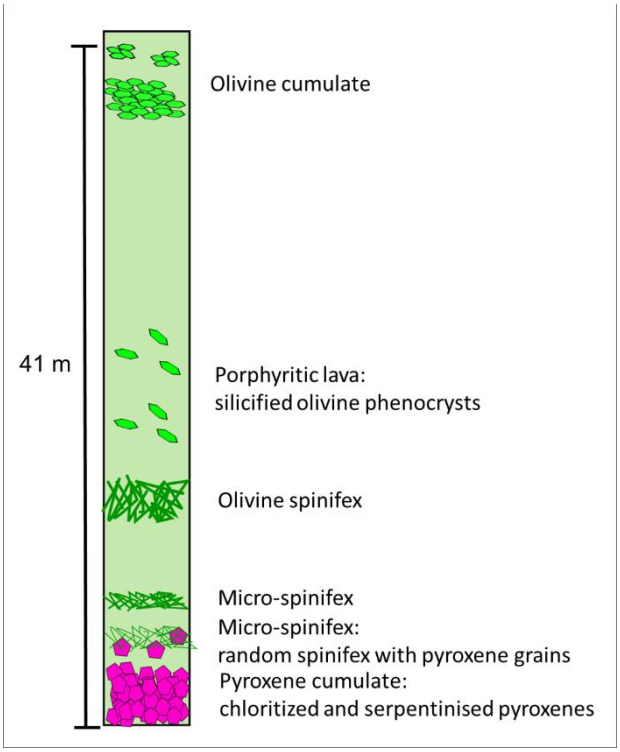

Figure 4. 3 Section through drillcore E5 showing the komatiite flow of the Westonaria Formation, from which some of the analysed samples were collected.

4.4 Results

4.4.1 Petrography

The samples show marked variation in phenocryst (pseudomorphed olivine and clinopyroxene) content and the extent of alteration. There is evidence in borehole E5 for the presence of multiple, composite komatiite flows, with cumulate, porphyritic and spinifex zones all preserved (Fig. 4.4). No primary (fresh) olivine is preserved. Pseudomorphed olivine and pyroxene phenocrysts are the dominant phases in the cumulate zones and porphyritic zones. Some of the porphyritic samples are characterised by glomerocrysts that locally contain aligned, euhedral olivine pseudomorphs (chloritized) and which are hosted in a fine-grained matrix of secondary actinolite (Fig. 4.4a-d). The cumulate zones are well developed, and they vary in their crystal content (up to 90 % modal abundance). Figure 4.4 shows cumulate (c and d) and phenocryst-rich zones (a and b) composed of chloritized orthopyroxene that appears to have replaced olivine. Some pseudomorphed olivine phenocrysts show resorbed, and amoeboid, textures (Fig. 4.4a-b). These phenocrysts are hosted in an actinolite-rich matrix, and they display a preferred orientation (Fig. 4.4 a-b). There are also clinopyroxene-rich cumulate zones (Fig. 4.4i-j). Serpentinization is apparent in the cumulate zones (Fig. 4.4j). Locally there are silicified (pseudomorphed) olivine phenocrysts crosscut by calcite-filled fractures, and which are hosted in an actinolite- and chlorite-rich matrix (Fig. 4.4f). Randomly oriented needles of actinolite spinifex are also present (Fig. 4.4g and h). The elongated grains are secondary actinolite needles. A TIMA image of the spinifex zone shows possible relict olivine specks, between the secondary actinolite needles as well as chloritized matrices (Fig. A1.1). The coarse spinifex texture grades into a microspinifex zone with microphenocryst pseudomorphs (Fig. 4.4g and h). Coarse clinopyroxene phenocrysts are set in the microspinifex zone (Fig. 4.4 i and j) and which grades into a clinopyroxene-rich cumulate. Calcite-, quartz- and chlorite-rich veins are observed in some sections (Fig. A1.2 and A1.3). Secondary titanite, talc, epidote and ankerite are also present in all samples.

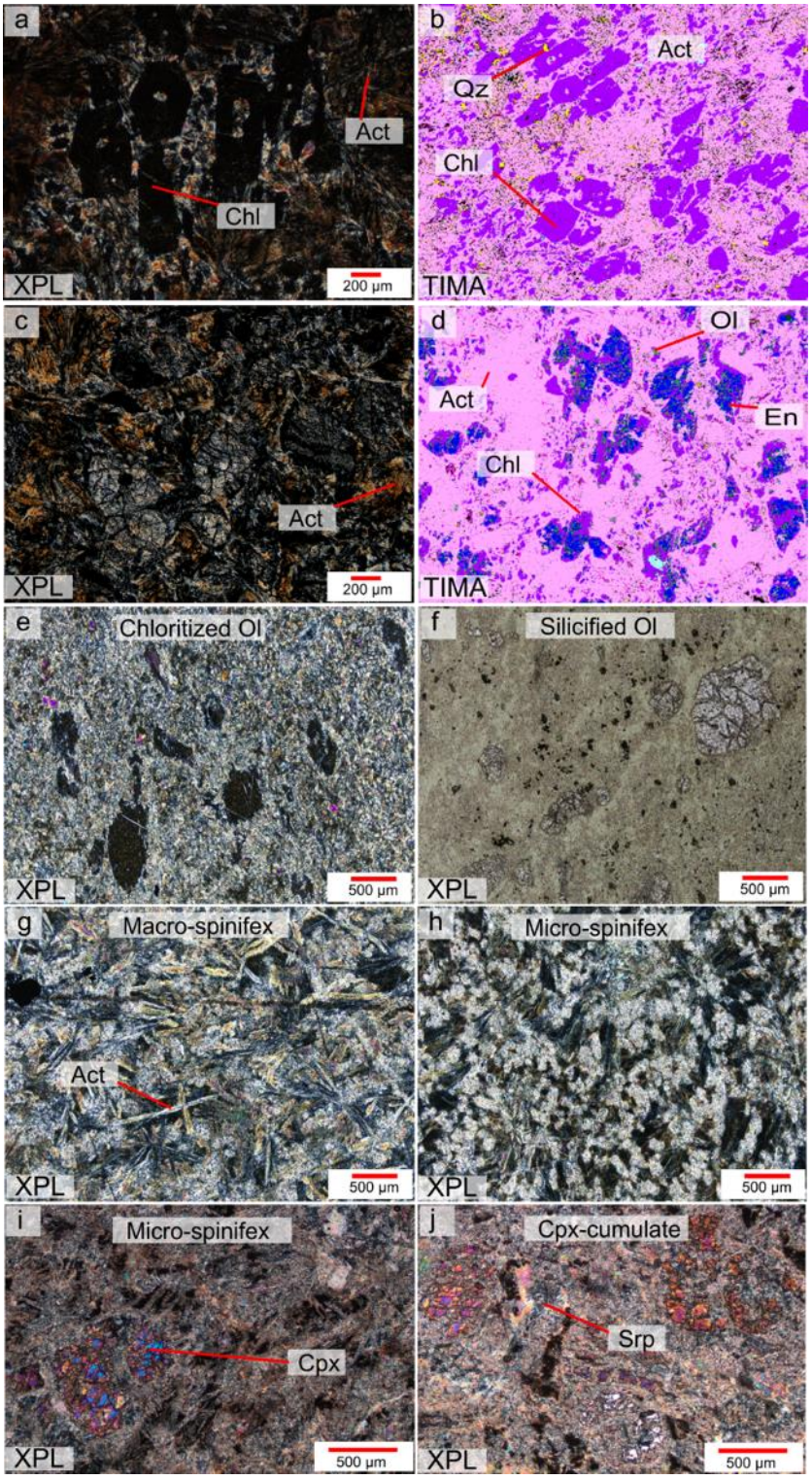

Figure 4. 4 Petrographic sections through the komatiite flow of the Westonaria Formation showing a well-developed flow. a) and b) show the pockets of cumulus phase that has been chloritized and hosted in an actinolite matrix. The chlorite has resorbed olivine inclusions. c and d) show the cumulate made up of partially chloritized pyroxene with relict olivine. e and f) show porphyritic texture with chloritized and silicified phenocrysts, previously olivine. g and h) show the spinifex textures that vary in length of the needles. i) shows clinopyroxene phenocrysts set in the micro-spinifex, and j) shows few cumulus clinopyroxene crystals in the pyroxene cumulate zone. Act = actinolite, Chl = chlorite, En = enstatite, Ol = olivine, Qz = quartz, Cpx = clinopyroxene, and Srp = serpentine.

4.4.2 Major and trace element chemistry

The Westonaria lavas have MgO contents that correspond to picrite and komatiitic compositions (14–25 wt. %: Table A3.1, Fig. 4.5, Fig. 4.6: Myers et al., 1990). Major elements (SiO_2, Al_2O_3, FeO_t, CaO and Na_2O) all display poor negative correlations with MgO (Fig. A1.4). The samples classify as komatiitic basalts using the cation classification from Jensen (1976). Trace elements (Cr, Zr, Ce) show poor negative correlations with MgO (Fig. A1.5). Nickel shows a weak positive correlation with MgO with uniform Ni contents (~1000 ppm) observed over a range of MgO values (19–24 wt. %). Cr values are scattered, with most samples having Cr concentrations of 1000-1200 ppm (Table A3.1). A moderate negative trend is observed between Zr and MgO. Ce plots show scattering versus MgO, however, there is an overall decrease in Ce content with increasing MgO, excluding outlier samples (R359 and R362) at lower MgO which show extensive alteration and recrystallization.

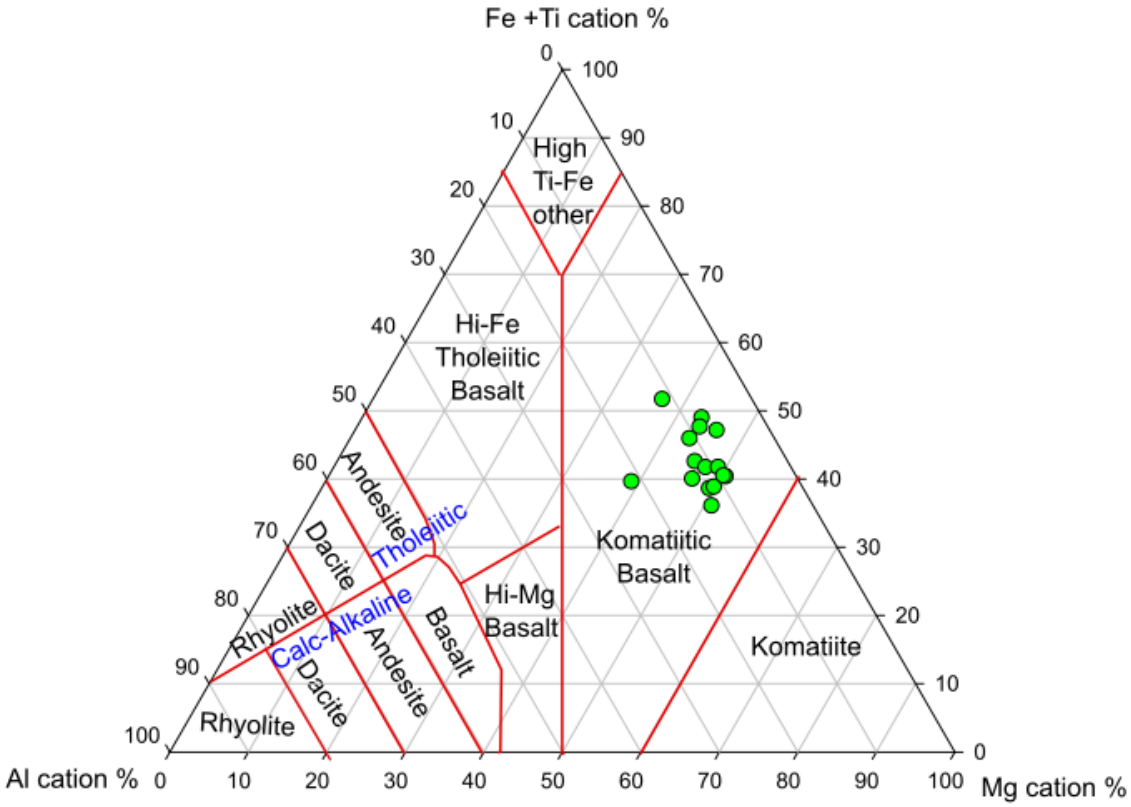

Figure 4. 5 Cation classification plot after Jensen (1976) for the analysed Westonaria samples.

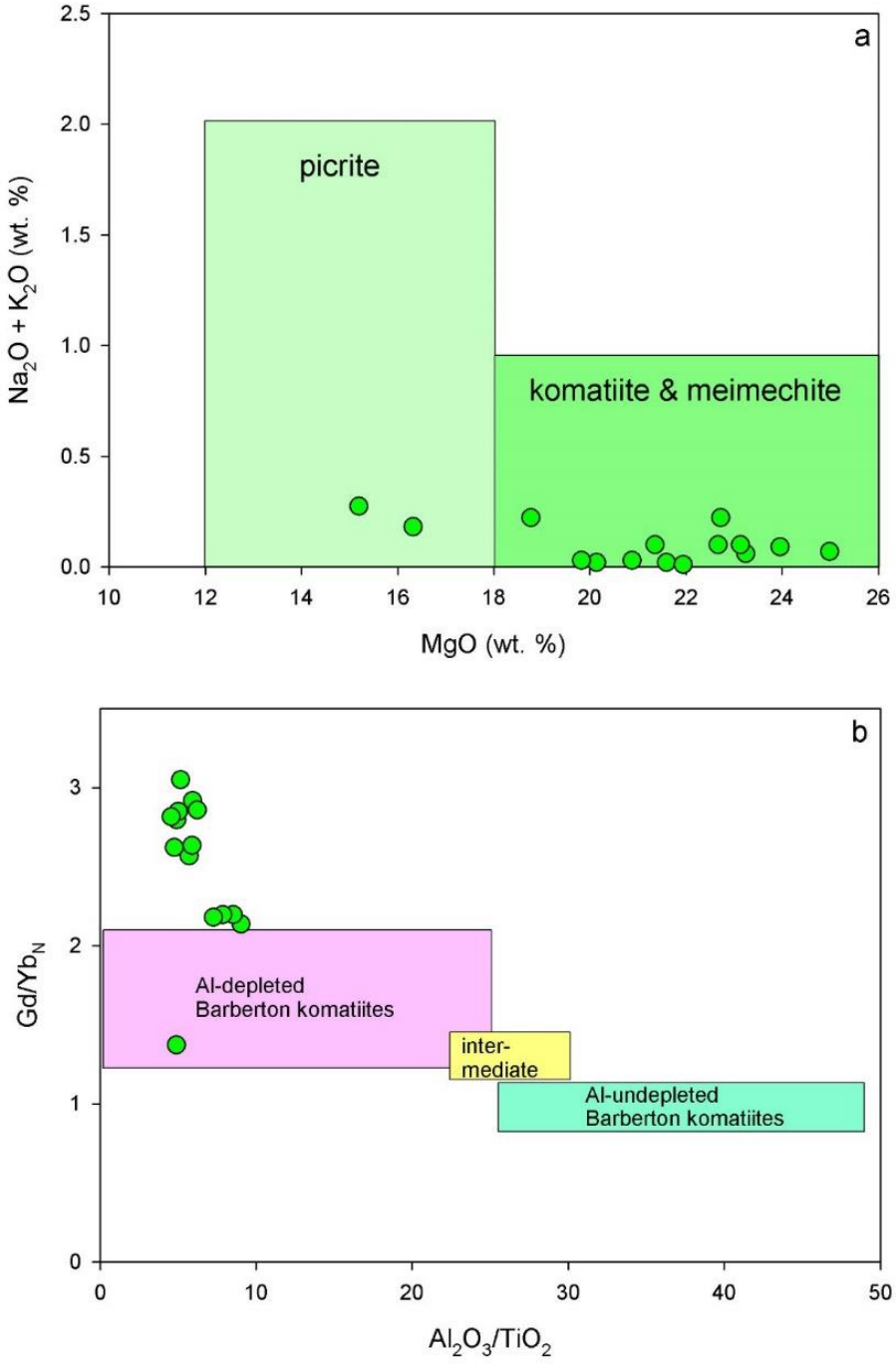

Figure 4. 6 IUGS classification of the Westonaria Formation after Le Bas (2000) showing the samples selected in our study are generally komatiite in composition. b) Westonaria komatiites showing Al-depletion and elevated MREE/HREE compared to Barberton Al-depleted komatiites.

We used drillcore E5 to assess stratigraphic variations in chemistry in the Westonaria lavas (Fig. A1.6). The TIMA element maps clearly show the phenocrystic cargo in these lavas from E5 (Fig. A1.7). There is a good correlation between the chemistry of the samples and the

abundance of olivine pseudomorph phenocrysts they contain. For example, the highest MgO contents (25 wt %) correspond to the olivine microspinifex zone (~7 m height from the drillcore base: Fig. A1.6). TIMA images show that Mg is concentrated in the matrix surrounding the spinifex needles (identified as secondary actinolite) and is highly concentrated in the pseudomorphed olivine in the cumulate cumulate. Regions of high Cr- and Ca-content occur in the matrix of spinifex needles and make up <5 % of the olivine cumulate and spinifex zones. The pyroxene cumulate zone has some of the highest Cr and Ni contents (Fig. A1.6). The lowest MgO contents (20 wt. %) correspond to the fine-grained aphyric zone (~31 m: Fig. A1.6). MgO increases to ~25 wt % at the pseudomorphed olivine cumulate zone (~38 m). Both the microspinifex and cumulate zones have the highest Ni concentrations (1246 ppm and 1280 ppm respectively). An entire composite komatiite flow can be identified and the variation in MgO can be used to delimit its extent (Fig. A1.6). SiO_2 and CaO behave similarly to MgO (Fig. A1.6). High CaO contents are observed in heavily chloritized samples and in samples that contain silicified olivine pseudomorphs that have calcite-filled fractures. Elemental mapping shows that the high Ca content observed in the olivine cumulate zone is mainly hosted in the matrix and the crosscutting veins (Fig. A1.7). In contrast, the high Ca contents (4.5 wt.%) in the pyroxene cumulate zone (at 2 m) are hosted in clinopyroxene. The clinopyroxene is of diopside composition (Table A3.2 and Fig. 4.7).

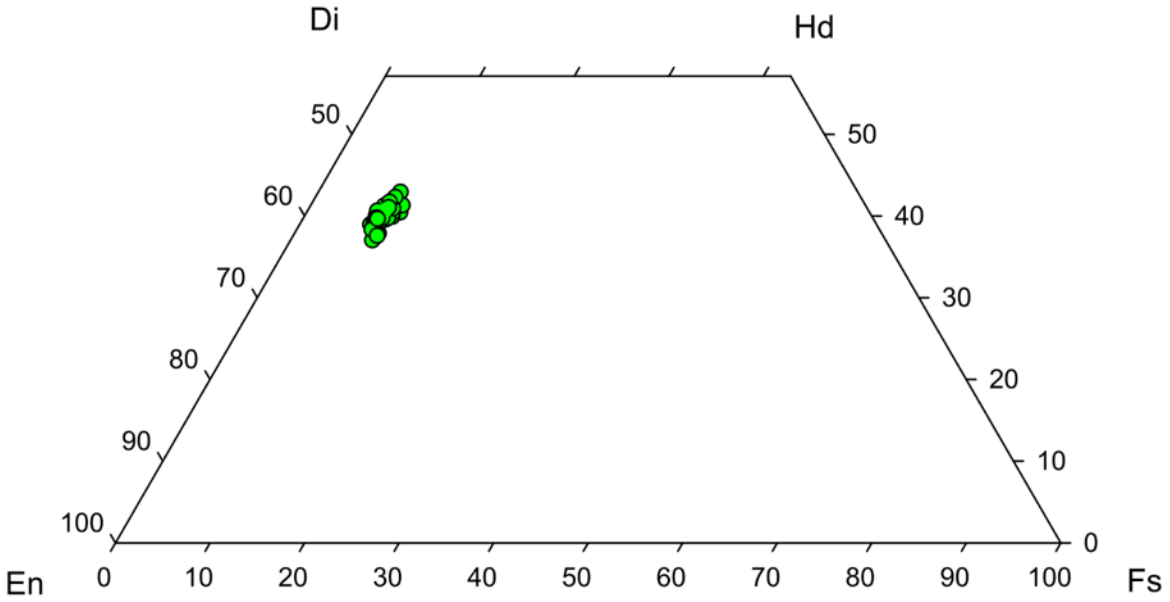

Figure 4. 7 Classification of clinopyroxene grains in the Westonaria komatiites showing that they are of diopside composition.

The Westonaria lavas show enrichment in light rare earth elements (REE) (La/Yb_N = 3.13-9.67: Fig. 4.8a). L/MREE (average La/Sm_N = 2.26, n = 12) is less lower than M/HREE (average Gd/Yb_N = 2.64, n = 12), excluding samples R503 and R509 (Fig. 4.8a). Sample R503 has a positive L/MREE (La/Sm_N) slope of 0.77 and a low M/HREE (Gd/Yb_N) slope of 2.18. Sample R509 displays a sinusoidal pattern (Fig. 4.8a). The L/MREE-enrichment of the Westonaria lavas can be subdivided into two groups: (1) Lavas with low La/Sm_N (average = 1.61, n = 5); and (2) lavas with high La/Sm_N (average = 2.72, n = 7). Sample R359, which has the lowest MgO (16 wt%) and Ni (484 ppm) contents, also has the flattest REE slope. The Westonaria lavas have almost parallel M/HREE slopes with a small amount of enrichment relative to primitive mantle for the relatively immobile elements (Fig. 4.8). Some of the lavas are depleted in Rb-Ba-Ta relative to primitive mantle and show negative Zr-Hf-Nb-Ta-Ti-Th-Sr-Rb-Ba anomalies (Fig. 4.8b). Sample R359 is the only sample that shows depletion in Ta relative to the primitive mantle. R502 has a positive Eu anomaly (Eu/Eu^*_N) of 1.27 and sample R507 has a negative Eu anomaly of 0.85.

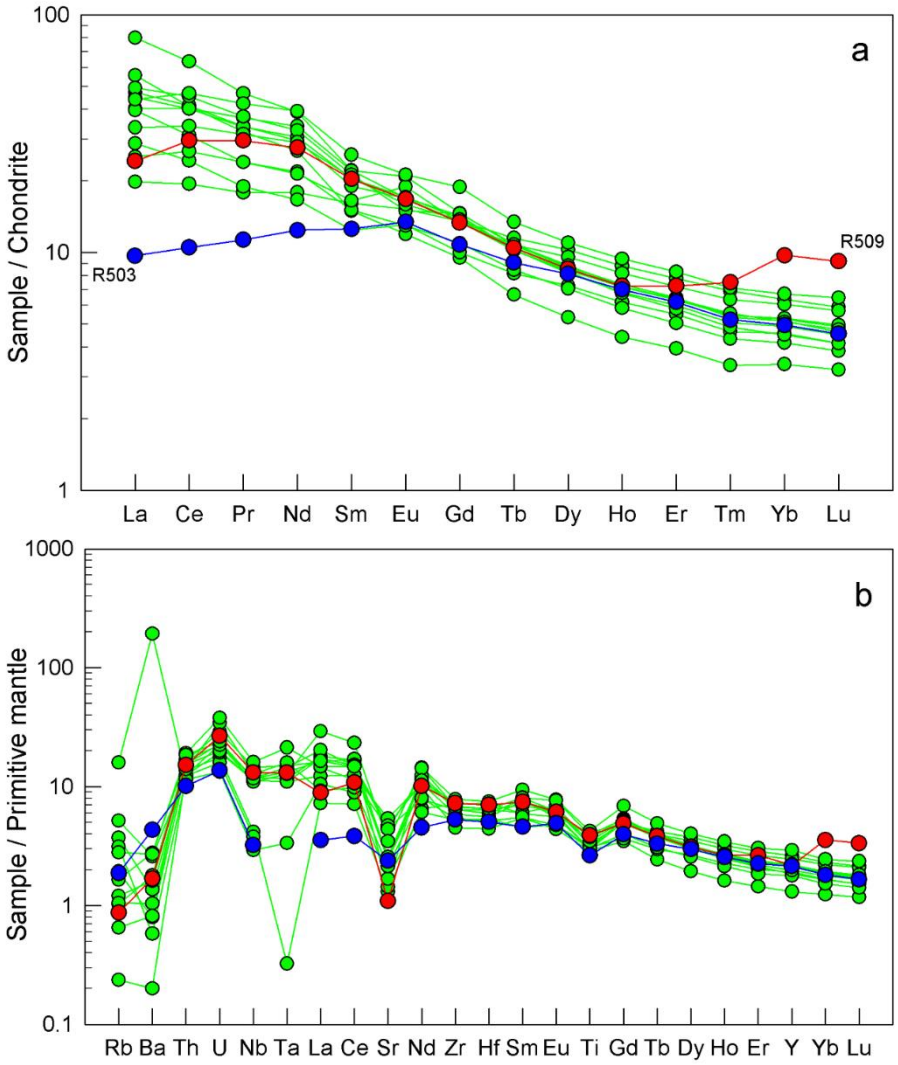

Figure 4. 8 a) A chondrite normalised REE diagram of the Westonaria samples analysed in this study showing L/HREE enrichment as well as samples R503 and R509 displaying unusual patterns b) Multi-lithophile diagram for the Westonaria komatiitic lavas normalized to the primitive mantle. Normalizing values are from McDonough and Sun (1995).

4.4.3 Isotope chemistry

Our new high-precision radiogenic isotope data are the first combined Sr-Nd-Hf isotope data for the Westonaria lavas (Table 4.1). Fifteen neodymium isotopic analyses were reported previously for various lavas in the Klipriviersberg Group (Marsh et al., 1992).

Table 4. 1 Sr-Nd-Hf isotopic compositions of the Westonaria komatiites.

	Hf (ppm)	Lu (ppm)	$^{176}Lu/^{177}Hf$	$^{176}Hf/^{177}Hf$	1SE	$^{176}Hf/^{177}Hf$ (T)	$\varepsilon_{Hf\,(T)}$	1 SE
R048	1.126	0.080	0.010	0.28149	4.28E-06	0.28095	-1.33	0.15
R141	1.879	0.126	0.009	0.28109	1.62E-05	0.28058	-14.66	0.58
R359	2.271	0.153	0.010	0.28160	7.76E-06	0.28109	3.60	0.28
R360	1.387	0.108	0.011	0.28159	4.29E-06	0.28100	0.24	0.15
R362	1.468	0.095	0.009	0.28157	1.49E-05	0.28108	3.11	0.53
R434	1.674	0.114	0.010	0.28149	3.92E-06	0.28097	-0.69	0.14
R432	1.875	0.145	0.011	0.28154	4.70E-06	0.28096	-1.16	0.17
R502	2.047	0.157	0.011	0.28163	3.43E-06	0.28105	2.05	0.12
R503	1.773	0.127	0.010	0.28157	3.33E-06	0.28102	1.13	0.12
R505	1.976	0.116	0.008	0.28147	6.25E-06	0.28103	1.40	0.22
R506	1.870	0.127	0.010	0.28146	4.46E-06	0.28094	-1.79	0.16
R507	2.090	0.130	0.009	0.28143	2.96E-06	0.28096	-1.02	0.11
R508	2.296	0.173	0.011	0.28152	2.69E-06	0.28095	-1.62	0.10
R509	2.030	0.124	0.009	0.28148	6.52E-06	0.28102	0.96	0.23
R511	1.780	0.109	0.009	0.28143	2.93E-06	0.28097	-0.89	0.10
	Nd (ppm)	**Sm (ppm)**	$^{147}Sm/^{144}Nd$	$^{143}Nd/^{144}Nd$	**1SE**	$^{143}Nd/^{144}Nd$ (T)	**e Nd (T)**	**1 SE**
R048	9.503	1.817	0.116	0.51118	2.95E-06	0.50905	0.64	0.06
R141	14.162	2.900	0.124	0.51137	4.75E-06	0.50909	1.41	0.09
R359	8.585	2.556	0.180	0.51226	2.51E-06	0.50895	-1.44	0.05
R360	7.376	1.825	0.150	0.51184	2.84E-06	0.50909	1.36	0.06
R362	8.389	1.937	0.140	0.51150	1.35E-05	0.50893	-1.72	0.27
R434	16.137	3.320	0.124	0.51129	2.65E-06	0.50901	-0.25	0.05
R432	27.806	5.328	0.116	0.51120	3.13E-06	0.50907	0.89	0.06
R502	9.540	2.454	0.156	0.51193	2.50E-06	0.50907	0.92	0.05
R503	5.991	1.935	0.195	0.51271	1.17E-05	0.50912	1.89	0.23
R505	30.951	5.775	0.113	0.51120	1.60E-06	0.50913	2.16	0.03
R506	15.511	3.182	0.124	0.51131	2.23E-06	0.50903	0.24	0.04
R507	15.308	3.180	0.126	0.51136	2.66E-06	0.50905	0.62	0.05
R508	19.102	3.952	0.125	0.51138	3.36E-06	0.50908	1.24	0.07
R509	12.660	3.042	0.145	0.51165	2.29E-06	0.50897	-0.92	0.04
R511	13.150	3.072	0.141	0.51158	2.05E-06	0.50898	-0.79	0.04
	Sr (ppm)	**Rb (ppm)**	$^{87}Rb/^{86}Sr$	$^{87}Sr/^{86}Sr$	**1SE**	$^{87}Sr/^{86}Sr$ (T)	**1 SE**	
R048	48.618	0.089	0.005	0.71561	5.27E-06	0.71539	5.27E-06	
R141	100.055	0.590	0.017	0.71350	6.76E-06	0.71281	6.76E-06	
R359	27.295	2.274	0.241	0.72069	6.20E-06	0.71095	6.2E-06	
R360	34.818	1.716	0.143	0.71691	5.41E-06	0.71115	5.41E-06	
R362	42.151	1.056	0.072	0.70952		0.70659	1.3E-05	
R434	88.209	0.351	0.012	0.70759	3.78E-06	0.70713	3.78E-06	
R432	140.439	12.987	0.268	0.71085	3.53E-06	0.70005	3.53E-06	
R502	93.530	9.782	0.303	0.72312	3.24E-06	0.71089	3.24E-06	
R503	49.999	1.098	0.064	0.71892	4.12E-06	0.71636	4.12E-06	
R505	76.339	0.972	0.037	0.71043	1.23E-05	0.70894	1.23E-05	
R506	51.203	1.569	0.089	0.71791	4.75E-06	0.71433	4.75E-06	
R507	54.617	0.769	0.041	0.71770	3.46E-06	0.71605	3.46E-06	
R508	30.203	0.569	0.055	0.71738	7.62E-06	0.71518	7.62E-06	
R509	22.098	0.451	0.059	0.71688	5.11E-06	0.71449	5.11E-06	
R511	130.873	3.640	0.081	0.71714	2.74E-06	0.71389	2.74E-06	

Rb, Sr, Sm, Nd, Lu and Hf concentrations were determined by isotope dilution MC-ICP-MS. $^{143}Nd/^{144}Nd$ was normalized for mass fractionation to $^{146}Nd/^{144}Nd$= 0.7219 and $^{176}Hf/^{177}Hf$ was normalized to $^{179}Hf/^{177}Hf$= 0.7325. Initial $^{87}Sr/^{86}Sr$, ε_{Nd} and ε_{Hf} values were calculated at T= 2.78 Ga using $\lambda^{87}Rb$ =1.42 x 10^{-11} y^{-1} (Steiger & Jager, 1977), $\lambda^{147}Sm$= 6.54 × 10^{-12} y^{-1} (Begemann et al., 2001) and $\lambda^{176}Lu$= 1.867 × 10^{-11} y^{-1} (Soderlund et al., 2004). CHUR values used: $^{143}Nd/^{144}Nd$= 0.512638, $^{147}Sm/^{144}Nd$= 0.1967 (Jacobsen & Wasserburg, 1980; Wasserburg et al., 1981), $^{176}Hf/^{177}Hf$= 0.282785 and $^{176}Hf/^{177}Hf$= 0.0336 from Bouvier et al. (2008).

The initial ε_{Nd} values (calculated at 2.78 Ga) have a narrow range (ε_{Nd} = -1.72 to +2.16: Fig. 4.9) corresponding to $^{143}Nd/^{144}Nd$ of 0.50893 to 0.50913. Samples with initial ε_{Nd} values <0 have relatively low L/MREE (average La/Sm_N = 1.61, n = 5), with the exception of samples

R508 and R509. Sample R508 has a positive initial ε_{Nd} value of+1.24 ($^{143}Nd/^{144}Nd$ = 0.50908) and R509 has a negative initial ε_{Nd} value of -0.92 ($^{143}Nd/^{144}Nd$ = 0.50897) and it displays a sinusoidal REE pattern (Fig. 4.9a). Samples with positive initial ε_{Nd} values have high L/MREE (average La/Sm_N = 2.27, n = 7). Initial $^{87}Sr/^{86}Sr$ ratios (calculated at 2.78 Ga) are highly variable, and range from 0.70659 to 0.71636, with exception of sample R432, which has an initial ratio of 0.70005. The samples form a sub-horizontal array at relatively constant ε_{Nd} values of ~0 (Fig. 4.9). Initial ε_{Hf} values (calculated at 2.78 Ga) range from -1.798 to 3.60 corresponding to $^{176}Hf/^{177}Hf$ of 0.28094 to 0.28109 (Fig. 4.9b). Oxygen isotope compositions ($\delta^{18}O_{cpx}$) of the clinopyroxene grains range from +4.13 ‰ to +5.68 ‰ with an average of +5.28 ± 0.25 ‰ (n = 49 spots: Table 4.2, Fig. 4.10). Variation plots of $\delta^{18}O_{cpx}$ against major element are shown in Figure A1.8. There is no variation in $\delta^{18}O_{cpx}$ with varying major element concentrations.

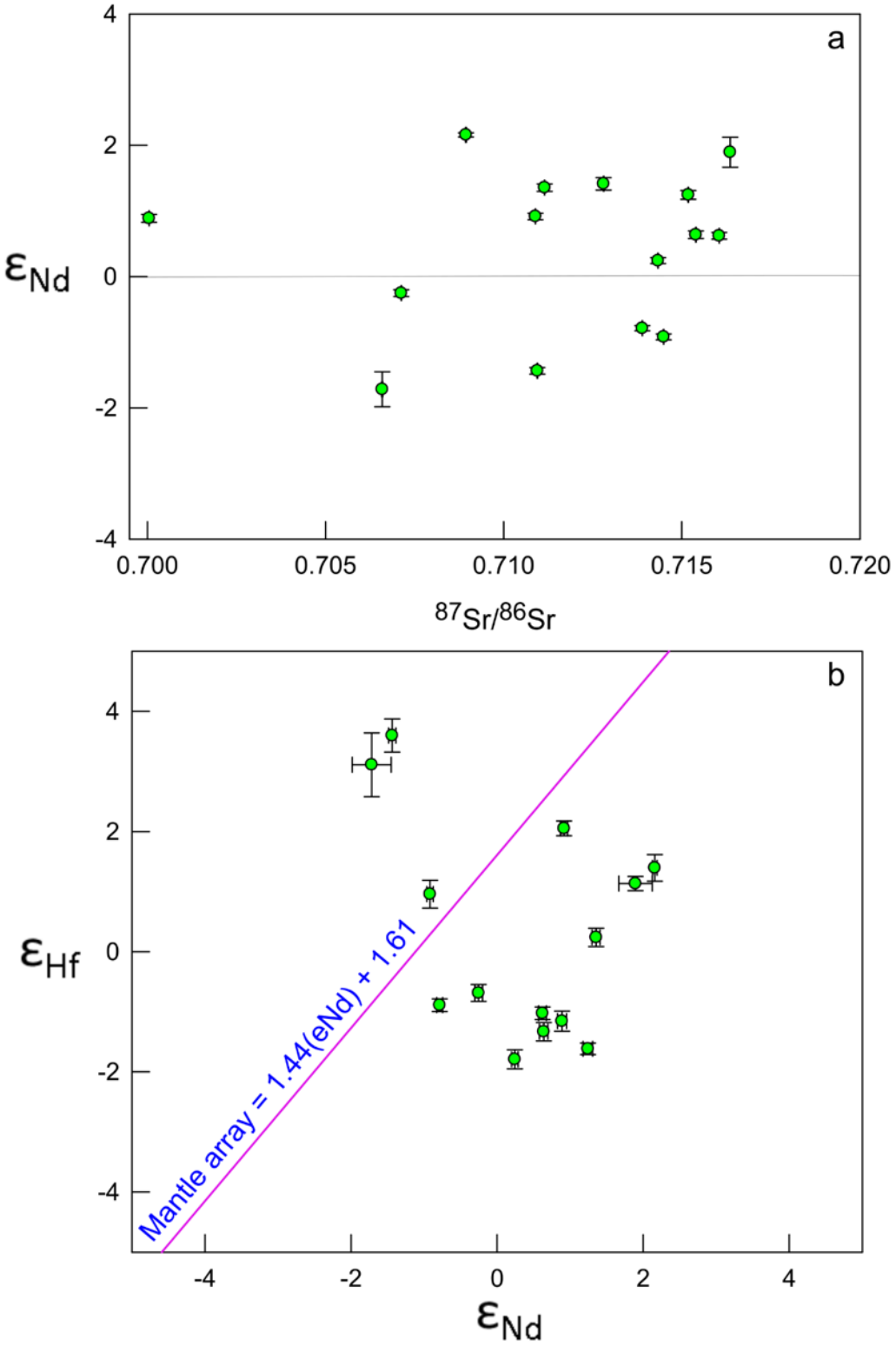

Figure 4.9 2.78 Ga Sr-Nd-Hf isotopic compositions of the Westonaria Formation. a) ε_{Nd} versus $^{87}Sr/^{86}Sr$ and b) εNd versus εHf. The Hf-Nd mantle array follows the relationship ε_{Hf} =1.44ENd +1.61 (Vervoort et al., 1999).

Table 4. 2 Oxygen isotope compositions of clinopyroxene in the Westonaria komatiites

Sample	Spot #	$^{18}O/^{16}O$ measured	(1SE, ‰)	$^{18}O/^{16}O$	$\delta^{18}O$ (V-SMOW) ‰	Uncertainty (1SE, ‰)
R510B_3	B1b@1	0.0020218	0.0065339	0.0020158	5.29	0.007
	B1b@2	0.0020217	0.0089256	0.0020156	5.20	0.009
	B1b@3	0.0020216	0.0077122	0.0020156	5.19	0.008
	B1b@4	0.0020221	0.0075032	0.0020161	5.42	0.008
	B1b@5	0.0020210	0.0087964	0.0020150	4.88	0.009
	B1b@6	0.0020226	0.0071582	0.0020165	5.65	0.007
	B1b@7	0.0020215	0.0081660	0.0020154	5.10	0.008
	B1b@8	0.0020216	0.0073078	0.0020156	5.19	0.007
	B1c@1	0.0020195	0.0092304	0.0020135	4.13	0.009
	B1c@3	0.0020209	0.0083593	0.0020149	4.82	0.008
R511B_1	B2a@1	0.0020210	0.0053467	0.0020156	5.18	0.005
	B2a@2	0.0020208	0.0061196	0.0020154	5.10	0.006
	B2a@3	0.0020208	0.0083387	0.0020154	5.07	0.008
	B2a@4	0.0020212	0.0089243	0.0020158	5.30	0.009
	B2a@5	0.0020212	0.0068660	0.0020158	5.30	0.007
	B2a@6	0.0020214	0.0061730	0.0020160	5.37	0.006
	B2a@7	0.0020211	0.0070619	0.0020157	5.21	0.007
	B2a@8	0.0020217	0.0083907	0.0020163	5.55	0.008
R511B_2	B2b@1	0.0020211	0.0100910	0.0020157	5.23	0.010
	B2b@2	0.0020208	0.0079835	0.0020154	5.07	0.008
	B2b@3	0.0020217	0.0098151	0.0020163	5.54	0.010
	B2b@4	0.0020211	0.0093177	0.0020157	5.26	0.009
	B2b@5	0.0020214	0.0087788	0.0020160	5.40	0.009
	B2b@6	0.0020213	0.0057974	0.0020159	5.35	0.006
	B2b@7	0.0020218	0.0076234	0.0020164	5.61	0.008
	B2b@8	0.0020213	0.0098868	0.0020159	5.33	0.010
R511C_1	Ca@1	0.0020208	0.0069318	0.0020154	5.08	0.007
	Ca@2	0.0020209	0.0070279	0.0020155	5.13	0.007
	Ca@3	0.0020213	0.0093368	0.0020159	5.35	0.009
	Ca@4	0.0020212	0.0087788	0.0020158	5.28	0.009
R511C_4B	Cc1@1	0.0020208	0.0068197	0.0020154	5.11	0.007
	Cc1@2	0.0020216	0.0094721	0.0020162	5.47	0.009
	Cc1@3	0.0020215	0.0090465	0.0020161	5.43	0.009
	Cc1@4	0.0020210	0.0091133	0.0020156	5.16	0.009
	Cc1@5	0.0020216	0.0085641	0.0020162	5.48	0.009
	Cc1@6	0.0020214	0.0085796	0.0020160	5.40	0.009
	Cc1@7	0.0020213	0.0081322	0.0020159	5.36	0.008
	Cc1@8	0.0020211	0.0069666	0.0020157	5.22	0.007
R511C_4A	Cc2@1	0.0020216	0.0096163	0.0020162	5.46	0.010
	Cc2@2	0.0020215	0.0085587	0.0020161	5.41	0.009
	Cc2@3	0.0020213	0.0076319	0.0020159	5.35	0.008
R511C_2	Cb@1	0.0020217	0.0071798	0.0020163	5.55	0.007
	Cb@2	0.0020214	0.0111167	0.0020160	5.40	0.011
R511C_3B	Cd@1	0.0020220	0.0071515	0.0020166	5.68	0.007
	Cd@2	0.0020216	0.0060553	0.0020162	5.49	0.006
	Cd@3	0.0020214	0.0082123	0.0020159	5.36	0.008
	Cd@4	0.0020214	0.0077472	0.0020160	5.37	0.008
	Cd@5	0.0020211	0.0111341	0.0020156	5.21	0.011
R511C_5B	Cf@1	0.0020207	0.0073891	0.0020153	5.05	0.007

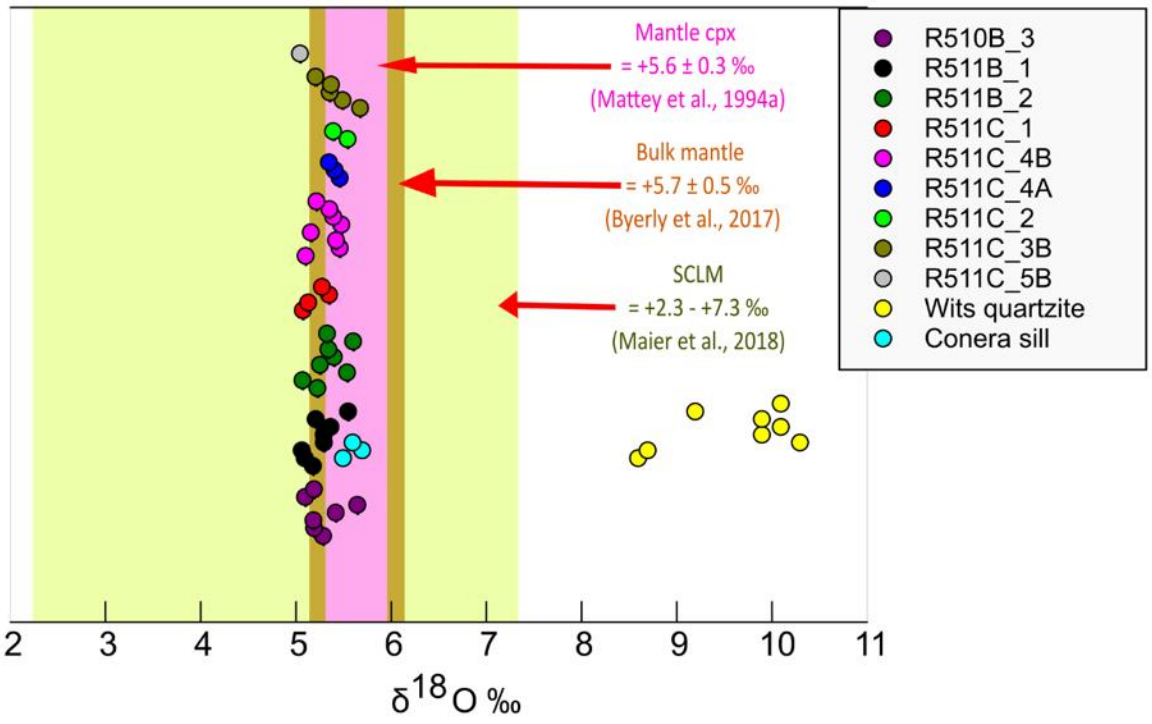

Figure 4.10 Oxygen isotope compositions of clinopyroxene grains in the Westonaria Formation komatiites. The composition ranges of mantle clinopyroxene, bulk mantle and the sub-continental lithospheric mantle (SCLM) are included. The Westonaria clinopyroxene grains have isotope compositions similar to the mantle clinopyroxene. They have similar composition to the Conera Sill linked to the Klipriviersberg Group that intrudes the Witwatersrand Supergroup. The data for the mantle clinopyroxene, bulk mantle, SCLM, Conera sill and the Wits quartzite are from Mattey et al. (1994), Byerly et al. (2017), Maier et al. (2018) and Harris and Watkins (1990), respectively.

4.5 Discussion

4.5.1 Evaluation of the effects of metamorphism and alteration

Given the age of the Westonaria lavas (2.78 Ga), it is important to evaluate the effects of metamorphism and alteration to constrain the extent of any disturbance of the Sr-Nd-Hf isotope systems before any interpretation can be made about their petrogenesis. The lavas are altered and the presence of actinolite, chlorite, serpentine, epidote and amphibole is consistent with extensive greenschist facies metamorphism (e.g. Fig. 4.4). The presence of calcite- and quartz-rich veins in the samples indicates that there was both carbonatisation and silicification (Fig. A1.2). The presence of chlorite, talc, titanite, epidote, amphibole, as well as serpentine, also indicates that there was a circulation of H_2O-rich fluids and replacement of Mg-rich minerals such as olivine. These observations are consistent with previous reports about the Westonaria lavas being altered to a talcose character (van der Westhuizen et al., 1991).

Elements may be mobilised by hydrothermal fluids. To assess this we plotted Sm, Nd, Lu, and Hf against Zr (Fig. A1.9). Zirconium was used as the reference of immobility in this study, although there are certain conditions of secondary processes where Zr could be mobile, Zr has a relatively low mobility compared to other elements, and it is hosted by minerals that are not easily altered. Sm and Hf show a moderately positive correlation, whereas Lu and Nd show a poor correlation with Zr (Fig. A1.9). This suggests that Lu and Nd may have been mobilised during a post-magmatic hydrothermal event, posing a challenge in inferring the magma source using the isotopes. Zirconium was used as the reference of immobility in this study, although there are certain conditions of secondary processes where Zr could be mobile, Zr has a relatively low mobility compared to other elements, and it is hosted by minerals that are not easily altered. The presence of epidote and titanite is consistent with REE-bearing fluids having played a role. Carbonic (CO_2-rich) fluids may form REE-complexes and preferentially mobilise L/HREE (Lahaye et al., 1995). There are carbonates in the overlying Transvaal Supergroup (age range of 2.5-2.3 Ga) that are a potential source for these REE-complexing fluids, in which the circulation of the CO_2-bearing fluids was triggered by later magmatic events such as the 2.4 Ga Ongeluk magmatism or the 2.22 Ga Hekpoort magmatism or the 2.06 Ga Bushveld magmatism. Duane et al. (2004) dated a craton-wide metamorphic

event at 2.0 Ga that might have resulted in the greenschist facies metamorphism and hydrothermal alteration. The Nd isotopic compositions have been shown to be affected by hydrothermal alteration and metamorphism, where elements that are thought to be immobile (e.g., REE and HFSE) are mobilized (Lahaye et al., 1995). The effect of this mobilization has been shown for the Abitibi komatiites (Alexo and Texmont) that have basaltic Nd isotopic compositions due to isotopic exchange with surrounding volcanic rocks during hydrothermal alteration (Lahaye et al., 1995).

Samples with positive ε_{Nd} values have steeper L/HREE patterns compared to samples with negative ε_{Nd} values. This difference can be explained by the presence of REE-carrier minerals such as epidote and titanite being more in the samples with steeper L/HREE patterns than the samples with less steep L/HREE patterns. This points to the possibility of an influence on the ε_{Nd} compositions by the varying proportions of REE-carrier minerals. Sample R505 has anomalously high Nd and Sm concentrations and it has the most juvenile ε_{Nd} value (+2.16: Table 4.1; Fig. 4.9) and it also contains a high proportion of the REE-bearing minerals (allanite and titanite), as well as abundant quartz, which is consistent with greater amounts of silicification. Sample R503 has relatively high L/MREE (Fig. 4.8a) and does not contain as many REE-bearing minerals as R505, although it also has a high ε_{Nd} value (+1.89: Table 4.1; Fig. 4.9). This suggests that the presence of REE-bearing minerals does not significantly affect the ε_{Nd} composition. The sinusoidal REE pattern of sample R509 is typical of an amphibole and/or titanite-bearing rock (Reichardt & Weinberg, 2012; Spandler et al., 2016). Alternatively, the disconnect between the isotopic compositions and REE patterns could be a result of the evident alteration and metamorphic event(s) that could have selectively modified the REEs and isotopic compositions, differently. As a result, the REEs and isotopes may record different events that the lavas have undergone.

Samples R505 and R503 have largely different initial $^{87}Sr/^{86}Sr$ compositions (Table 4.1), which suggests to us that hydrothermal alteration greatly disturbed the Rb-Sr isotope system. This disturbance is evident on the plot in Figure 4.9a as shown by the subhorizontal array of initial $^{87}Sr/^{86}Sr$ for relatively constant ε_{Nd}. The Rb-Sr isotope system was disturbed during hydrothermal alteration and greenschist metamorphism, with Sr affected during the formation of Ca-bearing minerals (e.g., calcite, epidote). The samples with low initial $^{87}Sr/^{86}Sr$ and low ε_{Nd} are from boreholes E3 and E4 that are located 23.2 and 9.4 kilometres from

borehole E5, respectively (Fig. 4.2 and Fig. 4.9a). Samples R432, R434, R359 and R362 plot to the left of the main cluster on a diagram of ε_{Nd}-$^{87}Sr/^{86}Sr$ and form a slight negative array that is parallel to the trend of the main cluster of data points. The samples with the most enriched ε_{Nd} values (R359 and R362) are from the same borehole (E3) and the samples with the most juvenile ε_{Nd} values (R432 and R434) are from borehole E4. These four samples display different textures compared with the samples from borehole E5 (Fig. A1.10). For instance, they contain coarse recrystallized amphiboles compared to borehole E5. The variation in ε_{Nd} and $^{87}Sr/^{86}Sr$ between the Westonaria samples is probably caused by varying degrees of alteration and metamorphism both vertically and laterally. Considering the possibility of the variable extent of alteration and its effect on the meaning of the isotopes, we used the samples from one locality (borehole E5) to plot the Sm-Nd and Lu-Hf isochrons to evaluate the degree of resetting of the isotope systematics. The Lu-Hf isochron yielded an age of 2972 ± 194 Ma (3166 – 2.778 Ma); the Sm-Nd isochron yielded an age of 2416.4 ± 16.4 Ma (2432 – 2399 Ma), Fig. 4.11. The Lu-Hf age is in agreement with the 2.78 Ga used in this study, whereas the Sm-Nd age is in agreement with the age of the Transvaal Supergroup, the proposed source of the carbonic fluids that affected the Westonaria komatiites.

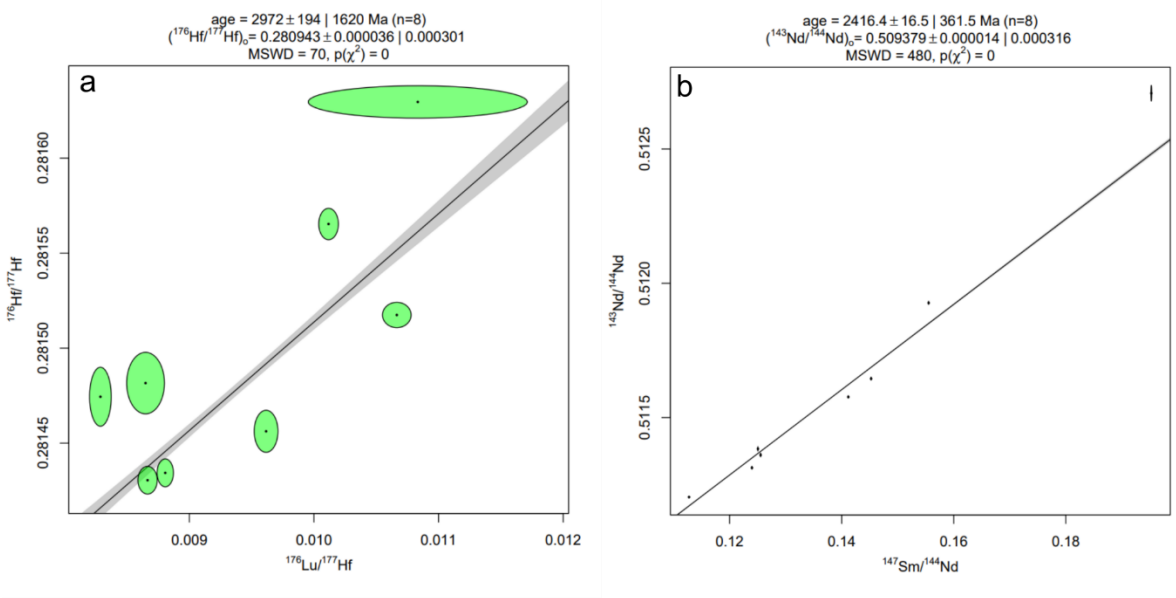

Figure 4. 11 Lu-Hf and Sm-Nd isochrons of the Westonaria Formation samples. The samples from boreholes E3 and E4 are excluded as the samples show extensive alteration and metamorphism.

In summary, this assessment of the effects of alteration on the Westonaria samples shows that the Rb-Sr isotopic system was greatly affected by metamorphism and alteration, and to some extent, the Sm-Nd isotope system was also affected. However, the Lu-Hf isotope system remains relatively robust and more faithfully preserves the primary isotopic signatures of the Westonaria lavas. Our oxygen isotope compositions of the clinopyroxene are mantle values despite alteration of the lavas. This indicates that the hydrothermal fluids that passed through crustal sequences with high $\delta^{18}O$ values did not exchange isotope composition with the clinopyroxene in the Westonaria komatiites. We will now use the whole rock and in-situ isotope data to assess the petrogenesis and mantle sources of the Westonaria komatiites.

4.5.2 Classifying the Westonaria komatiites

Komatiites (>18% MgO) are typically characterised by spinifex textures and thick komatiite flows that may be layered with cumulate, spinifex and chilled horizons (Arndt, 1986), as well as composite units (Viljoen & Viljoen, 1969; Arndt et al., 2008). Some komatiites also host important Archean-aged nickel sulphide deposits (Barnes & Fiorentini, 2012). The Westonaria lavas have MgO contents >18%, and they contain evidence of layered flows (e.g., cumulate, porphyritic, and spinifex horizons) that are characteristic of typical Archean komatiites.

There is evidence of olivine accumulation in the Westonaria lavas, however, so it is important to determine if the 'true' liquid compositions are komatiitic. We verified the komatiitic composition of the liquids by subtracting the cargo of olivine phenocrysts from the whole rock MgO-FeO composition (i.e., back-fractionation). The modal abundance of olivine was estimated for each thin section using point counting (e.g., sample R507 contains 5% psuedomorphed olivine). We estimated a forsterite (Fo) composition of Fo_{85} for olivine in equilibrium with the Westonaria magmas using least-squares regression analysis of the bulk rock MgO-FeO data for the Westonaria lavas (Fig. A1.11). Subtraction of 5% olivine with a composition of Fo_{85} from sample R507 results in a minor change in its MgO content (~1 wt%). This confirms the komatiitic composition of the Westonaria lavas.

The Westonaria lavas are enriched in TiO_2 (0.7 to 1.3 wt. %) compared to typical komatiites (e.g., Barberton komatiites contain <0.5 wt. %) and are comparable to meimechites with TiO_2 > 1 wt. % (Le Bas, 2000). We conclude that the high-Ti content of the Westonaria komatiites resulted in the abundant titanite observed in our samples. Komatiites have been further

divided into different chemical types, including: (1) Barberton-type komatiites that are Al-depleted (ADK: low Al_2O_3/TiO_2) with L/HREE enrichment; (2) Al-undepleted komatiites (AUK: intermediate Al_2O_3/TiO_2 of chondritic composition) with relatively flat REE patterns; (3) Munro-type komatiites that are Al-enriched (AEK: high Al_2O_3/TiO_2), and enriched in HREE, and (4) Karasjok-type komatiites that are enriched in Ti (Robin-Popieul et al., 2012; Blichert-Toft et al., 2015, Barnes & Arndt, 2019). The Westonaria komatiites are Al-depleted (Al_2O_3/TiO_2 = 4–9), have superchondritic Gd_N/Yb_N, and are enriched in L/HREE (Fig. 4.6b). They are comparable to siliceous high-magnesian basalts (SHMB) that are unusually enriched in incompatible elements and SiO_2 (Sensarma et al., 2002; Barnes & Arndt, 2019). Because of the relatively high SiO_2 contents and the L/HREE-enrichment of the Westonaria komatiites, it is therefore important to assess the evidence for crustal contamination. This is postulated to have played an important role in the origin of SHMB (e.g., Sensarma et al., 2002; Barnes & Arndt, 2019). However, as mentioned in the previous sections, there is also evidence of silicification shown by presence of quartz vein and silicified olivine phenocrysts that could explain the unusual enrichment of SiO_2 in the Westonaria komatiites.

4.5.3 Crustal contamination of the Westonaria magmas

We can use our isotope data to evaluate the role of crustal contamination in the petrogenesis of the Westonaria lavas. Crow & Condie (1988) suggested that there was minimal crustal contamination of the Ventersdorp magmas using element and element-ratio plots for elements that are enriched in the continental crust. Our in-situ oxygen isotope compositions of the fresh clinopyroxene present strong evidence for the minimal contamination of the Westonaria magmas by crustal components. We have shown that the oxygen isotope compositions do not carry alteration effects. The $\delta^{18}O_{cpx}$ values fall in a tight range within the mantle range and do not show any significant influence by crustal components that have high $\delta^{18}O$ values (Fig. 4.10). While the measured mantle-like oxygen isotopic compositions in our clinopyroxene samples indicate minimal contamination, there are also possible explanations for this that include (i) the possibility of the analysed clinopyroxene to have crystallised prior to crustal contamination, therefore not capturing the possible contamination of the magmas, and (ii) due to high abundance of oxygen in the mantle, it might be difficult for the isotopic signatures of the magma to be changed by crustal contamination.

The presence of zircon xenocrysts (2.9 Ga) that have been identified in two Klipriviersberg lavas lend further support to the proposed minimal crustal contamination by older crustal components, which might have occurred in the magmatic conduits during magma ascent or by incorporation of older sediments such as of the Witwatersrand Supergroup during the eruption (Armstrong et al., 1991). The enriched whole rock Hf isotope compositions attest to the proposed minimal contamination. Crustal rocks that could have been possible contaminants at the time of Westonaria magmatism include the 3.1 Ga Johannesburg Dome (JD) granites-granodiorites and tonalites. There are Sr-Nd isotope data reported for these rocks (Barton et al., 1999) that can be used as potential crustal contaminant endmembers in two-component bulk assimilation models (De Paolo & Wasserburg, 1979). However, the Sr isotope compositions of the Westonaria komatiites have been greatly affected by post-emplacement events (metamorphism and alteration), therefore, cannot be used to model the contamination extent. An assimilation and fractional crystallization (AFC) using rhyolite-MELTS+H2O-CO2 fluid (v1.2.0); Melts-batch-v1.2.0; of a depleted mantle magma and Johannesburg Dome granitoid as a contaminant using Nd isotopes was modelled using the Magma Chamber Simulator (MCS) (Fig. 4.12). The depleted mantle composition was sourced from Salters and Stracke (2004) and the Johannesburg Dome Nd isotopic composition was sourced from Barton et al. (1999). Major element compositions of the contaminant was sourced from Anhaeusser (1999) of a trondhjemitic gneiss sample (N15). The pressure was set at 1kbar. The Westonaria Formation do not fall on the liquid line of descent of the modelled AFC. This can either (i) indicate that the Westonaria magmas were not contaminated by the granitoids, or (ii) the Westonaria magmas might have interacted with different crustal components, or (iii) the parameter set for the model did not fit the evolution of the Westonaria magmas.

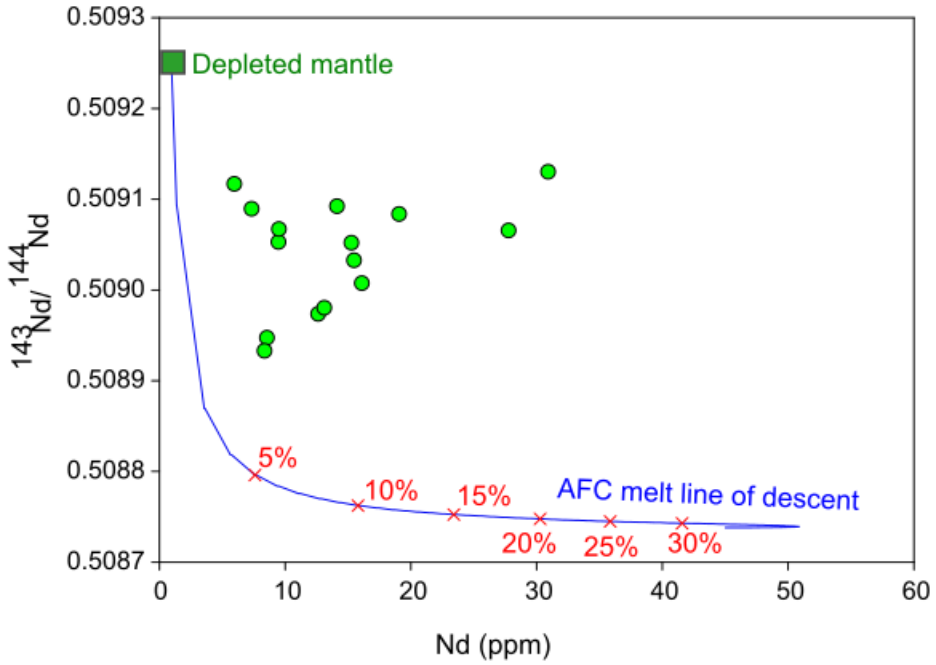

Figure 4. 12 Initial $^{143}Nd/^{144}Nd$ versus Nd concentration in the melt modelled using the Magma Chamber Simulator (MCS). The Westonaria samples do not indicate interaction of their depleted mantle-sourced magmas with Kaapvaal granitoids.

4.5.4 A heterogeneous sublithospheric mantle source

The mantle source(s) of komatiites is a matter of controversy. Mantle sources range from plume-asthenosphere models (Stiegler et al., 2012) to subduction zone settings (e.g., Grove et al., 1999; Parman et al., 2001). There is a similar controversy regarding the origin of voluminous basaltic magmas in large igneous provinces, with both sublithospheric mantle sources (Crow & Condie, 1988; Hatton, 1995; White, 1997; Campbell, 2007; Ashwal, 2021) and lithospheric mantle (SCLM) (Hawkesworth et al., 1984; 1990; Marsh et al., 1992; Jourdan et al., 2009; Humbert et al., 2019) sources proposed. It has been proposed that the lavas of the Klipriviersberg lavas and Allanridge lavas (i.e., the Pniel Group) were derived from the same source (a mantle wedge), and the lavas of the Platberg Group were derived from the enriched mantle lithosphere (Crow & Condie, 1988; Humbert et al., 2019). We critically evaluate these proposals below. We then use our trace element and Hf-O (~Nd) isotopes to provide important new constraints on the mantle sources of the Westonaria komatiites at the base of the Klipriviersberg Group.

An origin from the SCLM has been proposed for parts of the Klipriviersberg Group (Marsh et al., 1992; Humbert et al., 2019). Refertilisation of the SCLM beneath the Kaapvaal craton is required prior to 2.7 Ga to account for large-scale magma extraction without the destabilisation of the SCLM (Humbert et al., 2019). However, diamonds with ages of up to 3.5 Ga from the Kaapvaal SCLM provide evidence against large-scale heating of the SCLM, as these diamonds would have been destroyed (Ashwal, 2021). The enrichment of the Westonaria komatiites in incompatible elements may also be due to secondary processes such as alteration (carbonitisation), rather than inheritance from an enriched source as proposed in Humbert et al (2019). It might also be expected that the isotopic composition of the SCLM was modified to more enriched isotopic compositions and thus yielded the more enriched Westonaria lava compositions, compared to our depleted ε_{Nd} and ε_{Hf} compositions of up to +2.2 and +3.6, respectively. These isotopic compositions suggest a depleted mantle source that was not significantly modified by enriched components. Conversely, some have argued against a depleted mantle source for the lavas in the Klipriviersberg Group based on the expected ε_{Nd} values of a depleted mantle source at 2.7 Ga (Marsh et al., 1992; Humbert et al., 2019). For instance, the depleted mantle source of the komatiites would be expected to have ε_{Nd} of +4 and the derivative Klipriviersberg lavas would be expected to have ε_{Nd} of +2.2 at 2.7 Ga (Marsh et al., 1992; Humbert et al., 2019). However, the measured narrow range of oxygen isotope compositions and varying SCLM (subcontinental lithospheric mantle) composition do not necessarily exclude the possibility of the SCLM being the source of the magmas. The magmas may have been sourced from a zone of the SCLM with an overlapping composition as the deep mantle. However, we have analysed a sample from the Westonaria komatiites with an εNd value of +2.16. This clearly indicates the influence of a depleted mantle component in the mantle source, potentially originating from the deep mantle with depleted isotopic compositions. In addition, the narrow range of the oxygen isotope compositions of clinopyroxene observed in the lavas is- different from the reported variability of oxygen isotopes in the SCLM according to Maier et al. (2018). Putting into consideration the depleted isotopic compositions and the distinct narrow range of the oxygen isotope compositions, the possibility of a SCLM source is not supported by our data. Therefore, we favour a sublithospheric mantle source for the Westonaria komatiites. We compared our in-situ $\delta^{18}O_{cpx}$ data to the $\delta^{18}O_{WR}$ of the Conera Sill and the Wits quartzites reported in Harris and Watkins (1990). The Conera Sill intrudes the Witwatersrand Supergroup and has been

dated and linked to the Klipriviersberg Group. The Conera Sill and the Westonaria clinopyroxene have overlapping $\delta^{18}O$ values that fall within the mantle range, away from the crustal range. This also provides further evidence for the genetic link between the Conera Sill and the Klipriviersberg lavas.

There is some chemical evidence for the involvement of enriched lithospheric reservoirs in the petrogenesis of the Westonaria komatiites. The presence of negative Nb-Ta-Ti anomalies suggests an influence on the source by subduction-related material (Fig. 4.8b: Humbert et al., 2019). The Westonaria komatiites plot above the MORB-OIB array, towards the average Archean crust (Fig. A1.12). Together, Th/Yb-Nb/Yb, small negative Nb-Ta anomalies, and the Hf-O isotopic compositions indicate minor crustal contamination of the Westonaria magmas and the minor influence of subducted material on the magmas. Delta Nb ($\Delta Nb = 1.74 + \log Nb/Y - 1.92 \log Zr/Y$) can be used to quantify the abundance of Nb relative to Zr/Y (Fitton, 2007). Positive ΔNb values are associated with oceanic island basalts (OIB) and negative ΔNb values are associated with normal mid-ocean ridge basalts (MORB) that are derived from the depleted mantle (e.g., Luttinen, 2018). The presence of both positive and negative ΔNb in the Westonaria lavas, coupled with the ε_{Nd} data, indicates the presence of a heterogeneous sub-lithospheric mantle plume source that was composed of both enriched and depleted components. We cannot rule out that some of these enriched components were subducted material entrained in a mantle plume.

4.5.5 Nd-Hf isotopic decoupling in the Westonaria komatiites

Nd-Hf isotopes in the Westonaria komatiites are characterised by a slight negative slope, rather than a positive slope, as is expected for coupled Nd-Hf isotope evolution of the mantle (Fig. 4.9b). The decoupling of the Westonaria komatiites from the mantle array, along with aluminium depletion, superchondritic Gd/Yb_N, and, partly, the L/HREE-enrichment, can be explained by the presence of garnet in the mantle source. The decoupling of Nd-Hf isotopes can be caused by the retention of a phase that partitions Lu and Hf differently (e.g., garnet, Ca-perovskite and Mg-perovskite) in the source (Blichert-Toft & Puchtel, 2010; Boyet et al., 2021). We propose that the material bearing such a phase was entrained in the heterogeneous mantle source that was partially melted during the formation of the komatiitic magmas. However, with the realisation of the alteration effects on the Nd isotopes of our

whole-rock samples, the observed Nd-Hf decoupling can easily be explained by alteration and metamorphism.

4.6 Conclusions

The Westonaria komatiites at the base of the Neoarchean Ventersdorp Supergroup record the onset of magmatism in the Klipriviersberg large igneous province on the Kaapvaal Craton. The Westonaria komatiites (15-25 wt% MgO) are Al-depleted, have high SiO_2 (up to 54%) contents, and show enrichment in light/heavy rare earth elements, compared to typical Archean komatiites. Sr-Nd-Hf-O isotopes, in tandem with the major and trace element data, provide constraints on the composition of the mantle sources of the Westonaria komatiites. The Westonaria komatiites are highly altered, although they do preserve relict cumulate and spinifex textures, that are observed in komatiitic lavas elsewhere. Low-grade greenschist metamorphism has significantly altered the Rb-Sr isotopes. Sm-Nd isotopes were slightly affected, although Lu-Hf and O isotopes remain robust. Initial (at 2.78 Ga) Nd-Hf isotopic compositions (ε_{Nd} of -1.7 to +2.2 and ε_{Hf} of -1.8 to +3.6) indicate that the Westonaria komatiites were derived from a depleted mantle source. Crustal contamination can explain the high silica and light/heavy rare earth element-enrichment compositions of the Westonaria komatiites. The Al-depleted nature, and the Nd-Hf isotopic decoupling from the terrestrial mantle array, can be explained by melting in the presence of Mg- and/ or Ca-perovskite or garnet. We propose that the Westonaria komatiites are derived from a heterogeneous sublithospheric mantle source that was melted in response to the impingement of a mantle plume at the base of the Kaapvaal Craton.

Chapter 5: Radiogenic (Sr-Nd-Hf) isotope evidence for mantle sources in the magmatism of the Neoarchean Ventersdorp Large Igneous Provinces (South Arica) and implications for the Vaalbara supercraton

Khulekani B. Khumalo, Lewis D. Ashwal, Ben Hayes & Linda M. Iaccheri

The manuscript is to be submitted to the South African Journal of Geology for publication before the final submission of the Thesis in June 2023.

Contributions:

Khulekani Khumalo: Conceptualised the study; wrote the manuscript; conducted the Sr-Nd-Hf isotope dilution and mass spectrometry analyses; and conducted the petrographic analysis.

Lewis Ashwal: Conceptualised the study; Compiled literature data; and reviewed the manuscript drafts.

Ben Hayes: Conceptualised the study; reviewed and edited manuscript drafts.

Linda Iaccheri: Supervised the isotope dilution laboratory work; and reviewed manuscript drafts.

Please note that the detailed geological background and methodology sections are excluded from this manuscript chapter and are presented in Chapters 2 and 3.

5.1 Introduction

Large Igneous Provinces (LIPs) represent enormous volumes of intraplate magmatism emplaced or erupted in a short period of geological time (mostly < 10 million years). They are represented as either continental flood basalts (e.g., Karoo LIP, Deccan), mafic-ultramafic layered intrusions (e.g., Bushveld Complex), oceanic flood basalts (e.g., Ontong Java Plateau), sill complexes (e.g., Midland Valley) and dyke swarms (e.g., Mackenzie swarm) (see review by Ernst, 2014). LIP magmatism has been attributed to mantle plumes with the melting of either the asthenospheric mantle (Crow & Condie, 1988; Hatton, 1995; White, 1997, Eriksson et al., 2002, Campbell, 2005, 2007; Ashwal, 2021) or the subcontinental lithospheric mantle (SCLM) (Hawkesworth et al., 1984; Marsh et al., 1992; Jourdan et al., 2009; Humbert et al., 2019), with or without crustal contamination. The lavas in the Ventersdorp Supergroup are some of the oldest continental flood basalt province(s) in the world and are located on the Kaapvaal Craton of southern Africa. The Ventersdorp lavas provide an excellent natural laboratory to study the mantle sources and magmatic evolution of an Archean continental flood basalt and will provide important insights into the early Earth geodynamics (White, 1997; Marsh et al., 1992; Gumsley et al., 2020).

The lavas of the Ventersdorp Supergroup have previously been regarded as a single magmatic province. However, recent geochronological work has revealed that there are two disparate magmatic provinces in the Ventersdorp Supergroup that are at least 70 Myr apart: the 2.79-2.78 Ga Klipriviersberg LIP and the 2.71-2.68 Ga Allanridge LIP (Gumsley et al., 2020). There have been multiple studies on the Ventersdorp lavas to better understand its sources, its spatial distribution, and its duration (Fig. 5.1: Winter, 1976; Burke et al., 1985; Crow & Condie, 1988; Myers et al., 1990; Armstrong et al., 1991; van der Westhuizen et al., 1991, 2006; Hatton, 1995, White, 1997; de Kock et al., 2009, 2012; Cornell et al., 2017; Gumsley et al., 2020; Meintjes & van der Westhuizen, 2018; Gumsley et al., 2020). However, relatively little is still known about the magma source(s) of the Ventersdorp lavas because of the lack of data, especially isotopic data that have proven to be useful in identification of magma sources and contamination.

The Ventersdorp volcano-sedimentary succession on the Kaapvaal Craton has been proposed to have extended to the Pilbara Craton, Australia. The 2.77 Ga to 2.71 Ga Fortescue Group on

the Pilbara Craton has been correlated to the Ventersdorp Supergroup on the Kaapvaal Craton (Trendall, 1968; Button, 1979; Nelson et al., 1992; Wingate, 1999; Blake et al., 2004; de Kock et al., 2012). Geochemical and lithostratigraphy similarities between the two Neoarchean sequences are used as evidence to argue for a supercraton named Vaalbara, implying that the Kaapvaal and Pilbara Cratons were once adjoined.

In this study, we present major, trace and high-precision Sr-Nd-Hf isotope data for all the lavas of the Ventersdorp Supergroup. We use these data to constrain their magma sources and petrogenesis, and we discuss the possible effects of crustal contamination during their transport through the crust. This study adds to the previous study on the petrogenesis of the Westonaria Formation komatiites near the base of the Ventersdorp Supergroup in the Klipriviersberg Group, with a focus on the entire sequence of the Ventersdorp Supergroup including the Klipriviersberg Group, the Platberg Group and Pniel Group to investigate the proposed magmatic events. We then compare the isotopic data between the different lavas of the Ventersdorp Supergroup. Ultimately, the findings have implications for the viability of Vaalbara.

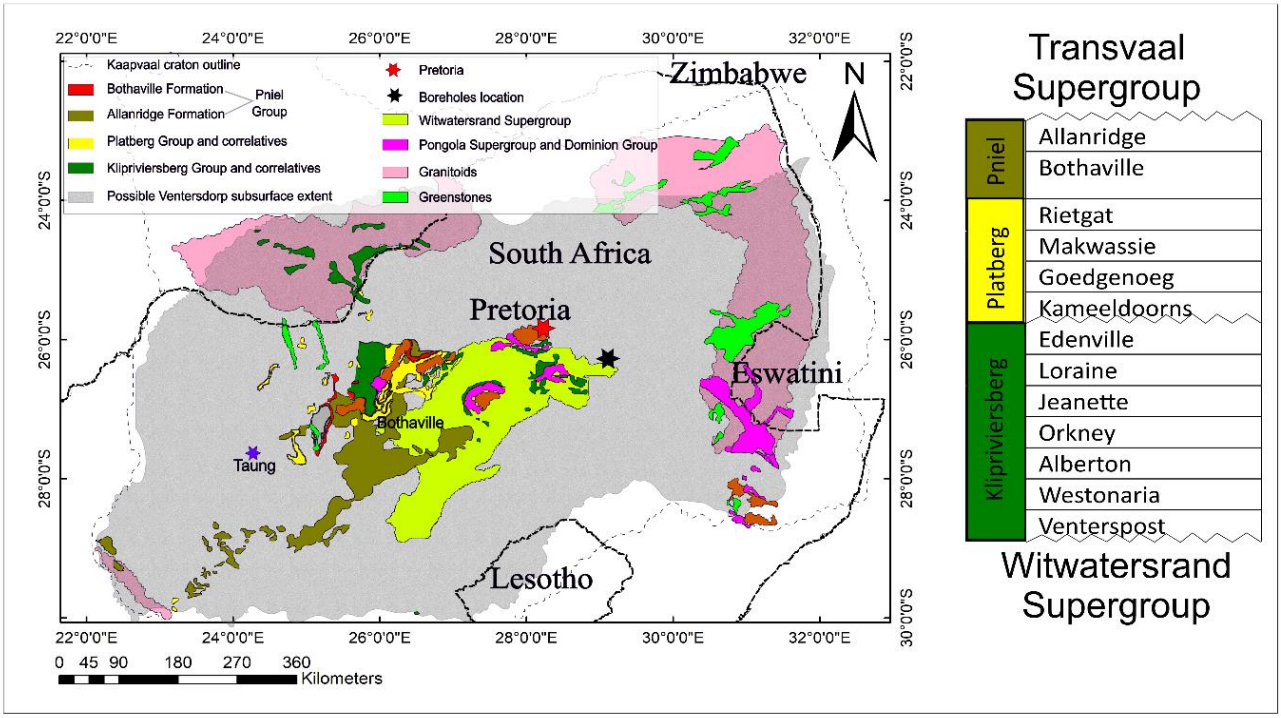

Figure 5. 1 Simplified geological map showing the surface distribution of the formations of the Ventersdorp Supergroup and their equivalents on the Kaapvaal craton (modified after Gumsley et al., 2017). It also shows the possible areal extent of the lavas. The stratigraphy of the volcano-sedimentary sequence is shown on the right. The location of the sample boreholes is shown as the black star.

5.2 Results

5.2.1 Classifying the Ventersdorp Supergroup lavas

We classify the lavas using the plot of Zr/Ti (fractionation index) versus Nb/Y (alkalinity index) which uses immobile elements that are unlikely to have been affected by secondary processes - a more preferred classification scheme than the TAS diagram of Cox et al. (1979) (Fig. 5.2a). The major element compositions of our selected samples are shown in Table A4.1. Two distinct trends are observed in the plot: (i) the relatively uniform Zr/Ti contents of the Klipriviersberg lavas form a horizontal array in the basaltic fields (basalt and basaltic andesite), and (ii) the relatively uniform Nb/Y contents of the Platberg volcanic rocks form a vertical array in the andesite and rhyolite fields. The komatiitic Westonaria lavas plot in the field of basalt and some plot in the field of alkali basalt at low Zr/Ti. The overlying five formations of the Klipriviersberg Group cluster slightly above the Westonaria lavas and are also classified as basalts and basaltic andesites (Fig. 5.2a). The Platberg volcanic rocks show a tight cluster in Nb/Y (i.e., alkalinity) and a wider range for Zr/Ti. The lavas classify as basalts, mostly as basaltic andesites, and some as dacites and rhyolites. The Goedgenoeg and Rietgat lavas cluster at lower Zr/Ti than the Makwassie lavas. The Allanridge lavas plot slightly above the Klipriviersberg lavas in the basalt and basaltic andesite fields, with a smaller range in Nb/Y (excluding the outliers) compared to the Klipriviersberg lavas. The cation classification plot after Jensen (1976) shows the Westonaria lavas to be komatiitic basalts, together with some of the Loraine-Edenville lavas. The rest of the Klipriviersberg lavas, Platberg lavas (Goedgenoeg and Rietgat Formations), and the Allanridge lavas of the Pniel Group classify as high-Fe tholeiitic basalts (Fig, 5.2b).

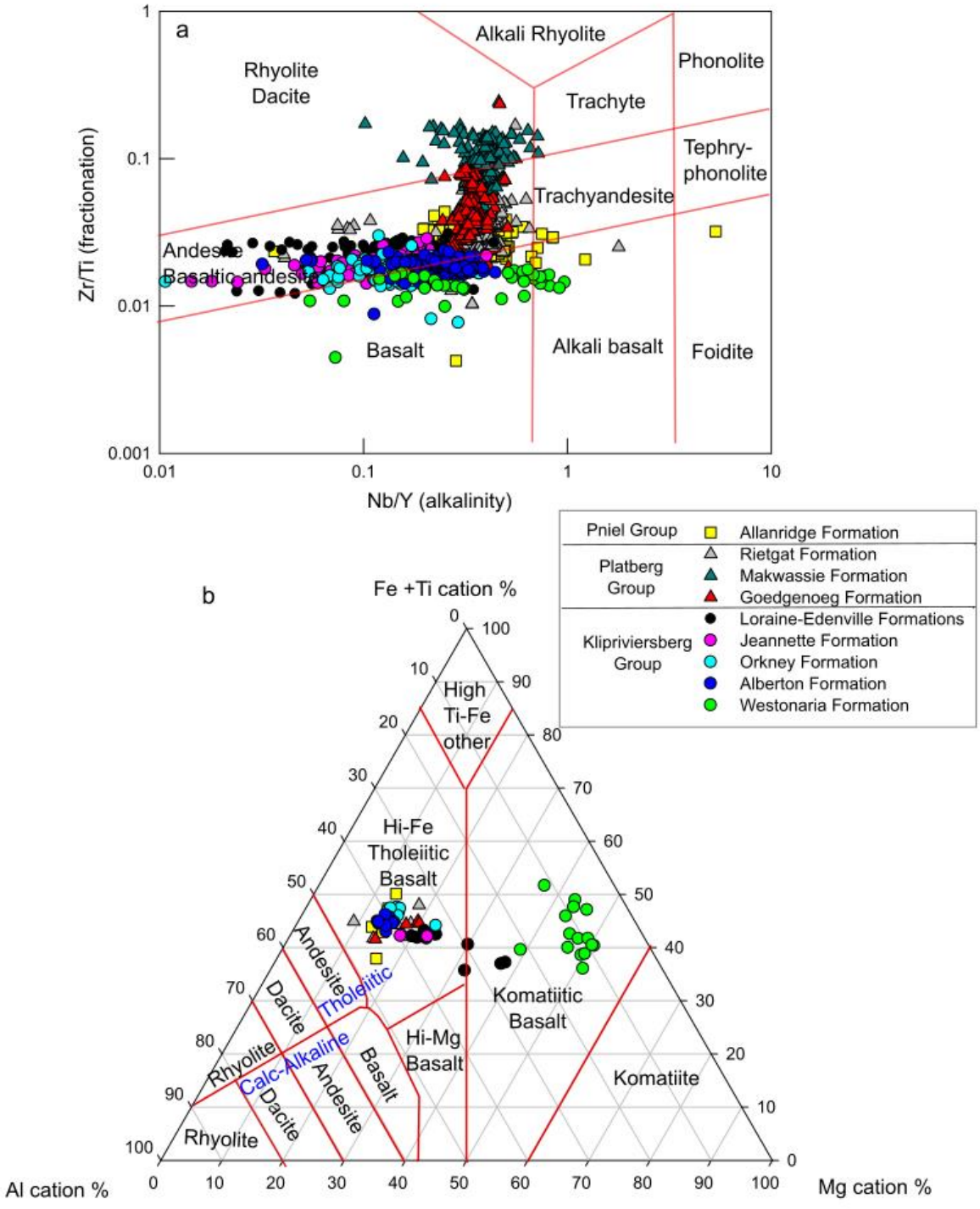

Figure 5. 2 Classification plots. (a) Zr/Ti versus Nb/Y (Pearce, 1996) shows the classification of the lavas. (b) cation classification plot (Jensen, 1976) showing the komatiitic Westonaria lavas analysed in Khumalo et al. (Chapter 4). The rest of the Ventersdorp lavas show tholeiitic affinities.

5.2.2 Major element geochemistry

The Westonaria lavas have higher MgO compared to the rest of the Klipriviersberg Group (Fig. 5.3a). Alberton, Orkney, and Jeanette lavas have uniform compositions and the Loraine-Edenville basalts plot between the Westonaria and the other three formations. The Klipriviersberg lavas generally display a gentle negative trend compared to the steep negative trends for the Platberg Group lavas (Fig. 5.3a). For the Platberg Group, the Goedgenoeg lavas display similar compositions to the Rietgat lavas. The Makwassie dacites and rhyolites have high SiO_2 contents and low MgO contents. A high-SiO_2 cluster of Goedgenoeg lavas overlaps with some of the Makwassie lavas. The Allanridge lavas have similar compositions to the Alberton, Orkney, and Jeanette lavas. There are five groups of TiO_2-MgO compositions that include the (i) Westonaria lavas that plot separately from the rest of the lavas at high MgO, (ii) Loraine-Edenville and Jeanette basalts, (iii) Alberton, Orkney and Allanridge basalts, (iv) Rietgat, high-TiO_2 Makwassie and Goedgenoeg lavas, and (v) low-TiO_2 Makwassie lavas (Fig. 5.3b). The Platberg lavas display a positive trend on the Al_2O_3 and MgO variation diagram whereas the Klipriviersberg lavas display a negative trend (Fig. 5.3c). The Alberton, Orkney, and Jeanette basalts plot within the basaltic composition (14-16 % Al_2O_3) and the picritic basalts of the Loraine-Edenville plot at lower Al_2O_3 (up to 9 wt. %) towards the komatiitic Westonaria lavas at less than 8 wt. % Al_2O_3. The Platberg lavas display a positive trend from the more evolved Makwassie to the Rietgat lavas that show similar total FeO contents to the Allanridge, Orkney, Alberton, and Jeanette basalts (Fig. 5.3d). This composition is at the pivot point of the Platberg-Klipriviersberg lavas showing a gentle positive trend. The Loraine-Edenville lavas plot towards the isolated cluster of the Westonaria lavas at higher MgO contents.

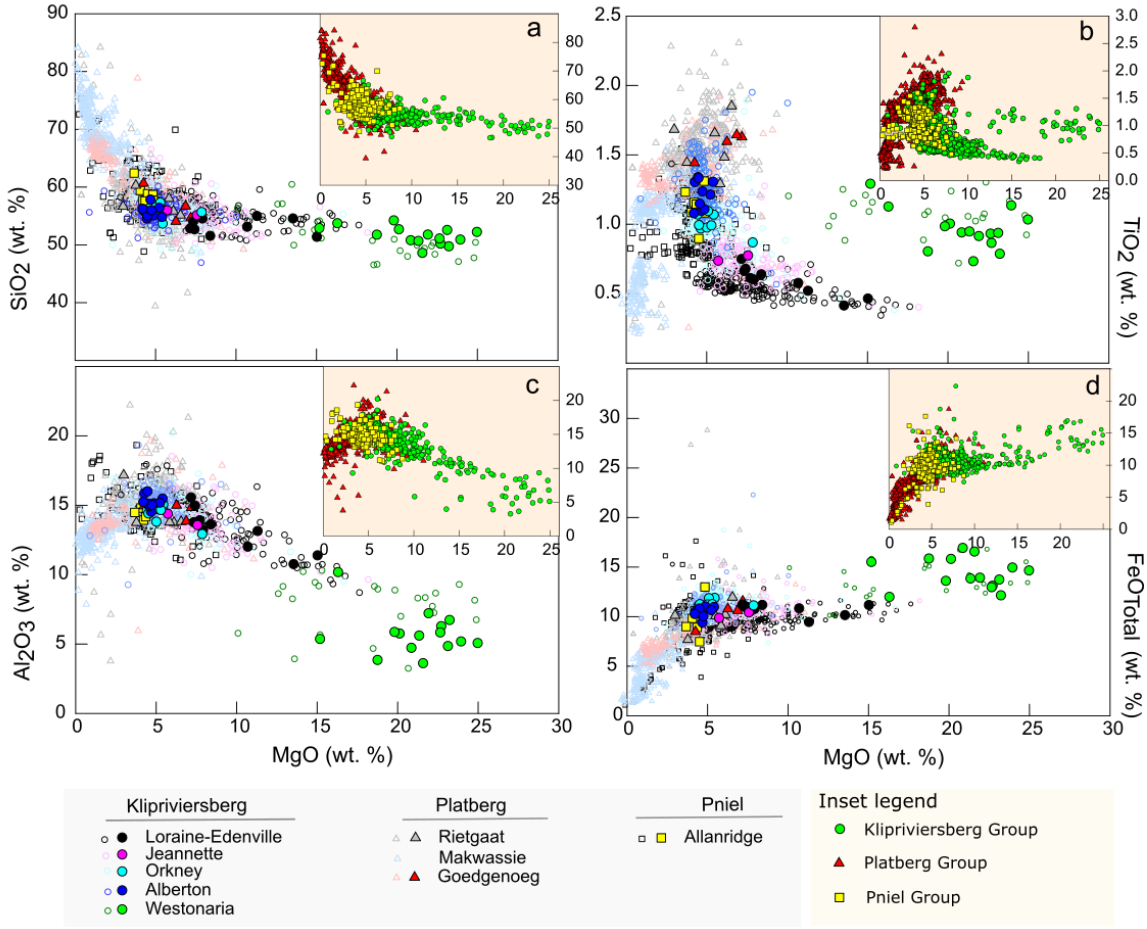

Figure 5. 3 Major element oxide variations of the Ventersdorp Supergroup lavas. The solid symbols are the samples analysed for Sr-Nd-Hf isotopes in this study. The open symbols represent literature data. The inset plots show the variations of the Klipriviersberg Group (green circles), the Platberg Group (red triangles) and the Allanridge Formation (yellow squares).

5.2.3 Trace element geochemistry

The trace element compositions are shown in Table 5.1. The Ti and Nd versus Zr plots discriminate between the Klipriviersberg lavas and Platberg lavas (Fig. 5.4). The komatiitic Westonaria lavas of the Klipriviersberg Group have low Sr contents (<70 ppm), plotting separately from the rest of the Klipriviersberg lavas (Fig. 5.4a). The rest of the Klipriviersberg lavas have Sr contents greater than 200 ppm, displaying a positive trend from the Loraine-Edenville and Jeanette lavas (with similar Zr content to Westonaria lavas) to the Alberton lavas that slightly overlap with the Allanridge lavas. The Goedgenoeg and Rietgat have higher Zr and Sr contents. Two groups that include the (i) Westonaria lavas with a wide range of Ni contents (483 to 1508 ppm) at a narrow Zr range (47 to 82), and the (2) rest of the Ventersdorp lavas show a narrow range of Ni (54 to 286 ppm) at a wide range of Zr (36 to 268) are shown in Figure 5.4b. The Formations still show grouping by Zr content. Nd and Ti show positive correlations with Zr, displaying similar groupings of the Formations (Fig. 5.4c and d). The Westonaria lavas plot between the Loraine-Edenville and Jeanette cluster and the rest of the Klipriviersberg lavas for Nd and Ti. The Allanridge Formation overlaps with the Alberton Formation in Nd and Zr contents. The Platberg Group lavas plot separately from the Klipriviersberg and Allanridge lavas (Fig. 5.4c). Two positive arrays are shown on the Ti versus Zr plot: the Klipriviersberg lavas, and the Platberg and Allanridge lavas (Fig. 5.4d).

Table 5. 1 New trace element compositions of the Ventersdorp Supergroup lavas.

Formation	Sample	Li	P	Sc	Ti	V	Cr	Co	Ni	Cu	Zn	Ga	Rb	Sr	Y	Zr	Nb	Sn	Sb	Cs	Ba
Westonaria	R048	2.85	182.61	10.55	3480.00	76.22	872.54	115.81	1343.28	306.62	142.86	5.87	0.14	47.99	5.63	47.44	7.74	0.88	1.74	0.24	1.32
	R141	8.46	368.97	11.99	3932.07	106.53	1085.39	101.63	1010.72	186.42	123.69	8.11	0.63	93.59	9.36	71.47	7.45	1.08	0.26	2.12	6.86
	R359	62.58	389.78	16.66	4910.14	184.16	1167.53	62.31	483.58	33.38	94.44	12.12	2.23	26.05	11.32	74.43	2.73	0.88	1.55	1.86	8.99
	R360	31.93	290.73	16.35	3740.33	130.69	1689.66	105.10	1508.81	212.36	83.59	10.15	1.88	33.30	8.20	55.10	1.92	0.86	5.60	3.26	3.82
	R362	7.04	325.39	12.43	3651.73	86.73	913.42	106.56	1058.02	202.51	119.66	6.32	1.16	42.46	7.64	56.83	8.38	1.37	0.66	1.36	5.27
	R434	5.45	345.41	12.51	4716.42	96.08	1023.77	109.16	1051.93	263.35	135.40	7.51	0.39	87.16	9.53	71.34	10.56	1.13	0.62	1.85	5.37
	R502	45.81	355.77	13.07	4026.65	171.37	1170.72	81.61	866.91	84.05	104.03	10.77	9.58	88.82	10.53	67.20	2.49	1.01	0.41	1.58	1274.43
	R503	26.13	326.14	11.35	3173.17	151.56	1439.41	102.46	1280.43	70.82	136.32	9.47	1.13	47.25	9.23	55.19	2.12	0.70	1.32	1.86	28.59
	R505	28.69	343.37	14.00	4184.45	95.28	1162.70	86.44	940.76	177.31	147.29	8.93	0.99	69.17	8.54	70.27	7.22	2.13	0.43	1.16	18.33
	R506	33.26	366.72	15.30	4528.67	103.96	1246.54	91.90	999.97	178.44	131.63	8.59	1.68	48.49	9.46	76.52	7.68	1.52	1.21	1.48	17.86
	R507	22.05	340.69	8.46	3667.13	107.34	1100.91	88.92	939.07	154.43	145.97	8.00	0.73	50.79	9.29	67.61	7.83	0.94	0.62	0.99	10.62
	R508	19.62	454.81	18.63	5103.79	132.31	842.04	91.97	968.55	244.11	87.87	8.24	0.61	28.44	12.50	82.31	9.53	1.51	0.42	1.52	11.80
	R509	17.99	393.96	15.86	4707.88	103.06	819.24	103.93	1246.31	180.22	103.53	7.18	0.52	21.72	9.33	76.14	8.60	0.96	0.22	1.46	11.12
	R511	25.73	329.76	9.29	3568.53	97.18	1159.26	95.48	1031.48	193.02	90.56	6.92	3.11	107.29	7.93	61.29	7.44	1.31	0.67	3.21	17.15
Alberton	LZ41	36.94	711.89	17.67	6154.06	148.70	114.80	38.76	131.17	114.11	87.67	18.63	64.21	450.55	16.71	125.15	5.22	1.72	1.49	1.75	817.70
	LZ31	15.71	550.92	20.62	5261.12	147.52	41.62	46.77	137.61	200.42	76.99	15.40	23.25	329.96	16.10	105.02	4.46	1.52	0.46	0.99	201.96
	R030	22.97	795.33	19.79	6567.46	148.43	141.13	49.58	141.89	131.35	106.98	17.78	47.74	322.66	17.21	130.99	6.02	1.43	0.45	1.58	324.67
	R038	20.20	843.63	19.23	7115.02	152.28	117.60	47.52	128.75	130.20	91.40	16.47	22.55	242.44	16.75	132.10	6.26	1.28	0.52	0.49	183.64
	R040	22.96	837.02	18.15	6605.35	163.95	110.41	46.26	129.74	169.61	117.30	21.20	44.91	444.62	17.10	121.65	5.84	1.58	0.33	0.72	570.45
	R129	24.66	750.68	18.99	6218.93	156.25	139.58	46.86	143.16	152.48	124.26	17.21	39.80	516.56	16.55	117.21	5.55	1.40	0.15	1.23	461.01
	R134	29.29	767.72	18.34	6414.65	146.84	108.17	47.67	125.29	112.84	96.31	19.79	36.34	552.54	17.79	132.51	5.79	2.04	0.39	0.87	780.13
	R357	24.32	897.85	21.81	7397.01	166.43	151.34	57.56	158.67	108.97	99.66	17.71	54.76	184.43	20.46	144.56	6.54	2.09	0.30	1.10	215.38
	R420	14.02	606.74	19.77	5415.58	161.10	68.13	47.12	127.81	154.52	84.21	17.58	45.69	413.70	16.19	105.50	4.83	1.80	0.32	0.78	463.63
Orkney	LZ18	16.14	374.74	26.14	3780.74	178.71	424.33	58.48	209.32	99.63	77.28	14.42	60.58	358.75	12.95	66.92	3.00	1.24	0.49	1.15	403.67
	LZ23	14.62	495.76	24.64	4981.08	190.08	19.30	55.61	118.78	90.12	87.41	17.96	107.72	305.84	15.80	88.01	4.18	1.56	1.00	1.78	700.20
	LZ29	12.90	472.08	21.49	5014.19	180.11	55.88	49.42	123.07	119.09	97.99	16.73	16.46	343.64	14.99	88.96	4.06	1.47	1.16	0.74	124.21
	R347	17.16	511.90	24.17	5415.65	199.07	58.22	54.22	128.43	178.78	90.52	16.26	31.23	394.45	16.27	95.43	4.94	16.99	0.82	0.63	478.67
	R105	32.59	504.00	23.57	4601.17	189.51	29.61	49.08	103.16	108.82	91.30	16.66	62.91	318.70	14.87	91.28	4.01	1.09	0.64	1.79	436.47
	R333	16.00	471.21	25.57	4840.64	179.96	31.38	62.08	117.08	285.67	124.76	11.51	6.91	155.24	15.15	92.69	4.21	1.55	0.34	0.27	91.15
	R335	12.99	517.68	24.94	4899.08	194.82	27.41	54.31	100.98	121.67	84.18	17.03	94.77	315.86	15.96	86.32	4.27	1.58	0.57	2.43	595.33
Jeannette	R326	10.58	366.97	26.05	3590.37	175.61	118.13	46.78	133.01	85.41	100.51	15.22	82.30	276.54	12.78	65.37	2.94	0.97	0.88	2.61	482.45
	LZ17	22.55	299.70	25.37	3208.41	167.13	978.99	62.59	286.03	103.39	74.79	12.15	47.88	224.88	11.12	42.54	2.30	4.61	0.96	1.23	410.51
Lora-Eden	KL136	11.49	311.29	27.39	3314.63	178.37	302.41	55.48	189.79	92.90	80.57	13.00	61.58	523.52	11.11	56.56	2.33	0.97	0.35	3.00	341.80
	KL142	10.09	296.69	29.08	3095.07	193.23	394.38	55.58	202.18	90.58	92.60	11.63	19.59	193.98	10.81	42.71	2.15	1.18	0.66	1.07	167.10
	KL145	12.76	273.84	27.19	2967.21	177.88	343.47	52.69	186.35	85.13	82.77	11.83	84.80	245.71	9.88	54.45	2.05	0.82	0.59	3.32	371.29
	KL147	10.33	357.56	32.07	3266.47	178.32	360.18	55.64	187.14	86.05	84.97	9.04	42.69	52.22	12.40	61.11	2.46	0.73	0.72	1.39	230.77
	KL150	11.21	322.82	27.72	3281.93	182.53	357.00	52.58	189.81	65.40	82.46	13.47	41.85	222.77	11.80	69.37	2.52	1.11	0.46	0.98	572.59
	KL156	19.99	204.51	28.82	2146.54	140.90	1432.42	64.50	341.82	52.99	90.80	10.02	12.16	211.92	7.73	36.74	1.40	0.51	0.35	0.97	102.23
Goedgenoeg	PG168	14.28	3167.37	21.62	8412.21	175.34	293.28	39.12	137.05	51.53	173.85	21.59	22.08	452.01	39.14	268.62	14.65	2.27	0.11	1.05	577.74
	PG163	16.01	2254.14	18.91	6777.81	178.64	256.13	34.28	134.63	46.30	145.46	16.71	22.86	349.05	34.13	187.34	9.50	1.37	0.37	0.93	796.50
Rietgat	PR472	33.97	2328.33	19.82	8463.31	128.59	13.28	15.52	9.55	2.58	98.10	33.98	60.27	275.01	62.28	681.12	27.82	5.75	0.34	2.60	949.90
	PR487	7.43	2963.01	18.61	7124.58	148.14	89.14	22.83	54.73	38.00	84.68	21.86	24.95	889.98	39.94	265.85	15.99	2.16	0.11	1.08	681.79
	PR484	30.35	2013.88	18.74	6262.05	161.64	320.96	33.81	133.14	39.57	115.97	19.49	49.24	471.12	33.70	220.75	10.98	1.81	0.41	1.76	848.73
	PR182	8.55	2173.11	17.42	6003.91	142.94	405.08	36.55	148.70	38.67	102.47	15.36	23.30	335.36	25.96	190.81	10.88	1.81	0.17	0.48	750.99
Allanridge	AR199	3.47	734.84	14.10	5468.37	144.22	15.70	43.34	117.54	142.86	90.27	15.27	35.90	1240.36	17.35	150.95	7.09	1.90	0.17	4.22	486.53
	AR446	7.62	1026.32	19.99	5950.79	153.33	44.99	51.19	124.19	117.21	99.42	17.43	41.15	382.88	19.36	173.70	7.55	1.74	0.04	0.71	710.21

	AR451	11.20	596.97	19.90	4261.63	156.41	131.98	39.04	94.87	129.68	56.81	15.20	46.61	401.48	14.24	123.97	5.45	2.57	0.19	0.43	733.21
	AR345	9.36	798.24	18.37	5179.75	160.51	42.24	55.30	144.73	64.87	128.34	19.12	16.08	437.77	17.27	148.63	6.14	1.60	0.10	1.02	309.19

The compositions are reported in ppm.

Table 5.1. *Continued*

Formation	Sample	La	Ce	Pr	Nd	Sm	Eu	Gd	Tb	Dy	Ho	Er	Tm	Yb	Lu	Hf	Ta	W	Tl	Pb	Th	U
Westonaria	R048	13.19	25.28	3.00	12.24	2.22	0.67	1.89	0.24	1.31	0.24	0.63	0.08	0.55	0.08	1.26	0.54	0.13	0.02	1.61	1.00	0.46
	R141	11.19	25.47	3.15	13.49	2.82	0.95	2.68	0.37	2.08	0.39	1.03	0.14	0.84	0.12	1.83	0.41	0.12	0.02	0.86	1.21	0.41
	R359	4.70	11.92	1.66	8.20	2.39	0.86	2.70	0.42	2.53	0.48	1.25	0.17	1.02	0.15	2.07	0.01	0.10	0.02	3.01	1.10	0.36
	R360	6.82	14.95	1.76	7.64	1.84	0.74	2.00	0.30	1.79	0.34	0.88	0.12	0.74	0.10	1.51	0.12	0.36	0.04	2.73	0.91	0.27
	R362	6.00	16.39	2.23	9.99	2.24	0.73	2.18	0.31	1.74	0.32	0.81	0.11	0.67	0.10	1.47	0.59	0.08	0.11	1.67	1.12	0.70
	R434	9.58	24.80	3.43	15.56	3.28	1.18	2.92	0.39	2.15	0.40	1.04	0.13	0.83	0.11	1.84	0.79	3.01	0.10	0.82	1.51	0.77
	R502	9.41	19.11	2.23	9.80	2.45	1.07	2.65	0.39	2.36	0.45	1.15	0.16	0.98	0.14	1.80	-0.01	0.14	0.09	3.91	0.98	0.32
	R503	2.30	6.44	1.05	5.68	1.86	0.76	2.15	0.33	2.00	0.38	0.99	0.13	0.80	0.11	1.43	-0.04	0.03	0.01	2.16	0.80	0.28
	R505	18.96	39.03	4.34	17.83	3.27	0.96	2.85	0.37	2.02	0.37	0.96	0.13	0.79	0.11	1.84	0.47	0.23	0.03	2.31	1.34	0.46
	R506	10.66	24.69	3.14	14.00	3.03	0.96	2.78	0.38	2.12	0.39	1.01	0.13	0.85	0.12	1.98	0.49	0.26	0.05	4.88	1.46	0.49
	R507	11.70	27.92	3.47	14.91	3.15	0.84	2.90	0.39	2.17	0.39	1.02	0.14	0.82	0.12	1.69	0.43	0.08	0.01	3.40	1.23	0.47
	R508	10.44	28.72	3.93	18.01	3.82	1.20	3.76	0.49	2.71	0.52	1.33	0.18	1.08	0.16	2.12	0.55	0.14	0.03	1.95	1.31	0.59
	R509	5.75	18.16	2.75	12.61	3.02	0.94	2.66	0.38	2.10	0.40	1.16	0.19	1.57	0.23	1.99	0.48	0.10	0.04	2.64	1.20	0.54
	R511	7.96	20.89	2.92	13.30	3.05	0.90	2.74	0.37	2.04	0.37	0.93	0.12	0.73	0.10	1.58	0.41	0.12	0.06	1.41	0.99	0.39
Alberton	LZ41	19.54	37.38	4.45	18.67	4.23	1.31	4.23	0.61	3.66	0.71	1.91	0.26	1.57	0.23	3.48	0.41	0.25	1.07	4.16	2.30	0.75
	LZ31	16.43	31.38	3.73	15.74	3.58	1.12	3.78	0.55	3.35	0.66	1.81	0.25	1.54	0.23	2.97	0.38	0.16	0.34	4.44	2.29	0.96
	R030	14.74	33.89	3.95	16.98	3.85	1.20	3.90	0.56	3.38	0.67	1.79	0.25	1.63	0.23	3.45	0.37	0.59	0.35	3.55	2.18	0.73
	R038	14.82	32.75	3.92	16.96	3.84	0.93	3.86	0.57	3.44	0.67	1.83	0.26	1.60	0.23	3.50	0.31	0.38	0.16	2.90	2.29	0.73
	R040	18.10	35.63	4.45	19.00	4.16	1.50	4.16	0.60	3.55	0.69	1.84	0.26	1.56	0.21	3.27	0.28	0.40	0.37	7.92	2.17	0.71
	R129	17.37	36.19	4.34	18.39	4.07	1.40	4.09	0.58	3.48	0.68	1.80	0.25	1.53	0.22	3.22	0.25	0.35	0.29	3.24	2.12	0.71
	R134	18.05	37.66	4.57	19.46	4.25	1.69	4.26	0.61	3.67	0.71	1.89	0.26	1.67	0.24	3.64	0.36	0.44	0.54	3.06	2.30	0.74
	R357	18.48	43.21	5.16	22.26	4.87	1.45	4.86	0.70	4.24	0.82	2.21	0.30	1.94	0.28	3.79	0.43	0.26	0.75	2.52	2.70	0.90
	R420	15.53	31.42	3.71	16.04	3.53	1.22	3.66	0.54	3.23	0.64	1.73	0.24	1.54	0.22	2.80	0.34	0.41	0.62	6.74	2.14	0.90
Orkney	LZ18	9.79	19.72	2.34	10.23	2.40	0.83	2.52	0.39	2.46	0.51	1.40	0.20	1.31	0.19	1.84	0.21	0.27	0.71	3.39	1.42	0.59
	LZ23	11.52	24.14	2.91	12.76	3.01	1.09	3.20	0.48	3.02	0.62	1.68	0.23	1.57	0.23	2.42	0.29	0.41	1.27	3.88	1.91	0.82
	LZ29	11.89	23.62	2.81	12.24	2.98	1.04	3.21	0.49	3.04	0.61	1.70	0.23	1.45	0.22	2.52	0.36	0.16	0.24	4.47	2.00	0.89
	R347	12.25	26.36	3.23	13.98	3.40	1.14	3.59	0.55	3.37	0.67	1.80	0.26	1.58	0.23	2.79	0.33	0.93	0.20	5.42	2.07	0.97
	R105	11.38	23.94	2.89	12.40	2.91	1.01	3.10	0.47	2.94	0.60	1.67	0.24	1.52	0.22	2.57	0.17	0.35	0.44	6.57	1.81	0.77
	R333	9.06	21.24	2.64	11.73	2.90	0.81	3.01	0.47	3.02	0.61	1.71	0.25	1.64	0.24	2.56	0.31	0.37	0.10	4.58	2.00	0.84
	R335	13.75	26.99	3.18	13.77	3.13	1.10	3.34	0.50	3.13	0.63	1.72	0.24	1.59	0.22	2.30	0.31	0.25	1.14	4.64	2.02	0.85
Jeannette	R326	10.12	20.54	2.41	10.06	2.30	0.84	2.45	0.38	2.44	0.51	1.45	0.21	1.37	0.20	1.84	0.05	0.30	0.62	5.49	1.52	0.56
	LZ17	8.55	15.99	1.89	8.27	1.98	0.78	2.16	0.34	2.19	0.44	1.22	0.17	1.08	0.15	1.26	0.16	0.41	0.58	3.72	1.07	0.44
Lora-Eden	KL136	8.41	16.40	1.91	8.18	2.04	0.73	2.31	0.36	2.38	0.49	1.40	0.20	1.26	0.19	1.66	0.19	0.09	0.76	4.00	1.37	0.52
	KL142	7.81	15.16	1.80	7.81	1.93	0.68	2.24	0.35	2.32	0.48	1.36	0.19	1.20	0.18	1.36	0.18	0.12	0.31	4.82	1.23	0.46
	KL145	7.42	14.48	1.73	7.43	1.85	0.66	2.06	0.33	2.12	0.45	1.29	0.18	1.19	0.19	1.59	0.17	0.09	0.96	2.61	1.23	0.46
	KL147	8.10	18.76	2.19	9.19	2.04	0.57	2.20	0.34	2.19	0.46	1.31	0.20	1.36	0.20	1.66	0.16	0.39	0.30	2.25	1.17	0.41
	KL150	8.43	17.43	2.11	9.07	2.25	0.75	2.47	0.39	2.55	0.54	1.55	0.23	1.46	0.23	1.99	0.21	0.08	0.64	2.46	1.52	0.54
	KL156	4.05	8.71	1.04	4.42	1.09	0.36	1.27	0.20	1.39	0.30	0.85	0.13	0.88	0.13	1.03	0.09	0.22	0.07	1.90	0.68	0.24
Goedgenoeg	PG168	49.24	115.21	14.51	60.38	11.22	2.84	9.98	1.34	7.68	1.52	4.18	0.59	3.88	0.57	6.20	0.80	0.73	0.13	3.40	1.48	0.32
	PG163	54.76	112.97	13.81	58.40	10.87	2.81	9.74	1.27	7.30	1.43	3.89	0.52	3.26	0.49	4.85	0.45	0.21	0.33	1.86	1.13	0.25
Rietgat	PR472	143.01	282.42	33.29	134.13	23.22	5.00	19.64	2.46	13.50	2.59	7.12	0.96	6.11	0.91	17.23	1.48	1.66	0.60	76.89	8.19	1.57
	PR487	59.55	133.06	16.19	66.10	12.10	3.08	10.63	1.40	7.87	1.53	4.13	0.57	3.69	0.52	6.07	0.84	0.85	0.12	7.39	2.14	0.42

	PR484	58.27	112.78	13.59	55.58	10.41	2.67	9.29	1.23	7.15	1.40	3.87	0.53	3.34	0.50	5.50	0.51	0.14	0.60	6.26	1.81	0.37
	PR182	53.85	103.53	12.23	50.05	8.96	2.30	7.79	1.00	5.67	1.08	2.95	0.40	2.49	0.36	4.69	0.51	0.17	0.30	3.53	2.17	0.44
Allanridge	AR199	26.62	51.52	6.07	25.47	5.24	1.76	4.98	0.68	3.87	0.74	1.98	0.27	1.65	0.25	3.97	0.61	2.82	0.51	5.48	2.39	0.63
	AR446	27.44	53.59	6.34	25.73	5.24	2.16	5.06	0.70	4.00	0.76	1.98	0.28	1.76	0.25	4.12	0.35	0.24	0.27	3.09	2.15	0.41
	AR451	25.42	46.30	5.06	20.29	4.15	1.29	3.97	0.56	3.22	0.62	1.66	0.22	1.39	0.21	3.36	0.50	0.12	0.50	2.50	3.59	1.02
	AR345	27.97	53.57	6.30	25.47	4.98	1.27	4.62	0.65	3.79	0.74	1.97	0.26	1.60	0.23	3.84	0.36	0.12	0.24	5.12	2.21	0.39

The compositions are reported in ppm.

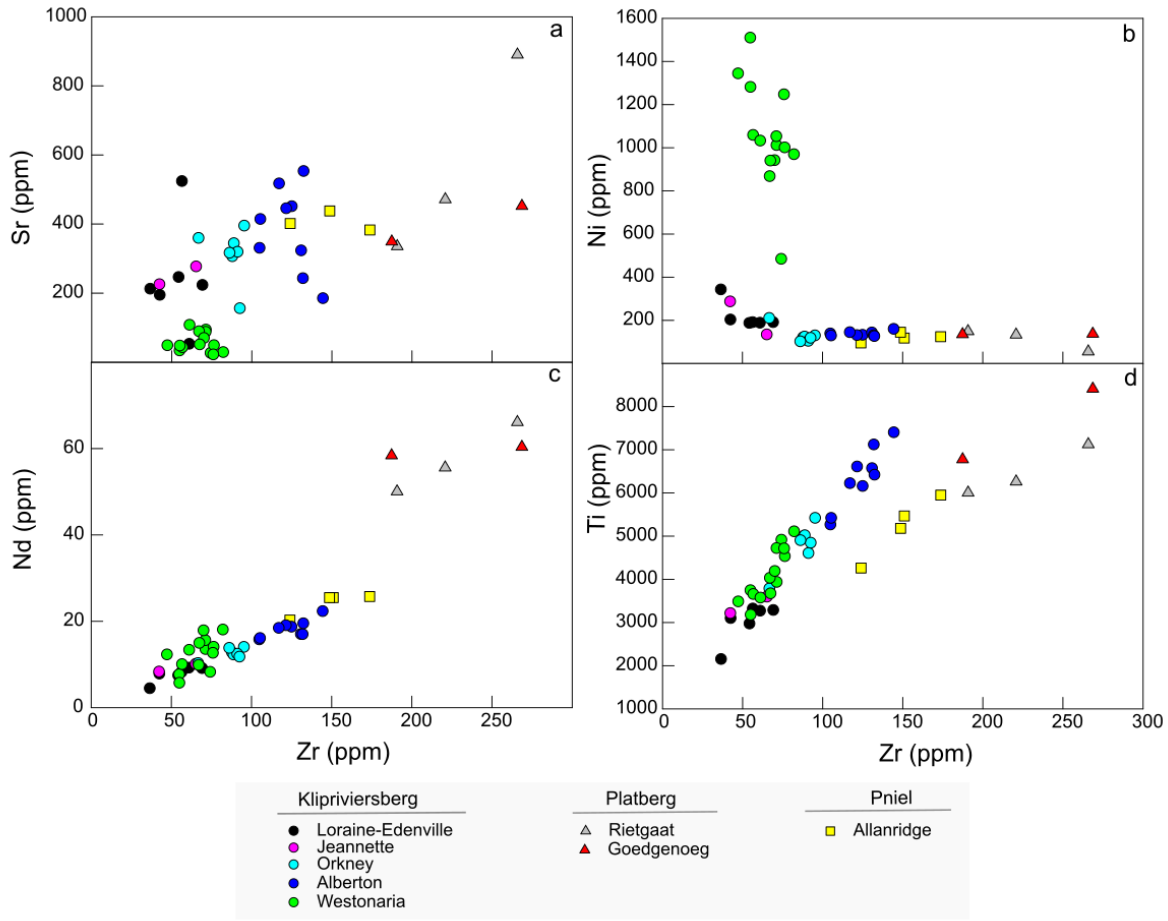

Figure 5. 4 Variations of trace elements (Sr, Ni, Nd, Ti and Zr) of the lavas that are analysed in this study.

The Ventersdorp Supergroup lavas display L/HREE enrichment patterns with weak Eu anomalies (Fig. 5.5). The lavas show greater variation in LREE than HREE (Fig. A2.1). The concentration of incompatible elements decreases up section from the Alberton Formation to the Loraine-Edenville Formation, whereas the Westonaria overlaps with the rest of the Klipriviersberg lavas. The Klipriviersberg lavas display a flattening of the HREE patterns from the Alberton Formation towards the Loraine-Edenville Formations, except for the Westonaria Formation which displays variation in the HREE patterns ($Gd/Yb_{(N)}$: 2.13 – 3.05) overlapping with the rest of the Klipriviersberg lavas ($Gd/Yb_{(N)}$: 1.17 – 2.60: Fig. 5.5a – e). The Platberg Group plot at higher values of enrichment relative to chondrites (above 40 for the LREE and 10 for the HREE), parallel to the Klipriviersberg Group samples (Fig. 5.5a and d). The Goedgenoeg and Rietgat lavas of the Platberg Group display greater L/HREE enrichment

compared to the Klipriviersberg lavas. The Allanridge lavas of the Pniel Group are parallel to both the Klipriviersberg and Platberg Groups (Fig. 5.5a and d).

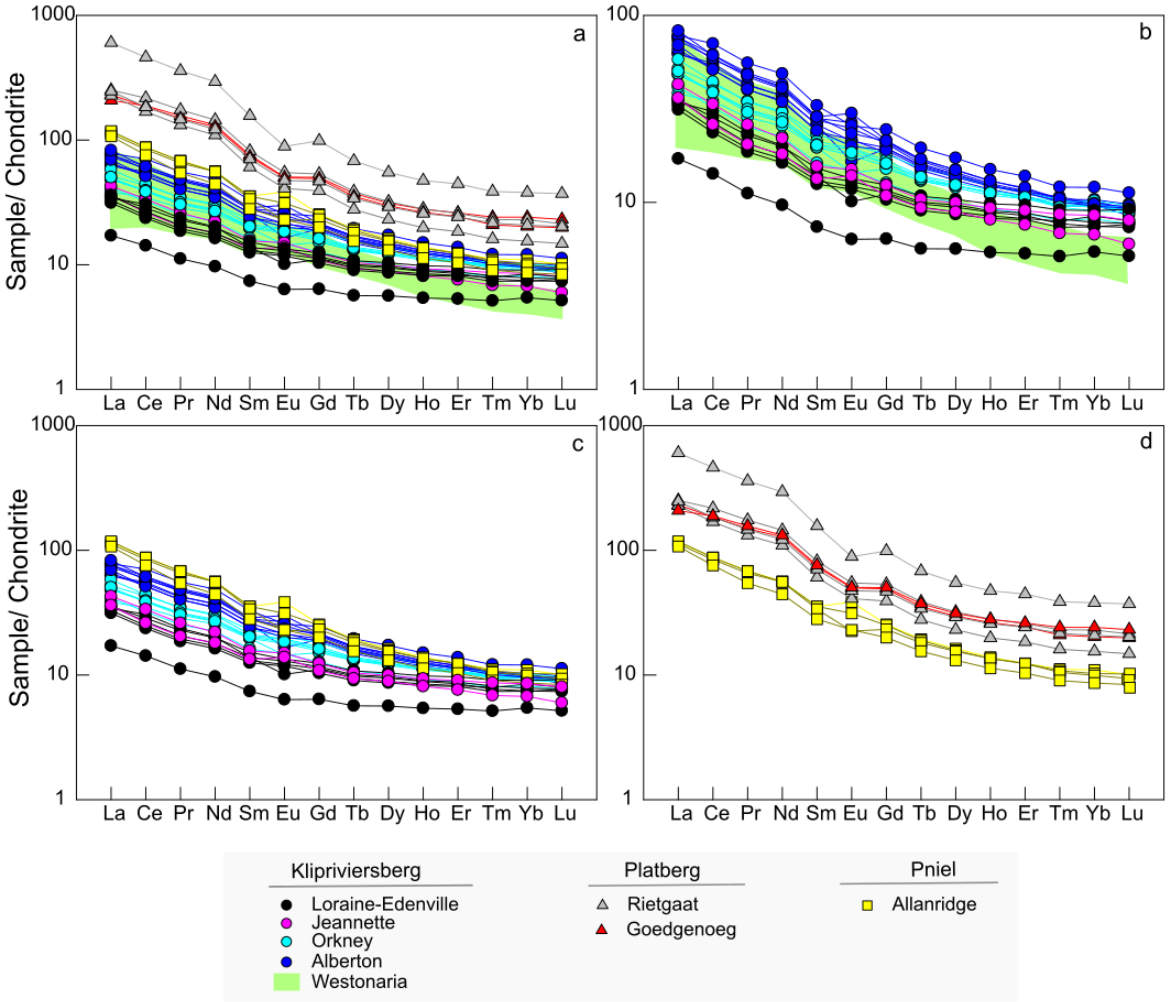

Figure 5. 5 Chondrite-normalised rare earth elements (REE) diagrams of the Ventersdorp lavas. The lavas show L/HREE enrichment. The Westonaria lavas in Khumalo et al. (Chapter 4) are shown by the green field (a and b). a) the entire Ventersdorp Supergroup, b) the entire Klipriviersberg Group, c) Allanridge Formation and the Klipriviersberg Group without the Westonaria Formation, and d) Platberg Group and the Allanridge Formation. The chondrite normalisation values are from McDonough and Sun (1995).

The multi-element diagrams normalized using primitive mantle values reported in McDonough and Sun (1995) are shown in Figure 5.6. The Allanridge Formation displays trace element enrichment patterns that are similar to those of the Alberton Formation of the Klipriviersberg Group. The Klipriviersberg lavas show less variation in the immobile elements. They display parallel trends with a small range of enrichment relative to the primitive mantle.

The Klipriviersberg lavas show uniform negative Ti anomalies, however, they are less pronounced than the Ti anomalies observed for the samples of the Platberg Group and Pniel Group (Fig. 5.6a and b). The Alberton, Orkney, Jeanette and Loraine-Edenville lavas display larger negative Nb-Ta-Th-U anomalies than the Westonaria lavas. The four elements produce a U-shaped trend for the Klipriviersberg lavas with the exception of the samples of the Westonaria Formation. The trough becomes more even (not step-like) and shows similar enrichment for Nb-Ta-Th-U in the Platberg Formation. Positive Sr anomalies are observed for the majority of the Klipriviersberg lavas, excluding the Westonaria lavas that have negative Sr anomalies. The samples of the Platberg Group plot at higher levels of enrichment for the least mobile elements and immobile elements (Fig. 5.6b). They show similar enrichment for the mobile elements (Rb, Ba and K) as well for Th and U as compared to the Klipriviersberg lavas. However, Nb and Ta are more enriched compared to the Klipriviersberg lavas. The samples of the Goedgenoeg Formation and Rietgat Formation display larger negative Ti anomalies and variable Sr anomalies with the Goedgenoeg Formation showing the greatest Sr anomaly. The relative enrichment between Rb and Ba for the Klipriviersberg and Platberg groups is different. The Allanridge Formation displays a similar trend and enrichment as the Alberton Formation.

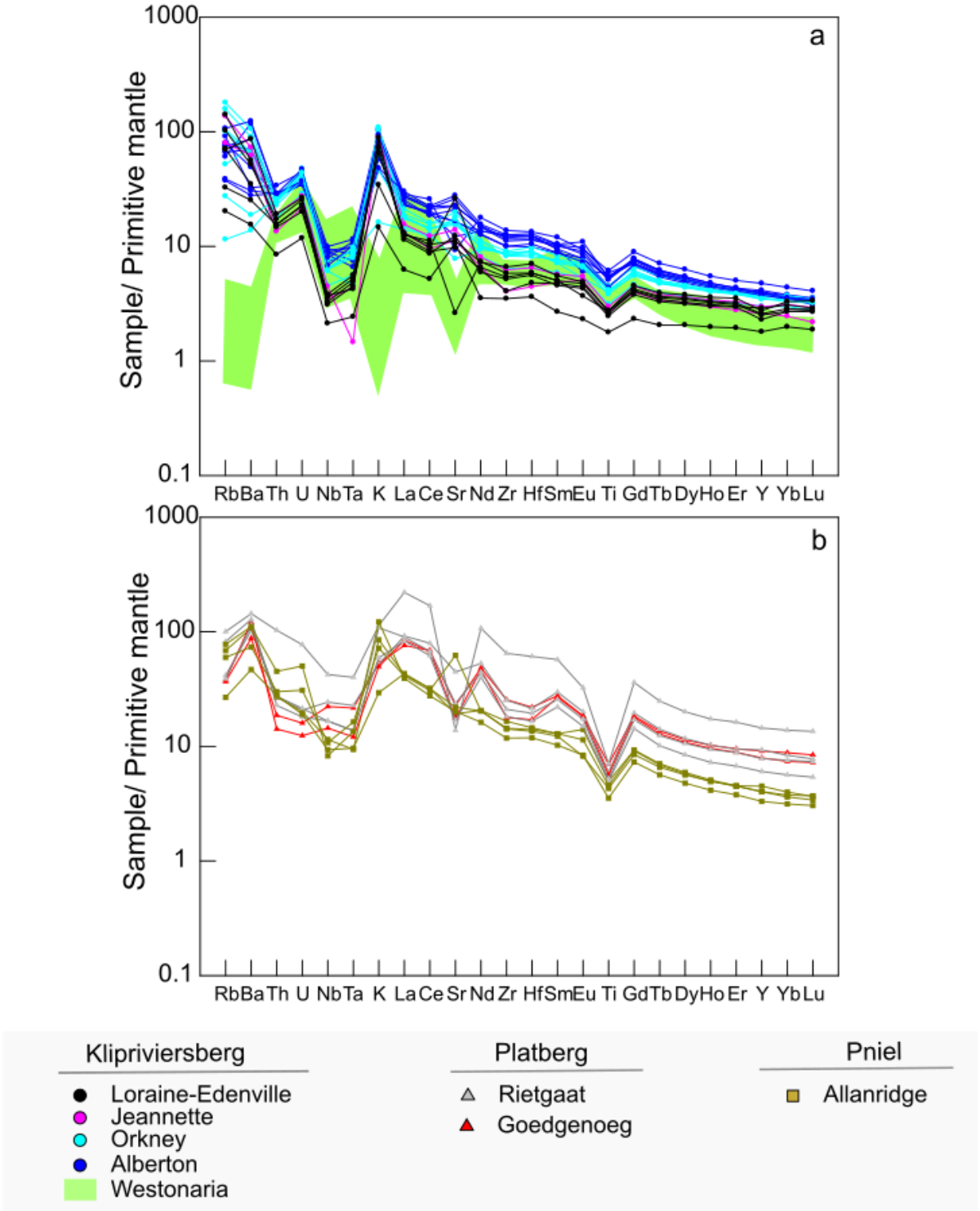

Figure 5. 6 Multi-element diagram of the Ventersdorp Supergroup lavas normalised to the primitive mantle composition. The lavas display Nb-Ta-Ti anomalies. The normalisation values are from McDonough and Sun (1995).

5.2.4 Sr-Nd-Hf isotopes

High-precision Sr-Nd-Hf isotope data are presented in Tables 5.2, 5.3 and 5.4, and Figure 5.7. The initial ε_{Nd} values calculated at 2.78 Ga for the Klipriviersberg Group lavas range from +1.06 ($^{143}Nd/^{144}Nd$ = 0.50907) to -1.16 ($^{143}Nd/^{144}Nd$ = 0.50896), excluding the Westonaria lavas that have a similar range of ε_{Nd} of -1.72 to +2.16 as reported in Khumalo et al. (Chapter 4). The Platberg lavas have ε_{Nd} (calculated at 2.72 Ga) ranging from -2.57 ($^{143}Nd/^{144}Nd$ = 0.50898) to -4.80 ($^{143}Nd/^{144}Nd$ = 0.50896). The Allanridge lavas (calculated at 2.68 Ga) have ε_{Nd} ranging from -2.44 ($^{143}Nd/^{144}Nd$ = 0.50904) to -3.74 ($^{143}Nd/^{144}Nd$ = 0.50897). Initial $^{87}Sr/^{86}Sr$ for the Klipriviersberg lavas (2.78 Ga) range from 0.69386 to 0.71201. The Platberg lavas (2.72 Ga) have initial $^{87}Sr/^{86}Sr$ that range from 0.69896 to 0.70352 and the Allanridge lavas have initial $^{87}Sr/^{86}Sr$ ranging from 0.70044 to 0.70269. Initial ε_{Hf} values for the Klipriviersberg lavas range from -4.26 ($^{176}Hf/^{177}Hf$ = 0.28087) to +1.51 ($^{176}Hf/^{177}Hf$ = 0.28103). These values overlap with the Westonaria Formation (-1.79 to +3.59; Khumalo et al., Chapter 4). The ε_{Hf} values for the Platberg lavas (calculated at 2.72 Ga) range from -10.12 ($^{176}Hf/^{177}Hf$ = 0.28075) to – 2.73 ($^{176}Hf/^{177}Hf$ = 0.28096) overlapping with the Allanridge Formation (at 2.68 Ga) that ranges from -7.31 to -2.80 ($^{176}Hf/^{177}Hf$ = 0.28086 to 0.28098).

Table 5. 2 Lu-Hf isotope composition of the Ventersdorp Supergroup lavas.

Formation	Sample	Age (Ga)	Hf (ppm)	Lu (ppm)	$^{176}Lu/^{177}Hf$	$^{176}Hf/^{177}Hf$	1SE	$^{176}Hf/^{177}Hf$ (t)	εHf (t)	1SE
Westonaria	R048	2.78	1.13	0.08	0.010	0.28149	4.00E-06	0.28095	-1.33	0.15
	R141	2.78	1.88	0.13	0.009	0.28109	1.60E-05	0.28058	-14.66	0.58
	R359	2.78	2.27	0.15	0.010	0.28160	8.00E-06	0.28109	3.60	0.28
	R360	2.78	1.39	0.11	0.011	0.28159	4.00E-06	0.28100	0.24	0.15
	R362	2.78	1.47	0.10	0.009	0.28157	1.50E-05	0.28108	3.11	0.53
	R434	2.78	1.67	0.11	0.010	0.28149	4.00E-06	0.28097	-0.69	0.14
	R432	2.78	1.87	0.14	0.011	0.28154	5.00E-06	0.28096	-1.16	0.17
	R502	2.78	2.05	0.16	0.011	0.28163	3.00E-06	0.28105	2.05	0.12
	R503	2.78	1.77	0.13	0.010	0.28157	3.00E-06	0.28102	1.13	0.12
	R505	2.78	1.98	0.12	0.008	0.28147	6.00E-06	0.28103	1.40	0.22
	R506	2.78	1.87	0.13	0.010	0.28146	4.00E-06	0.28094	-1.79	0.16
	R507	2.78	2.09	0.13	0.009	0.28143	3.00E-06	0.28096	-1.02	0.11
	R508	2.78	2.30	0.17	0.011	0.28152	3.00E-06	0.28095	-1.62	0.10
	R509	2.78	2.03	0.12	0.009	0.28148	7.00E-06	0.28102	0.96	0.23
	R511	2.78	1.78	0.11	0.009	0.28143	3.00E-06	0.28097	-0.89	0.10
Alberton	LZ41	2.78	3.74	0.28	0.011	0.28152	9.00E-06	0.28095	-1.45	0.31
	LZ31	2.78	3.06	0.25	0.011	0.28160	9.00E-06	0.28099	-0.03	0.32
	R030	2.78	3.63	0.25	0.010	0.28151	7.00E-06	0.28098	-0.38	0.24
	R038	2.78	3.81	0.27	0.010	0.28152	2.00E-06	0.28099	0.11	0.08
	R040	2.78	3.45	0.24	0.010	0.28153	7.00E-06	0.28101	0.57	0.24
	R129	2.78	3.38	0.27	0.011	0.28154	1.00E-05	0.28094	-1.75	0.35
	R134	2.78	3.31	0.27	0.011	0.28157	3.00E-06	0.28096	-1.27	0.11
	R357	2.78	3.77	0.34	0.013	0.28159	4.00E-06	0.28090	-3.33	
	R420	2.78	2.75	0.25	0.013	0.28163	3.00E-06	0.28095	-1.51	
Orkney	LZ18	2.78	2.08	0.22	0.015	0.28167	1.90E-05	0.28087	-4.26	0.69
	LZ23	2.78	2.66	0.25	0.014	0.28172	9.00E-06	0.28099	0.01	0.33
	LZ29	2.78	2.36	0.24	0.014	0.28172	3.00E-06	0.28096	-1.16	0.10
	R347	2.78	2.86	0.25	0.012	0.28169	7.00E-06	0.28103	1.51	0.24
	R005	2.78	2.24	0.25	0.015	0.28179	3.00E-06	0.28096	-1.17	0.12
	R105	2.78	2.89	0.28	0.014	0.28171	3.00E-06	0.28098	-0.21	0.11
	R333	2.78	2.52	0.29	0.016	0.28174	3.00E-06	0.28087	-4.14	
	R335	2.78	2.37	0.25	0.015	0.28174	3.00E-06	0.28094	-1.79	
Jeannette	R326	2.78	2.02	0.22	0.016	0.28181	9.00E-06	0.28097	-0.70	0.32
	LZ17	2.78	1.35	0.17	0.017	0.28192	1.90E-05	0.28099	-0.15	0.68
Loraine-Edenville	KL136	2.78	1.58	0.20	0.018	0.28192	4.00E-06	0.28093	-2.03	0.14
	KL141	2.78	1.15	0.17	0.021	0.28214	6.00E-06	0.28103	1.34	0.21
	KL142	2.78	1.56	0.22	0.020	0.28186	2.40E-05	0.28077	-7.83	0.87
	KL145	2.78	1.69	0.20	0.017	0.28190	1.50E-05	0.28099	0.11	0.52
	KL147	2.78	1.59	0.23	0.020	0.28200	3.00E-06	0.28092	-2.40	
	KL150	2.78	2.12	0.26	0.018	0.28197	1.40E-05	0.28103	1.42	0.50
	KL153	2.78	2.09	0.29	0.020	0.28188	3.00E-06	0.28082	-6.12	0.10
	KL155	2.78	1.43	0.27	0.027	0.28185	4.00E-06	0.28042		0.15
	KL156	2.78	1.10	0.14	0.018	0.28190	1.50E-05	0.28092	-2.62	0.52
	KL158	2.78	1.13	0.19	0.023	0.28216	6.00E-06	0.28090	-3.29	0.20
Goedgenoeg	PG166	2.72	5.52	0.63	0.016	0.28165	3.00E-06	0.28081	-8.09	0.12
	PG168	2.72	6.54	0.62	0.013	0.28166	6.00E-06	0.28096	-2.73	0.21
	PG163	2.72	6.02	0.59	0.014	0.28166	7.00E-06	0.28093	-3.67	0.26
	PG175	2.72	6.52	0.57	0.012	0.28151	3.00E-06	0.28086	-6.10	0.10
Rietgat	PR472	2.72	14.85	0.95	0.009	0.28139	2.00E-06	0.28091	-4.41	0.07
	PR487	2.72	7.10	0.59	0.012	0.28151	8.00E-06	0.28090	-4.94	0.27
	PR484	2.72	6.53	0.58	0.013	0.28158	9.00E-06	0.28093	-3.78	0.33
	PR182	2.72	4.94	0.46	0.013	0.28153	3.00E-06	0.28085	-6.58	0.12
	PR185	2.72	6.14	0.66	0.015	0.28164	3.00E-06	0.28084	-7.12	0.12
	PR189	2.72	7.51	0.77	0.014	0.28150	2.00E-06	0.28075	-10.12	0.08
Allanridge	AR199	2.68	3.68	0.27	0.009	0.28146	3.00E-06	0.28092	-4.88	0.11
	AR446	2.68	4.28	0.26	0.012	0.28140	6.00E-06	0.28095	-3.80	0.20
	AR451	2.68	3.57	0.22	0.013	0.28144	1.20E-05	0.28098	-2.80	0.42
	AR300	2.68	4.09	0.25	0.013	0.28135	3.00E-06	0.28091	-5.37	0.11
	AR305	2.68	3.86	0.26	0.015	0.28141	3.00E-06	0.28091	-5.49	0.10
	AR345	2.68	3.73	0.29	0.014	0.28142	2.00E-06	0.28086	-7.31	0.09
	AR364	2.68	3.86	0.27	0.010	0.28142	3.00E-06	0.28091	-5.32	0.12

Lu and Hf concentrations were determined by isotope dilution MC-ICP-MS. $^{176}Hf/^{177}Hf$ was normalized to $^{179}Hf/^{177}Hf$= 0.7325. Initial ε_{Hf} values were calculated at t (Ga) using $\lambda^{176}Lu = 1.867 \times 10^{-11}$ y^{-1} (Soderlund et al., 2004). CHUR values used are $^{176}Hf/^{177}Hf$= 0.282785 and $^{176}Hf/^{177}Hf$= 0.0336 from Bouvier et al. (2008).

Table 5. 3 Sm-Nd isotope composition of the Ventersdorp Supergroup lavas.

Formation	Sample	Age (Ga)	Nd (ppm)	Sm (ppm)	$^{147}Sm/^{144}Nd$	$^{143}Nd/^{144}Nd$	1SE	$^{143}Nd/^{144}Nd$ (t)	εNd (t)	1SE
Westonaria	R048	2.78	9.50	1.82	0.116	0.51118	3.00E-06	0.50905	0.64	0.06
	R141	2.78	14.16	2.90	0.124	0.51137	5.00E-06	0.50909	1.41	0.09
	R359	2.78	8.58	2.56	0.180	0.51226	3.00E-06	0.50895	-1.44	0.05
	R360	2.78	7.38	1.83	0.150	0.51184	3.00E-06	0.50909	1.36	0.06
	R362	2.78	8.39	1.94	0.140	0.51150	1.40E-05	0.50893	-1.72	0.27
	R434	2.78	16.14	3.32	0.124	0.51129	3.00E-06	0.50901	-0.25	0.05
	R432	2.78	27.81	5.33	0.116	0.51120	3.00E-06	0.50907	0.89	0.06
	R502	2.78	9.54	2.45	0.156	0.51193	2.00E-06	0.50907	0.92	0.05
	R503	2.78	5.99	1.93	0.195	0.51271	1.20E-05	0.50912	1.89	0.23
	R505	2.78	30.95	5.77	0.113	0.51120	2.00E-06	0.50913	2.16	0.03
	R506	2.78	15.51	3.18	0.124	0.51131	2.00E-06	0.50903	0.24	0.04
	R507	2.78	15.31	3.18	0.126	0.51136	3.00E-06	0.50905	0.62	0.05
	R508	2.78	19.10	3.95	0.125	0.51138	3.00E-06	0.50908	1.24	0.07
	R509	2.78	12.66	3.04	0.145	0.51165	2.00E-06	0.50897	-0.92	0.04
	R511	2.78	13.15	3.07	0.141	0.51158	2.00E-06	0.50898	-0.79	0.04
Alberton	LZ41	2.78	19.82	4.45	0.136	0.51153	1.00E-05	0.50903	0.17	0.19
	LZ31	2.78	15.91	3.62	0.138	0.51218	1.70E-04	0.50965		3.33
	R030	2.78	17.98	4.05	0.136	0.51151	3.00E-06	0.50900	-0.41	0.06
	R038	2.78	18.09	4.06	0.136	0.51154	2.00E-06	0.50905	0.53	0.04
	R040	2.78	19.60	4.31	0.133	0.51150	2.00E-06	0.50905	0.63	0.05
	R129	2.78	20.61	4.51	0.132	0.51148	2.00E-06	0.50905	0.62	0.05
	R134	2.78	21.06	4.57	0.131	0.51146	2.00E-06	0.50904	0.47	0.05
	R357	2.78	21.53	4.82	0.135	0.51150	5.00E-06	0.50901	-0.15	0.10
	R420	2.78	16.13	3.61	0.135	0.51150	6.00E-06	0.50901	-0.19	0.11
Orkney	LZ18	2.78	10.47	2.47	0.143	0.51164	2.50E-05	0.50902	-0.06	0.49
	LZ23	2.78	13.26	3.12	0.142	0.51163	8.00E-06	0.50902	-0.09	0.15
	LZ29	2.78	13.23	3.19	0.146	0.51169	4.00E-06	0.50901	-0.25	0.08
	R347	2.78	14.12	3.39	0.145	0.51170	4.00E-06	0.50903	0.22	0.07
	R005	2.78	12.13	2.84	0.141	0.51220	5.00E-06	0.50960		0.11
	R105	2.78	13.09	3.05	0.141	0.51163	3.00E-06	0.50905	0.50	0.05
	R333	2.78	12.37	3.02	0.148	0.51169	3.00E-06	0.50897	-0.96	0.06
	R335	2.78	14.04	3.25	0.140	0.51159	4.00E-06	0.50901	-0.19	0.08
Jeannette	R326	2.78	10.36	2.37	0.138	0.51157	1.00E-05	0.50902	0.07	0.19
	LZ17	2.78	8.53	2.06	0.146	0.51172	1.10E-05	0.50903	0.22	0.23
Loraine-Edenville	KL136	2.78	10.10	2.40	0.144	0.51172	3.00E-06	0.50907	1.06	0.07
	KL141	2.78	7.80	2.02	0.156	0.51186	5.00E-06	0.50899	-0.67	0.10
	KL142	2.78	8.30	2.08	0.151	0.51182	1.00E-05	0.50903	0.25	0.20
	KL145	2.78	7.81	1.89	0.146	0.51169	9.00E-06	0.50900	-0.32	0.18
	KL147	2.78	7.97	1.98	0.150	0.51176	5.00E-06	0.50899	-0.58	0.09
	KL150	2.78	10.16	2.40	0.143	0.51163	1.30E-05	0.50901	-0.26	0.25
	KL156	2.78	4.77	1.16	0.147	0.51173	7.00E-06	0.50902	0.03	0.14
	KL158	2.78	5.19	1.33	0.156	0.51182	4.00E-06	0.50896	-1.16	0.08
Goedgenoeg	PG166	2.72	59.97	11.20	0.113	0.51097	4.00E-06	0.50895	-3.14	0.59
	PG168	2.72	62.71	11.73	0.113	0.51098	2.00E-06	0.50895	-3.13	0.05
	PG163	2.72	61.08	11.39	0.113	0.51099	8.00E-06	0.50897	-2.78	0.15
	PG175	2.72	60.47	11.06	0.111	0.51089	4.00E-06	0.50890	-4.01	0.56
Rietgat	PR472	2.72	179.62	28.94	0.097	0.51073	2.00E-06	0.50898	-2.57	0.04
	PR487	2.72	69.16	12.62	0.110	0.51093	2.00E-06	0.50895	-3.08	0.04
	PR484	2.72	58.90	10.90	0.112	0.51098	8.00E-06	0.50897	-2.75	0.15
	PR182	2.72	50.56	9.13	0.109	0.51091	5.00E-06	0.50895	-3.05	0.10
	PR185	2.72	67.37	12.59	0.113	0.51095	4.00E-06	0.50892	-3.71	0.55
	PR189	2.72	72.10	13.21	0.111	0.51090	5.00E-06	0.50891	-3.89	0.71
Allanridge	AR199	2.68	26.41	5.55	0.127	0.51125	4.00E-06	0.50900	-3.09	0.09
	AR446	2.68	26.57	5.43	0.124	0.51119	3.00E-06	0.50900	-3.11	0.06
	AR451	2.68	20.40	4.13	0.122	0.51117	1.00E-05	0.50901	-2.96	0.20
	AR300	2.68	27.32	5.43	0.120	0.51113	3.00E-06	0.50901	-3.01	0.41
	AR305	2.68	26.13	5.24	0.121	0.51118	3.00E-06	0.50904	-2.45	0.41
	AR345	2.68	26.28	5.16	0.119	0.51110	4.00E-06	0.50900	-3.16	0.08
	AR364	2.68	27.64	5.64	0.123	0.51115	5.00E-06	0.50897	-3.74	0.66

Sm and Nd concentrations were determined by isotope dilution MC-ICP-MS. $^{143}Nd/^{144}Nd$ was normalized for mass fractionation to $^{146}Nd/^{144}Nd = 0.7219$. The initial ε_{Nd} values were calculated at t (Ga) using $\lambda^{147}Sm = 6.54 \times 10^{-12}$ y^{-1} (Begemann et al., 2001). CHUR values used are $^{143}Nd/^{144}Nd = 0.512638$.

Table 5. 4 Rb-Sr isotope composition of the Ventersdorp Supergroup lavas.

Formation	Sample	Age (Ga)	Sr (ppm)	Rb (ppm)	$^{87}Rb/^{86}Sr$	$^{87}Sr/^{86}Sr$	1SE	$^{87}Sr/^{86}Sr$ (t)	1SE
Westonaria	R048	2.78	48.62	0.09	0.005	0.71561	5.00E-06	0.71539	5.00E-06
	R141	2.78	100.05	0.59	0.017	0.71350	7.00E-06	0.71281	7.00E-06
	R359	2.78	27.29	2.27	0.241	0.72069	6.00E-06	0.71095	6.00E-06
	R360	2.78	34.82	1.72	0.143	0.71691	5.00E-06	0.71115	5.00E-06
	R362	2.78	42.15	1.06	0.072	0.70952		0.70659	1.30E-05
	R434	2.78	88.21	0.35	0.012	0.70759	4.00E-06	0.70713	4.00E-06
	R432	2.78	140.44	12.99	0.268	0.71085	4.00E-06	0.70005	4.00E-06
	R502	2.78	93.53	9.78	0.303	0.72312	3.00E-06	0.71089	3.00E-06
	R503	2.78	50.00	1.10	0.064	0.71892	4.00E-06	0.71636	4.00E-06
	R505	2.78	76.34	0.97	0.037	0.71043	1.20E-05	0.70894	1.20E-05
	R506	2.78	51.20	1.57	0.089	0.71791	5.00E-06	0.71433	5.00E-06
	R507	2.78	54.62	0.77	0.041	0.71770	3.00E-06	0.71605	3.00E-06
	R508	2.78	30.20	0.57	0.055	0.71738	8.00E-06	0.71518	8.00E-06
	R509	2.78	22.10	0.45	0.059	0.71688	5.00E-06	0.71449	5.00E-06
	R511	2.78	130.87	3.64	0.081	0.71714	3.00E-06	0.71389	3.00E-06
Alberton	LZ41	2.78	527.14	66.44	0.365	0.71479		0.70006	5.00E-06
	LZ31	2.78	366.17	24.57	0.194	0.70903		0.70119	6.00E-06
	R030	2.78	308.40	8.11	0.076	0.71508	5.00E-06	0.71201	5.00E-06
	R038	2.78	246.44	21.65	0.254	0.71150	3.00E-06	0.70124	3.00E-06
	R040	2.78	502.86	43.00	0.247	0.71189	3.00E-06	0.70190	3.00E-06
	R129	2.78	601.91	39.13	0.188	0.70953	3.00E-06	0.70194	3.00E-06
	R134	2.78	589.40	34.72	0.170	0.71097	3.00E-06	0.70409	3.00E-06
	R357	2.78	190.45	51.35	0.781	0.72540	5.00E-06	0.69386	5.00E-06
	R420	2.78	424.97	43.54	0.297	0.71444	4.00E-06	0.70247	4.00E-06
Orkney	LZ18	2.78	382.10	57.60	0.436	0.71619		0.69857	5.00E-06
	LZ23	2.78	335.44	101.86	0.881	0.73300		0.69744	8.00E-06
	LZ29	2.78	386.60	16.72	0.125	0.71151	2.00E-06	0.70646	
	R347	2.78	434.25	31.20	0.208	0.70948	3.00E-06	0.70109	3.00E-06
	R005	2.78	356.08	49.90	0.406	0.71768	3.00E-06	0.70130	3.00E-06
	R105	2.78	329.88	60.89	0.535	0.72103	3.00E-06	0.69945	3.00E-06
	R333	2.78	165.36	16.50	0.289	0.71135	3.00E-06	0.69970	
	R335	2.78	325.96	88.33	0.785	0.72846	4.00E-06	0.69675	
Jeannette	R326	2.78	278.80	81.14	0.843	0.72846	5.00E-06	0.69441	5.00E-06
	LZ17	2.78	241.89	45.99	0.551	0.71890		0.69667	1.40E-05
Lora-Eden	KL136	2.78	588.34	61.09	0.301	0.71539	4.00E-06	0.70326	
	KL141	2.78	317.59	78.60	0.717	0.72758	4.00E-06	0.69862	
	KL142	2.78	230.96	21.18	0.265	0.71296		0.70224	8.00E-06
	KL145	2.78	277.42	83.72	0.875	0.73015		0.69483	5.00E-06
	KL147	2.78	50.61	38.53	2.214	0.76073	5.00E-06		
	KL150	2.78	276.72	44.48	0.466	0.71858		0.69979	7.00E-06
	KL153	2.78	150.02	61.27	1.185	0.73520	8.00E-06		
	KL155	2.78	402.53	50.77	0.365	0.71438	3.00E-06	0.69965	
	KL156	2.78	215.07	11.42	0.154	0.70872	8.00E-06	0.70252	8.00E-06
	KL158	2.72	126.39	9.01	0.206	0.70992	4.00E-06	0.70160	
Goedgenoeg	PG166	2.72	444.66	13.04	0.085	0.70558	3.00E-06	0.70224	3.00E-06
	PG168	2.72	493.98	20.93	0.123	0.70636	4.00E-06	0.70154	4.00E-06
	PG163	2.72	402.25	24.75	0.178	0.70844		0.70143	9.00E-06
	PG175	2.72	292.54	43.81	0.433	0.71558	3.00E-06	0.69851	3.00E-06
Rietgat	PR472	2.72	332.51	63.12	0.550	0.72208	4.00E-06	0.70043	
	PR487	2.72	954.03	41.18	0.125	0.70561	3.00E-06	0.70070	3.00E-06
	PR484	2.72	540.32	53.43	0.286	0.71279		0.70152	6.00E-06
	PR182	2.72	385.09	24.48	0.184	0.70885	2.00E-06	0.70161	
	PR185	2.72	706.95	12.52	0.051	0.70459	4.00E-06	0.70257	4.00E-06
	PR189	2.72	805.88	2.99	0.011	0.70393	3.00E-06	0.70351	3.00E-06
Allanridge	AR199	2.68	1470.45	38.72	0.076	0.70560	4.00E-06	0.70265	4.00E-06
	AR446	2.68	402.28	36.75	0.264	0.71080	5.00E-06	0.70055	5.00E-06
	AR451	2.68	457.47	50.43	0.319	0.71281		0.70044	5.00E-06
	AR300	2.68	65.87	63.73	2.818	0.78039	4.00E-06	0.67108	4.00E-06
	AR305	2.68	50.85	30.23	1.727	0.75134	4.00E-06	0.68435	4.00E-06
	AR345	2.68	490.99	16.83	0.099	0.70653	3.00E-06	0.70269	3.00E-06
	AR364	2.68	615.37	29.43	0.138	0.70709	4.00E-06	0.70173	4.00E-06

Rb and Sr concentrations were determined by isotope dilution MC-ICP-MS. Initial $^{87}Sr/^{86}Sr$ values were calculated at t (Ga) using $\lambda^{87}Rb = 1.42 \times 10^{-11}\ y^{-1}$ (Steiger & Jager, 1977).

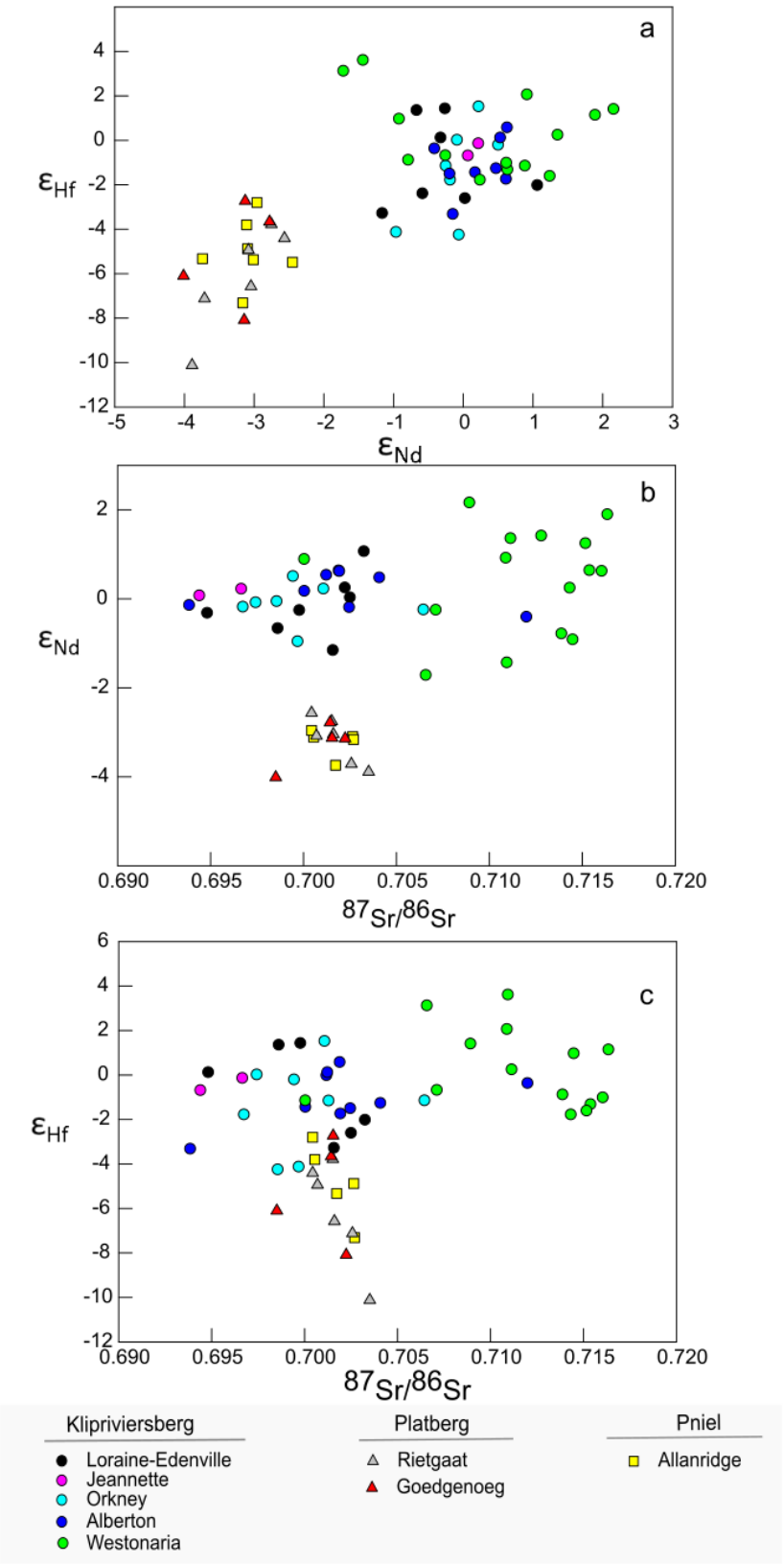

Figure 5. 7 Radiogenic isotope compositions of the Ventersdorp Supergroup lavas at 2.7 Ga (a) ε_{Nd} versus $^{87}Sr/^{86}Sr$, b) ε_{Nd} versus ε_{Hf} and c) ε_{Hf} versus $^{87}Sr/^{86}Sr$). The Klipriviersberg samples show overlapping compositions for Hf and Nd, and large differences in the Sr compositions. The Klipriviersberg Group lavas have depleted mantle-like compositions. The Platberg Group and Allanridge lavas have more enriched isotopic compositions.

5.3 Discussion

5.3.1 Ventersdorp magmatic events

The lavas of the Ventersdorp Supergroup have previously been regarded as a single large igneous province that was formed in less than 10 million years. However, recent geochronological studies by Gumsley et al. (2020) have shown that the Ventersdorp Supergroup is comprised of at least two LIPs – the 2.79-2.78 Ga Klipriviersberg LIP and the 2.71-2.68 Ga Allanridge LIP, which are both separated by the 2.75-2.71 Ga Platberg volcanic province. These age constraints have strengthened the concept of multiple igneous provinces in the Ventersdorp Supergroup that have been based on lithostratigraphy studies as well as previously published dates (Wingate, 1988; Klausen et al., 2010; Cornell et al. 2017; Gumsley et al., 2020).

Ernst (2014) discriminated LIPs from non-LIPs based on their (i) volume, (ii) areal extent, (iii) duration, (iv) nature of magmatism, and (v) tectonic setting. The first two mentioned criteria (i and ii) have been set to a minimum of 0.1 million km^3 and 0.1 million km^2 to meet the definition of a LIP (Ernst, 2014). The next two criteria (iii and iv) require the determination of precise ages to understand the age and rate of magmatic emplacement, with LIPs being emplaced in less than 10 million years. Taking the above-mentioned criteria and the new dates into consideration, the Ventersdorp Supergroup can be subdivided into at least two substantial LIPs. The genetic linkage between the disparate magmatic events of the Ventersdorp Supergroup is considered in this study.

The Klipriviersberg flood basalts cover an area of at least 20 000 km^2 (this is the present-day coverage excluding the estimated sub-surface areal extent) and are ~2 km thick (van der Westhuizen et al., 1991, 2006). Their volume, and the angular unconformity between the Klipriviersberg Group and the Platberg Group, suggest to us that the Klipriviersberg Group is a single LIP.

The 2.75 – 2.71 Ga Platberg Group volcanics comprise the Goedgenoeg and Makwassie felsic lavas (~1.8 km) and the Rietgat mafic-intermediate lavas (~1.3 km) as well as interbedded lavas in the graben sedimentary rocks of the Kameeldoorns Formation. The dominance of mafic igneous rocks is the basis for a LIP definition and mantle-melting origin, although, *sensu*

stricto LIPs are also associated with dominant silicic components (Ernst, 2014). Taking the volume and intraplate setting of the Platberg volcanics into consideration, the Platberg Group can be considered as its own LIP – a Silicic Large Igneous Province (SLIP) with subordinate basaltic Rietgat lavas. Silicic LIPs are one of the continental LIP varieties (Ernst, 2014). The Platberg silicic LIP occurred over a long interval of 40 million years. This implies that the Ventersdorp Supergroup comprises three LIPs – 2 Continental Flood Basalts Provinces and 1 Silicic Large Igneous Province.

The Allanridge Formation of the Pniel Group at the top of the Ventersdorp Supergroup covers an area of over 200 000 km^2 and it is 1km thick (Gumsley et al., 2020). The Allanridge Formation can also be regarded as a single LIP. The Allanridge lavas have been age constrained between 2.71 and 2.68 Ga using the dates from the Makwassie Formation as the upper limit (2.71 Ga: Klausen et al., 2010; Olsson et al., 2010; Cornell et al., 2017). Gumsley et al. (2020) also suggested the possibility of the Platberg lavas being part of a combined Platberg-Allanridge LIP. However, the age (2.71 Ga) used to constrain the Allanridge Formation is doubtful as the lavas are only linked to the 2.70-2.68 Ga Rykoppies Dyke Swarm, the 2.66-2.65 Ga White Mfolozi Dyke Swarm, and the 2.66 Ga lavas of the Buffelsfontein Formation (Allanridge Formation correlative). Therefore, there is a 10 million-year gap that suggests the Platberg and the Allanridge volcanism are separate magmatic events. This is supported by the unconformity between the Platberg Group and the Pniel Group, indicating a time gap between the two magmatic events. Dating of the uppermost unit of the Platberg Group, the Rietgat Formation, will better constrain the timing of the Platberg Group and the Pniel Group (i.e., the onset of the Allanridge LIP).

5.3.2 Alteration of the lavas

The Ventersdorp Supergroup lavas are 2.7 billion years old and show evidence of multiple secondary processes, such as the 2.0 Ga Kaapvaal Craton-wide metamorphic event in Duane et al. (2004) and the Limpopo orogeny. The effects of alteration and metamorphism on the isotopic compositions of the Ventersdorp lavas are investigated before we use these data to constrain the magma source(s).

The wide range of initial $^{87}Sr/^{86}Sr$ isotopic compositions of the Klipriviersberg Group lavas suggests there is a disturbance of the Rb-Sr isotope system, possibly by hydrothermal fluids

that percolated through the lavas, which may have caused the loss and/or gain of radiogenic Sr. Evidence of hydrothermal fluids passing through the lavas include (i) calcite-chlorite and chlorite-quartz veins as well as (ii) epidote-quartz amygdales (Figs. A2.2 and A2.3 and A2.4). The addition of Rb due to its high mobility lowered the initial $^{87}Sr/^{86}Sr$ below ~0.700 (Fig. 5.8a). Alteration processes readily mobilize Rb which affects the Rb/Sr ratios and the initial $^{87}Sr/^{86}Sr$ ratios. Removal of Rb from a system will result in lower Rb/Sr ratios and higher initial $^{87}Sr/^{86}Sr$ ratios; whereas addition of Rb will cause higher Rb/Sr ratios, resulting in lower initial $^{87}Sr/^{86}Sr$ ratios (Fig. 5.8a). The loss of Rb resulted in the higher initial $^{87}Sr/^{86}Sr$ ratios of the Westonaria lavas. Carbonic (CO_2-rich) fluids and silicic fluids that exploited the rift- and graben-faults of the Ventersdorp basin altered the lavas, and the carbonic fluids might have formed REE complexes, as they have the ability to mobilize the REE (Lahaye et al., 1995). Therefore, the effect of element mobility by the fluids on the bulk isotope systems should be considered when interpreting the Sm-Nd and Lu-Hf isotopic compositions in terms of the composition of the mantle source.

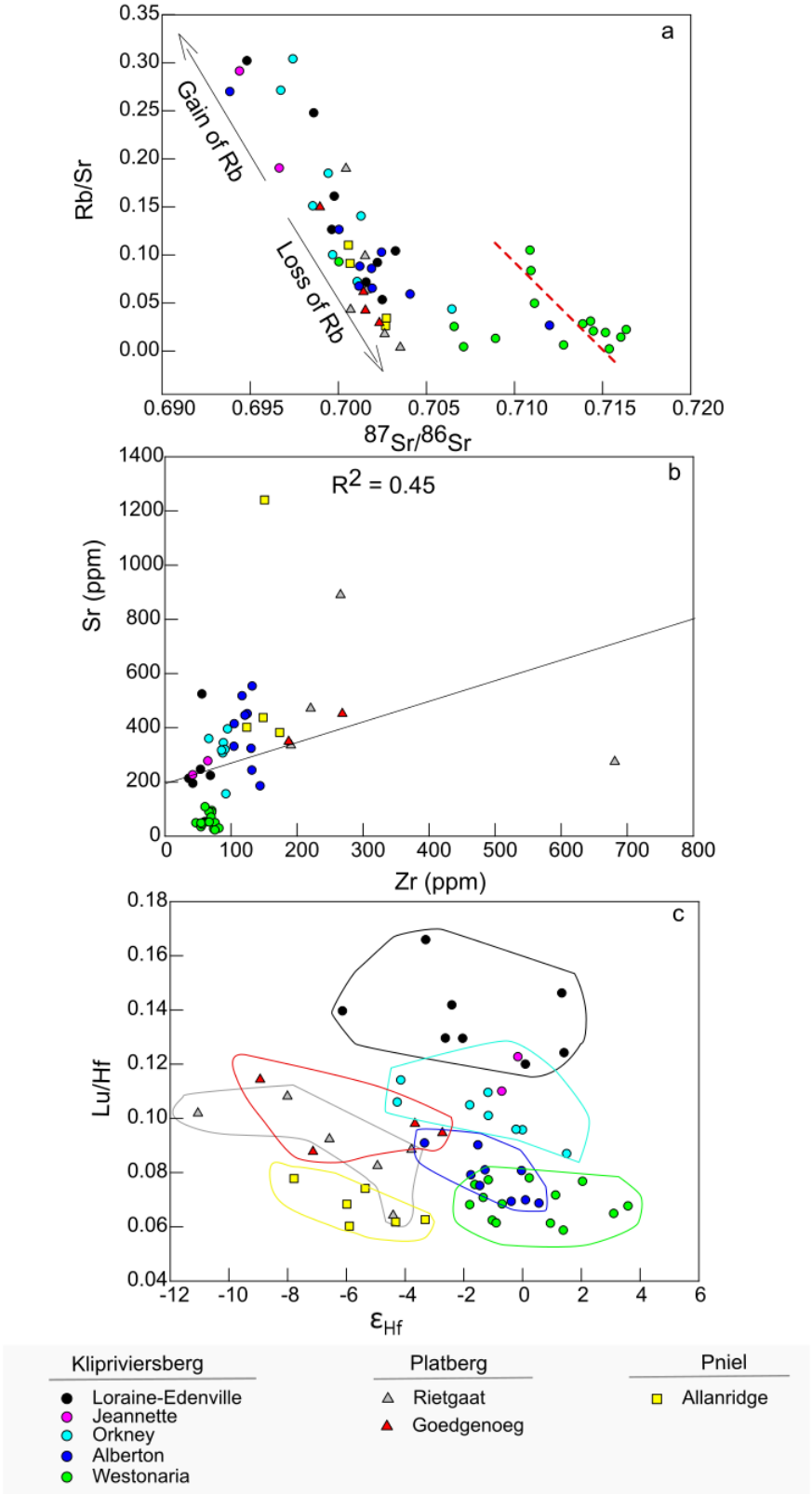

Figure 5. 8 a) Rb/Sr versus $^{87}Sr/^{86}Sr$ shows the effect of the hydrothermal alteration on the Sr isotope compositions. The addition of Rb in the lavas resulted in lower initial isotope ratios and the loss of Rb resulted in higher ratios. b) Sr versus Zr (immobile element) shows the mobility of Sr with a poor correlation with Zr. c) Lu/Hf versus ε_{Hf} plot shows the minimal effect of alteration on the Hf composition. The alteration did not homogenise the composition of the lavas.

Khumalo et al. (Chapter 4) proposed that carbonates in the overlying 2.5-2.3 Ga Transvaal Supergroup were the potential source for the carbonic fluids. Duane et al. (2004) determined a 2.0 Ga craton-wide metamorphic event (thermal and hydrothermal) to have metamorphosed and altered the Ventersdorp Supergroup lavas. The alteration possibly contributed to the formation of the Pb-Zn deposits in the Allanridge Formation with the hydrothermal fluids sourcing these metals from the Makwassie Quartz Porphyry (Whitelaw, 1998; Duane et al., 2004). The presence of actinolite, epidote, pumpellyite and quartz in the Klipriviersberg Group basalts indicates prehnite-pumpellyite to greenschist metamorphic conditions (Chapter 4). The different isotopic compositions between the stratigraphic units of the Ventersdorp Supergroup indicate small-scale modification of the Sm-Nd and Lu-Hf isotopic systems as opposed to a large-scale modification that would have homogenized the isotopic compositions. Therefore, it is assumed that any disturbance in the isotopic systems happened at a small scale and that samples still possess isotopic compositions that allow constraints to be placed on the petrogenesis of the Ventersdorp Supergroup. This certainly applies to the Sm-Nd and the Lu-Hf systems as the conditions (<400 °C) of the greenschist metamorphism would only significantly affect the Rb-Sr system (Scherer et al., 2000). Khumalo et al. (Chapter 4) show that the Sm-Nd system was less disturbed compared to the Rb-Sr system, and that the Lu-Hf system remained robust in the komatiitic Westonaria lavas. This is seen in the wide range in the initial $^{87}Sr/^{86}Sr$ compositions and the relatively narrow range of ε_{Nd} and ε_{Hf} values of the Ventersdorp lavas. The scatter in K, Rb, Ba and Sr within individual formations indicate the mobilization of these elements, and this is evident because of the poor correlation between Sr and Zr (Fig. 5.8b). The LREE compositions of the Westonaria lavas show that the mobilization of LREE and the disturbance of the Rb-Sr isotopic system was more enhanced in the Westonaria lavas than in the other overlying formations. This is evident from the wide range (scattering) of the Westonaria LREE compositions, which overlap with the other Klipriviersberg lavas, instead of exhibiting the narrow range or uniform compositions typically expected for unaltered lavas observed in other formations (Fig. 5.5). In addition, the Westonaria lavas have large negative anomalies of readily mobilized elements such as K, Ba, Rb and Sr (Fig. 5.6). The plot of Lu/Hf versus ε_{Hf} better discriminates the Formations indicating that the alteration effect on the HREE and Lu-Hf isotope system was minimal (Fig. 5.8c). This testifies to the reliability of the isotopes used in our work and the effectiveness of using the three isotope systems with different strengths against alteration

and metamorphism (Lu-Hf > Sm-Nd > Rb-Sr). Despite the secondary processes discussed in this section, the effects of the alteration and metamorphism were not significant except for the Rb-Sr isotopic system. In addition, the Lu-Hf and Sm-Nd isotopic systems are robust and can be used to infer the mantle sources of the lavas in the Ventersdorp Supergroup.

5.3.3 Mantle source(s) and the contamination history of lavas in the Ventersdorp Supergroup

The Nd-Hf isotopes show different sources and petrogenetic processes for the three provinces of the Ventersdorp Supergroup. The isotope signatures indicate that the magma source of the Klipriviersberg LIP was the depleted mantle (Fig. 5.9a). The basal komatiitic lavas of the Westonaria Formation have depleted initial ε_{Nd} of +2.2 and ε_{Hf} of +3.6; the rest of the Klipriviersberg lavas have similarly depleted compositions of ε_{Nd} of +1.06 (Loraine-Edenville picritic basalt) and ε_{Hf} of +1.51 (Orkney basalt).

The Westonaria komatiites contain evidence for the influence of asthenospheric mantle in their genesis; whereas the rest of the Klipriviersberg lavas show lithospheric mantle influence or interaction with subduction-modified mantle (Fig. 5.9b). The negative Nb-Ta anomalies in the Klipriviersberg lavas also indicates that their depleted mantle source was influenced by subduction or inherited subduction signatures (Fig. 5.6a). The Westonaria Formation has weak negative Nb-Ta anomalies indicating the minimal influence of the lithosphere in the source (possibly a mantle plume) during Westonaria komatiitic magmatism. Komatiites or high-temperature magmas are the first products of mantle plumes and in the case of the Klipriviersberg mantle plume, the Westonaria komatiites were extruded prior to the extensive interaction (contamination) of the mantle plume with the lithosphere mantle.

The 2.75-2.71 Ga Platberg SLIP and the 2.70-2.68 Ga Allanridge LIP possess uniform enriched isotopic signatures that indicate magma derivation from enriched sources. They also have uniform Hf isotopic compositions that are similar to those of the more enriched Klipriviersberg lavas. The enriched isotope signatures and silicic nature of the Platberg volcanics can be explained by the derivation of magmas from the enriched mantle and lower crustal sources. The lavas show strong negative Nb-Ta-Ti anomalies that suggest the derivation of magmas from a mantle that was strongly influenced by earlier subduction of crustal components.

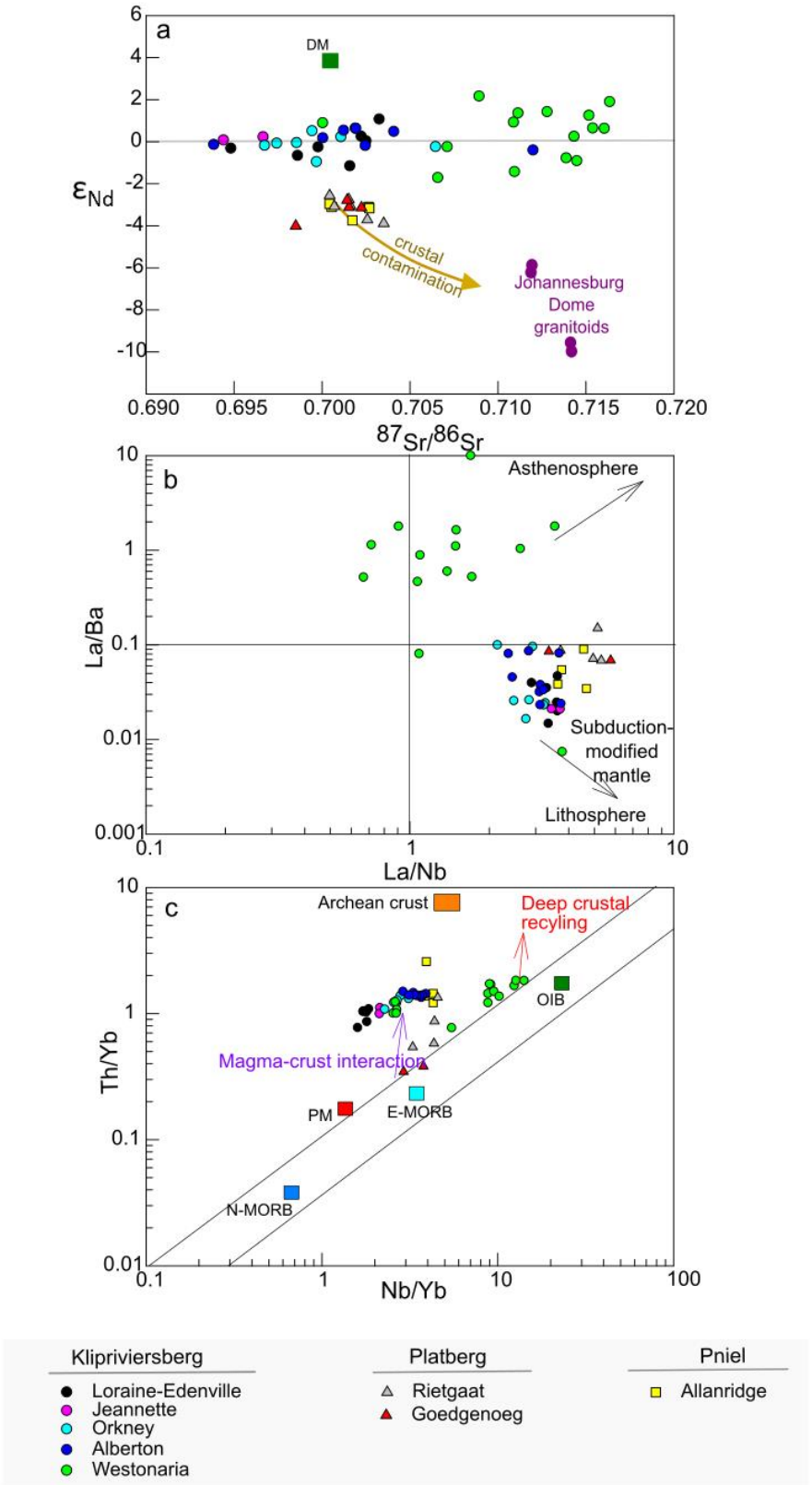

Figure 5. 9 Initial Nd-Sr isotope plot showing a wide range of initial Sr isotope compositions as a result of alteration. The isotope compositions of the Platberg Group and Allanridge Formation indicate possible crustal contamination by the Johannesburg Dome granitoids. b) La/Ba versus La/Nb (Saunders et al., 1992) shows the asthenospheric influence on the Westonaria magmas whereas the rest of the Ventersdorp magmas indicates the influence of lithospheric mantle that was modified by subducted components. c) Th/Yb versus Nb/Yb plot (Pearce, 2008) shows the influence of crustal recycling in the Westonaria magmas and the interaction of the magmas of the rest of the Ventersdorp magmas with the crust.

All of the lavas of the Ventersdorp LIPs plot above the OIB-MORB array on the Th/Yb-Nb/Yb plot of Pearce (2008), similar to other CFBs, indicating the interaction of the magmas with lithospheric components (Fig. 5.9c). The komatiitic Westonaria Formation plots closely to the OIB-MORB array compared to the other Formations, which suggests that the Westonaria magmas had minimal interaction with enriched lithosphere that would have dragged their compositions towards the crustal compositions, hence having the most depleted isotopic signatures. However, the Westonaria lavas have similar REE patterns to the rest of the Klipriviersberg lavas that were derived from a depleted source that had been influenced by a lithospheric mantle and lower crust as evident from the Th/Yb-Nb/Yb ratios. The disconnect between the isotopic compositions and REE patterns could be a result of the evident alteration and metamorphic event(s) that could have selectively modified the REEs and isotopic compositions. This modifies the distribution and concentrations of the REEs as well as the isotopic compositions of the lavas. As a result, the observed REE patterns may not accurately represent their primary compositions, as suggested in chapter 4 for the Westonaria lavas. Similarly, the isotopic compositions, which are indicative of the mantle source, may have also undergone modifications due to mobilisation of certain isotopes during the secondary processes. Consequently, the REEs and isotopes of the lavas may record distinct events or processes undergone by the lavas. Therefore, the REE patterns might provide insights into the effects of alteration and/ or metamorphism on the elemental composition of the lavas, while the isotopic compositions can still reflect the primary mantle source signatures. The interaction of the Klipriviersberg lavas with the lithospheric mantle and the lower crust is also evident on the isotope plots where the Klipriviersberg lavas plot towards the lower crust composition (Fig. 5.9a). Crustal input is evident in the trace elements (REE, Th/Yb, Nb/Yb) of the Platberg SLIP and Allanridge LIP lavas. The lavas show an array on the Th/Yb-Nb/Yb plot above the OIB-MORB array towards the upper crustal composition indicating magma-crust interaction. A contamination array is observed for the Platberg SLIP and Allanridge LIP magmas on the isotope plots where the lavas form an array towards the upper crust composition. Isotopic and MgO-SiO_2 compositions of the Ventersdorp lavas show changes in the influence of the lithospheric mantle and crust between the three Ventersdorp LIPs (Fig. 5.10). A crustal contamination array is observed from the least contaminated Klipriviersberg lavas to the Platberg and Allanridge lavas on the plots of ε_{Hf} and ε_{Nd} against MgO and SiO_2 (Fig. 5.10). While this can show varying degrees of contamination between the

3 LIPs, it is suggested that some of the SiO_2 in the lavas is due to post-magmatic processes that might have introduced additional SiO_2 in the lavas.

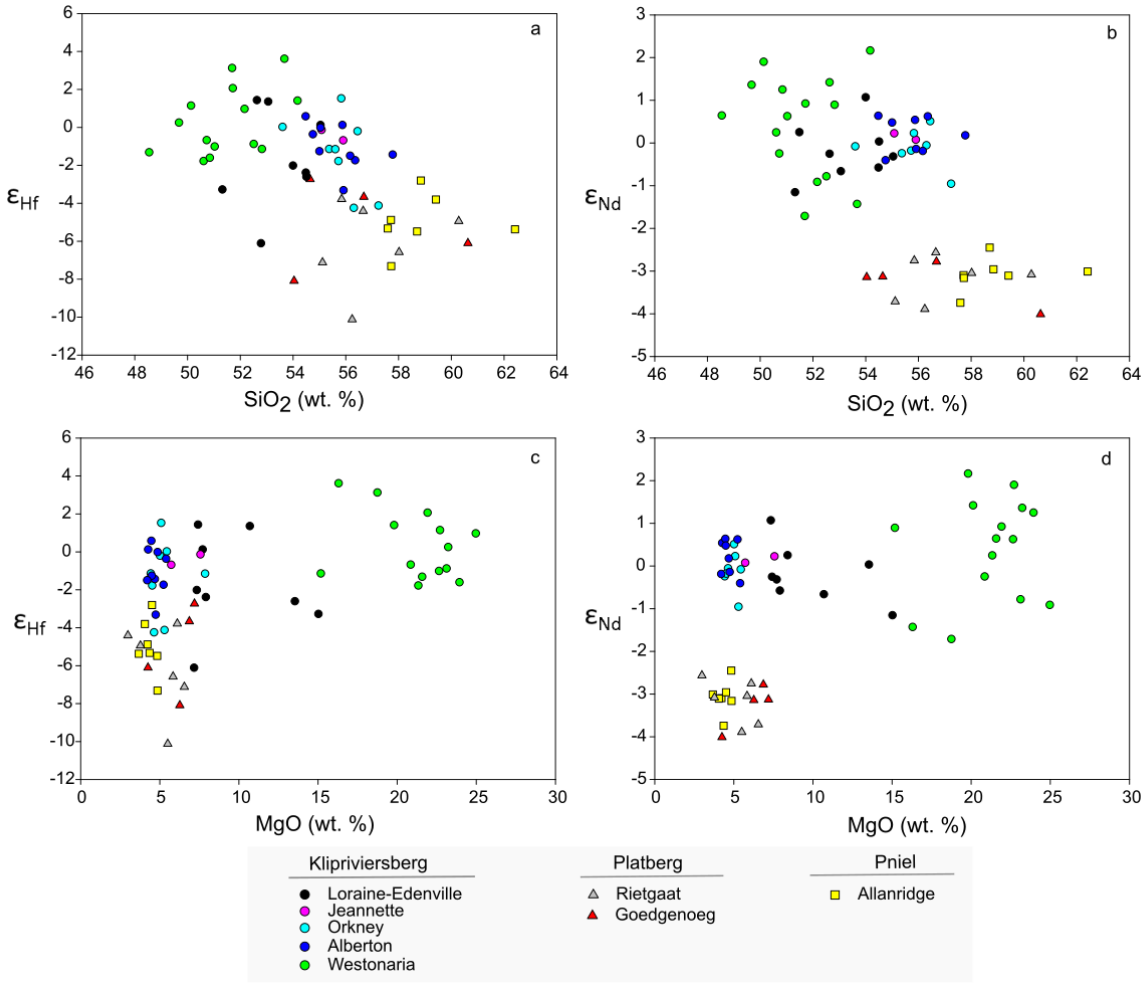

Figure 5. 10 Plots of Nd-Hf isotope compositions versus MgO and SiO_2 showing the evolution of the Ventersdorp Supergroup magmas by lithospheric mantle and crustal contamination. Poor correlation for the Klipriviersberg Group lavas suggest that there was minor crustal contamination.

5.3.4 Petrogenetic evolution of the Ventersdorp LIPs

The petrogenesis of the Ventersdorp magmas can be explained by batch partial melting of different sources. The partial melting of a sublithospheric mantle plume produced the magmas of the Klipriviersberg LIP. The first products were the komatiitic magmas of the Westonaria Formation that do not show significant contamination either by lithospheric mantle or continental crust. The clustering of the major and trace elements of the Westonaria lavas from the rest of the Klipriviersberg lavas suggests differences in the production of the magmas. This further suggests the evolution of the source in terms of its composition or

different source(s) for the rest of the Klipriviersberg magmas. The occurrence of the Westonaria komatiitic lavas at the base, the overlying evolved basalts, and the less evolved picritc-basalts of the Loraine-Edenville Formations at the top of the Klipriviersberg LIP can be explained as follows:

1) Production of komatiitic lavas in a sublithospheric mantle plume and extrusion on the Kaapvaal Craton to form the basal volcanic unit.

2) Progressive interaction of the sublithospheric mantle plume with the subduction-modified SCLM and production of the basalts, explaining the negative Nb-Ta anomalies in the basalts.

3) Initial basaltic magmas interacted with enriched contaminants during ascent, therefore, becoming more evolved and having enriched isotopic compositions.

4) The less evolved basalts (Orkney, Jeanette and Loraine-Edenville Formations) are because of the decrease in the interaction of the magmas with contaminants, possibly because of the casing of conduit walls by precursor magmas such as the Alberton magmas.

The silicic Platberg volcanics may be explained by partial melting of the enriched lower crust by heat from underplating sublithospheric mantle material. The Platberg SLIP contains the basaltic andesites of the Goedgenoeg and Rietgat Formations that have enriched mantle isotopic compositions and are strongly enriched in incompatible elements (REE). The rhyolitic lavas of the Makwassie Formation are between the Goedgenoeg and Rietgat Formations. The production of the Platberg magmas can be explained by the partial melting of the enriched lithospheric mantle (possibly the mantle that interacted with the Klipriviersberg magma source), and subsequent crustal contamination during their ascent. This was followed by partial melting of the lower crust to produce the Makwassie felsic magmas (ε_{Nd} = -3 to -6: Walraven et al., 1991; Nelson et al., 1992) that were significantly contaminated by the upper crust. Re-melting of the Goedgenoeg magma source (enriched lithospheric mantle) produced the Rietgat magmas that were also contaminated by the crust.

The Allanridge lavas have enriched isotopic compositions that are similar to the Platberg basaltic lavas, however, they have major and trace element compositions that are between the mafic Klipriviersberg and silicic Platberg lavas. They also overlap with the most evolved

lavas of the Klipriviersberg LIP (the Alberton lavas). Considering the (i) isotopic and trace element compositions presented in this study, and the (ii) occurrence of rare komatiitic basalts at the base of the formation reported in van der Westhuizen et al. (2006), the Allanridge can be explained by the re-melting of underplated mantle material with enriched compositions due to the interaction with enriched lithospheric material. In such settings, the silicic and mafic magmas are expected to have similar isotopic signatures as observed for the Platberg lavas (Goedgenoeg and Rietgat Formations) and the Allanridge lavas.

5.3.5 Implications for Vaalbara supercraton

It has been proposed that the Ventersdorp Supergroup on the Kaapvaal Craton and the Fortescue Group on the Pilbara Craton are correlatives (de Kock et al., 2009, 2012; Gumsley, 2017). Lithostratigraphy, geochemistry, geochronology and paleomagnetic evidence have been provided to support the concept that the two cratons were once adjoined during the formation of the two Neoarchean volcano-sedimentary sequences – the Vaalbara supercraton (Wingate, 1988; Nelson et al., 1992; de Kock et al., 2009, 2012; Kampmann et al., 2015; Gumsley, 2017). We compare our new Sm-Nd isotopic results of the Ventersdorp Supergroup lavas (because of the lack of Lu-Hf isotope data of Fortescue Group) to published Sm-Nd isotope data of the Fortescue lavas as well as to the correlatives lavas on the Kaapvaal Craton (Fig. 5.11). The volcanics of the Fortescue Group have uniform Sm-Nd isotopic compositions throughout the whole stratigraphy except for the Pyradie komatiites that have depleted Nd isotope compositions, whereas there is a clear ε_{Nd} distinction between the older Klipriviersberg LIP and the younger Platberg and Allanridge LIPs of the Ventersdorp Supergroup. The 2.78 Ga Klipriviersberg basalts on the Kaapvaal Craton have similar ε_{Nd} compositions to the 2.72 Ga Pyradie komatiites on the Pilbara Craton. The Platberg Group and the Pniel Group of the Ventersdorp Supergroup have similar enriched ε_{Nd} compositions to their proposed equivalents of the Fortescue Group. The differences in the Sm-Nd isotopic compositions of the Klipriviersberg lavas and the Mount Roe basalts do not support the Vaalbara theory, unless there was a large variation in the contamination of the primary komatiitic magmas across the Vaalbara craton, where the magmas ascending through the Kaapvaal section were least contaminated compared to their equivalents ascending through the Pilbara section, and/or they were contaminated by different contaminants. In addition,

we propose that the Klipriviersberg komatiitic magmas were contaminated by enriched lithospheric mantle, whereas the Fortescue komatiitic magmas were contaminated by crustal components. Another critical issue is that the Pyradie komatiites are stratigraphically higher than the Mount Roe lavas, which are correlated with the Klipriviersberg lavas as opposed to the Westonaria komatiites that occur at the base of the Ventersdorp Supergroup. However, despite the 60 Myr gap, these komatiites are Al-depleted, enriched in incompatible elements, enriched in SiO_2, and have depleted Nd isotopic compositions. In addition to the Vaalbara debate, the new dates of the Usushwana Complex (2989 ± 1 Ma, 2990 ± 2 Ma, 2978 ± 2 Ma) on the Kaapvaal Craton no longer correlate with its proposed equivalent, the 2860 ± 20 Ma Millindinna Complex, on the Pilbara Craton (Schmidt and Embleton,1985; Gumsley et al., 2015). These new dates do not support the existence of the Vaalbara supercraton during the formation of the Usushwana and Millindinna Complexes.

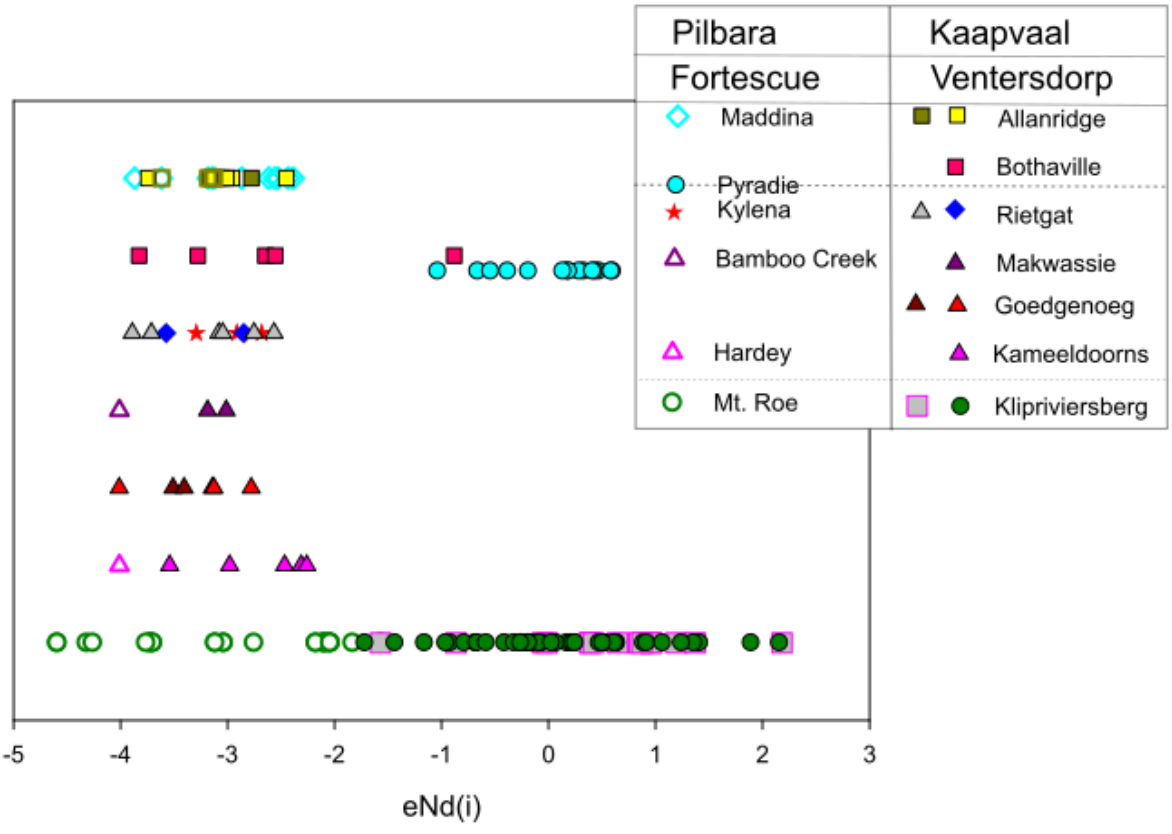

Figure 5. 11 Nd isotopic compositions of the Ventersdorp lavas and Fortescue lavas as well as of the correlatives lavas on the Kaapvaal craton. The plot shows that the Klipriviersberg Group and the proposed equivalent, the Mount Roe, on the Pilbara craton possess different Nd isotopic signatures. However, the rest of both sequences have uniform isotopic signatures except for the Pyradie komatiites. The data for the correlatives are from Walraven et al. (1991), Marsh et al. (1992), Nelson et al. (1992), Scheinderhan et al. (2011), Altermann and Lenhardt (2012) and Mole et al. (2018).

5.4 Conclusion

The Ventersdorp Supergroup comprises three distinct large igneous provinces that include the 2.79-2.78 Ga Klipriviersberg LIP at the base, 2.75-2.71 Ga Platberg SLIP in the middle and the 2.70-2.68 Allanridge LIP at the top. Our Sr-Nd-Hf isotope data in combination with trace element data show that the magmas of the Ventersdorp Supergroup were derived from different sources – depleted and enriched mantle sources. We show that the Klipriviersberg LIP magmas were derived from a depleted mantle source, and the Platberg SLIP and the Allanridge LIP were derived from enriched sources. The geochemistry of the Klipriviersberg LIP indicates the production of the Westonaria komatiitic magmas in a sublithospheric mantle source before the significant interaction with a subduction-modified lithospheric mantle during the production of the rest of the Klipriviersberg LIP magmas. The production of the Platberg SLIP magmas is explained by the melting of enriched lithospheric mantle together with the lower crust. The isotopic geochemistry of the Allanridge LIP indicates its production from a mantle source with enriched isotopic compositions to explain the komatiitic basalts reported at the base of the lava sequence. The magmas of the Klipriviersberg LIP, Platberg SLIP and Allanridge LIP were contaminated by different contaminants to different extents. A comparison of the Nd isotopic compositions of the Ventersdorp lavas to the Fortescue lavas shows the contrast between the Klipriviersberg lavas on the Kaapvaal Craton and the Fortescue lavas on the Pilbara Craton. This finding does not support the concept of the Vaalbara supercraton during the magmatism of the Klipriviersberg LIP.

Chapter 6: Ni-PGE and multiple sulphur isotope compositions of the Klipriviersberg Large Igneous Province, Ventersdorp Supergroup, South Africa

Khulekani B. Khumalo, Lewis D. Ashwal & Ben Hayes

The manuscript is to be submitted in 2023 to a journal.

Contributions:

Khulekani Khumalo: Conceptualised the study; wrote the manuscript and conducted the petrographic analysis.

Lewis Ashwal: Conceptualised the study and reviewed the manuscript drafts.

Ben Hayes: Conceptualised the study; reviewed and edited manuscript drafts.

Please note that the detailed geological background and methodology sections are excluded from this manuscript chapter and are presented in Chapters 2 and 3.

6.1 Introduction

Magmatism of large igneous provinces (LIP) involves enormous amounts of energy and ore metals that can either form primary or secondary ore deposits. The deposits that are related to LIP events can be (i) hosted by the LIPs (orthomagmatic), (ii) concentrated by LIPs that provide the heat, driving the hydrothermal systems or source of the metals or structural and barriers for metal collection, (iii) weathering products of LIPs (Ernst & Jowitt, 2013). Knowledge of how ore deposits are linked to LIPs has crucial implications on exploring for deposits (Schulz et al., 2010). Reconstruction of previously connected crustal blocks that are mineralized is another way of exploration of ore deposits using LIPs (Ernst & Jowitt, 2013). Ore deposits studies have shown a temporal and spatial linkage between LIPs and kimberlites (diamonds), carbonatites (Nb-Ta-REE-P), Ni-Cu-PGE, Fe-Ti-V and Cr deposits (Naldrett et al., 1992; Torsvik et al., 2010; Schulz et al., 2010; Dobretsov et al., 2012; Ernst & Jowitt, 2013). The majority of mineralization is in the vicinity of the plume centre, which is related to the high-temperature centres and greater volumes where there are higher chances of sulphur saturation (Naldrett et al., 1992). The heat brought by LIPs drives the mobilization of metals within LIPs or host rocks to form ore deposits (e.g., copper and gold).

Platinum group elements (PGE: Pt, Pd, Rh, Ir, Ru and Os) are siderophile and chalcophile elements that are subdivided into chalcophile Palladium group (Pd-PGE: Pd, Pt and Rh) and siderophile Iridium group (Ir-PGE: Ir, Os and Ru) based on their physical and chemical behaviour (Barnes et al., 1985; Tredoux et al., 1995). The elements are useful for understanding the early Earth differentiation, mantle heterogeneity, core-mantle interaction and origin of mantle magmas (Maier et al., 2009; Ma et al., 2009; Mondal, 2011). These elements have economic benefits as well (Naldrett et al., 1992). The PGE concentrate more in mafic-ultramafic igneous rocks and are mostly hosted in sulphides (Maier, 2005). Due to their high affinity for metal phases than silicate phases, the PGEs are thought to have partitioned into the core during the core-mantle formation (Mondal, 2011).

Maier et al. (2009) showed that most early Archean komatiites are relatively depleted in PGE compared to late Archean and younger komatiites, suggesting a change in the mantle PGE through the Archean. However, the late Archean Westonaria komatiites and early Archean Komati komatiites on the Kaapvaal Craton have similar PGE concentrations (Maier et al.,

2003). The PGE concentrations in the Archean mantle and their behaviour during magmatic processes remain controversial and less well constrained (Maier et al., 2003; Mondal, 2011). However, due to their chalcophile and siderophile nature, the concentration of PGE in igneous rocks are controlled by sulphide minerals in the mantle during partial melting (Maier et al., 2003; Maier & Barnes, 2004). Therefore, the concentrations of PGE in igneous rocks are dependent on the nature of the source rocks (depleted or enriched in PGE), the degree of partial melting of the source, and the sulphur saturation of the magma. However, it has also been suggested that other non-sulphide phases host PGE in the mantle (Barnes & Picard, 1993; Maier et al., 2003; Maier & Barnes, 2004).

Platinum group elements (PGE) are associated with magmatic events - for example, the Bushveld LIP – and are sourced from the mantle from which the magmas are derived. PGE studies on komatiites have shown that a significant number of the high-MgO lavas have low PGE contents leading to the conclusion that the Archean mantle was PGE-depleted or the PGE were not evenly distributed in the mantle (Maier et al., 2003; Waterton et al., 2021). An isolated PGE-enriched source that remained untapped during the Archean has been also proposed and suggested to have mixed at the end of the Archean and post-Archean (Maier et al., 2009; Waterton et al., 2021). Sulphide retention in the mantle source during partial melting is also proposed in explaining the PGE depletion of the komatiites (Barnes & Picard, 2003; Maier et al., 2003; Maier & Barnes, 2004). Waterton et al. (2021) attributed the low PGE contents of the 1.9 Ga Winnipegosis komatiites of Canada to moderate degrees and depth of partial melting of the source, rather than a PGE-depleted source, arguing against a temporal change in the PGE contents of komatiites. This is in agreement with Maier et al. (2003), who reported similar PGE contents in the 3.5 Ga Komati komatiites and 2.7 Ga Westonaria komatiites. In addition to different mantle sources and different degrees of partial melting, other controls of PGE contents in lavas are sulphide segregation in the magmas on their way to the surface and/or during emplacement as well as crystal fractionation (Barnes & Picard; 1993; Maier et al., 2003). The formation of magmatic PGE deposits requires the magma to reach sulphur saturation, separation and concentration of PGE-rich sulphide liquid (Ripley & Li, 2003). The sulphur saturation has been shown by sulphur isotope data to be attained through contamination – the addition of external sulphur from country rocks and/ or xenoliths (Ripley & Li, 2003; Smith et al., 2016). It has been demonstrated that sulphur

isotopes are useful indicators of crustal sulphur input and are applicable to understanding the ore-forming processes of magmatic PGE deposits (Keays & Lightfoot, 2010; Smith et al., 2016). However, Seat et al. (2009) propose that sulphur from the mantle can be sufficient to promote ore formation. In addition, fractional crystallization and mixing of magmas are also possible mechanisms for achieving sulphur saturation (Ripley & Li, 2003). In addition to sulphide saturation, the sulphide concentration should be economic, which depends on the magma volume, rate, and duration of magmatism (Ripley & Li, 2003). Keays (1995) reports that most komatiites remain sulphur undersaturated during their ascent and emplacement and that they are useful in understanding the roles of silicate and oxide phases on PGE fractionation. There are no known magmatic economic deposits of the large igneous provinces of the Ventersdorp Supergroup. The Westonaria komatiites together with the basalts of the rest of the Klipriviersberg LIP present an opportunity to study the PGE fractionation in both the komatiites and basalts.

In this study, we report Ni-Cu-PGE concentrations in 32 samples, and multiple sulphur isotope compositions of 21 samples of the Klipriviersberg LIP. The research aims to assess the possibility of sulphide segregation from the magmas of the Klipriviersberg LIP during their ascent as this might imply a possible PGE ore deposit in the subsurface. In addition to sulphur isotopes, we also apply stable (O) and radiogenic isotope (Sr-Nd-Hf) compositions to assess the role of contamination in the PGE concentrations of the LIP.

6.2 Geological background

The 2.7 Ga Ventersdorp Supergroup consists of the volcanic Klipriviersberg LIP, the Platberg silicic LIP and the Allanridge LIP (Fig. 6.1: Chapter 5). The volcanic formations of the Klipriversberg LIP (2.78 -2.75 Ga) are the Westonaria, Alberton, Orkney, Jeanette and Loraine-Edenville Formations. The Westonaria Formation occurs at the base consisting of komatiites, overlying the Ventersdorp Contact Reef (VCR) at its contact with the gold-rich Witwatersrand Supergroup (van der Westhuizen et al., 2006). The rest of the Klipriviersberg LIP consists of mafic flood basalts. The group unconformably underlies the Platberg Group made up of mafic-felsic lavas and clastic-chemical sediments (van der Westhuizen et al., 2006). The Pniel Group consists of the Bothaville sediments and Allanridge lavas (van der Westhuizen et al., 2006). Numerous intrusions in the Witwatersrand Supergroup are also reported to form part of the

plumbing system that fed the Klipriviersberg and Allanridge lavas (Harris & Watkins, 1990; McCarthy et al., 1990; Olsson et al., 2010; Klausen et al., 2010; Gumsley, 2017; Gumsley et al., 2020). The Allanridge Formation hosts Pb-Zn mineralization in amygdales and breccia zones in the southwestern part of the Ventersdorp basin (Whitelaw, 1998). Please refer to Chapter 2 for the detailed geological background.

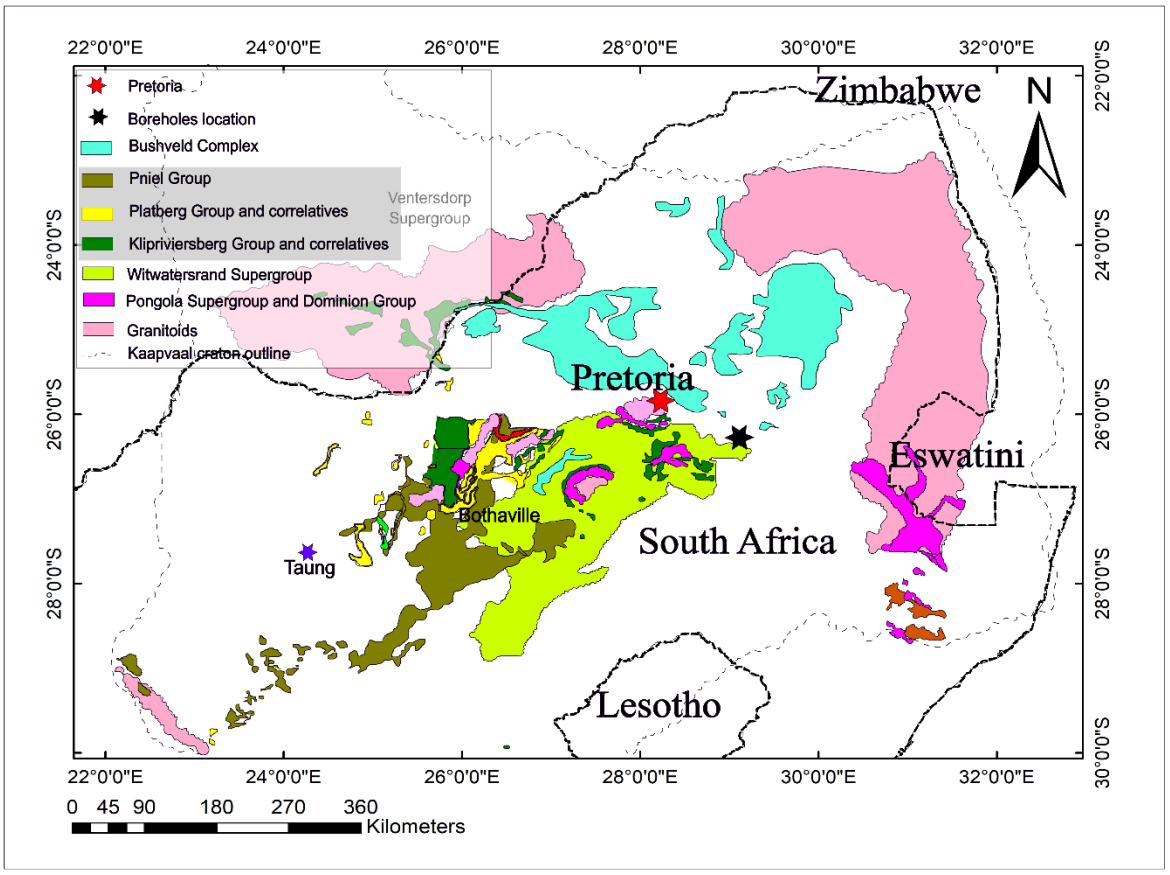

Figure 6. 1 Simplified geological map showing the surface distribution of the groups of the Ventersdorp Supergroup and their equivalents on the Kaapvaal craton (modified after Gumsley et al., 2017). It also shows the possible areal extent of the lavas. The stratigraphy of the volcano-sedimentary sequence is shown on the right. The location of the sample boreholes is shown as the black star.

6.3 Results

The petrographic analysis of the Klipriviersberg lavas using reflected light shows that the sulphide phases are associated with secondary features such as veins and amygdales (Fig. 6.2) The observed sulphides include chalcopyrite, pyrite (solid and sieve forms) and pyrrhotite that

is associated with chalcopyrite. In some samples, an overgrowth of chalcopyrite is observed around pyrite (Fig. 6.2c).

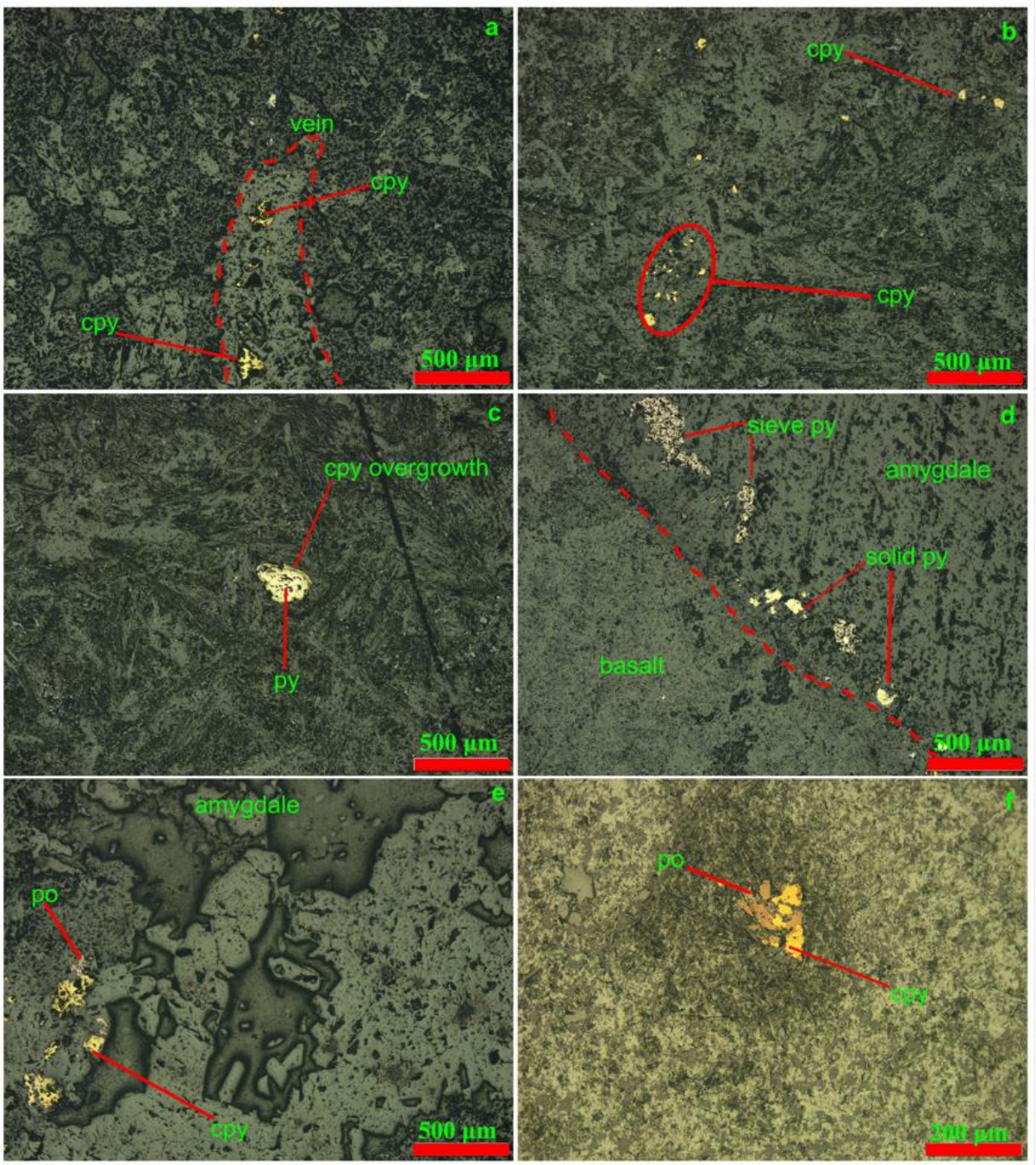

Figure 6. 2 Reflected light photographs of sulphides minerals in the Klipriviersberg lavas. (a) chalcopyrite hosted in silicate vein. (b) and (c) chalcopyrite and pyrite specks in the spinifex zone of the Westonaria komatiites, (c) pyrite grain with an overgrowth rim of chalcopyrite. (d) sieve pyrite and solid pyrite along the boundary of an amygdale in the basalt. (e) pyrrhotite and chalcopyrite in a quartz-epidote filled amygdale of the Alberton Formation basalt. (f) pyrrhotite and chalcopyrite in the porphyritic zone of the Westonaria komatiites. Py = pyrite, cpy = chalcopyrite and po = pyrrhotite.

The PGE concentrations of the Klipriviersberg LIP are presented in Table 6.1. The plots of PGEs against MgO, Cr and Ni show clear differences between the Ir-PGEs and Pd-PGEs, and a clear grouping of the Westonaria komatiites from the basalts of the rest of the Klipriviersberg LIP (Fig. 6.3 and Fig. 6.4). The distinct trends of the Ir-PGEs and Pd-PGEs show overall positive trends for the Ir-PGEs for the Klipriviersberg LIP. The komatiites show a positive trend for the Pd-PGE and Cr, although they show a slight negative trend for Ni. The rest of the Klipriviersberg LIP basalts show uniform concentrations for the Ir-PGEs (vary within 0.5 ppb) forming a plot cluster (e.g., Ir versus Ni) and slight linear trends (e.g., Ru versus Cr). The basalts have a broader range in their Pd-PGEs concentration and narrower ranges for Cr and Ni concentrations compared to the Westonaria komatiites. The basalts clearly form their own positive trend for the Pd-PGEs, separate from the komatiites trend. The Pd-PGE concentrations increase up the stratigraphy from the evolved Alberton basalts to the Loraine-Edenville picritic basalts. The Westonaria komatiites have relatively lower Pd-PGE concentration and higher Ir-PGE concentrations than the basalts.

Table 6. 1 Ni-Cu-PGE concentrations in the lavas of the Klipriviersberg LIP.

Formation	Sample	Ni	Cu	Ru	Rh	Pd	Os	Ir	Pt	Au	Pt/Pd	Pd/Ir	Cu/Pd	Ni/Cu
Westonaria	R432	n.a	n.a	0.50	0.35	2.61	0.26	<Lod	2.96	1.14	1.13			
	R434	1051.93	263.35	1.66	0.44	2.55	0.71	0.70	2.65	6.13	1.04	3.62	103.18	3.99
	R502	866.91	84.05	1.41	0.50	4.82	1.29	0.67	4.58	0.61	0.95	7.18	17.42	10.31
	R503	1280.43	70.82	2.54	0.63	4.11	3.27	1.40	4.67	1.00	1.14	2.92	17.25	18.08
	R505	940.76	177.31	2.00	0.51	2.78	1.88	0.91	2.56	0.97	0.92	3.05	63.86	5.31
	R506	999.97	178.44	1.93	0.49	3.54	2.05	0.88	2.39	1.18	0.68	4.03	50.39	5.60
	R507	939.07	154.43	2.08	0.54	2.87	2.00	1.00	4.16	0.58	1.45	2.87	53.88	6.08
	R508	968.55	244.11	1.80	0.51	3.01	1.43	0.88	2.78	1.12	0.92	3.44	81.02	3.97
	R511	1031.48	193.02	2.21	0.54	2.41	1.65	1.03	2.61	0.64	1.08	2.34	80.19	5.34
	R360	1508.81	212.36	2.59	0.51	4.47	3.65	1.64	3.54	1.33	0.79	2.73	47.46	7.11
	R141	1010.72	186.42	2.06	0.48	2.56	2.42	0.95	2.58	1.08	1.01	2.71	72.86	5.42
	R048	1343.28	306.62	1.58	0.30	1.78	1.44	0.82	1.54	3.12	0.87	2.18	171.81	4.38
Alberton	R030	141.89	131.35	<Lod	<Lod	0.62	0.57	0.04	1.50	0.75	2.43	16.12	212.79	1.08
	R040	129.74	169.61	0.20	0.38	5.72	0.34	0.12	5.60	2.19	0.98	46.80	29.63	0.76
	R129	143.16	152.48	<Lod	<Lod	1.23	0.22	0.04	1.59	0.57	1.29	27.37	124.14	0.94
	R134	125.29	112.84	0.15	0.34	6.29	0.27	0.10	4.93	0.69	0.78	61.22	17.93	1.11
	R420	127.81	154.52	0.30	0.57	6.69	0.33	0.08	6.33	0.98	0.95	83.70	23.09	0.83
	LZ31	137.61	200.42	0.20	0.50	7.72	0.42	0.06	6.35	1.72	0.82	121.95	25.96	0.69
	LZ41	131.17	114.11	0.14	0.28	5.00	0.42	0.11	4.73	1.25	0.95	45.73	22.81	1.15
Orkney	LZ18	209.32	99.63	0.39	0.65	7.19	0.27	0.09	5.67	1.08	0.79	78.83	13.87	2.10
	LZ29	123.07	119.09	<Lod	0.36	8.59	0.17	<Lod	5.16	1.20	0.60		13.86	1.03
	R005	n.a	n.a	<Lod	0.26	11.67	0.14	0.04	10.10	1.04	0.87	280.67		
	R105	103.16	108.82	<Lod	<Lod	0.47	0.26	<Lod	0.41	0.47	0.87		231.52	0.95
	R335	100.98	121.67	<Lod	<Lod	<Lod	0.24	<Lod	0.51	0.58				0.83
	R347	128.43	178.78	0.18	0.50	10.57	0.19	0.04	6.78	1.02	0.64	272.80	16.92	0.72
Jeannette	LZ17	286.03	103.39	1.28	2.03	10.69	0.37	0.31	9.35	1.18	0.87	34.36	9.68	2.77
	R326	133.01	85.41	0.22	0.40	10.57	0.35	0.03	7.49	1.82	0.71	347.70	8.08	1.56
	KL136	189.79	92.90	0.41	1.05	12.54	0.26	<Lod	10.02	0.75	0.80		7.41	2.04
	KL142	202.18	90.58	0.39	0.97	13.01	0.22	0.03	14.80	1.24	1.14	435.10	6.96	2.23
	KL147	187.14	86.05	0.28	0.54	10.57	0.26	0.06	11.25	0.75	1.07	163.07	8.14	2.17
	KL150	189.81	65.40	0.32	0.75	12.04	0.31	0.07	11.91	0.44	0.99	166.85	5.43	2.90
	KL153	n.a	n.a	0.26	0.43	10.76	0.24	0.04	7.45	2.79	0.69	240.90		
Allanridge	AR345	144.73	64.87	0.16	0.72	6.68	0.29	0.09	6.44	<Lod	0.96	72.45	9.72	2.23

Ni and Cu are in ppm. The PGE-Au are in ppb. The major elements and trace elements of the samples are presented in Chapter 5. n.a = not analysed. <Lod = below the limit of detection

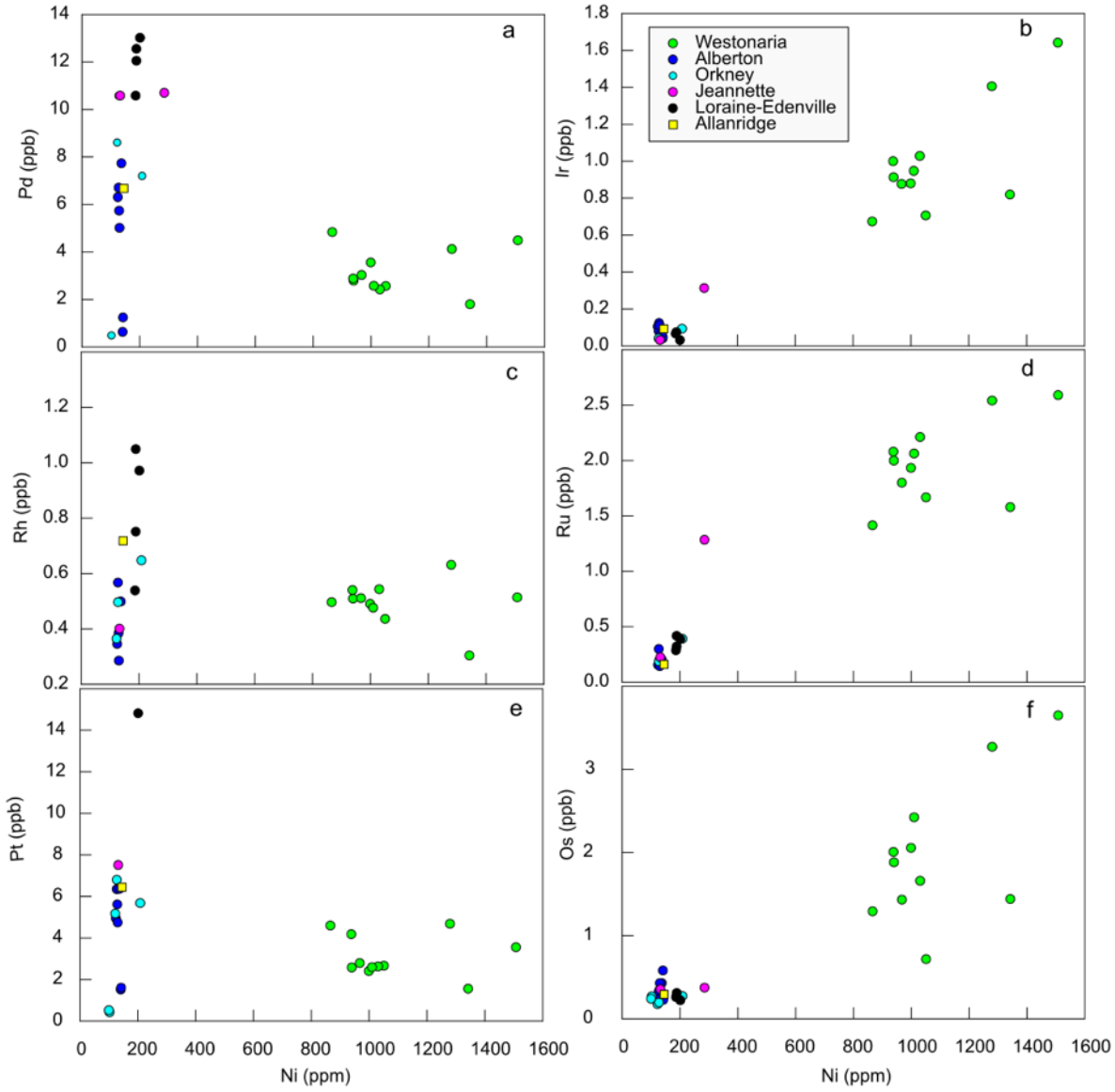

Figure 6. 3 Variation plots of PGE versus Ni. The Westonaria Formation shows different variations for the Ir-PGE and Pd-PGE compared to the rest of the Klipriviersberg lavas.

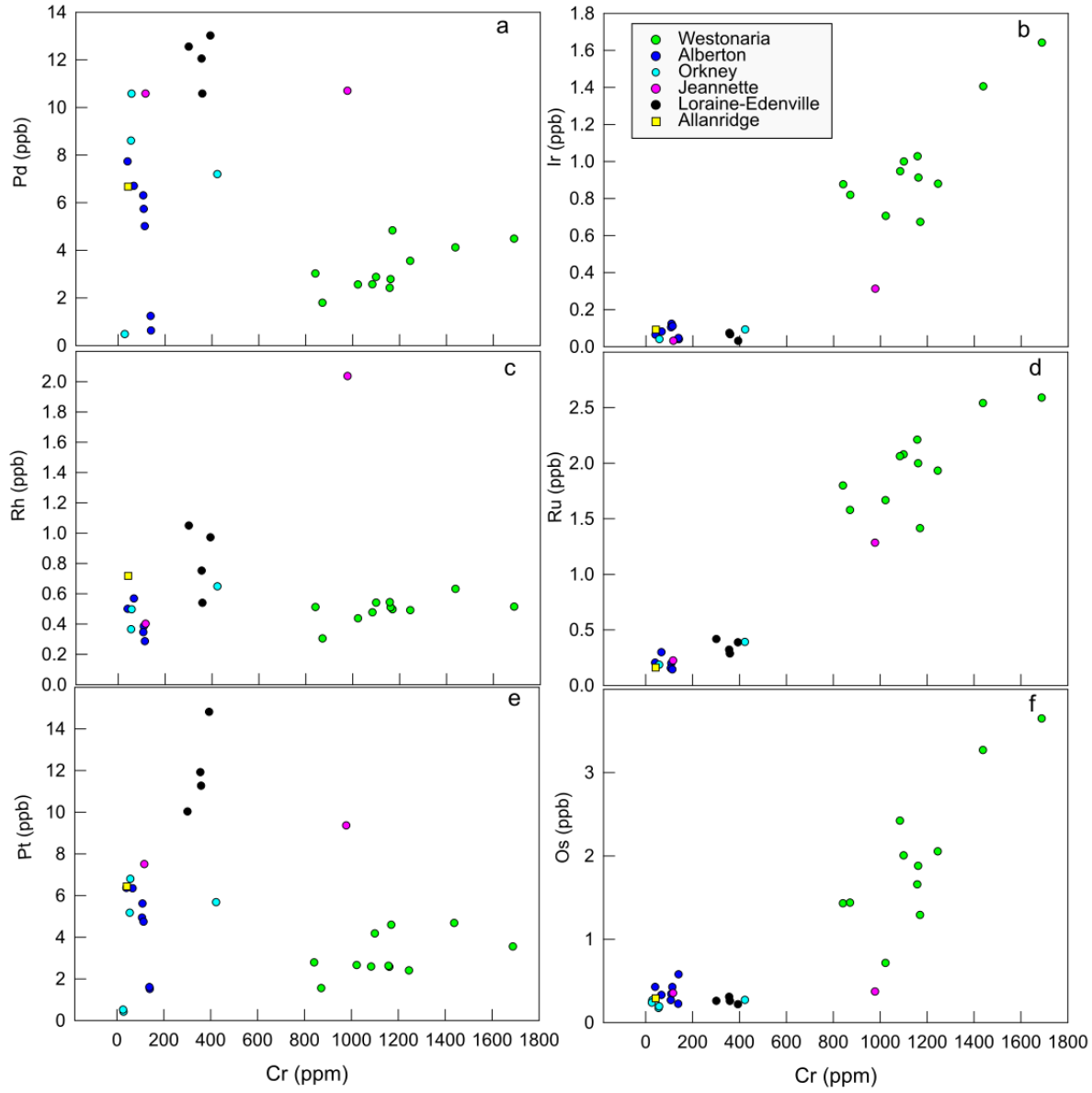

Figure 6. 4 Variation plots of PGE versus Cr. Similar observations to Ni variation are made for Cr. The Westonaria Formation shows different variations for the Ir-PGE and Pd-PGE compared to the rest of the Klipriviersberg lavas.

The basalts have uniform Ir-PGE concentrations over variable MgO content, and the komatiites show a poor positive trend (Fig. 6.5). An opposite observation is made for the Pd-PGEs where the basalts display moderate positive trends and also form a scattered cluster for the komatiites. The Westonaria komatiites display a vertical scatter of Cu concentration over four wt.% of MgO (Fig. 6.5h). The basalts display a negative trend with high Cu concentration (65 – 200 ppm) in the evolved Alberton basalts and low Cu concentrations in the Loraine-Edenville picritic basalts (Fig. 6.5h). There is an overall negative trend of Cu and Pd, with a decrease in the Pd concentrations up the stratigraphy (Fig. 6.6a). However, the Westonaria komatiites display a negative trend, whereas the individual basalt Formations of the rest of the Klipriviersberg LIP display positive trends. The Ir shows a negative trend against Cu for the Westonaria komatiites and a relatively horizontal trend for the basalts (Fig. 6.6b). Primitive-mantle normalized Ni-Cu-PGE patterns of the Klipriviersberg LIP lavas show positively inclined patterns (Fig. 6.7). The Westonaria komatiites show a gently inclined pattern, whereas the basalts show a steeply inclined pattern. The komatiites are a bit depleted in the Ni-PGE relative to the primitive mantle, except for Ru. The Au and Cu are a bit enriched for the komatiites relative to the primitive mantle. They display strong negative Ir and positive Ru anomalies as well as weak negative Pt anomalies for some of the samples. The basalts also display strong negative Ir and Au anomalies. They show more depletion in Ni-(Ir-PGE) than the Westonaria komatiites.

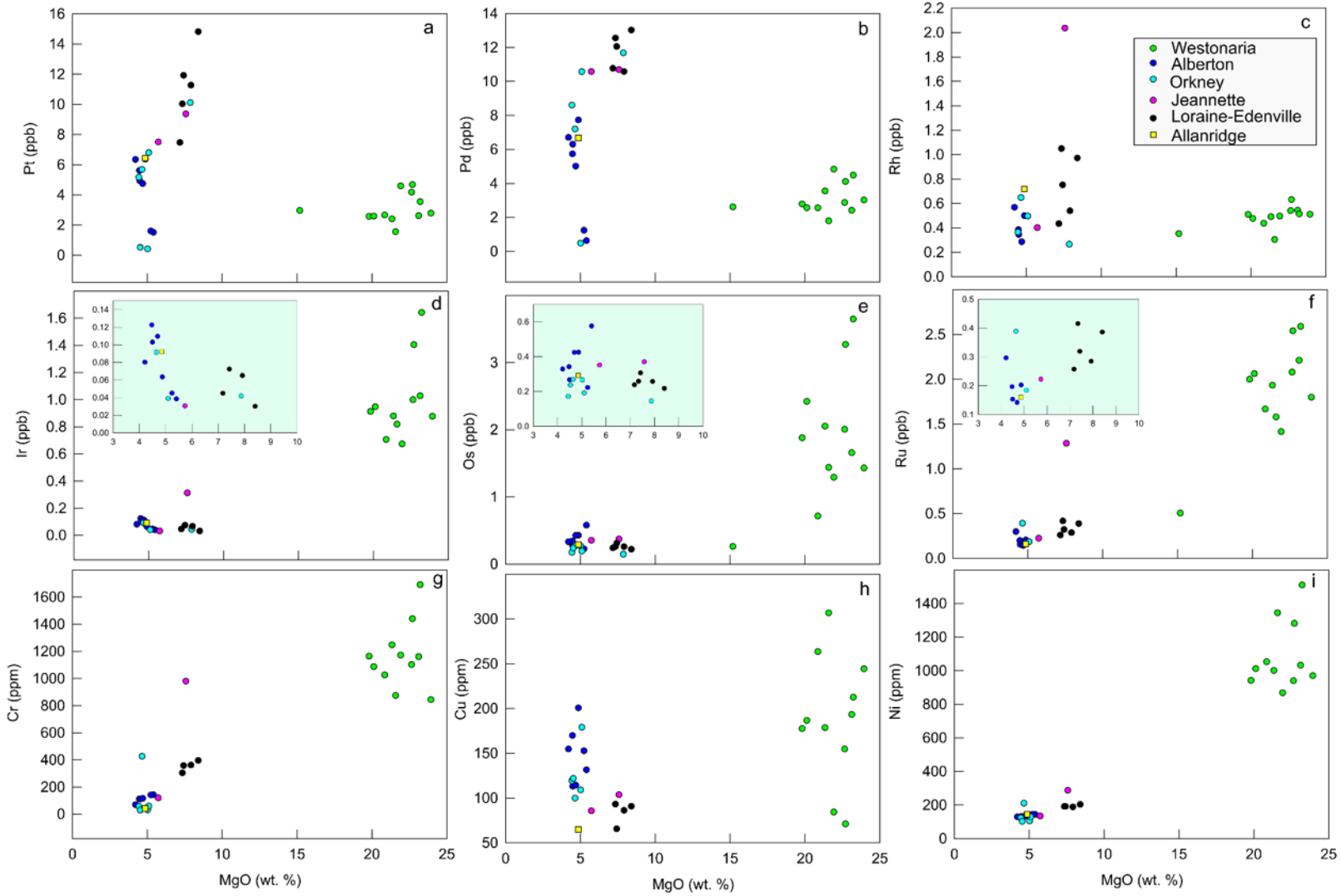

Figure 6. 5 Variations of (a-f) PGE, (g) Cr, (h) Cu and (i) Ni versus MgO. The inset plots in (d), (e) and (f) show variations between the basalts of the Klipriviersberg LIP.

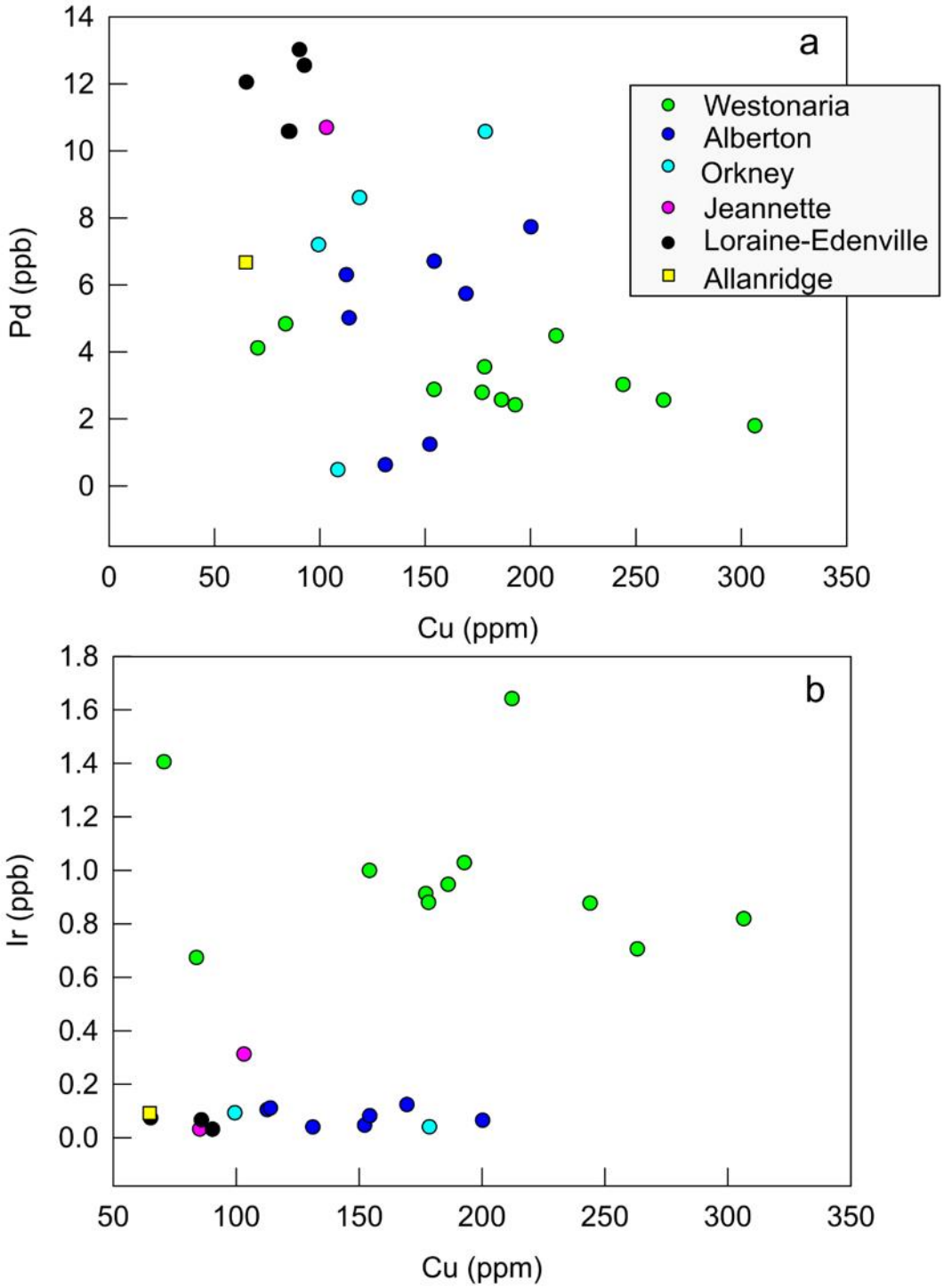

Figure 6. 6 Plots of Cu against (a) Pd and (b) Ir displaying different behaviour between the Ir-PGE and Pd-PGE.

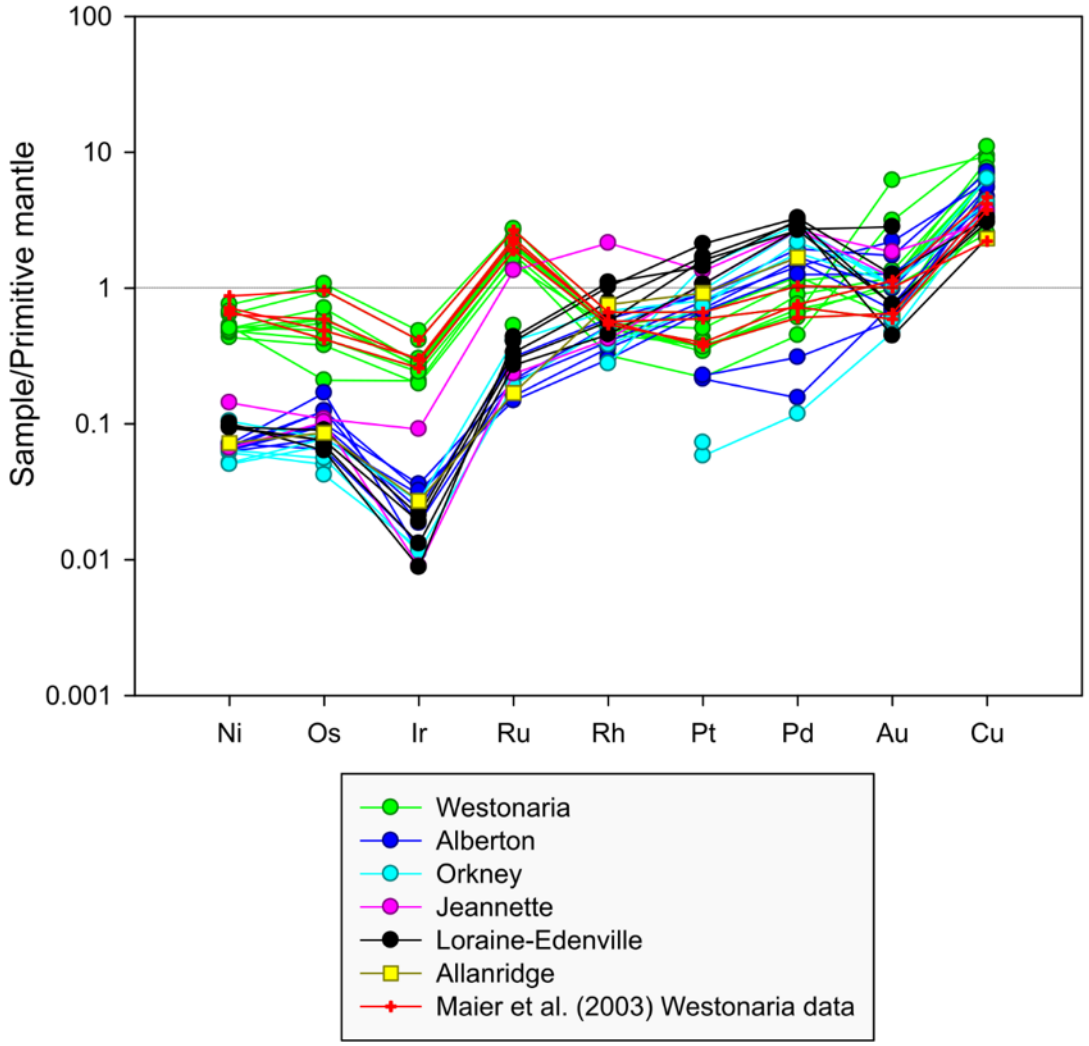

Figure 6. 7 Primitive-mantle normalised PGE patterns showing two different patterns between the komatiites and the associated basalts of the Klipriviersberg LIP. The red and black symbols are the komatiites from the Westonaria Formation. The normalising vales are from Barnes and Maier (1999).

The $\delta^{34}S$, $\Delta^{33}S$ and $\Delta^{36}S$ values of the samples range from -1.704 to +0.492 ‰, -0.225 to -0.004 ‰, and -0.352 to +0.119 ‰ (Fig. 6.8 and Table 6.2). The sulphur isotope compositions vary according to the Formations. The Westonaria komatiites have the most negative $\Delta^{33}S$, overlapping with the Loraine-Edenville basalts. The evolved Alberton basalts have the least negative $\Delta^{33}S$ with near-zero $\Delta^{33}S$ and $\delta^{34}S$ values. The Westonaria komatiites cover wider ranges for $\delta^{34}S$ (-1.704 to +0.492 ‰) and $\Delta^{36}S$ (-0.352 to +0.061 ‰), overlapping with the rest of the Formations.

Table 6. 2 Multiple sulphur isotope compositions of the Kliprivіersberg LIP.

Name	$\delta^{34}S$ cdt (‰)	$\Delta^{33}S$ cdt (‰)	$\Delta^{36}S$ cdt (‰)	Comment
KL142	-1.163	-0.114	-0.095	
KL150	-1.093	-0.167	0.119	
LZ17 2	-1.152	-0.034	-0.151	Replicate
LZ17	-1.154	-0.051	-0.134	Replicate
R005	-0.582	-0.022	-0.157	
R030	0.003	-0.002	-0.244	
R040	0.062	-0.007	-0.181	
R048	-0.959	-0.155	-0.267	
R105	-1.340	-0.004	-0.190	
R129	-0.244	-0.022	-0.257	
R141	-0.736	-0.204	-0.204	
R360	-0.926	-0.162	-0.122	
R434	0.492	-0.155	-0.352	
R502	-0.363	-0.131	-0.109	
R503	-0.280	-0.137	0.061	
R505	-0.881	-0.135	-0.146	Replicate
R505 b	-1.092	-0.142	-0.039	Replicate
R506	-1.423	-0.166	-0.093	
R507	-1.365	-0.153	-0.047	
R508	-1.704	-0.187	-0.067	
R511	-1.158	-0.225	0.012	

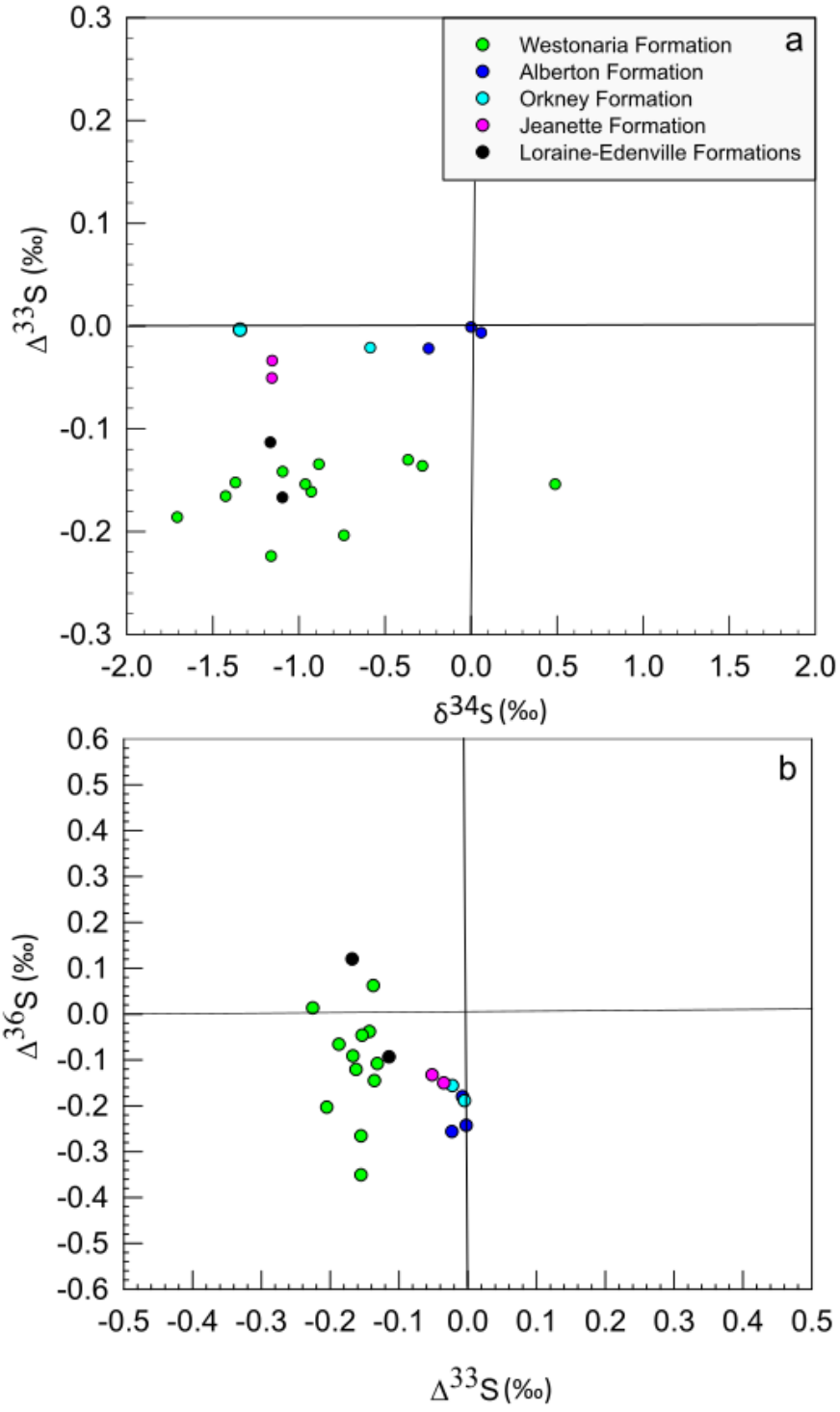

Figure 6. 8 Plots of (a) $\Delta^{33}S$ versus $\delta^{34}S$ and (b) $\Delta^{36}S$ versus $\Delta^{33}S$ for the lavas of the Klipriviersberg LIP. The multiple sulphur isotopes plots show mass-independent fractionated sulphur isotope (SMIF) compositions in the Klipriviersberg LIP lavas.

6.4 Discussion

6.4.1 PGE nature of the magma source(s)

Our previous work on the Sr-Nd-Hf isotope of the Ventersdorp Supergroup showed that the magmas of the Klipriviersberg LIP were sourced from a sublithospheric mantle that interacted with the subcontinental lithospheric mantle (SCLM) that had been influenced by a subduction event. Khumalo et al. (Chapter 4) propose that the Westonaria komatiites were the first products of the partial melting of an asthenospheric mantle that interacted with the SCLM during the production of the rest of the Klipriviersberg magmas. The lavas of the Klipriviersberg LIP are PGE-depleted and this can be explained by either derivation of magmas from a PGE-depleted mantle source, sulphide retention during the partial melting of the mantle source, or sulphide segregation during the ascent of the magmas. The Klipriviersberg LIP has higher Cu/Pd ratios than the mantle, except for the Loraine-Edenville lavas that overlap with the mantle ratios (Fig. 6.9). The Loraine-Edenville Formation has picritic composition and possibly have Ni-Cu-PGE composition similar to or close to the mantle source. The Westonaria komatiites have some of the highest Cu/Pd ratios within the LIP and they were formed earlier than the other magmas, possibly by a high degree of partial melting of the source which may have caused the partial melting of the sulphides in the source as well as sulphur enrichment in the komatiitic melt. Barnes and Picard (1993) approximate at least 20 % of partial melting of the mantle source to start melting the sulphides in the source. The high degree of partial melting required to produce komatiites produces an average PGE composition of the source, and in the case of the PGE-depleted Westonaria komatiites, the possibility of the retention of sulphide in the mantle source to explain the PGE depletion of the Westonaria komatiites can be eliminated, leaving a PGE depleted source or sulphide segregation as a result of magma-crust interaction as plausible explanations. Sulphide segregation during the ascent of the magma results in high Cu/Pd ratios (PGE depleted) due to high partition coefficients of PGEs for sulphides compared to Cu (Barnes & Picard, 1993). Other komatiites are said to have formed by small degrees of partial melting (e.g., Komati komatiites; Roelofse et al., 2002), which may retain Pd in the source, causing high Cu/Pd ratios. Komatiites are high-temperature magmas that required high degrees of partial melting of their sources (Arndt et al., 2008; Sossi et al., 2016). Based on high occurrence of komatiites

and extensive mantle plume activity in the Archean, we argue against small degrees of partial melting to produce the Westonaria komatiites. Mantle plumes have the capacity for significant heat transfer and large-scale melting.

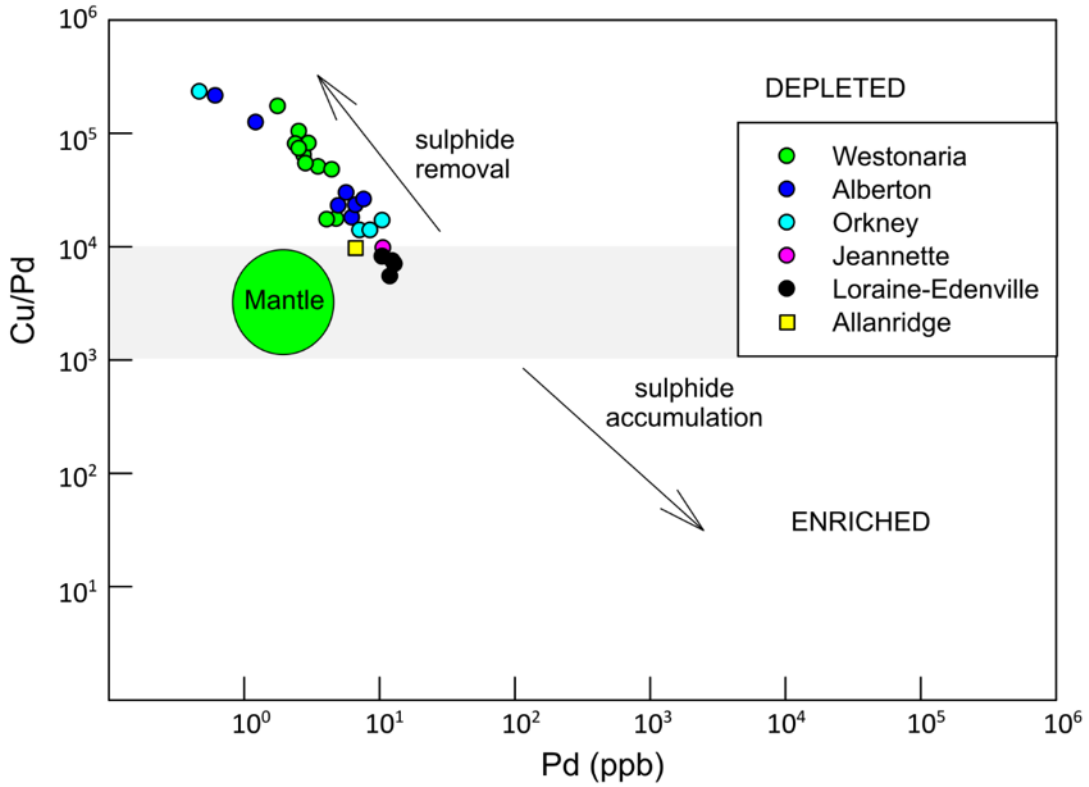

Figure 6. 9 Cu/Pd plotted against Pd in the Klipriviersberg LIP lavas showing PGE depletion in the magmas.

The Westonaria komatiites have similar Pt/Pd ratios as the rest of the Klipriviersberg basalts and lower Pd/Ir ratios compared to the basalts (Fig. 6.10) – a commonly observed fractionation trend between basalts and associated komatiites (Tredoux et al., 1995). Overall, the whole Klipriviersberg LIP has lower Pt/Pd and higher Pd/Ir than the primitive mantle. The observation points to the similarity of the magma sources for the komatiites and the basalts, and the insignificance of varying degrees of partial melting in the fractionation of Pt and Pd. However, the differences in the Pd/Ir ratios show the influence of the differences in the degrees and conditions of partial melting, and sulphide segregation as well as possible sulphide segregation in the Westonaria magmas during ascent or emplacement. The effect of different degrees of partial melting is evident in the primitive mantle-normalised PGE patterns of the komatiites and basalts. The low degree of partial melting of the mantle to

produce basalts fractionated the PGE by enriching the partial melts in the light Pd-PGE, forming positive steep patterns as opposed to the large degrees of partial melting to produce the komatiites that led to melting of the phases that host PGE (especially the mantle compatible Ir-PGE), thus producing relatively horizontal patterns (Fig. 6.7). Maier and Barnes (2004) suggested that the low Pt/Pd ratios of komatiites are indicative of the partial melting of a dry mantle source.

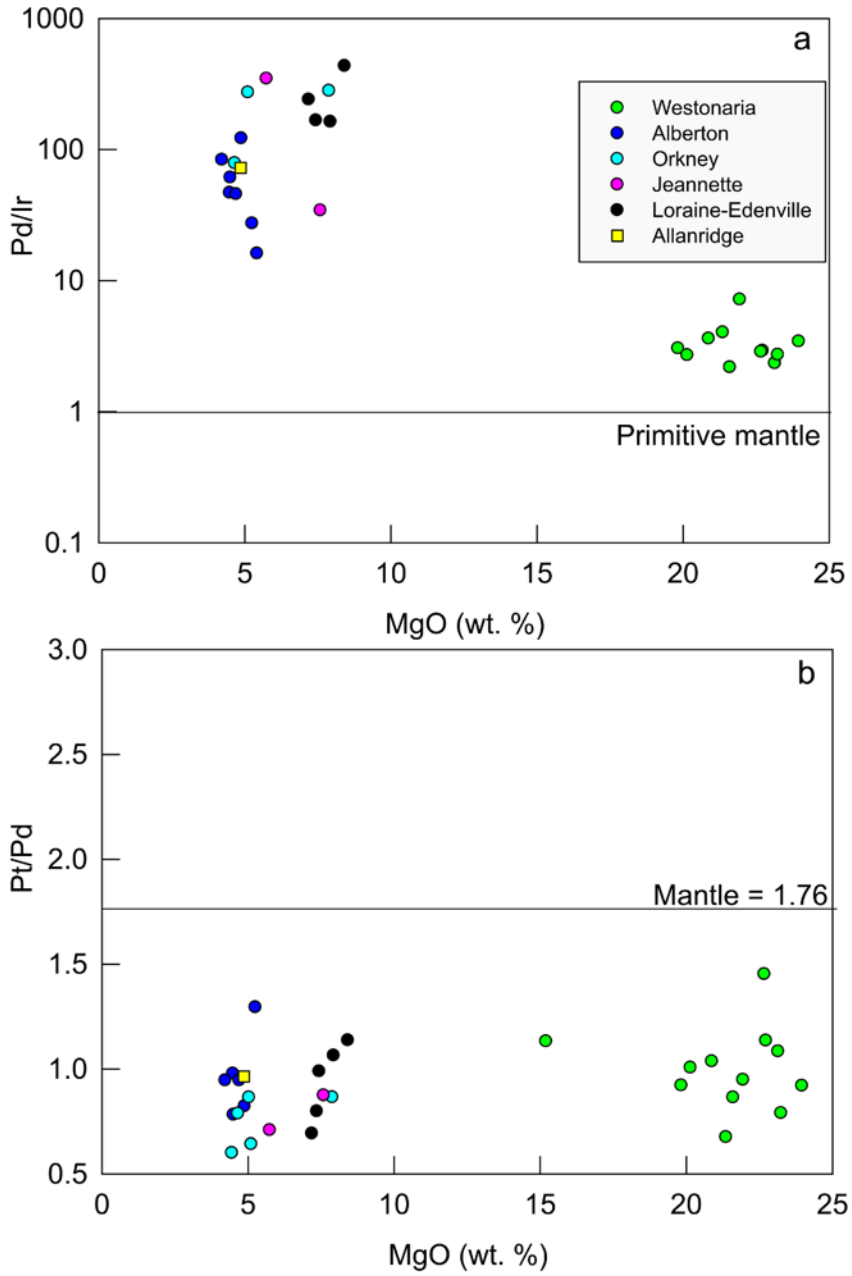

Figure 6. 10 a) Pd/Ir, and (b) Pt/Pd ratios of Klipriviersberg lavas plotted against MgO.

Crustal contamination of the Klipriviersberg LIP magmas would have decreased the temperature of the magmas as well as the sulphur solubility in the magmas, causing the magmas to reach sulphur saturation by the addition of external sulphur, resulting in sulphide segregation. Our radiogenic isotope study of the lavas shows that there was insignificant crustal contamination of the magmas as indicated by the depleted isotopic compositions (Chapter 5). This was substantiated by the narrow range of $\delta^{18}O$ of clinopyroxene in the Westonaria komatiites that show that the magmas originated from the sublithospheric mantle without the influence of crustal material (Chapter 4). The basalts of the Klipriviersberg LIP show negative Nb-Ta anomalies that we attributed to the interaction of the sublithospheric mantle plume with the SCLM that was modified by subduction event(s). In this study, we use sulphur isotopes to further assess crustal contamination of the Klipriviersberg magmas and the role of externally derived sulphur in the PGE contents of the lavas. The Klipriviersberg lavas have mass-independent fractionated sulphur (S-MIF) isotopic compositions (Fig. 6.8). These are non-zero $\Delta^{36}S$ and $\Delta^{33}S$ values that were produced by photochemical reactions during the Archean when the atmosphere was anoxic (Farquhar et al., 2000; Bekker et al., 2009; Kubota et al., 2022). The observed S-MIF signatures in the Klipriviersberg lavas indicate the presence of sulphur that was derived from the surface before ca. 2.4 Ga, the age of the Great Oxidation Event. Kubota et al. (2022) propose three potential processes to explain S-MIF signature in Archean mantle rocks and these include (1) hydrothermal alteration of the rocks to S-MIF signatures and variable $\delta^{34}S$ compositions, (2) assimilation of crustal components with S-MIF signatures, or (3) presence of subducted Archean crustal material with S-MIF signatures in the mantle source. The Klipriviersberg lavas are altered and metamorphosed (see Chapters 4 and 5), and Hiebert et al. (2016) show that the sulphur is readily modified by alteration fluids due to its high mobility, which might have affected our sulphur isotope compositions. The S-MIF signatures of the Klipriviersberg lavas can be explained by post-emplacement alteration of the lavas by hydrothermal fluids carrying S-MIF species from the underlying sedimentary Witwatersrand and/ or overlying sedimentary Transvaal Supergroup (Fig. 6.11).

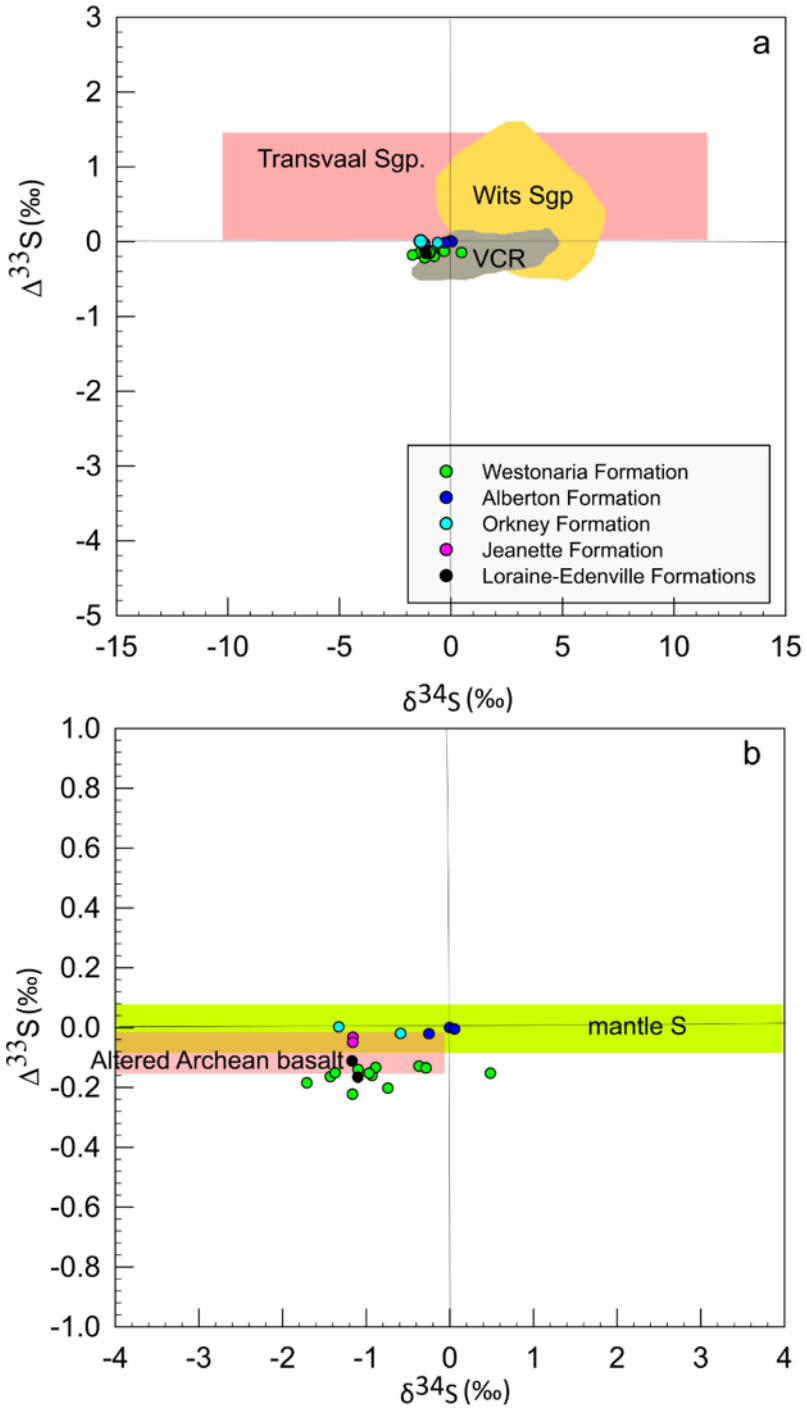

Figure 6. 11 Plots of (a and b) $\Delta^{33}S$ versus $\delta^{34}S$ for the lavas of the Klipriviersberg LIP. (a) shows that the Klipriversberg lavas have similar sulphur isotope compositions to the Ventersdorp Contact Reef compared to the Witwatersrand and Transvaal Supergroups. (b) The Klipriviersberg lavas fall in the altered Archean basalt composition defined in Aoyama and Ueno (2018). The composition of the mantle sulphur is from Bekker et al. (2009). The data for the Transvaal Supergroup, Witwatersrand Supergroup and the Ventersdorp Contact Reef are from Guo et al. (2009), Guy et al. (2012) and Hofmann et al. (2009), respectively.

Despite the alterated nature of the Klipriviersberg lavas that can easily explain the observed S-MIF signatures, our overall study of the Ventersdorp Supergroup has also shown the:

1) Influence of subduction on the Klipriviersberg magmas evident with negative Nb-Ta anomalies.

2) Unaltered (no isotope exchange) mantle oxygen isotopic compositions of fresh clinopyroxene in the Westonaria komatiites.

3) Insignificant crustal contamination of the Klipriviersberg magmas using depleted mantle Nd-Hf isotopic and the clinopyroxene mantle oxygen isotopic compositions.

Therefore, alteration cannot solely be used to explain the presence of S-MIF signatures without considering the presence of subducted Archean surface sulphur in the mantle source of the Klipriviersberg magmas. The proposed subduction component in the Klipriviersberg lavas could have introduced the S-MIF signatures to the magmas. We also note the differences between our oxygen and sulphur isotope analyses, in which the oxygen isotopes do not indicate significant alteration or isotope exchange between hydrothermal fluids and clinopyroxene. However, the oxygen isotope analysis was done by the in-situ analysis of freshly preserved clinopyroxene grains, whereas the sulphur isotope analysis was the whole rock analysis, which is generally more extensively altered compared to the clinopyroxene phenocrysts. Therefore, alteration cannot be convincingly ruled out as a plausible explanation for the origin of the S-MIF signatures in the Klipriviersberg lavas.

The behaviour of PGE during alteration is not well constrained. Maier et al. (2003) and Zaccarini et al. (2005) show that PGEs are immobile during alteration. The greenschist metamorphism and alteration events of the Ventersdorp Supergroup had an insignificant effect on the PGE concentrations of the Klipriviersberg LIP as there is little scatter of PGE. We presume that the observed PGE concentrations of the Klipriviersberg LIP lavas are primary concentrations. The three possible explanations for the PGE-depletion for the Klipriviersberg lavas include (1) a PGE-poor mantle source, (2) sulphide retention during partial melting of the mantle source, or (3) sulphide segregation during the ascent of the magmas by assimilation of sulphur-rich country rocks. The retention of sulphide phases hosting the PGE in the mantle source during partial melting is eliminated based on the high-degree partial melting required to produce the komatiitic magmas that would have melted the sulphides into the komatiitic magmas. Therefore, any sulphides or PGE-host phases in the mantle source

of the Klipriviersberg magmas were melted into the magma. The sulphur saturation of the magmas by contamination of the Klipriviersberg magmas during their ascent and sulphide segregation is not evident based on the clinopyroxene oxygen isotope and Nd-Hf isotope compositions. This suggests that the mantle source of magmas of the Klipriviersberg LIP was poor in PGE. The underlying ~8 km thick Witwatersrand Supergroup has large amounts of sulphides and has the economic potential of PGEs of placer origin (Mondal, 2011). Our sulphur isotope data do not show evidence of interaction between the Klipriviersberg magmas, and the sulphur-rich sediments of the Witwatersrand Supergroup as the Interaction would have resulted in positive isotopic values (Fig. 6.11a). Sulphur isotope studies (e.g., Hofmann et al., 2009; Guy et al., 2014) analysed diagenetic, epigenetic and detrital pyrite in the Ventersdorp Contact Reef (VCR) that have sulphur isotope compositions that overlap with our results, with the Westonaria komatiites that directly overlie the VCR having the most negative $\Delta^{33}S$. This attests to the post-emplacement modification of sulphur isotopes by hydrothermal alteration.

6.4.2 Fractionation of PGE during magma emplacement

The lavas of the Klipriviersberg LIP show control of PGE behaviour by crystal fractionation. The observed PGE concentrations and variations indicate that the Ir-PGEs were compatible during the emplacement of the komatiites, and the Pd-PGEs were more compatible during the emplacement of the basalts. The positive correlations of Ni, Cr and Ir-PGEs for the Westonaria komatiites suggest that the Cr was controlled by the crystallisation of the olivine and/or pyroxene, and possibly, chromite. No chromite was observed in the samples, which is uncommon in komatiitic and basaltic sequences, possibly due to its conversion to other minerals by metamorphic processes. The basalts have lower Ni concentrations (<300 ppm) and lower Cr concentrations (<450 ppm) than the komatiites, although they have higher Pd-PGE concentrations indicating that they were less compatible during the emplacement of the komatiites as shown by the gentle positive correlation of Cr with Pd-PGEs. Further evidence for the control of PGE concentration during the ascent or emplacement of the magma is shown in Figure 6.12. The Pt positively correlates with Pd indicating uniform behaviour for the Pd-PGEs during crystallisation. Rhodium (Rh) displays positive correlations with Pd for individual Formations suggesting discrete pulses for the Formations. Another explanation for

the slight differences in the behaviour of Rh from Pt and Pd is that the Rh has a higher partition coefficient for the mantle than Pt and Pd and may be hosted not only by sulphides (Barnes and Picard, 1993; Maier et al., 2003; Maier and Barnes, 2004). Generally, the Pd concentrations generally increase up the stratigraphy as well as for the individual Formations except for the high-MgO Formations (Westonaria and Loraine-Edenville Formations) that show an upward decrease in the Pd concentrations (Fig. 6.13). This suggests incompatibility of the Pd-PGEs for high-Mg phases. The sharp decrease in Ir and Ni up the stratigraphy and the constant concentrations clearly support the compatibility of the Ir-PGEs and Ni for the early forming phases. The observed behaviour of the PGE groups has been observed in other komatiite studies (Crocket & McRae, 1986; Brugmann et al., 1987; Dowling & Hill, 1992; Ripley & Li., 2013). Copper (Cu) shows a systematic gradual decrease in concentration up the stratigraphy, suggesting a control on the Cu concentration during the emplacement of the magmas.

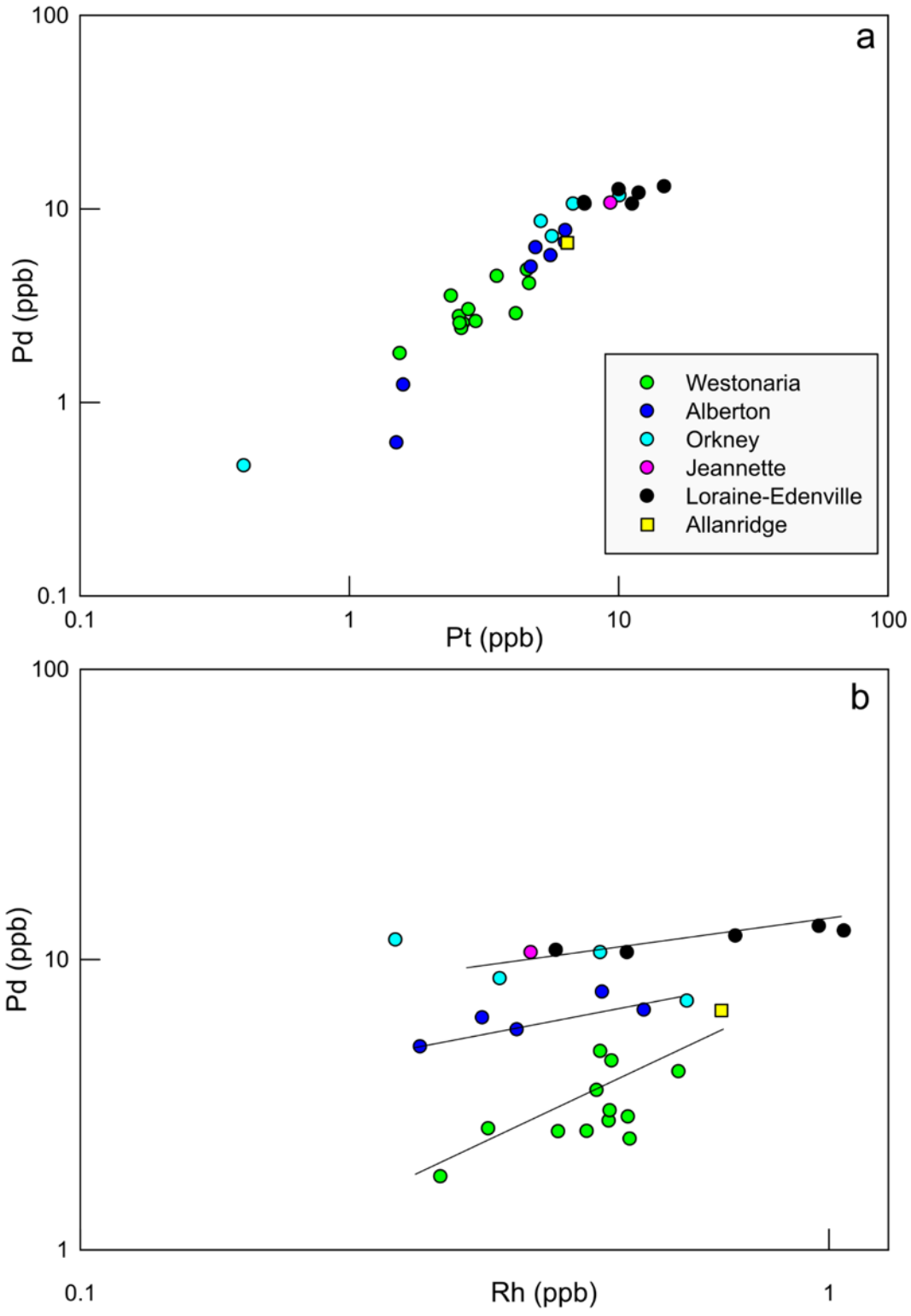

Figure 6. 12 Variation plots of (a) Pd versus Pt, and (b) Pd versus Rh showing the control of the PGE concentration during the ascent or emplacement of the magmas. The black lines show the trends for individual Formations.

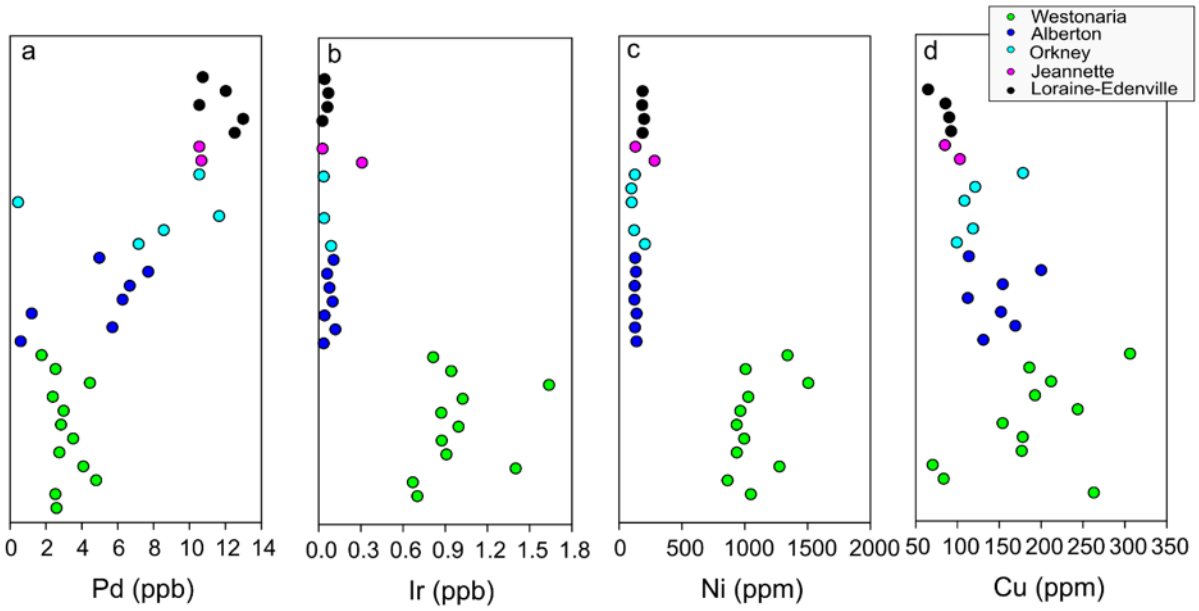

Figure 6. 13 Plots of (a) Pd, (b) Ir, (c) Ni and (d) Cu against the stratigraphy of the Klipriviersberg LIP, showing the behaviour of the elements during the emplacement of the magmas.

6.5 Conclusions

The Klipriviersberg LIP, a mafic flood basalt sequence with a komatiite at the base, has mass-independent fractionated sulphur isotopes (SMIF) and the lavas are PGE depleted. We establish that the magmas of the Klipriviersberg LIP were derived from a mantle source that was poor in PGE by showing that there was insignificant contamination of the magmas to form immiscible sulphide liquid that might have segregated from the magmas. The differences in the PGE concentrations between the Westonaria komatiites and the basalts of the LIP are attributed to the differences in the degrees of partial melting. The Cu/Pd ratios of the komatiites and basalts do not point to a potential PGE ore deposit associated with the Klipriviersberg LIP magmatism. The presence of SMIF shown by the multiple sulphur isotope compositions implies the influence of subducted sulphur in the magma source or during the ascent of the magmas. The magmas might have acquired the SMIF signatures during the proposed interaction of their source with the subduction-modified lithospheric mantle. Alternatively, the extensive alteration of the lavas is a possible mechanism to have introduced the SMIF signatures post emplacement of the lavas. The ease of S mobilization, as observed in the character of the sulphides in the samples, further supports the significant likelihood of alteration processes being responsible for the SMIF signatures in the Klipriviersberg LIP.

Chapter 7: Conclusion

In this thesis, new geochemical approaches on petrogenesis of the Neoarchean Ventersdorp Supergroup on the Kaapvaal Craton are presented. This study significantly increased the Sr-Nd-Hf-O-S isotope data of the Ventersdorp Supergroup lavas that has been largely lacking. New whole-rock trace element data, platinum group elements- (PGE) and in-situ major element data are also presented in this thesis. The multi-source data enabled the meticulous analysis of the altered samples of the Ventersdorp Supergroup for their magma source compositions and the extent of crustal contamination. The study shows distinct geochemical signatures of the three large igneous provinces (LIPs) in the Ventersdorp Supergroup. The LIPs include the basal Klipriviersberg LIP, the medial Platberg silicic LIP and the uppermost Allanridge LIP. The Rb-Sr isotope system of the Ventersdorp LIPs has been altered to an extent that proved not to be useful for inferring primary signatures.

However, the Sm-Nd and Lu-Hf isotope systems do not appear to have been affected extensively and the isotopic composition of the magma sources can still be inferred using these isotopic systems, together with the primary processes that probably affected the magmas. Despite the alteration nature of the Westonaria komatiites at the base of the Klipriviersberg LIP, thin section analyses identified fresh clinopyroxene grains that were analysed for their oxygen isotope compositions. The in-situ oxygen isotope analysis revealed that the source of the Westonaria Formation was a sublithospheric mantle source and that the magmas were not affected by crustal contamination, or the magma had not been crustally contaminated during the crystallization of clinopyroxene. The analysis also shows the resistance of clinopyroxene for oxygen isotope exchange by hydrothermal alteration that affected the whole-rock Rb-Sr isotope system. The sublithospheric mantle source is also indicated by the depleted Nd-Hf isotope compositions. The mantle source of the Klipriviersberg LIP interacted with a subduction-modified sub-continental lithospheric mantle (SCLM), inheriting the subduction signatures. The Westonaria magmas were produced first, prior to a higher degree of interaction of the source with the SCLM.

The magmas of the Platberg silicic LIP, unlike their precursors, were derived from enriched lower crustal sources, and subsequently contaminated by upper crust components. The Nd isotope compositions of the Ventersdorp Supergroup on the Kaapvaal Craton and of the

Fortescue Group of the Pilbara Craton were compared to investigate the proposed Vaalbara supercraton that implies that the Kaapvaal Craton and Pilbara Craton were adjoined during the magmatism of the Ventersdorp Supergroup. The investigation showed distinct Nd isotopic compositions for the Ventersdorp LIPs, whereas, the entire Fortescue Group has uniform Nd isotope composition, except for the Pyradie komatiites in the upper section of the sequence. The Vaalbara concept cannot be validated using Nd isotopes.

The investigation of potential PGE mineralisation associated with the Ventersdorp Supergroup, specifically the Klipriviersberg LIP, proved to be a challenge due to the alteration nature of the lavas, and the high mobility of sulphur during alteration. The Klipriviersberg lavas have low PGE content that can be explained either by derivation from a PGE-poor source, or sulphide segregation by assimilation of external sulphur, or retention of sulphide in the source. The latter is discarded due to high degrees of partial melting required for the production of the Westonaria komatiitic magmas. The investigation of assimilation of external sulphur using multiple sulphur isotopes show that the lavas have mess-independent sulphur isotope (SMIF) signatures that formed at the surface before the Great Oxidation Event. This implies that the sublithospheric mantle source was influenced by subduction, which has been proposed in the earlier investigations in this study. However, the SMIF signatures can be explained by post-emplacement modification of the lavas by hydrothermal fluids, which is evident in the lavas Of the Klipriviersberg LIP.

Regardless of the alteration of the lavas and considering the defiance of certain minerals to the secondary processes experienced by the lavas, to extract primary signatures of the lavas and their source compositions, it is recommended that future studies focus on in-situ analyses, as they can minimise the effects of secondary processes. Field, petrography and geochemistry investigations of the plumbing system of the Ventersdorp Supergroup is also recommended for better understanding of the PGE potential. In-situ analyses of sulphide minerals will also provide better understanding of PGE fractionation in the Ventersdorp Supergroup magmatic system.

8. References

Altermann, W. and Lenhardt, N., 2012. The volcano-sedimentary succession of the Archean Sodium Group, Ventersdorp Supergroup. South Africa: Volcanology, sedimentology, and geochemistry. *Precambrian Research*, 214–215, 60–81. doi:10.1016/j.precamres.2012.02.012.

Anderson, D.L., 2007. New Theory of the Earth: The nature and cause of the mantle heterogeneity. Cambridge University Press, New York, 312.

Anhaeusser, C.R., 1999. Archaean crustal evolution of the central Kaapvaal Craton, South Africa: evidence from the Johannesburg Dome. *South African Journal of Geology*, *102*(4), pp.303-322.

Aoyama, S. and Ueno, Y., 2018. Multiple sulfur isotope constraints on microbial sulfate reduction below an Archean seafloor hydrothermal system. *Geobiology*, 16(2), 107-120.

Armstrong, R. A., Compston, W., Retief, E. A., Williams, I. S. and Welke, H. J., 1991. Zircon ion microprobe studies bearing on the age and evolution of the Witwatersrand triad. *Precambrian Research,* 53, 243-266. doi.org/10.1016/0301-9268(91)90074-K.

Arndt, N.T., Nelson, D.R., Compston, W., Trendall, A.F. and Thorne, A.M., 1991. The age of the Fortescue Group, Hamersley Basin, Western Australia, from ion microprobe zircon U-Pb results. *Australian Journal of Earth Sciences*, *38*(3), pp.261-281.

Arndt, N., Lesher, M.C., and Barnes, S.J., 2008. Komatiite. Cambridge University Press, Cambridge.

Arndt, N.T., 1986. Differentiation of komatiitic flows. *Journal of Petrology*, 27, 279-301.

Ashwal, L.D., 2021. Sub-lithospheric mantle sources for overlapping southern African Large Igneous Provinces. *South African Journal of Geology*, 124, 421–442. doi.org/10.25131/sajg.124.0023.

Ashwal, L.D., 2017. Oppenheimer Fellowship Award application. (not in public).

Baertschi, P., 1976. Absolute18O content of standard mean ocean water. *Earth and Planetary Science Letters*, *31*(3), 341-344.

Ballmer, M.D., van Keken, P.E. and Ito, G., 2015. Hotspots, large igneous provinces, and melting anomalies. Elsevier.

Barnes S-J., Naldrett A. J., and Gorton M. P., 1985. The origin of the fractionation of the platinum-group elements in terrestial magmas. *Chemical Geology*, 53, 303-323.

Barnes, S.-J., and Picard, C. P., 1993. The behaviour of platinum group elements during partial melting, crystal fractionation, and sulphide segregation: an example from the Cape Smith Fold Belt, northern Quebec. *Geochimica et Cosmochimica Acta*, 57, 79-87.

Barnes, S.J. and Maier, W.D., 1999. The fractionation of Ni, Cu and the noble metals in silicate and sulfide liquids. In: Keays, R. R., Lesher, C. M., Lightfoot, P. C. & Farrow, C. E. G. (eds) Dynamic Processes in Magmatic Ore Deposits and their Application to Mineral Exploration. Geological Association of Canada, Short Course Notes 13, 69-106.

Barnes, S.J., and Arndt, N.T., 2019. Distribution and Geochemistry of Komatiites and Basalts Through the Archean, in: Earth's Oldest Rocks. Elsevier, 103–132. doi.org/10.1016/B978-0-444-63901-1.00006-X.

Barnes, S.J., and Fiorentini, M.L., 2012. Komatiite Magmas and Sulfide Nickel Deposits: A Comparison of Variably Endowed Archean Terranes. *Economic Geology*, 107, 755–780. doi.org/10.2113/econgeo.107.5.755.

Barton, E. S., Compston, W., Williams, I. S., Bristow, J. W., Hallbauer, D. K. and Smith, C. B., 1990. Provenance ages for the Witwatersrand Supergroup and the Ventersdorp contact reef; constraints from ion microprobe U–Pb ages of detrital zircons; reply. *Economic Geology and the Bulletin of the Society of Economic Geologists*, 85(8), 1951–1952. doi.org/10.2113/gsecongeo.85.8.1951.

Barton, J.M., Barton, E.S., and Kroner, A., 1999. Age and isotopic evidence for the origin of the Archaean granitoid intrusives of the Johannesburg Dome, South Africa. *Journal of African Earth Sciences*, 28, 693-702.

Begemann, F., Ludwig, K.R., Lugmair, G.W., Min, K., Nyquist, L.E., Patchett, P.J., Renne, P.R., Shih, C.Y., Villa, I.M., and Walker, R.J., 2001. Call for an improved set of decay constants for geochronological use. *Geochimica et Cosmochimica Acta* 65, 111–121. doi.org/10.1016/S0016-7037(00)00512-3.

Bekker, A., Barley, M.E., Fiorentini, M.L., Rouxel, O.J., Rumble, D., and Beresford, S.W., 2009. Atmospheric sulfur in Archean Komatiite-hosted nickel deposits. *Science,* 326, 1086–1098.

Blake, T.S., Buick, R., Brown, S.J.A., and Barley, M.E., 2004. Geochronology of a Late Archaean flood basalt province in the Pilbara Craton, Australia: constraints on basin evolution, volcanic and sedimentary accumulation, and continental drift rates. *Precambrian Research*, 133, 143–173.

Blichert-Toft, J., Arndt, N.T., Wilson, A., and Coetzee, G., 2015. Hf and Nd isotope systematics of early Archean komatiites from surface sampling and ICDP drilling in the Barberton Greenstone Belt, South Africa. *American Mineralogist*, 100, 2396–2411. doi.org/10.2138/am-2015-5325.

Blichert-Toft, J., and Puchtel, I.S., 2010. Depleted mantle sources through time: Evidence from Lu-Hf, and Sm-Nd isotope systematics of Archean komatiites. *Earth and Planetary Science Letters*, 297, 598–606. doi.org/10.1016/j.epsl.2010.07.012.

Bouvier, A., Vervoort, J.D., and Patchett, P.J., 2008. The Lu-Hf and Sm-Nd isotopic composition of CHUR: Constraints from unequilibrated chondrites and implications for the bulk composition of terrestrial planets. *Earth and Planetary Science Letters*, 273, 48–57. doi.org/10.1016/j.epsl.2008.06.010.

Bowen, M. P., 1984. The petrogenesis of the volcanic rocks of the Witwatersrand Triad in the Klerksdorp area, Transvaal. M.Sc. Thesis, Rhodes University, Grahamstown, 204.

Boyet, M., Garçon, M., Arndt, N.T., Carlson, R.W., and Konc, Z., 2021. Residual liquid from deep magma ocean crystallization in the source of komatiites from the ICDP drill core in the Barberton Greenstone Belt. *Geochimica et Cosmochi mica Acta*, 304, 141–159.

Brugmann, G. E., Arndt, N. T., Hofmann, A. W. and Tobschall, H. J., 1987. Noble metal abundances in komatiite suites from Alexo, Ontario, and Gorgona Island, Colombia. *Geochimica et Cosmochi mica Acta*, 51, 2159-2169.

Bryan, S. E., and Ferrari, L., 2013. Large igneous provinces and silicic large igneous provinces: progress in our understanding over the last 25 years. *Geological Society of America Bulletin*, 125, 1053-1078. doi:10.1130/B30820.1.

Burke, K., Kidd, W.S.F., and Kusky, T., 1985. Is the Ventersdorp Rift System of Southern Africa related to a continental collision between the Kaapvaal and Zimbabwe Cratons at 2.64 Ga ago? *Tectonophysics*, 115, 1–24. doi.org/10.1016/0040-1951(85)90096-4.

Button, A., 1979. Transvaal and Hamersley Basins—review of basin development and mineral deposits. *Minerals Science and Engineering*, 8, 262–290.

Byerly, B.L., Kareem, K., Bao, H. and Byerly, G.R., 2017. Early Earth mantle heterogeneity was revealed by light oxygen isotopes of Archaean komatiites. *Nature Geoscience*, 10(11), 871-875.

Cagney, N., Crameri, F., Newsome, W., Lithgow-Bertelloni, C., Cotel, A., Hart, S.R. and Whitehead, J.A., 2015. Constraining the source of mantle plumes. *Earth and Planetary Science Letter*, 435, 55- 63, doi:10.1016/j.epsl.2015.12.008.

Campbell, I.H., 2005. Large igneous provinces and the mantle plume hypothesis. *Elements*, 1(5), 265–269, doi:10.2113/gselements.1.5.265.

Campbell, I.H., 2007. Testing the plume theory. *Chemical Geology*, 241, 153–176. doi.org/10.1016/j.chemgeo.2007.01.024.

Coffin, M. F., and Eldholm, O., 1994. Large igneous provinces: Crustal structure, dimensions, and external consequences. *Reviews of Geophysics, 32, 1 – 36.*

Cornell, D. H., Meintjes, P. G., van der Westhuizen, W. A., and Frei, D., 2017. Microbeam U-Pb Zircon dating of the Makwassie Formation and underlying units in the Ventersdorp Supergroup of South Africa. *South African Journal of Geology*, 120.4, 525-540. doi:10.25131/gssajg.120.4.525.

Cox, K. G., Bell, J. D., and Pankhurst, R. J., 1979. The Interpretation of Igneous Rocks. George, Allen and Unwin, London.

Crocket, J. H., and McRae, W. E., 1986. Platinum-group element distribution in komatiitic and tholeiitic volcanic rocks from Munro Township, Ontario. *Economic Geology*, 81, 1242-1251.

Crow, C., and Condie, K.C., 1988. Geochemistry and origin of late Archean volcanics from the ventersdorp supergroup, South Africa. *Precambrian Research*, 42, 19–37. doi.org/10.1016/0301-9268(88)90008-3.

Davies, D.R., Goes, S. and Sambridge, M., 2015. On the relationship between volcanic hotspot locations, the reconstructed eruption sites of large igneous provinces and deep mantle seismic structures. *Earth Planetary Science Letters*, 411, 121–130. doi:10.1016/j.epsl.2014.11.052.

Davies, J.H., and Bunge, H.P., 2006. Are splash plumes the origin of minor hotspots? *Geology*, 34, 349–352.

de Kock, M.O., Beukes, N.J., and Armstrong, R.A., 2012. New SHRIMP U–Pb zircon ages from the Hartswater Group, South Africa: Implications for correlations of the Neoarchean Ventersdorp Supergroup on the Kaapvaal craton and with the Fortescue Group on the Pilbara craton. *Precambrian Research*, 204–205, 66–74. doi.org/10.1016/j.precamres.2012.02.007.

de Kock, M.O., Evans, D.A.D., and Beukes, N.J., 2009. Validating the existence of Vaalbara in the late Neoarchean. *Precambrian Research*, 174, 145–154. doi:10.1016/j.precamres.2009.07.002

DePaolo, D.J., and Wasserburg, G.J., 1979. Petrogenetic mixing models and Nd-Sr isotopic patterns. *Geochimica et Cosmochimica Acta* , 43, 615–627. doi.org/10.1016/0016-7037(79)90169-8.

Dobretsov, N. L., Borisenko, A. S. and Izokh, A. E., 2012. Thermochemical Mantle Plumes as the Source of the Earth‘s Ore Resources. *Science First Hand*, N3 (33).

Dowling, S. E., and Hill, R. R. T., 1992. The distribution of PGE in fractionated Archean komatiites, Western and Central ultramafic units, Mt. Keith region, Western Australia. *Australian Journal of Earth Science*, 39, 349-363.

Duane, M.J., Kruger, F.J., Turner, A.M., Whitelaw, H.T., Coetzee, H., and Verhagen, B.T., 2004. The timing and isotopic character of regional hydrothermal alteration and associated epigenetic mineralization in the western sector of the Kaapvaal Craton (South Africa). *Journal of African Earth Sciences*, 38, 461–476. doi.org/10.1016/j.jafrearsci.2004.03.002.

Eriksson, P.G., Condie, K.C., Westhuizen, W. van der, Merwe, R. van der, Bruiyn, H. de, Nelson, D.R., Altermann, W., Catuneanu, O., Bumby, A.J., Lindsay, J., and Cunningham, M.J., 2002. Late Archaean superplume events: a Kaapvaal–Pilbara perspective. *Journal of Geodynamics*, 34, 207–247. doi.org/10.1016/S0264-3707(02)00022-4.

Ernst R. E., 2014. Large igneous provinces. Cambridge University Press, Cambridge, UK, 653.

Ernst, R. E. and Bell, K., 2009. Large igneous provinces and carbonatites. *Mineral Petrology*, 98, 55 – 76. doi: 10.1007/s00710-009-0074-1.

Ernst, R. E. and Jowitt, S. M., 2013. Large Igneous Provinces and Metallogeny. *Society of Economic Geologists, Inc*. Special Publication, 17, 17 – 51.

Ernst, R.E., and Bleeker, W., 2010. Large igneous provinces (LIPs), giant dyke swarms, and mantle plumes: significance for breakup events within Canada and adjacent regions from 2.5 Ga to present Canadian. *Journal of Earth Sciences*, 47,695-739. doi: 10.1139/E10-025.

Ernst, R.E., and Buchan, K.L., 2001. Large mafic magmatic events through time and links to mantle-plume heads. In: Mantle Plumes: Their Identification Through Time. Edited by R.E. Ernst, and K.L. Buchan. *Geological Society of America Special Paper*, 352, 483- 575.

Farquhar, J., Bao, H., and Thiemens, M., 2000. Atmospheric influence of Earth's earliest sulfur cycle. *Science*, 289, 756–758. doi.org/10.1126/science.289.5480

Fitton, J.G., 2007. The OIB paradox, in: Special Paper 430: Plates, Plumes and Planetary Processes. *Geological Society of America*, 387–412. doi.org/10.1130/2007.2430(20).

Foulger, G. R., 2010. Plates vs Plumes: A Geological Controversy. Wiley-Blackwell, Sussex, 364.

French, J.E., and Heaman, L.M., 2010. Precise U–Pb dating of Paleoproterozoic mafic dyke swarms of the Dhar war craton, India: Implications for the existence of the Neoarchean supercraton Sclavia. *Precambrian Research*, 183, 416–441.

Greenough, J.D. and McDivitt, J.A., 2017. Earth's evolving subcontinental lithospheric mantle: inferences from LIP continental flood basalt geochemistry. *International Journal Earth Sciences*, 107,787–810. doi.10.1007/s00531-017-1493-6.

Grobler, D.F. and Walraven, F., 1993. Geochronology of Gaborone Granite Complex extensions in the area north of Mafikeng, South Africa. *Chemical Geology*, 105(4),319-337.

Grobler, N.J., van der Westhuizen, W.A., and Tordiffe, E.A.W., 1989.The Sodium Group, South Africa: Reference section for late Archaean - early Proterozoic cratonic cover sequences. *Australian Journal of Earth Sciences*, 36, 41-64.

Grove, T., Parman, S., J., and Dann, J., 1999. Conditions of magma generation for Archean komatiites from the Barberton Mountainland, South Africa, in Mantle Petrology: Field Observations and High-Pressure Experimentation, a Tribute to Francis R. (Joe) Boyd, edited by Y. Fei, C. Bertka, and B. Mysen, 155-167, Geochemical Society, Houston, Texas.

Gums Van der Westhuizen, W.A., de Bruiyn, H. and Meintjes, P.G., 1991. The Ventersdorp Supergroup: an overview. *Journal of African Earth Sciences*, 13, 83-105.

Gumsley, A., 2017. 'Validating the existence of the supercraton Vaalbara in the Mesoarchaean to Palaeoproterozoic', Doctor, Department of Geology, Lund.

Gumsley, A., Olsson, J., Söderlund,U., de Kock, M., Hofmann, A. and Klausen, M., 2015. Precise U-Pb baddeleyite age dating of the Usushwana Complex, southern Africa – Implications for the Mesoarchaean magmatic and sedimentological evolution of the Pongola Supergroup, Kaapvaal Craton. *Precambrian Research*, 267, 174–185. dx.doi.org/10.1016/j.precamres.2015.06.010.

Gumsley, A., Rådman, J., Söderlund, U. and Klausen, M., 2015. U–Pb baddeleyite geochronology and geochemistry of the White Mfolozi Dyke Swarm: unravelling the complexities of 2.70-2.66 Ga dyke swarms across the eastern Kaapvaal Craton, South Africa. *GFF* 138, 1–18. doi.org/10.1080/11035897.2015.1122665.

Gumsley, A., Stamsnijder, J., Larsson, E., Söderlund, U., Naeraa, T., de Kock, M., Sałacińska, A., Gawęda, A., Humbert, F., and Ernst, R., 2020. Neoarchean large igneous provinces on the Kaapvaal Craton in southern Africa re-define the formation of the Ventersdorp Supergroup and its temporal equivalents. *Geological Society of America Bulletin*, 132, 1829–1844. doi.org/10.1130/B35237.1.

Guo, Q., Strauss, H., Kaufman, A.J., Schröder, S., Gutzmer, J., Wing, B., Baker, M.A., Bekker, A., Jin, Q., Kim, S.T. and Farquhar, J., 2009. Reconstructing Earth's surface oxidation across the Archean-Proterozoic transition. *Geology*, 37(5), 399-402.

Guy, B.M., Ono, S., Gutzmer, J., Kaufman, A.J., Lin, Y., Fogel, M.L. and Beukes, N.J., 2012. A multiple sulfur and organic carbon isotope record from non-conglomeratic sedimentary rocks of the Mesoarchean Witwatersrand Supergroup, South Africa. *Precambrian Research*, 216, 208-231.

Guy, B.M., Ono, S., Gutzmer, J., Lin, Y. and Beukes, N.J., 2014. Sulfur sources of sedimentary “buckshot” pyrite in the auriferous conglomerates of the Mesoarchean Witwatersrand and Ventersdorp Supergroups, Kaapvaal Craton, South Africa. *Mineralium Deposita*, 49(6), 751-775.

Harris, C., and Watkins, R.T., 1990. Fluid interaction in the Witwatersrand gold fields: Oxygen isotope geochemistry of Ventersdorp-age dolerite intrusions. *South African Journal of Geology*, 93, 611–615.

Hastie, A.R., Fitton, J.G., Kerr, A.C., McDonald, I., Schwindrofska, A., and Hoermle, K., 2016. The composition of mantle plumes and the deep Earth. *Earth and Planetary Science Letters*, 444, 13–25, doi:10.1016/j.epsl.2016 .03.023.

Hatch, F.H., 1903. The Boulder Beds of Ventersdorp (Transvaal). Grocott and Sherry, printers.

Hatton, C.J., 1995. Mantle plume origin for the Bushveld and Ventersdorp magmatic provinces. *Journal of African Earth Sciences*, 21, 571–577. doi.org/10.1016/0899-5362(95)00106-9.

Hawkesworth, C., and Scherstén, A.,2007. Mantle plumes and geochemistry. *Chemical Geology*, 241, 319-331. doi.org/10.1016/j.chemgeo.2007.01.018.

Hawkesworth, C.J., Kempton, P.D., Rogers, N.W., Ellam, R.M., and van Calsteren, P.W., 1990. Continental mantle lithosphere, and shallow-level enrichment processes in the Earth's mantle. *Earth and Planetary Science Letters*, 96, 256-268.

Hawkesworth, C.J., Marsh, J.S., Duncan, A.R., Erlank, A.J., and Norry, M.J., 1984. The role of continental lithosphere in the generation of the Karoo volcanic rocks: evidence from combined Nd- and Sr-isotope studies. In: Erlank AJ (ed) Petrogenesis of the volcanic rocks of the Karoo Province. *Geological Society of South Africa*, 13, 341–354.

Hiebert, R.S., Bekker, A., Houlé, M.G., Wing, B.A. and Rouxel, O.J., 2016. Tracing sources of crustal contamination using multiple S and Fe isotopes in the Hart komatiite-associated Ni–Cu–PGE sulfide deposit, Abitibi greenstone belt, Ontario, Canada. *Mineralium Deposita*, 51(7), 919-935.

Hofmann, A., Bekker, A., Rouxel, O., Rumble, D. and Master, S., 2009. Multiple sulphur and iron isotope composition of detrital pyrite in Archaean sedimentary rocks: A new tool for provenance analysis. *Earth and Planetary Science Letters*, 286(3-4), 436-445.

Humbert, F., de Kock, M., Lenhardt, N., and Altermann, W., 2019. Neoarchaean to Early Palaeoproterozoic Within-Plate Volcanism of the Kaapvaal Craton: Comparing the Ventersdorp Supergroup and the Ongeluk and Hekpoort Formations (Transvaal Supergroup), in: Kröner, A., Hofmann, A. (Eds.), The Archaean Geology of the Kaapvaal Craton, Southern Africa, Regional Geology Reviews. Springer International Publishing, Cham, 277–302. doi.org/10.1007/978-3-319-78652-0_11.

Iwamori, H., and Nakamura, H., 2014. Isotopic heterogeneity of oceanic, arc, and continental basalts and its implications for mantle dynamics. *Gondwana Research*, 27, 1131 – 1152. dx.doi.org/10.1016/j.gr.2014.09.003.

Jacobsen, S.B., and Wasserburg, G.J., 1980. Sm-Nd isotopic evolution of chondrites. *Earth and Planetary Science Letters*, 50, 139–155. doi.org/10.1016/0012-821X(80)90125-9.

Jahn, B.M., Vidal, P. and Tilton, G.R., 1980. Archaean mantle heterogeneity: evidence from chemical and isotopic abundances in Archaean igneous rocks. *Philosophical Transactions of the Royal Society of London. Series A, Mathematical and Physical Sciences*, *297*(1431), 353-364. doi.org/10.1098/rsta.1980.0221.

Jensen, L.S. 1976. A new cation plot for classifying subalkalic volcanic rocks. Ontario Division of Mines, *Miscellaneous Paper* 66, 22.

Jerram, D.A., and Widdowson, M., 2005. The anatomy of Continental Flood Basalt Provinces: geological constraints on the processes and products of flood volcanism. *Lithos*, 79(3-4), 385-405.

Jourdan, F., Bertrand, H., Féraud, G., Le Gall, B., and Watkeys, M.K., 2009. Lithospheric mantle evolution monitored by overlapping large igneous provinces: Case study in southern Africa. *Lithos*, 107, 257–268. doi.org/10.1016/j.lithos.2008.10.011.

Jourdan, F., Bertrand, H., Schärer, U., Blichert-Toft, J., Féraud, G., and Kampunzu, A.B., 2007. Major and trace element and Sr, Nd, Hf, and Pb isotope compositions of the Karoo large igneous province, Botswana–Zimbabwe: lithosphere vs mantle plume contribution. *Journal of Petrology*, 48(6), 1043-1077.

Kampmann, T.C., Gumsley, A.P., de Kock, M.O., and Söderlund, U., 2015. U–Pb geochronology and paleomagnetism of the Westerberg Sill Suite, Kaapvaal Craton – Support for a coherent Kaapvaal–Pilbara Block (Vaalbara) into the Paleoproterozoic? *Precambrian Research*, 269, 58–72. doi.org/10.1016/j.precamres.2015.08.011.

Kasemann, S., Meixner, A., Rocholl, A., Vennemann, T., Rosner, M., Schmitt, A.K., and Wiedenbeck, M., 2001. Boron and oxygen isotope composition of certified reference materials NIST SRM 610/612 and reference materials JB-2 and JR-2. *Geostandards Newsletter*, *25*(2-3), 405-416.

Keays, R. R., 1995. The role of komatiitic and picritic magmatism and S-saturation in the formation of ore deposits. *Lithos*, 34, 1-18.

Keays, R.R. and Lightfoot, P.C., 2010. Crustal sulfur is required to form magmatic Ni–Cu sulfide deposits: evidence from chalcophile element signatures of Siberian and Deccan Trap basalts. *Mineralium Deposita*, 45(3), 241-257.

Klausen, M.B., Söderlund, U., Olsson, J.R., Ernst, R.E., Armoogam, M., Mkhize, S.W., Petzer, G., 2010. Petrological discrimination among Precambrian dyke swarms: Eastern Kaapvaal craton (South Africa). *Precambrian Research*, 183, 501–522. doi:10.1016/j.precamres.2010.01.013.

Kubota, Y., Matsu'ura, F., Shimizu, K., Ishikawa, A. and Ueno, Y., 2022. Sulfur in Archean komatiite implies early subduction of the oceanic lithosphere. *Earth and Planetary Science Letters*, 598, 117826.

Lahaye, Y., Amdt, N. T., Byerly, G., Chauvel, C, Fourcade, S. & Gruau, G., 1995. The influence of alteration on the trace element and Nd isotopic compositions of komatiites. *Chemical Geology*, 126, 43-64.

Le Bas, M.J., 2000. IUGS reclassification of the high-Mg and picritic volcanic rocks. *Journal of Petrology*, 41(10), 1467-1470.

Linton, P. L., 1992. The geochemical stratigraphy of the Klipriviersberg Group along the western margin of the Witwatersrand Basin. M.Sc. Thesis, University of the Witwatersrand, Johannesburg.

Lohmann, F.C., Hort, M. and Morgan, J.P., 2009. Flood basalts and ocean island basalts: A deep source or shallow entrainment? *Earth and Planetary Science Letters*, 284(3-4), 553-563.

Luttinen, A.V., 2018. Bilateral geochemical asymmetry in the Karoo large igneous province. *Scientific Reports*, 8, 5223. doi.org/10.1038/s41598-018-23661-3.

Ma, Y., Tao, Y., Zhong, H., Zhu, F. and Zhou, J., 2009. Geochemical characteristics of the platinum-group elements in the Abulangdang ultramafic intrusion, Sichuan Province, China. *Chinese Journal of Geochemistry*, 28(3), 320-327.

Magalhães, N., Farquhar, J., Bybee, G., Penniston-Dorland, S., Rumble III, D., Kinnaird, J. and McCreesh, M., 2019. Multiple sulfur isotopes reveal a possible non-crustal source of sulfur for the Bushveld Province, southern Africa. *Geology*, 47(10), 982-986.

Maier, W.D. and Barnes, S.J., 2004. Pt/Pd and Pd/Ir ratios in mantle-derived magmas: a possible role for mantle metasomatism. *South African Journal of Geology*, 107(3), 333-340.

Maier, W.D., 2005. Platinum-group element (PGE) deposits and occurrences: Mineralization styles, genetic concepts, and exploration criteria. *Journal of African Earth Sciences*, 41(3), 165-191.

Maier, W.D., Barnes, S.J., Campbell, I.H., Fiorentini, M.L., Peltonen, P., Barnes, S.J. and Smithies, R.H., 2009. Progressive mixing of meteoritic veneer into the early Earth's deep mantle. Nature, 460(7255), 620-623.

Maier, W.D., Prevec, S.A., Scoates, J.S., Wall, C.J., Barnes, S.J. and Gomwe, T., 2018. The Uitkomst intrusion and Nkomati Ni-Cu-Cr-PGE deposit, South Africa: trace element geochemistry, Nd isotopes, and high-precision geochronology. *Mineralium Deposita*, 53(1), 67-88.

Maier, W.D., Roelofse, F. and Barnes, S.J., 2003. The concentration of the platinum-group elements in South African komatiites: implications for mantle sources, melting regime and PGE fractionation during crystallization. *Journal of Petrology*, 44(10), 1787-1804.

Manzi, M.S.D., Hein, K.A.A., King, N., and Durrheim, R.J., 2013. Neoarchaean tectonic history of the Witwatersrand Basin and Ventersdorp Supergroup: New constraints from high-resolution 3D seismic reflection data. *Tectonophysics*, 590, 94-105.

Marsh, J.S., Bowen, M.P., Rogers, N.W., and Bowen, T.B., 1992. Petrogenesis of Late Archaean Flood-Type Basic Lavas from the Klipriviersberg Group, Ventersdorp Supergroup, South Africa. *Journal of Petrology*, 33, 817–847. doi.org/10.1093/petrology/33.4.817.

Mattey, D., Lowry, D. and Macpherson, C., 1994. Oxygen isotope composition of mantle peridotite. *Earth and Planetary Science Letters*, 128(3-4), 231-241.

McCarthy, TS, McCallum, K., Myers, R, E., and Linton, P., 1990. Stress states along the northern margin of the Witwatersrand Basin during Klipriviersberg Group volcanism. *South African Journal of Geology*, 93(1), 245-260.

McDonough, W.F., and Sun, S.S., 1995. The composition of the Earth. *Chemical Geology*, 120(3-4), 223-253.

Meier, D.L., Heinrich, C.A., and Watts, M.A., 2009. Mafic dikes displacing Witwatersrand gold reefs: Evidence against metamorphic-hydrothermal ore formation. *Geology*, 37, 607–610.

Meintjes, P. G. and van der Westhuizen, W. A., 2018. Stratigraphy and Geochemistry of the Goedgenoeg and Makwassie Formations, Ventersdorp Supergroup, in the Bothaville area of South Africa. *South African Journal of Geology*, 121, 339-362. doi:10.25131/sajg.121.0021.

Meintjes, P.G., and van der Westhuizen, W.A., 2018. Borehole LLE1 – an intra-caldera succession of the Goedgenoeg and Makwassie Formations, Ventersdorp Supergroup. *South African Journal of Geology* 121, 363–382. doi.org/10.25131/sajg.121.0034.

Mole, D.R., Fiorentini, M.L., Thebaud, N., Cassidy, K.F., McCuaig, T.C., Kirkland, C.L., Romano, S.S., Doublier, M.P., Belousova, E.A., Barnes, S.J., and Miller, J., 2014. Archean komatiite volcanism controlled by the evolution of early continents. *Proceedings of National Academy of Sciences*, 111, 10083–10088. doi.org/10.1073/pnas.1400273111.

Mondal, S.K., 2011. Platinum group element (PGE) geochemistry to understand the chemical evolution of the Earth's mantle. *Journal of the Geological Society of India*, 77(4), 295-302.

Montelli, R., Nolet, G., Dahlen, F.A., Masters, G., Engdahl, E.R., and Hung, S.H., 2004. Finite frequency tomography reveals a variety of plumes in the mantle. *Science*, 303, 338-343.

Moore, M., Davis, D.W., Robb, L.J., Jackson, M.C. and Grobler, D.F., 1993. Archean rapakivi granite-anorthosite-rhyolite complex in the Witwatersrand basin hinterland, southern Africa. *Geology*, 21(11), 1031-1034.

Morgan, W.J., 1971. Convection plumes in the lower mantle. *Nature*, 230(5288), 42-43.

Munker, C., Weyer, S., Scherer, E., and Mezger, K., 2001. Separation of highfield strength elements (Nb, Ta, Zr, Hf) and Lu from rock samples for MC-ICP-MS measurements, *Geochemistry Geophysics Geosystems*, 2 (12). doi:10.1029/2001GC000183.

Myers, J.M., 1990. The stratigraphy and geochemistry of the Klipriviersberg and Platberg groups of the Ventersdorp supergroup in the Klerksdorp area, Western Transvaal.

Myers, R. E, Cawthorn, R G., McCarthy, T. S., and Anhaeusser, C. R., 1987. Fundamental uniformity in the trace element patterns of the volcanics of the Kaapvaal Craton from 3000 to 2100 Ma: evidence for the lithospheric origin of these continental tholeiites. In: Pharaoh, T. C, Beckinsale, R. D., & Rickard, D. (eds.) Geochemistry and Mineralization of Proterozoic Volcanic Suites. *Geological Society Special Publication*, 33, 315-25.

Myers, R.E., McCarthy, T.S., Bunyard, M., Cawthorn, R.G., Falatsa, T.M., Hewitt, T., Linton, P., Myers, J.M., Palmer, K.J., and Spencer, R., 1990. Geochemical stratigraphy of the Klipriviersberg Group volcanic rocks. *South African Journal of Geology* 93, 224-238.

Naldrett, A.J., Lightfoot, P.C., Fedorenko, V., Doherty, W. and Gorbachev, N.S., 1992. Geology and geochemistry of intrusions and flood basalts of the Noril'sk region, USSR, with implications for the origin of the Ni-Cu ores. *Economic Geology*, 87(4), 975-1004.

Nelson, D.R., Trendall, A.F., de Laeter, J.R., Grobler, N.J., and Fletcher, I.R., 1992. A comparative study of the geochemical and isotopic systematics of late Archaean flood basalts from the Pilbara and kaapvaal cratons. *Precambrian Research*, 54, 231–256. doi.org/10.1016/0301-9268(92)90072-V.

Neumann, E.R., Svensen, H., Galerne, C.Y. and Planke, S., 2011. Multistage evolution of dolerites in the Karoo large igneous province, Central South Africa. *Journal of Petrology*, 52(5), 959-984.

Ohtani, E., Kawabe, I., Moriyama, J., and Nagata, Y., 1989. Partitioning of elements between majorite garnet and melt and implications for the petrogenesis of komatiite. *Contributions to Mineralogy and Petrology*, 103, 263–269. doi.org/10.1007/BF00402913.

Olsson, J. R., Söderlund, U., Hamilton, M. A., Klausen, M. B., and Helffrich, G. R. J. N. G., 2011. A late Archaean radiating dyke swarm as possible clue to the origin of the Bushveld Complex. *Nature Geoscience*, 4, 865.

Olsson, J.R., Söderlund, U., Klausen, M.B., and Ernst, R.E., 2010. U-Pb baddeleyite ages of major Archean dyke swarms and the Bushveld Complex, Kaapvaal Craton (South Africa); correlations to volcanic rift forming events. *Special Issue Precambrian Research*, 183, 490–500.

O'Reilly, S.Y., Griffin, W.L., Poudjom, Y.H. and Morgan, P., 2001. Are lithosphere forever? Tracking changes in subcontinental lithospheric mantle through time. GSA Today, 11, 4–10.

Parman, S.W., Grove, T.L., and Dann, J.C., 2001. The production of Barberton komatiites in an Archean Subduction Zone. *Geophysical Research Letters*, 28, 2513–2516. doi.org/10.1029/2000GL012713.

Pearce, J.A., 1996. A user's guide to basalt discrimination diagrams. Trace element geochemistry of volcanic rocks: applications for massive sulphide exploration. *Geological Association of Canada, Short Course Notes*, 12(79), 113.

Pearce, J.A., 2008. Geochemical fingerprinting of oceanic basalts with applications to ophiolite classification and the search for Archean oceanic crust. *Lithos*, 100, 14-48. 10.1016/j.lithos.2007.06.016.

Poujol, M., Kiefer, R., Robb, L. J., Anhaeusser, C. R., and Armstrong, R. A., 2005. New U-Pb data on zircons from the Amalia greenstone belt, southern Africa: insights to the Neoarchean evolution of the Kaapvaal Craton. *South African Journal of Geology*, 108, 317-332. doi.org/10.2113/108.3.317.

Puchtel, I.S., Blichert-Toft, J., Horan, M.F., Touboul, M. and Walker, R.J., 2022. The komatiite testimony to ancient mantle heterogeneity. *Chemical Geology*, 120776.

Raymond, A. C. and Murchison, D. G., 1991. The relationship between organic maturation, the widths of thermal aureoles, and the thicknesses of sills in the Midland Valley of Scotland and Northern England. *Journal of the Geological Society*, 148, 215-218. doi.org/10.1144/gsjgs.148.2.0215

Reddy, V., and Germs, G.J.B., 1994. Stratigraphy and facies of the Venterspost Conglomerate Formation at Western Areas Gold Mine. *South African Journal of Geology*, 97, 288-296.

Reichardt, H., and Weinberg, R.F., 2012. Hornblende Chemistry in Meta- and Diatexites and its Retention in the Source of Leucogranites: An Example from the Karakoram Shear Zone, NW India. *Journal of Petrology*, 53, 1287–1318. doi.org/10.1093/petrology/egs017.

Ripley, E.M., and Li, C., 2003. Sulfur isotope exchange and metal enrichment in the formation of magmatic Cu-Ni-(PGE) deposits. *Economic Geology*, 98(3), 635-641.

Ripley, E.M. and Li, C., 2013. Sulfide saturation in mafic magmas: Is external sulfur required for magmatic Ni-Cu-(PGE) ore genesis? Economic Geology, 108(1), 45-58.

Robin-Popieul, C.C.M., Arndt, N.T., Chauvel, C., Byerly, G.R., Sobolev, A.V., and Wilson, A., 2012. A New Model for Barberton Komatiites: Deep Critical Melting with High Melt Retention. *Journal of Petrology*, 53, 2191–2229. doi.org/10.1093/petrology/egs042.

Roelofse, F., Maier, W.D., and Barnes, S.J., 2002. Platinum-Group Elements in Komatiites from the Komati Formation, Barberton Greenstone Belt.

Salters, V.J. and Stracke, A., 2004. Composition of the depleted mantle. *Geochemistry, Geophysics, Geosystems*, *5*(5).

Saunders, A.D., Jones, S.M., Morgan, L.A., Pirece, K.L., Widdowson, M., and Xu, Y.G., 2007. Regional uplift associated with continental large igneous provinces: The roles of 30 mantle plumes and lithosphere. *Chemical Geology*, 241, 282-318. doi:10.1016/j.chemgeo.2007.01.017.

Saunders, A.D., Storey, M., Kent, R.W., and Norry, M.J., 1992. Consequences of plume-lithosphere interactions. *Geological Society, London, Special Publications*, 68(1), 41-60.

Savard, D., Barnes, S.J., and Meisel, T., 2010. Comparison between nickel-sulfur fire assay Te co-precipitation and isotope dilution with high-pressure asher acid digestion for the determination of platinum-group elements, rhenium, and gold. *Geostandards and Geoanalytical Research*, 34(3), 281-291.

Scherer, E.E., Cameron, K.L. and Blichert-Toft, J., 2000. Lu–Hf garnet geochronology: closure temperature relative to the Sm–Nd system and the effects of trace mineral inclusions. *Geochimica et Cosmochimica Acta*, 64(19), 3413-3432.

Schmidt, P. W. and Embleton, B. J. J., 1985. Prefolding and overprint magnetic signatures in Precambrian (2.9 – 2.7 Ga) Igneous rocks from the Pilbara Craton and Hamersley Basin, NW Australia. *Journal of Geophysical Research, Solid Earth*, 90, 2967–2984. doi.org/10.1029/JB090iB04p02967

Schneiderhan, E., Zimmermann, U., Gutzmer, J., Mezger, K., and Armstrong, R., 2011. Sedimentary Provenance of the Neoarchean Ventersdorp Supergroup, Southern Africa: Shedding Light on the Evolution of the Kaapvaal Craton during the Neoarchean. *The Journal of Geology*, 119 (6), 575 – 596. doi.org/10.1086/661988.

Schulz, K.J., Chandler, V.W., Nicholson, S.W., Piatak, Nadine, Seall, II, R.R., Woodruff, L.G., and Zientek, M.L., 2010. Magmatic sulfide-rich nickel-copper deposits related to picrite and (or) tholeiitic basalt dike-sill complexes—A preliminary deposit model: U.S. *Geological Survey Open-File Report*, 2010–1179, 25.

Seat, Z., Beresford, S.W., Grguric, B.A., Gee, M.M. and Grassineau, N.V., 2009. Reevaluation of the role of external sulfur addition in the genesis of Ni-Cu-PGE deposits: Evidence from the Nebo-Babel Ni-Cu-PGE deposit, West Musgrave, Western Australia. *Economic Geology*, 104(4), 521-538.

Sensarma, S., Palme, H., and Mukhopadhyay, D., 2002. Crust-Mantle interaction in the Genesis of Siliceous High Magnesian Basalts (SHMB): Evidence from the Early Proterozoic Dongargarh Supergroup, India. *Chemical Geology*, 187, 21-37.

Sharkov, E., Bogina, M., and Chistyakov, A., 2017. Magmatic systems of large continental igneous provinces. *Geoscience Frontiers*, 8, 621 – 640. dx.doi.org/10.1016/j.gsf.2016.03.006

Shirey, S.B., and Richardson, S.H., 2011. Start of the Wilson cycle at 3 Ga shown by diamonds from subcontinental mantle. *Science*, 333, 434-436. doi: 10.1126/science.1206275.

Smart, K. A., Tappe, S., Stern, R. A., Webb, S. J., and Ashwal, L. D., 2016. Early Archaean tectonics and mantle redox recorded in Witwatersrand diamonds. *Nature Geoscience* 9, 255-259. doi:10.1038/NGE2628.

Smirnov, A.V., Evans, D.A., Ernst, R.E., Söderlund, U., and Li, Z.X., 2013. Trading partners: Tectonic ancestry of southern Africa and western Australia, in Archean supercratons Vaalbara and Zimgarn. *Precambrian Research*, 224, 11-22.

Smith, J.W., Holwell, D.A., McDonald, I., and Boyce, A.J., 2016. The application of S isotopes and S/Se ratios in determining ore-forming processes of magmatic Ni–Cu–PGE sulfide deposits: A cautionary case study from the northern Bushveld Complex. *Ore Geology Reviews*, 73, 148-174.

Söderlund, U., Patchett, P.J., Vervoort, J.D., and Isachsen, C.E., 2004. The 176Lu decay constant determined by Lu–Hf and U–Pb isotope systematics of Precambrian mafic intrusions. Earth and Planetary Science Letters, 219, 311–324. doi.org/10.1016/S0012-821X(04)00012-3.

Sossi, P.A., Eggins, S.M., Nesbitt, R.W., Nebel, O., Hergt, J.M., Campbell, I.H., O'Neill, H.S.C., Van Kranendonk, M. and Davies, D.R., 2016. Petrogenesis and geochemistry of Archean komatiites. *Journal of Petrology*, *57*(1), pp.147-184.

Spandler, C., Hammerli, J., Sha, P., Hilbert-Wolf, H., Hu, Y., Roberts, E., and Schmitz, M., 2016. MKED1: A new titanite standard for in situ analysis of Sm-Nd isotopes and U–Pb geochronology. *Chemical Geology*, 425, 110–126. doi.org/10.1016/j.chemgeo.2016.01.002.

Stamsnijder, J., 2017. New geochronological constraints on the Klipriviersberg Group: defining a new Neoarchean large igneous province on the Kaapvaal Craton, South Africa. Dissertations in Geology at Lund University, 524, 21. 45 hp (45 ECTS credits).

Steiger, R.H., and Jäger, E., 1977. Subcommission on geochronology: Convention on the use of decay constants in geo- and cosmochronology. *Earth and Planetary Science Letter,* 36, 359–362. doi.org/10.1016/0012-821X(77)90060-7.

Stiegler, M.T., Cooper, M., Byerly, G.R., Lowe, D.R., 2012. Geochemistry and petrology of komatiites of the Pioneer Ultramafic Complex of the 3.3Ga Weltevreden Formation, Barberton greenstone belt, South Africa. *Precambrian Research,* 212–213, 1–12. doi.org/10.1016/j.precamres.2012.04.017.

Stow, G.W. and Jones, T.R., 1874. Geological Notes upon Griqualand West: With Descriptions of the Specimens. *Quarterly Journal of the Geological Society*, 30(1-4), 581-680.

Tanaka, T., Togashi, S. Kamioka, H., Amakawa, H., Kagami, H., Hamamoto, T., Yuhara, M., Orihashi, Y., Yoneda, S., Shimizu, H., Kunimaru, T., Takahashi, K., Yanagi, T., Nakano, T., Fujimaki, H., Shinjo, R., Asahara, Y., Tanimizu, M., and Dragusanu, C., 2000. JNdi-1: a neodymium isotopic reference in consistency with LaJolla neodymium. *Chemical Geology*, 168, 279-281.

Tang, G.Q., Su, B.X., Li, Q.L., Xia, X.P., Jing, J.J., Feng, L.J., Martin, L., Yang, Q. and Li, X.H., 2019. High-Mg# olivine, clinopyroxene and orthopyroxene reference materials for in situ oxygen isotope determination. *Geostandards and Geoanalytical Research*, 43(4), 585-593.

Tang, Y.J., Zhang, H.F., Ying, J.F. and Su, B.X., 2013. Widespread refertilization of cratonic and circum-cratonic lithospheric mantle. *Earth Science Review*, 118, 45-68. dx.doi.org/10.1016/j.earscirev.2013.01.004.

Taylor, B., 2006. The single largest oceanic plateau: Ontong Java–Manihiki–Hikurangi. *Earth and Planetary Science Letters*, 241, 372 – 380. doi:10.1016/j.epsl.2005.11.049

Torsvik, T. H., Burke, K., Steinberger, B., Webb, S. J., and Ashwal, L. D., 2010. Diamonds sampled by plumes from the core–mantle-boundary. *Nature*, 466, 352–358. doi:10.1038/nature09216.

Torsvik, T.H., Steinberger, B., Cocks, L.R.M., and Burke, K., 2008. Longitude: linking Earth's ancient surface to its deep interior. *Earth and Planetary Science Letters*, 276(3-4), 273-282.

Torsvik, T.H., van der Voo, R., Doubrovine, P.V., Burke, K., Steinberger, B., Ashwal, L.D., Trønnes, R.G., Webb, S.J., and Bull, A.L., 2014. Deep mantle structure as a reference frame for movements in and on the Earth. *Proceedings of the National Academy of Sciences*, 111(24), 8735-8740.

Tredoux, M., Davies, G., McDonald, I., and Lindsay, N.M., 1995. The fractionation of platinum-group elements in magmatic systems, with the suggestion of a novel causal mechanism. *South African Journal of Geology*, 98(2), 157-167.

Trendall, A.F., 1968. Three great basins of Precambrian iron formation deposition: a systematic comparison. *Geological Society of America Bulletin*, 79, 1527–1533

Tyler, N., 1979. Stratigraphy, geochemistry, and correlation of the Ventersdorp Supergroup in the Derdepoort area, west-central Transvaal. *South African Journal of Geology*, 82(1), 133-147.

Van der Westhuizen, W. A., de Bruiyn, H., and Meintjes, P. G., 2006. The Ventersdorp Supergroup. In: Johnson, M.R., Anhaeusser, C.R., and Thomas, R.J. (Eds.): The Geology of South Africa. Geological Society of South Africa Johannesburg and the Council for Geoscience Pretoria. 187-208.

Vervoort, J.D., and Blichert-Toft, J., 1999. Evolution of the depleted mantle: Hf isotope evidence from juvenile rocks through time. *Geochimica et Cosmochimica Acta*, 63, 533–556. doi.org/10.1016/S0016-7037(98)00274-9.

Viljoen, M.J., and Viljoen, R.P., 1969. The geology and geochemistry of the lower ultramafic unit of the Onverwacht group and a proposed new class of igneous rocks. *Geological Society of South Africa*, 2, 55–86.

Walraven, F., Smith, C, B., and Kruger, F., 1991. Age determinations of the Zoetlief Group-a Ventersdorp Supergroup correlative. *South African Journal of Geology*, 94(2), 220-227.

Walraven, F., Grobler, D.F. and Key, R.M., 1996. Age equivalence of the Plantation Porphyry and the Kanye volcanic formation, southeastern Botswana. *South African Journal of Geology*, 99(1), 23-31.

Walraven, F., Grobler, D.F. and Key, R.M., 1996. Age equivalence of the Plantation Porphyry and the Kanye volcanic formation, southeastern Botswana. *South African Journal of Geology*, 99(1), 23-31.

Walraven, F., Retief, E, A., and Moen, H., 1994. Single-zircon Pb-evaporation evidence for 2.77 Ga magmatism in northwestern Transvaal, South Africa. *South African Journal of Geology*, 97(2), 107-113.

Wang, Y., Santosh, M., Luo, Z., and Hao, J., 2014. Large igneous provinces linked to supercontinent assembly. *Journal of Geodynamics*. dx.doi.org/10.1016/j.jog.2014.12.001.

Wasserburg, G.J., Jacobsen, S.B., DePaolo, D.J., McCulloch, M.T., and Wen, T., 1981. Precise determination of SmNd ratios, Sm and Nd isotopic abundances in standard solutions. *Geochimica et Cosmochimica Acta*, 4-5, 2311–2323. doi.org/10.1016/0016-7037(81)90085-5.

Waterton, P., Mungall, J., and Pearson, D.G., 2021. The komatiite-mantle platinum-group element paradox. *Geochimica et Cosmochimica Acta*, 313, 214-242.

Weis, D., Kieffer, B., Hanano, D., Nobre Silva, I., Barling, J., Pretorius, W., Maerschalk, C., and Mattielli, N., 2007. Hf isotope compositions of U.S. Geological Survey reference materials. *Geochemistry Geophysics Geosystems,* 8, Q06006. doi: 10.1029/2006GC001473.

White, R. S., 1997. Mantle plume origin for the Karoo and Ventersdorp flood basalts, South Africa. *South African Journal of Geology,* 100 (4), 271-282.

Whitelaw, H.T., 1998. Hydrothermal alteration and Pb/Zn mineralisation in the Allanridge Formation, Ventersdorp Supergroup, near Douglas, Northern Cape Province, South Africa (Doctoral dissertation, University of the Free State).

Wingate, M. T. D., 1998. A palaeomagnetic test of the Kaapvaal – Pilbara (Vaalbara) connection at 2.78 Ga. *South African Journal of Geology,* 101, 257–274.

Wingate, M.T.D., 1999. Ion microprobe baddeleyite and zircon ages for Late Archaean mafic dykes of the Pilbara Craton, Western Australia. *Australian Journal of Earth Sciences*, 46(4), 493-500.

Winter, H. de la R., 1976. A lithostratigraphic classification of the Ventersdorp succession. *Transactions of the Geological Society of South Africa*, 79, 31-48.

Wyatt, B.A., 1976. The geology and geochemistry of the Klipriviersberg volcanics, Ventersdorp Supergroup, south of Johannesburg. M.S. Thesis, Univ. Witwatersrand, Johannesburg, South Africa: 178. (unpublished).

Wyley, A., 1859. Notes of a Journey in Two Directions Across the Colony, Made in the Years 1857-8, with a View to Determine the Character and Order of the Various Geological Formations. Saul Solomon.

Yu, X., Chen, L.H. and Zeng, G., 2017. Magmatic recharge buffers the isotopic compositions against crustal contamination in formation of continental flood basalts. *Lithos*, 284, 1-10.

Zaccarini, F., Proenza, J.A., Ortega-Gutierrez, F., and Garuti, G., 2005. Platinum group minerals in ophiolitic chromitites from Tehuitzingo (Acatlan complex, southern Mexico): implications for post-magmatic modification. *Mineralogy and Petrology*, 84(3), 147-168.

Zeh, A., Gerdes, A. and Barton Jr, J.M., 2009. Archean accretion and crustal evolution of the Kalahari Craton—the zircon age and Hf isotope record of granitic rocks from Barberton/Swaziland to the Francistown Arc. *Journal of Petrology*, *50* (5), 933-966.

Zhao D., 2004. Global tomographic images of mantle plumes and subducting slabs: insight into deep earth dynamics. *Physics of the Earth and Planetary Interiors*, 1 – 2 (146), 3—34. doi.org/10.1016/j.pepi.2003.07.032

Appendices

Appendix 1

Table A1. 1 Summary of published dates for the Ventersdorp Supergroup on the Kaapvaal craton. The dates are from lithologies from the Witwatersrand block, and also from correlatives on the Kimberley and Pietersburg blocks, as well as intrusions linked to the units.

Formation	Date	Methodology	Comments
Allanridge	2701 ± 11 Ma, 2698 ± 3.6 Ma, 2692 ± 1.4 Ma, 2674 ± 11 Ma, 2659 ± 13 Ma [1]	U-Pb baddeleyite	Mafic sills linked to Allanridge lavas
Bothaville			
Rietgat	2724 ± 5.8 Ma [2]	U-Pb zircon	Dated Phokwane Formation
Makwassie	2709 ± 4 Ma [3] 2721 Ma, 2722 Ma, 2723 Ma, 2718 Ma (± 6 Ma; 4) 2729.1 ± 3 Ma [5]	U-Pb zircon U-Pb zircon	 2718 ± 6 Ma from the Kareefontein Formation of the Zoetlief Group
Goedgenoeg	2746 ± 9 Ma [4]		
Kameeldoorns	2733 ± 3.4 Ma [2] 2739 ± 39 Ma [6]	U-Pb zircon U-Pb zircon	Mohle Formation Ongers River Formation
Edenville			
Loraine			
Jeanette			
Orkney			
Alberton	2809 ± 45 Ma [7] 2714 ± 8 Ma [3]	U-Pb zircon U-Pb zircon	
Westonaria	2787 ± 2 Ma, 2789 ± 4 Ma [7]	U-Pb baddeleyite	Mafic sills linked to Klipriviersberg lavas
Venterpost	2780 ± 5 Ma [8]	U-Pb zircon	
Derdepoort volcanics Lobatse volcanics Kanye	2769 ± 2 Ma [9] 2769.3 ± 4.6 Ma [10] 2781.1 ± 4.4 Ma [11] 2781.7 ± 2 Ma [12] 2784 ± 2 Ma [13] 2785 ± 2 Ma [14]	 U-Pb zircon U-Pb zircon Pb-Pb zircon U-Pb zircon	These units have been correlated with the lower Klipriviersberg lavas

1. Olsson et al. (2010), 2. De Kock et al. (2012), 3. Armstrong et al. (1991), 4. Cornell et al. (2017), 5. Poujol et al. (2005), 6. Altermann and Lenhardt (2012), 7. Gumsley et al. (2020), 8. Barton et al. (1990), 9. Walraven et al. (1996), 10. Walraven et al. (1994), 11. Wingate (1998), 12. Walraven et al. (1996), 13. Grobler and Walraven (1993), and 14. Moore et al. (1993).

Table A1. 2 Stratigraphic column of the Ventersdorp Supergroup and the equivalents of the Ventersdorp type area formations after Grobler et al. (1989), de Kock et al. (2012), Altermann and Lenhardt (2012) and Cornell et al. (2017).

Type Area Formations	**Sodium Group Formations**	**Zoetlief Group Formations**	**Taung Area Formations**	**Amalia Group Formations**	**Fortescue Group Formations**
Allanridge					Maddina Basalt
Bothaville					Tumbiana
Rietgat	Omdraaivlai		Phokwane		Kylena Basalt
Makwassie	T'Kuip	Kareefontein		Paardefontein	Bamboo Creek/ Spinaway Porphyry
Goedgenoeg					
Kameeldoorns	Ongers River		Mohle		Hardey Sandstone
Edenville					Mt. Roe Basalt lavas
Loraine					
Jeanette					
Orkney					
Alberton					
Westonaria					
Venterspost					

Table A1. 3 *Summary of the lithological correlations between the Ventersdorp Supergroup (Kaapvaal) and the Fortescue Group (Pilbara), adapted after Grobler et al. (1989) and Nelson et al. (1992).*

Age (Ga)	Ventersdorp Supergroup	Lithology	Fortescue Group	Age (Ga)
2.68[1]	Allanridge Formation	Amygdaloidal basaltic\ andesitic lava, minor tuffs	Maddina Basalt	**2.71**[4]
	Bothaville Formation	Quartzite, shale, tuff, stromatolitic carbonates	Tumbiana Formation	**2.72**[4]
	Rietgat Formation	Amygdaloidal basalt, minor limestone, tuff, agglomerate sandstone	Kylena Basalt	
2.72[2]	Makwassie Formation	Felsic volcanic rocks and sub-volcanic intrusions	Bamboo Creek/ Spinaway Porphyry	
2.74[2]	Goedgenoeg Formation	Porphyritic basalt lavas		
	Kameeldoorns Formation	Sandstone and conglomerate with intercalated shales and siltstones. Minor tuff, basalt and stromatolites	Hardey Sandstone	
2.78[3]	Klipriviersberg Group	Amygdaloidal basalts, minor agglomerate, tuff	Mt. Roe Basalt	**2.78**[5]

1. Olsson et al. (2010), 2. Cornell et al. (2017), 3. Gumsley et al. (2020), 4. Blake et al. (2004) and 5. Arndt et al. (1991)

Appendix 2

Table A2. 1 List of samples analysed in this study and the analyses performed on them.

Sample	Formation	Sr-Nd-Hf isotopes	TE	PGE	S isotopes	TIMA	EPMA	O isotopes
R432	Westonaria	■		■				
R434	Westonaria	■	■	■	■			
R502	Westonaria	■	■	■	■	■		
R503	Westonaria	■	■	■	■	■		
R505	Westonaria	■	■	■	■			
R506	Westonaria	■	■	■	■			
R507	Westonaria	■	■	■	■	■		
R508	Westonaria	■	■	■	■			
R509	Westonaria	■	■					
R510	Westonaria		■			■	■	■
R511	Westonaria	■	■	■	■	■	■	■
R359	Westonaria	■	■					
R360	Westonaria	■	■	■	■			
R362	Westonaria	■	■					
R141	Westonaria	■	■	■	■			
R048	Westonaria	■	■	■	■			
R030	Alberton	■	■	■	■			
R040	Alberton	■	■	■	■			
R333	Orkney	■	■					
R347	Orkney	■	■	■				
R038	Alberton	■	■					
R005	Orkney	■		■	■			
R129	Alberton	■	■	■	■			
R105	Orkney	■	■	■	■			
LZ17	Jeannette	■	■	■	■			
R326	Jeannette	■	■	■				
LZ18	Orkney	■	■	■				
LZ23	Orkney	■	■					
LZ29	Orkney	■	■	■				
LZ31	Alberton	■	■	■				
LZ35	Alberton	■						
LZ41	Alberton	■	■	■				
R420	Alberton	■	■	■				
R357	Alberton	■	■					
R134	Alberton	■	■	■				
R335	Orkney	■	■	■				
PR472	Rietgat	■	■					
PR487	Rietgat	■	■					
PR182	Rietgat	■	■					
PR185	Rietgat	■						
PR189	Rietgat	■						
PR484	Rietgat	■	■					
KL136	Lora-Eden	■	■	■				

KL141	Lora-Eden	
KL142	Lora-Eden	
KL145	Lora-Eden	
KL147	Lora-Eden	
KL150	Lora-Eden	
KL153	Lora-Eden	
KL155	Lora-Eden	
KL156	Lora-Eden	
KL158	Lora-Eden	
PG163	Goedgenoeg	
PG168	Goedgenoeg	
PG166	Goedgenoeg	
PG175	Goedgenoeg	
AR199	Allanridge	
AR300	Allanridge	
AR305	Allanridge	
AR345	Allanridge	
AR364	Allanridge	
AR446	Allanridge	
AR451	Allanridge	

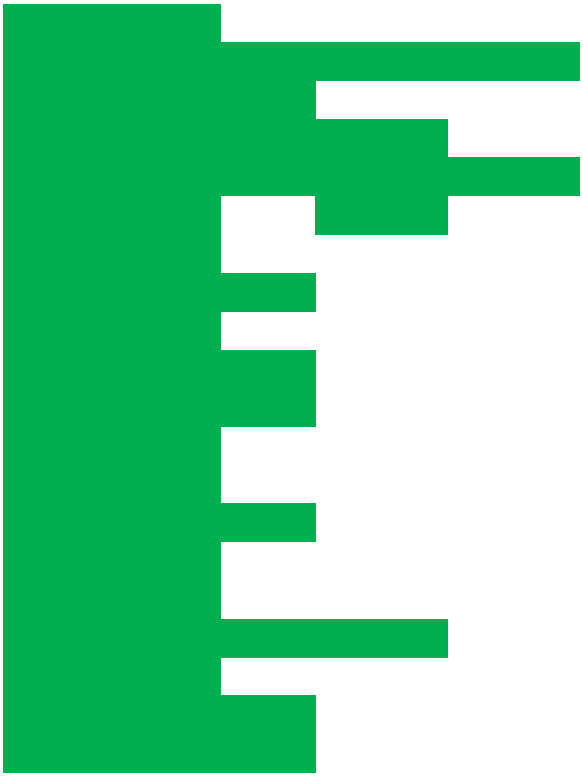

Lora-Eden = Loraine-Edenville Formations

Table A2. 2 Lu-Hf compositions of Certified Reference Materials analysed in this study.

CRM	$^{176}Hf/^{177}Hf$ final	1 SD	1SE	true value	ppm Hf	1SD	1SE	accepted	ppm Lu	1SD	1SE	accepted
KK8-AGV2	0.28296	5.79E-05	7.54E-06	0.28297	5.045	0.002678		5.137	0.2350	0.000365		0.2507
AGV2	0.28296	2.04E-05	2.97E-06	0.28297	4.541	0.001245	0.00018	5.137	0.2381	0.000221	4.93E-05	0.2507
SM-8 AGV2	0.28299	1.82E-05	2.66E-06	0.28297	4.596	0.000968	0.000141	5.137	0.2437	0.002625	0.000602	0.2507
SM2-7 AGV2	0.28299	2.01E-05	2.88E-06	0.28297	4.600	0.001209	0.000175	5.137	0.2390	0.000262	6.01E-05	0.2507
BCR2	0.28286	5.03E-05	6.73E-06	0.28286	4.993	0.00237		4.972	0.4998	0.001232		0.5049
BCR2	0.28286	3.34E-05	4.43E-06	0.28286	4.856	0.001581		4.972	0.4814	0.002883	0.000644	0.5049
MS1 BCR2	0.28288	2.45E-05	3.25E-06	0.28286	4.846	0.001339	0.000174	4.972	0.4849	0.000695	0.00016	0.5049
CJ-1-8 BCR2	0.28289	1.46E-05	2.18E-06	0.28286	4.346	0.000964	0.000141	4.972	0.4911	0.00126	0.000282	0.5049
F-7 BCR2	0.28289	2.48E-05	3.58E-06	0.28286	4.355	0.001269	0.000181	4.972	0.4914	0.001286	0.000287	0.5049
BH1 BCR2	0.28288	2.06E-05	2.94E-06	0.28286	4.359	0.001366	0.000199	4.972	0.4906	0.00165	0.000369	0.5049
WD2-1 BCR2	0.28288	3.18E-05	5.9E-06	0.28286	4.353	0.001117	0.000215	4.972	0.4912	0.002021	0.000452	0.5049
BHVO2	0.28305	5.69E-05	7.6E-06	0.28308	4.439	0.002414		4.47	0.2721	0.000577		0.275
D4 BHVO2	0.28308	2.23E-05	2.93E-06	0.28308	4.487	0.001098	0.000147	4.47	0.2815	0.000894	0.0002	0.275
J1 BHVO2	0.28306	2.57E-05	3.35E-06	0.28308	4.493	0.001226	0.000161	4.47	0.2823	0.000379	8.69E-05	0.275
G-8 BHVO2	0.28309	2.64E-05	3.77E-06	0.28308	3.928	0.000879	0.000127	4.47	0.2706	0.000697	0.000156	0.275
K8b BHV02	0.28311	2.08E-05	3.01E-06	0.28308	3.902	0.00094	0.000133	4.47	0.2673	0.000832	0.000186	0.275
M8b BHV02	0.28310	2.81E-05	4.01E-06	0.28308	3.923	0.000898	0.00013	4.47	0.2738	0.003868	0.000864	0.275
WD1-1 BHV02	0.28310	2.86E-05	4.05E-06	0.28308	3.931	0.001203	0.000174	4.47	0.2788	0.003651	0.000837	0.275

AGV2 = Guano Valley Andesite, BCR2 = Columbia River Basalt, BHVO2 = Hawaiian Basalt

The letters and numbers before the CRM name are batch IDs.

Table A2. 3 Sm-Nd compositions of the Certified Reference Materials used in this study.

CRM	$^{143}Nd/^{144}Nd$ final	1 SD	1SE	Accepted	ppm Nd	1SD	1 SE	Accepted	ppm Sm	1SD	1 SE	Accepted	$^{147}Sm/^{144}Nd$	1SD	1 SE	Accepted
KK-8 AGV2	0.5128	2.58E-05	3.42E-06	0.51279	29.79	8.81E-03		30.49	5.35	4.7E-04		5.51	0.10848	3.35E-05		0.109
AGV2	0.51279	2.78E-05	3.69E-06	0.51279	30.22	1.43E-02		30.49	5.42	5.0E-04		5.51	0.10849	5.22E-05		0.109
Li-4 AGV2	0.51277	2.11E-05	3.11E-06	0.51279	30.54	1.17E-02	1.69E-03	30.49	5.52	3.8E-04	5.4E-05	5.51	0.10923	4.25E-05	6.14E-06	0.109
Li-5 AGV2	0.51277	3.10E-05	4.48E-06	0.51279	30.6	1.37E-02	1.95E-03	30.49	5.53	2.8E-04	4.0E-05	5.51	0.10923	4.91E-05	7.02E-06	0.109
AGV2	0.51282	2.65E-05	3.82E-06	0.51279	30.29	1.39E-02	2.01E-03	30.49	5.47	2.4E-04	5.5E-05	5.51	0.10918	5.03E-05	7.31E-06	0.109
BCR2	0.51266	5.09E-05	6.74E-06	0.51264	28.4	2.18E-02		28.26	6.48	6.7E-04		6.55	0.13787	0.000107		0.138
BCR2	0.51263	2.69E-05	3.57E-06	0.51264	28.28	9.43E-03		28.26	6.44	5.4E-04		6.55	0.13774	4.74E-05		0.138
C5 BCR2	0.51264	1.77E-05	2.30E-06	0.51264	28.34	6.31E-03	8.36E-04	28.26	6.45	2.0E-04	4.7E-05	6.55	0.13751	3.09E-05	4.18E-06	0.138
MS1 BCR2	0.51264	5.02E-05	6.65E-06	0.51264	28.38	1.71E-02	2.28E-03	28.26	6.49	6.2E-04	1.4E-04	6.55	0.13837	8.43E-05	1.15E-05	0.138
F-7 BCR2	0.51265	2.74E-05	4.00E-06	0.51264	28.58	1.26E-02	1.82E-03	28.26	6.56	4.2E-04	9.5E-05	6.55	0.13877	6.18E-05	9.05E-06	0.138
BH1 BCR2	0.5126	2.54E-05	3.66E-06	0.51264	28.76	1.32E-02	1.89E-03	28.26	6.58	3.8E-04	9.0E-05	6.55	0.13841	6.41E-05	9.28E-06	0.138
WD2-1 BCR2	0.51263	2.60E-05	3.75E-06	0.51264	28.51	1.29E-02	1.85E-03	28.26	6.55	1.9E-04	4.4E-05	6.55	0.13880	6.31E-05	9.05E-06	0.138
JM6-4 BCR2	0.51261	2.36E-05	3.37E-06	0.51264	28.52	1.14E-02	1.64E-03	28.26	6.55	3.8E-04	8.6E-05	6.55	0.13886	5.63E-05	8.17E-06	0.138
BHVO2	0.51298	3.67E-05	4.86E-06	0.51298	24.22	1.27E-02		24.27	5.99	5.3E-04		6.02	0.14954	7.92E-05		0.150
JM8 BHVO2	0.513	2.49E-05	3.33E-06	0.51298	24.23	7.96E-03	1.05E-03	24.27	5.99	3.8E-04	8.8E-05	6.02	0.14951	5.00E-05	6.81E-06	0.150
D4 BHVO2	0.51299	2.44E-05	3.21E-06	0.51298	24.32	8.61E-03	1.14E-03	24.27	6.01	3.0E-04	6.8E-05	6.02	0.14950	5.34E-05	7.21E-06	0.150
J1 BHVO2	0.51304	3.60E-05	4.86E-06	0.51298	24.49	1.26E-02	1.67E-03	24.27	6.05	3.5E-04	7.8E-05	6.02	0.14939	7.75E-05	1.04E-05	0.150
KD7 BHVO2	0.51299	2.24E-05	2.94E-06	0.51298	24.25	7.04E-03	9.25E-04	24.27	6.00	3.4E-04	7.7E-05	6.02	0.14947	4.42E-05	6.01E-06	0.150
BHVO2	0.51298	2.23E-05	3.16E-06	0.51298	24.22	7.00E-03	1.01E-03	24.27	5.99	2.7E-04	6.1E-05	6.02	0.14948	4.37E-05	6.42E-06	0.150
JB-4 BHVO2	0.51303	7.66E-05	1.12E-05	0.51298	24.12	2.84E-02	4.06E-03	24.27	5.96	1.3E-03	2.9E-04	6.02	0.14945	0.000179	2.62E-05	0.150
K8 BHVO2	0.51298	3.22E-05	4.60E-06	0.51298	24.37	1.24E-02	1.79E-03	24.27	6.07	4.3E-04	9.6E-05	6.02	0.15053	7.75E-05	1.13E-05	0.150
JM2-8 BHVO2	0.513	3.75E-05	5.35E-06	0.51298	24.5	1.32E-02	1.88E-03	24.27	6.10	4.3E-04	9.9E-05	6.02	0.15050	8.15E-05	1.18E-05	0.150
RP1 BHVO2	0.51298	3.29E-05	4.75E-06	0.51298	24.52	1.09E-02	1.61E-03	24.27	6.10	4.3E-04	9.5E-05	6.02	0.15046	6.77E-05	1.01E-05	0.150
CR1 BHVO2	0.51295	4.61E-05	6.72E-06	0.51298	24.48	1.76E-02	2.54E-03	24.27	6.09	3.2E-04	7.4E-05	6.02	0.15046	0.000108	1.57E-05	0.150
WD1-1 BHVO2	0.51296	3.58E-05	5.12E-06	0.51298	24.51	1.25E-02	1.81E-03	24.27	6.10	3.6E-04	8.1E-05	6.02	0.15060	7.74E-05	1.13E-05	0.150
JM4-1 BHVO2	0.51296	3.03E-05	4.34E-06	0.51298	24.5	9.72E-03	1.40E-03	24.27	6.10	3.8E-04	8.6E-05	6.02	0.15056	6.04E-05	8.88E-06	0.150
M8 BHVO2	0.51295	2.85E-05	4.07E-06	0.51298	24.47	9.41E-03	1.36E-03	24.27	6.09	5.6E-04	1.3E-04	6.02	0.15059	5.95E-05	8.91E-06	0.150

AGV2 = Guano Valley Andesite, BCR2 = Columbia River Basalt, BHVO2 = Hawaiian Basalt

The letters and numbers before the CRM name are batch IDs.

Table A2. 4 Rb-Sr compositions of the Certified Reference Material analysed in this study.

CRM	$^{87}Sr/^{86}Sr$ final	1 SD	1SE	Accepted	ppm Sr	1SD	1SE	Accepted	ppm Rb	1SD	1SE	Accepted
KK_8 AGV2	0.70393	2.34E-05	3.52E-06	0.70399	639.43	2.33E-01		659.5	67.15	5.51E-03		67.79
Li-4 AGV2	0.70401	1.40E-05	2.16E-06	0.70399	649.49	1.10E-01	1.67E-02	659.5	67.76	1.80E-02	4.02E-03	67.79
Li-5 AGV2	0.70391	1.75E-05	2.64E-06	0.70399	649.84	1.07E-01	1.62E-02	659.5	68.06	1.33E-02	2.97E-03	67.79
GG1-6 AGV2	0.70400	2.29E-05	3.46E-06	0.70399	650.41	1.21E-01	1.87E-02	659.5	68.04	1.45E-02	3.43E-03	67.79
GG3-4 AGV2	0.70397	2.15E-05	3.24E-06	0.70399	645.30	1.17E-01	1.74E-02	659.5	67.48	1.91E-02	4.27E-03	67.79
GG4-4 AGV2	0.70397	2.01E-05	3.10E-06	0.70399	652.77	1.38E-01	2.08E-02	659.5	68.17	2.76E-02	6.17E-03	67.79
LS1 AGV2	0.70393	2.16E-05	3.34E-06	0.70399	643.20	2.41E-01	3.63E-02	659.5	67.66	3.81E-03	8.53E-04	67.79
BHVO2	0.70343	3.29E-05	4.96E-06	0.70348	392.23	2.10E-01		394	9.26	2.57E-03		9.261
D4 BHVO2	0.70346	3.64E-05	5.49E-06	0.70348	393.37	1.16E-01	1.76E-02	394	9.24	6.87E-04	1.54E-04	9.261
J6 BHVO2	0.70348	2.49E-05	3.67E-06	0.70348	394.94	1.93E-01	2.88E-02	394	9.31	9.07E-04	2.03E-04	9.261
JM8 BHVO2	0.70346	3.36E-05	5.06E-06	0.70348	394.94	1.88E-01	2.87E-02	394	9.22	2.15E-03	4.94E-04	9.261
GB8 BHVO-2	0.70346	2.66E-05	3.97E-06	0.70348	388.87	2.90E-01	4.37E-02	394	9.25	1.23E-02	2.83E-03	9.261
M8 BHV02	0.70343	2.82E-05	4.25E-06	0.70348	386.48	1.32E-01	2.06E-02	394	9.15	6.71E-04	1.54E-04	9.261
BCR2	0.70495	2.98E-05	4.44E-06	0.70492	337.23	3.01E-01		337	47.68	9.43E-03		46.02
BCR2	0.70499	2.09E-05	3.16E-06	0.70492	332.99	5.30E-02	8.00E-03	337	46.89	1.26E-02	2.82E-03	46.02
MS1 BCR2	0.70504	2.74E-05	4.09E-06	0.70492	335.78	2.09E-01	3.12E-02	337	47.00	5.61E-03	1.25E-03	46.02
Li-3 BCR2	0.70494	1.96E-05	2.95E-06	0.70492	334.93	1.33E-01	1.98E-02	337	47.44	4.69E-03	1.08E-03	46.02
F7 BCR2	0.70500	1.81E-05	2.74E-06	0.70492	334.31	1.21E-01	1.78E-02	337	46.90	2.50E-03	5.89E-04	46.02
GG5-1 BCR2	0.70501	1.81E-05	2.70E-06		332.42	7.73E-02	1.15E-02		46.72	1.42E-02	3.26E-03	
BH1 BCR2	0.70501	2.37E-05	3.58E-06	0.70492	332.71	1.39E-01	2.09E-02	337	47.03	7.29E-03	1.67E-03	46.02
GG7-7 BCR2	0.70499	2.77E-05	4.22E-06	0.70492	333.93	9.40E-02	1.43E-02	337	47.16	5.99E-03	1.34E-03	46.02
E8 GSP2	0.76522	2.11E-05	3.42E-06	0.76496	233.66	3.77E-02	6.04E-03	230	242.46	1.52E-01	3.39E-02	245

AGV2 = Guano Valley Andesite, BCR2 = Columbia River Basalt, BHVO2 = Hawaiian Basalt

The letters and numbers before the CRM name are batch IDs

Table A2. 5 Concentration of sulphur from sulphides in the samples

Sample	Mass (g)	Mass (mg)	Approximate S content (%)
	1st Batch		
KL150	1.2273	0.65	0.053%
KL153	1.2552	0.94	0.075%
KL142	1.2235	1.11	0.091%
R503	1.5454	1.29	0.083%
LZ17	2.051	1.51	0.074%
R502	1.9856	1.93	0.097%
R505	2.2596	1.94	0.086%
R507	1.9612	2.3	0.117%
R105	1.9633	2.54	0.129%
R129	1.4596	2.58	0.177%
R360	1.4205	2.82	0.199%
R506	2.0419	3.03	0.148%
R005	1.44	3.1	0.215%
R141	1.9847	3.22	0.162%
R508	1.4143	3.22	0.228%
R040	2.0619	3.31	0.161%
R511	1.9762	3.35	0.170%
R030	2.0698	4.53	0.219%
R048	1.9836	6.52	0.329%
R434	1.9537	33.11	1.695%
	2nd batch		
KL150 b	1.2544	0.618	0.049%
KL153 b	1.1827	0.83	0.070%
KL142 b	0.9179	0.672	0.073%
LZ17 b	2.1457	1.222	0.057%
	3rd batch		
R503 b	1.6825	1.18	0.070%
LZ17 c	1.7192	1.219	0.071%
R502 b	1.7655	1.192	0.068%
R505 b	1.7875	4.687	0.262%

Table A2. 6 Fluorination yield results

Day of purification	Name	Weight Ag2S (mg)	Fluorination yield (%)	Comment
20-10-2022	KL142 AB-CM	1.762	**84**	KL142 + KL142 b
24-10-2022	KL150 AB-CM	1.267	**79**	KL150 + KL150 b
21-10-2022	LZ17 AB-CM	1.463	**87**	
20-10-2022	LZ17 2 AB-CM	2.468	**86**	LZ17 b + LZ17 c
20-10-2022	R005 AB-CM	3.138	**81**	
21-10-2022	R030 AB-CM	4.897	**43**	
21-10-2022	R040 AB-CM	3.337	**86**	
04-10-2022	R048 AB-CM	2.727	**97**	
20-10-2022	R105 AB-CM	2.573	**64**	
21-10-2022	R129 AB-CM	2.546	**84**	
20-10-2022	R141 AB-CM	3.285	**87**	
21-10-2022	R360 AB-CM	2.608	**49**	
04-10-2022	R434 AB-CM	4.560	**106**	
19-10-2022	R502 AB-CM	3.457	**66**	R502 + R502 b
19-10-2022	R503 AB-CM	2.447	**67**	R503 + R503 b
20-10-2022	R505 AB-CM	1.806	**104**	
20-10-2022	R505 b AB-CM	2.250	**94**	
21-10-2022	R506 AB-CM	3.027	**97**	
21-10-2022	R507 AB-CM	2.315	**91**	
21-10-2022	R508 AB-CM	3.344	**70**	
20-10-2022	R511 AB-CM	3.500	**83**	
19-10-2022	KL 153	1.699	**88**	KL153 + KL153 b

Appendix 3

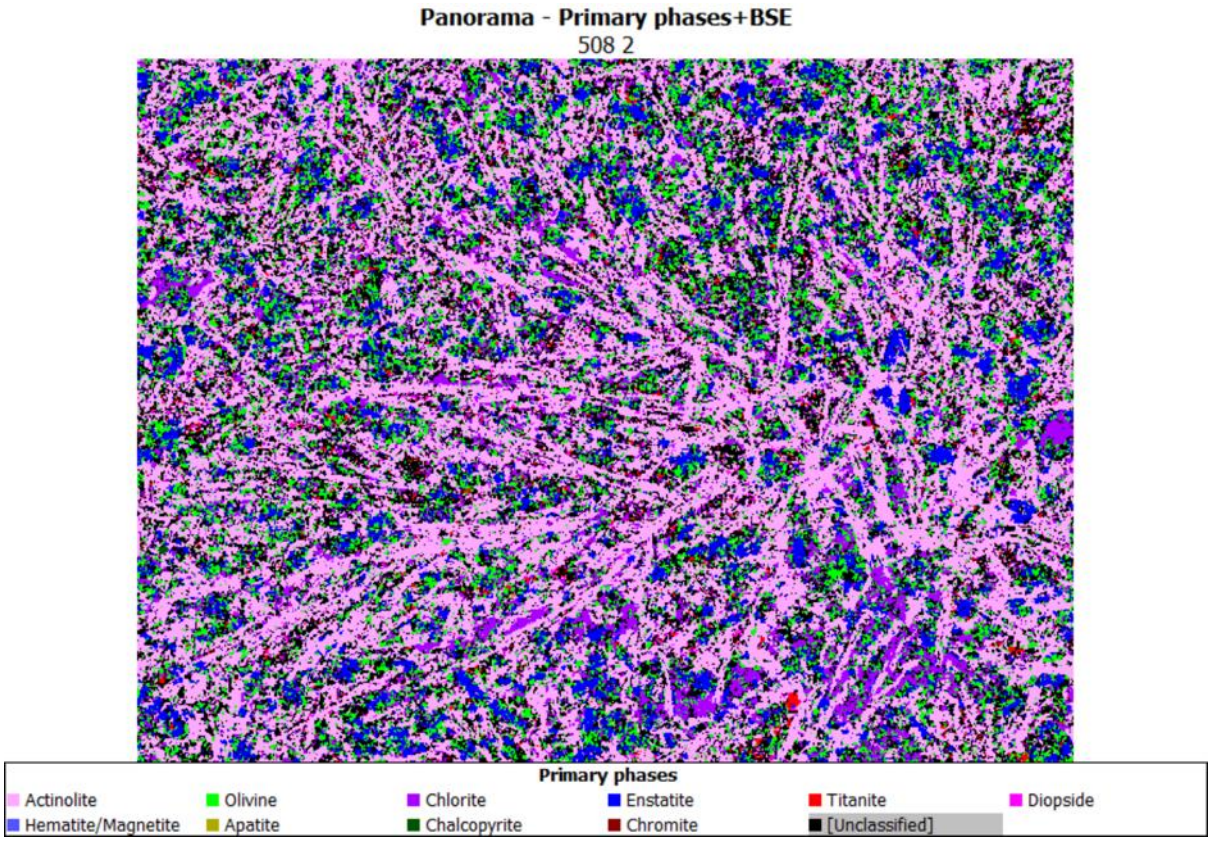

Figure A1. 1TIMA image of the macro-spinifex showing secondary actinolite needles and matrix made up of enstatite, chlorite, titanite and possible olivine.

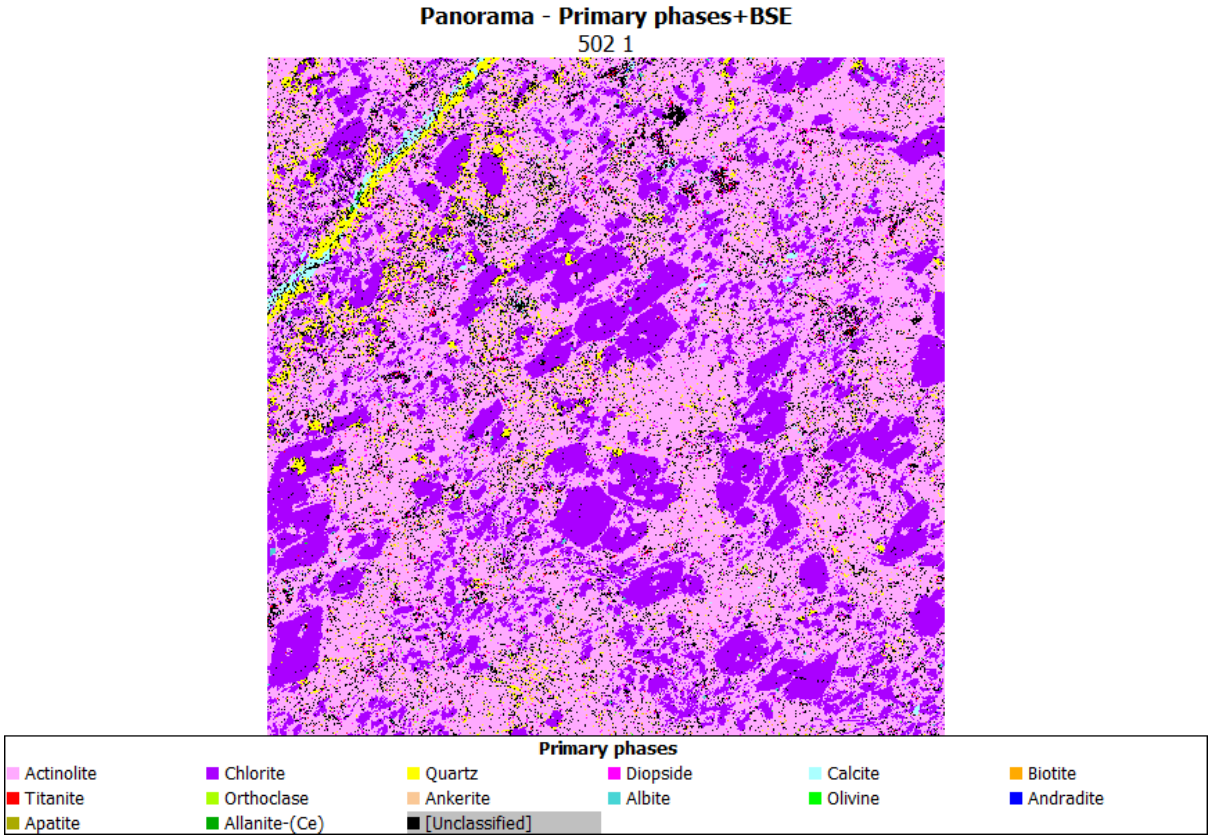

Figure A1. 2 TIMA image of phenocrystic-rich section showing a calcite-quartz vein. The chloritized phenocrysts show alignment and clustering in 'pockets'.

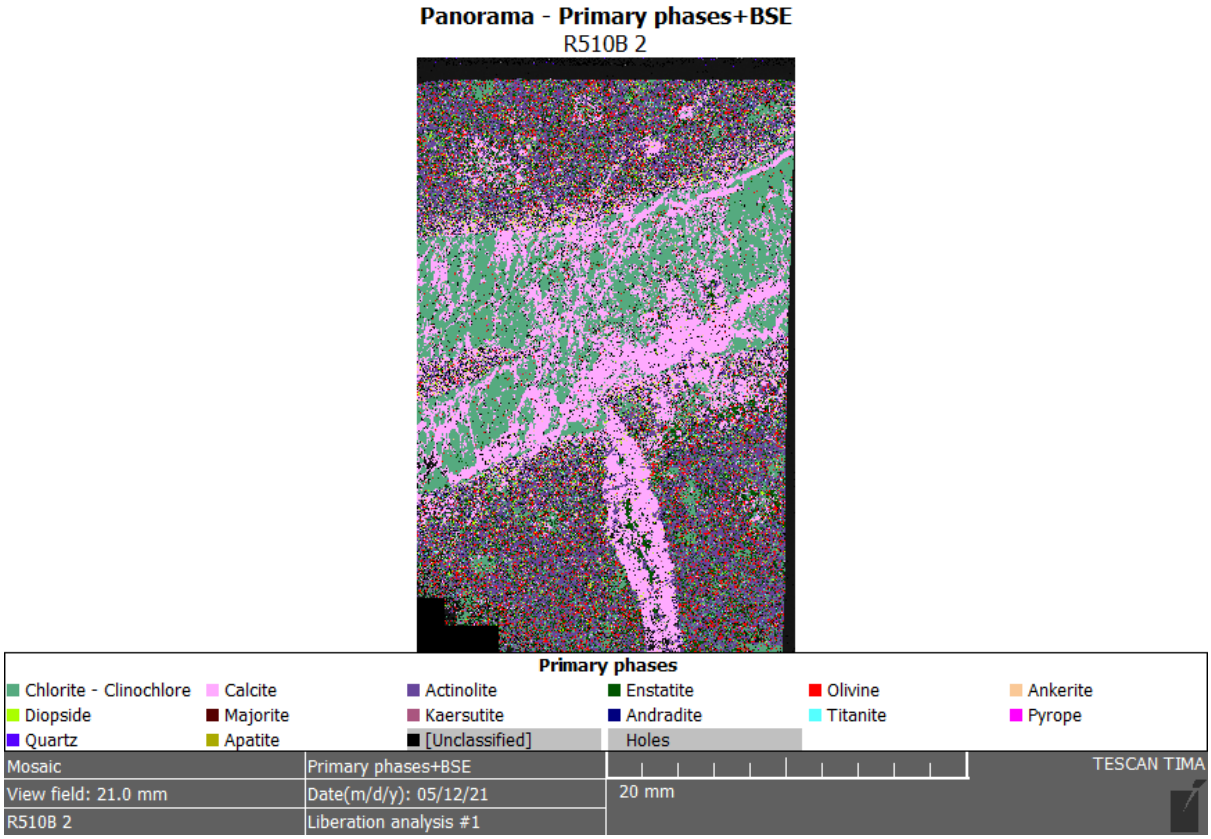

Figure A1. 3 TIMA image of a full thin section of the pyroxene cumulate zone showing a calcite-chlorite vein.

Table A3. 1 Major and trace element compositions of the Westonaria komatiites

Borehole	**E0**	**E1**		**E3**		**E4**					**E5**				
Location	-26.427561	-26.451571		-26.456388		-26.412318					-26.463085				
	29.06953	28.921364		29.144573		28.987718					28.911404				
Position above base (m)	4	4	20	16	2	1	6	41	38	31	22	17	13	7	2
wt. %	**R048**	**R141**	**R359**	**R360**	**R362**	**R434**	**R432**	**R502**	**R503**	**R505**	**R506**	**R507**	**R508**	**R509**	**R511**
SiO2	48.55	52.64	53.68	49.69	51.70	50.74	52.83	51.73	50.14	54.18	50.62	51.04	50.85	52.17	52.52
TiO2	0.73	1.00	1.13	0.78	0.80	0.94	1.29	0.91	0.86	0.98	0.95	0.93	1.13	1.03	0.93
Al2O3	3.59	5.73	10.16	6.71	3.82	4.70	5.35	7.19	6.27	5.85	5.58	5.81	5.16	5.05	4.83
FeO*	13.82	13.20	10.00	10.13	13.24	14.13	12.95	11.62	10.94	11.35	11.55	10.82	12.48	12.23	11.46
Fe2O3*	2.71	2.59	1.96	1.99	2.60	2.77	2.54	2.28	2.15	2.23	2.27	2.12	2.45	2.40	2.25
MnO	0.21	0.17	0.22	0.19	0.20	0.21	0.24	0.18	0.16	0.14	0.17	0.17	0.14	0.15	0.18
MgO	21.60	20.14	16.32	23.24	18.77	20.87	15.20	21.94	22.72	19.82	21.35	22.66	23.96	24.99	23.14
CaO	8.69	4.40	6.24	7.13	8.54	5.52	9.22	4.05	6.45	5.33	7.31	6.25	3.63	1.80	4.49
Na2O			0.10	0.02	0.06		0.11		0.18	0.01	0.07	0.09	0.09	0.06	0.06
K2O	0.02	0.02	0.08	0.04	0.16	0.03	0.16	0.01	0.04	0.02	0.03	0.01		0.01	0.04
P2O5	0.06	0.10	0.11	0.08	0.10	0.09	0.11	0.09	0.09	0.09	0.10	0.10	0.11	0.11	0.10
Total	100	100	100	100	100	100	100	100	100	100	100	100	100	100	100
LOI	11.18	6.52	5.16	6.23	2.94	5.39	6.24	5.64	5.48	4.95	4.71	5.6	5.18	5.46	5.85
ppm															
Li	2.85	8.46	62.58	31.93	7.04	5.45		45.81	26.13	28.69	33.26	22.05	19.62	17.99	25.73
P	182.61	368.97	389.78	290.73	325.39	345.41		355.77	326.14	343.37	366.72	340.69	454.81	393.96	329.76
Sc	10.55	11.99	16.66	16.35	12.43	12.51		13.07	11.35	14.00	15.30	8.46	18.63	15.86	9.29
Ti	3480.00	3932.07	4910.14	3740.33	3651.73	4716.42		4026.65	3173.17	4184.45	4528.67	3667.13	5103.79	4707.88	3568.53
V	76.22	106.53	184.16	130.69	86.73	96.08		171.37	151.56	95.28	103.96	107.34	132.31	103.06	97.18
Cr	872.54	1085.39	1167.53	1689.66	913.42	1023.77		1170.72	1439.41	1162.70	1246.54	1100.91	842.04	819.24	1159.26
Co	115.81	101.63	62.31	105.10	106.56	109.16		81.61	102.46	86.44	91.90	88.92	91.97	103.93	95.48
Ni	1343.28	1010.72	483.58	1508.81	1058.02	1051.93		866.91	1280.43	940.76	999.97	939.07	968.55	1246.31	1031.48
Cu	306.62	186.42	33.38	212.36	202.51	263.35		84.05	70.82	177.31	178.44	154.43	244.11	180.22	193.02
Zn	142.86	123.69	94.44	83.59	119.66	135.40		104.03	136.32	147.29	131.63	145.97	87.87	103.53	90.56
Ga	5.87	8.11	12.12	10.15	6.32	7.51		10.77	9.47	8.93	8.59	8.00	8.24	7.18	6.92
Rb	0.14	0.63	2.23	1.88	1.16	0.39		9.58	1.13	0.99	1.68	0.73	0.61	0.52	3.11
Sr	47.99	93.59	26.05	33.30	42.46	87.16		88.82	47.25	69.17	48.49	50.79	28.44	21.72	107.29
Y	5.63	9.36	11.32	8.20	7.64	9.53		10.53	9.23	8.54	9.46	9.29	12.50	9.33	7.93
Zr	47.44	71.47	74.43	55.10	56.83	71.34		67.20	55.19	70.27	76.52	67.61	82.31	76.14	61.29
Nb	7.74	7.45	2.73	1.92	8.38	10.56		2.49	2.12	7.22	7.68	7.83	9.53	8.60	7.44
Sn	0.88	1.08	0.88	0.86	1.37	1.13		1.01	0.70	2.13	1.52	0.94	1.51	0.96	1.31
Sb	1.74	0.26	1.55	5.60	0.66	0.62		0.41	1.32	0.43	1.21	0.62	0.42	0.22	0.67
Cs	0.24	2.12	1.86	3.26	1.36	1.85		1.58	1.86	1.16	1.48	0.99	1.52	1.46	3.21
Ba	1.32	6.86	8.99	3.82	5.27	5.37		1274.43	28.59	18.33	17.86	10.62	11.80	11.12	17.15

La	13.19	11.19	4.70	6.82	6.00	9.58	9.41	2.30	18.96	10.66	11.70	10.44	5.75	7.96
Ce	25.28	25.47	11.92	14.95	16.39	24.80	19.11	6.44	39.03	24.69	27.92	28.72	18.16	20.89
Pr	3.00	3.15	1.66	1.76	2.23	3.43	2.23	1.05	4.34	3.14	3.47	3.93	2.75	2.92
Nd	12.24	13.49	8.20	7.64	9.99	15.56	9.80	5.68	17.83	14.00	14.91	18.01	12.61	13.30
Sm	2.22	2.82	2.39	1.84	2.24	3.28	2.45	1.86	3.27	3.03	3.15	3.82	3.02	3.05
Eu	0.67	0.95	0.86	0.74	0.73	1.18	1.07	0.76	0.96	0.96	0.84	1.20	0.94	0.90
Gd	1.89	2.68	2.70	2.00	2.18	2.92	2.65	2.15	2.85	2.78	2.90	3.76	2.66	2.74
Tb	0.24	0.37	0.42	0.30	0.31	0.39	0.39	0.33	0.37	0.38	0.39	0.49	0.38	0.37
Dy	1.31	2.08	2.53	1.79	1.74	2.15	2.36	2.00	2.02	2.12	2.17	2.71	2.10	2.04
Ho	0.24	0.39	0.48	0.34	0.32	0.40	0.45	0.38	0.37	0.39	0.39	0.52	0.40	0.37
Er	0.63	1.03	1.25	0.88	0.81	1.04	1.15	0.99	0.96	1.01	1.02	1.33	1.16	0.93
Tm	0.08	0.14	0.17	0.12	0.11	0.13	0.16	0.13	0.13	0.13	0.14	0.18	0.19	0.12
Yb	0.55	0.84	1.02	0.74	0.67	0.83	0.98	0.80	0.79	0.85	0.82	1.08	1.57	0.73
Lu	0.08	0.12	0.15	0.10	0.10	0.11	0.14	0.11	0.11	0.12	0.12	0.16	0.23	0.10
Hf	1.26	1.83	2.07	1.51	1.47	1.84	1.80	1.43	1.84	1.98	1.69	2.12	1.99	1.58
Ta	0.54	0.41	0.01	0.12	0.59	0.79	-0.01	-0.04	0.47	0.49	0.43	0.55	0.48	0.41
W	0.13	0.12	0.10	0.36	0.08	3.01	0.14	0.03	0.23	0.26	0.08	0.14	0.10	0.12
Tl	0.02	0.02	0.02	0.04	0.11	0.10	0.09	0.01	0.03	0.05	0.01	0.03	0.04	0.06
Pb	1.61	0.86	3.01	2.73	1.67	0.82	3.91	2.16	2.31	4.88	3.40	1.95	2.64	1.41
Th	1.00	1.21	1.10	0.91	1.12	1.51	0.98	0.80	1.34	1.46	1.23	1.31	1.20	0.99
U	0.46	0.41	0.36	0.27	0.70	0.77	0.32	0.28	0.46	0.49	0.47	0.59	0.54	0.39

The major element data were collected from Myers (1990). FeO* is the Fe2+ calculated from the total Fe oxide with Fe2+/Fe3+ set at 0.85. BCR2 and BHVO2 are the Certified Reference Materials (CRM) measured to monitor the precision and accuracy of the ICPMS data.

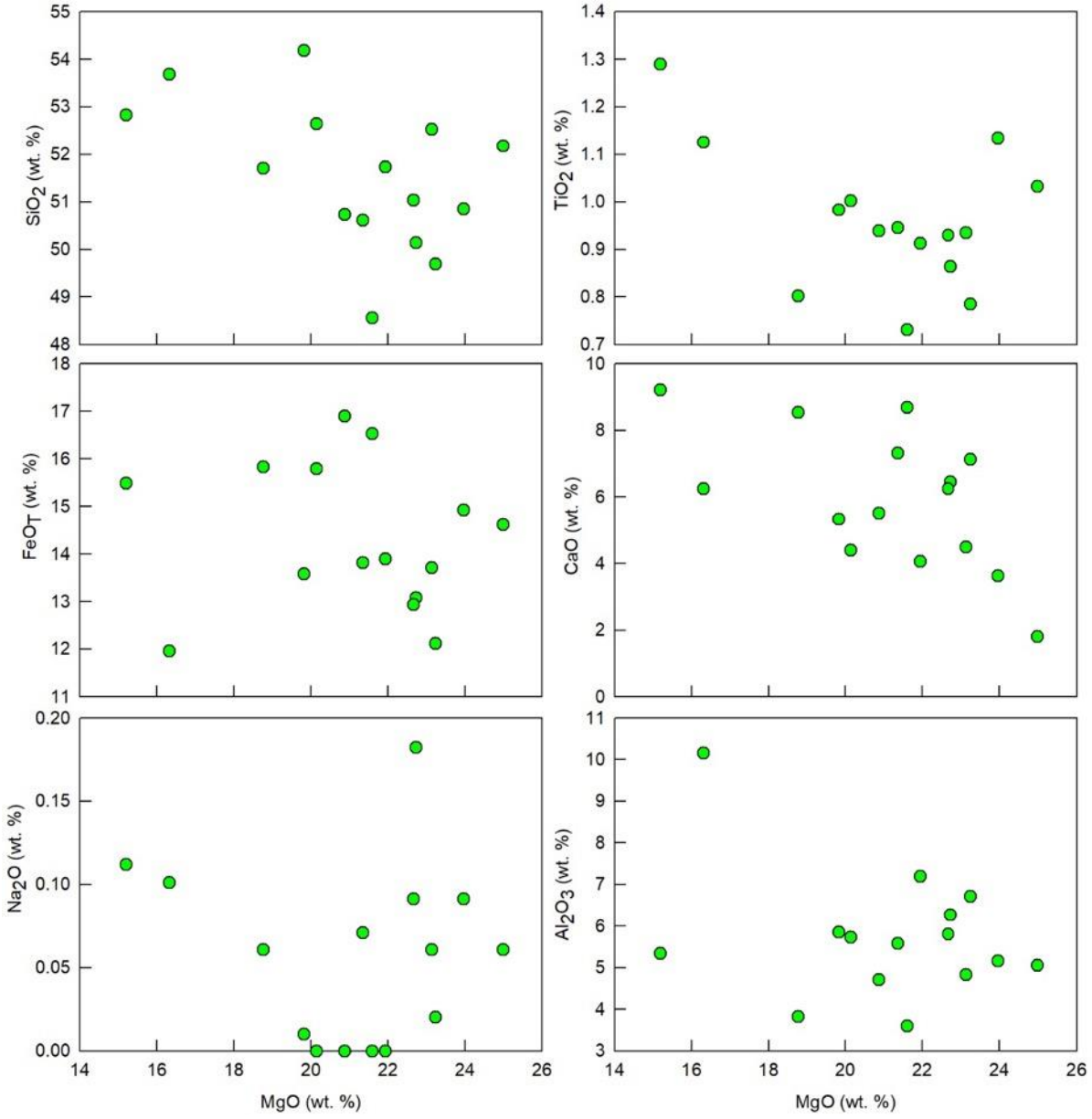

Figure A1. 4 Variation plots for major elements if the Westonaria whole rock samples. Almost all major elements display scattered (poor constrained trends) plots against MgO. The major elements display poor negative correlations with MgO.

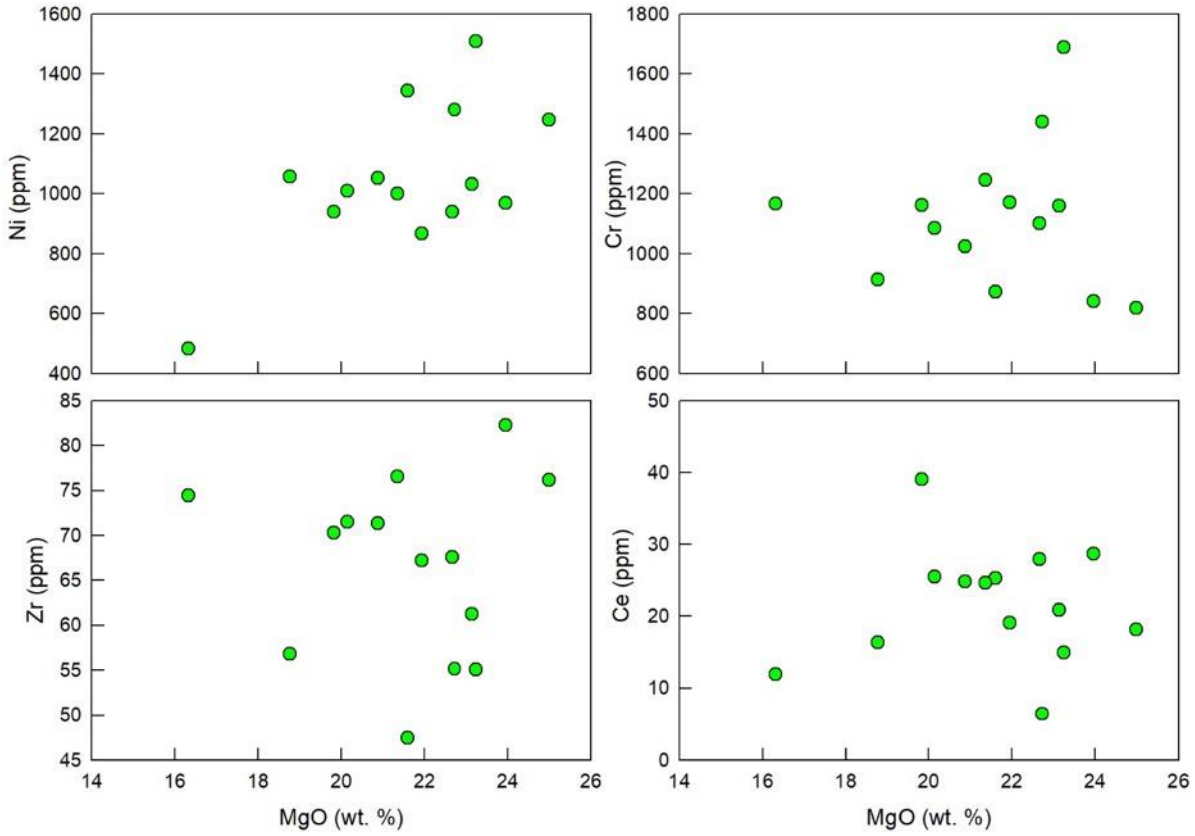

Figure A1. 5 MgO variation plots of Ni, Cr, Zr and Ce of the Westonaria samples. Nickel shows a weak positive correlation with MgO with unifrom Ni contents (~1000 ppm) observed over a range of MgO values (19–24 wt. %). Cr values are scattered, with most samples having Cr concentrations of 1000-1200 ppm.

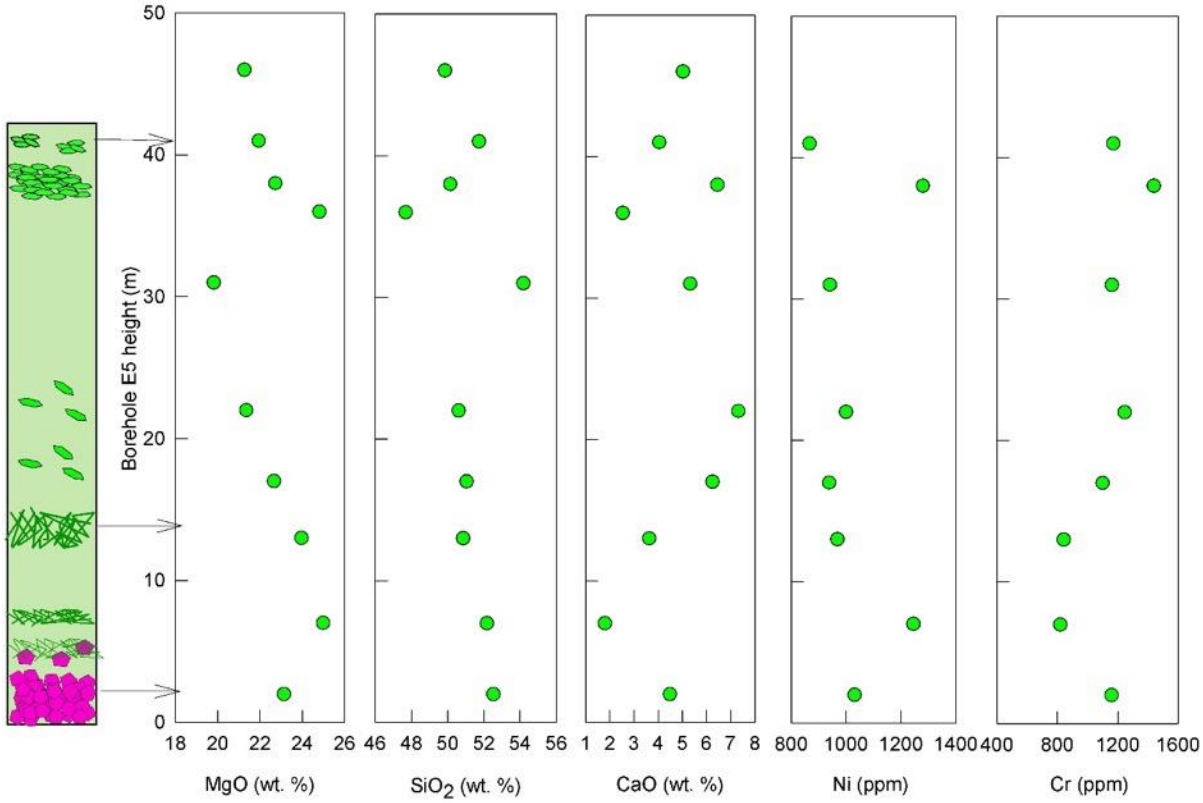

Figure A1. 6 Variations in major and trace elements in sections across borehole E5 displaying a well developed komatiite flow.

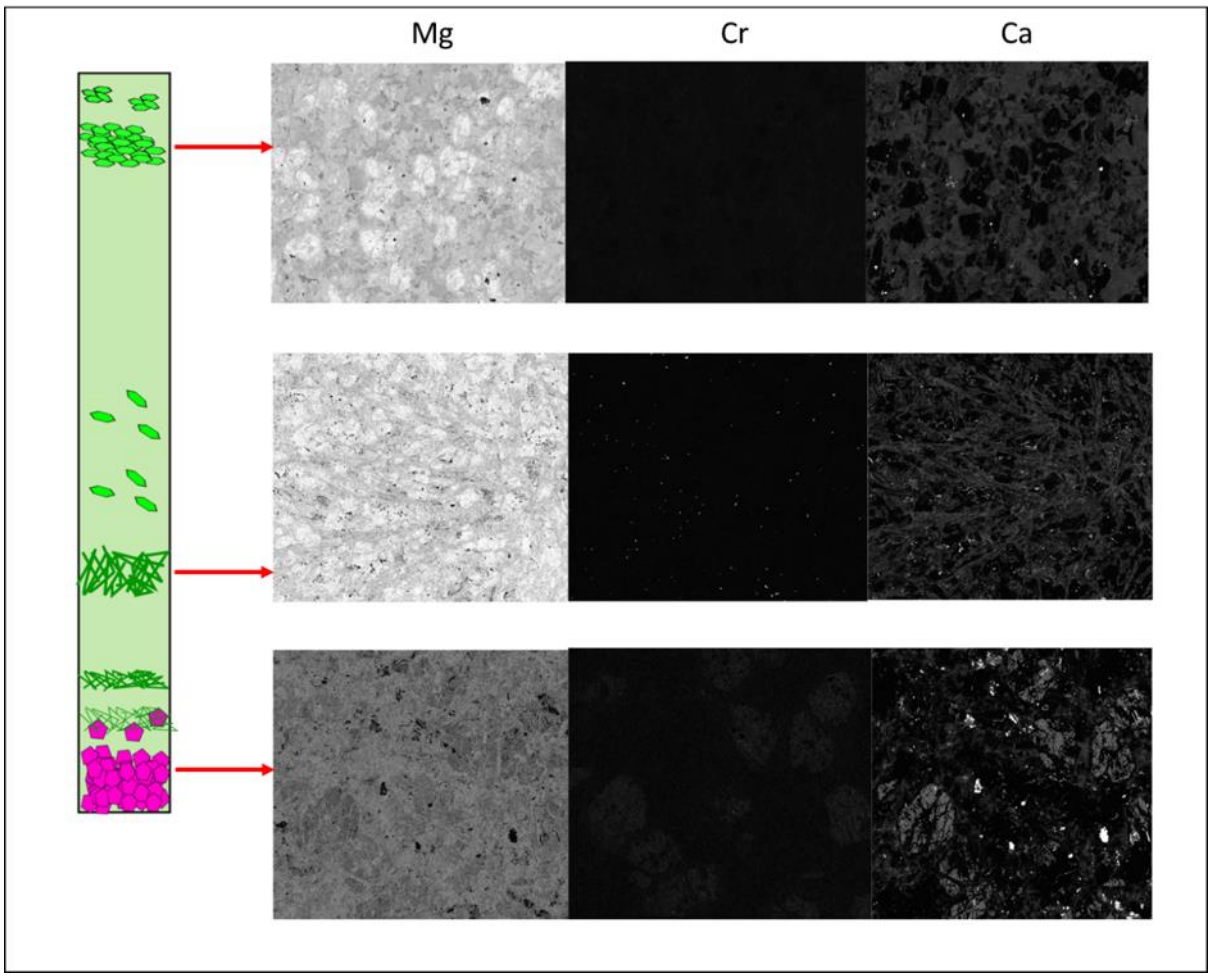

Figure A1. 7 Variations in Mg Cr and Ca, between cumulates and spinifex zones, and the element distribution between phenocrysts and matrix.

Table A3. 2 Major element composition of clinopyroxene grains in the Westonaria komatiites

Spot ID	Sample	SiO2	Al2O3	TiO2	Cr2O3	FeO	MnO	MgO	NiO	ZnO	CaO	Na2O	K2O	Total
B1b@1	R510B_3	55.66	0.50	0.34	0.91	5.50	0.21	18.24	0.08	0.00	18.03	0.46	0.07	100
B1b@2		53.75	0.47	0.29	0.88	5.66	0.16	19.66	0.10	0.00	18.64	0.38	0.02	100
B1b@3		53.58	0.60	0.33	0.99	5.12	0.15	19.05	0.10	0.00	19.62	0.45	0.00	100
B1b@4		53.60	0.45	0.31	1.01	5.59	0.22	19.22	0.15	0.02	18.94	0.48	0.00	100
B1b@6		54.00	0.50	0.31	0.78	5.18	0.16	19.37	0.08	0.01	19.20	0.40	0.01	100
B1b@7		55.51	0.50	0.24	0.81	5.57	0.12	18.58	0.15	0.02	18.13	0.37	0.00	100
B1b@8		54.36	0.50	0.30	0.90	5.44	0.17	19.01	0.11	0.01	18.75	0.42	0.02	100
B2a@1	R511B_1	54.44	0.58	0.40	0.61	5.78	0.15	17.75	0.05	0.04	19.73	0.48	0.00	100
B2a@2		53.81	0.51	0.36	0.86	5.32	0.16	18.26	0.11	0.04	20.12	0.44	0.01	100
B2a@3		52.42	0.63	0.34	0.97	5.13	0.14	19.56	0.10	0.00	20.23	0.48	0.00	100
B2a@4		52.41	0.65	0.50	0.69	5.92	0.18	18.83	0.06	0.00	20.29	0.48	0.00	100
B2a@5		53.28	0.59	0.40	0.78	5.54	0.16	18.59	0.08	0.02	20.09	0.47	0.00	100
B2a@6		52.98	0.60	0.40	0.82	5.48	0.16	18.81	0.09	0.01	20.18	0.47	0.00	100
B2a@7		52.77	0.62	0.41	0.81	5.51	0.16	18.95	0.08	0.01	20.20	0.48	0.00	100
B2a@8		52.86	0.61	0.43	0.78	5.61	0.16	18.79	0.08	0.01	20.19	0.48	0.00	100
B2b@1	R511B_2	53.79	0.67	0.55	0.93	5.64	0.14	17.66	0.09	0.00	20.02	0.50	0.01	100
B2b@2		53.84	0.57	0.40	0.96	5.26	0.16	18.45	0.14	0.04	19.72	0.47	0.00	100
B2b@3		53.65	0.71	0.39	1.18	5.19	0.12	17.68	0.11	0.00	20.45	0.51	0.00	100
B2b@4		53.76	0.65	0.45	1.03	5.36	0.14	17.93	0.11	0.01	20.06	0.50	0.00	100
B2b@5		53.75	0.64	0.41	1.06	5.27	0.14	18.02	0.12	0.02	20.08	0.49	0.00	100
B2b@6		53.72	0.67	0.42	1.09	5.27	0.14	17.87	0.11	0.01	20.20	0.50	0.00	100
B2b@7		53.74	0.65	0.42	1.06	5.30	0.14	17.94	0.11	0.01	20.11	0.50	0.00	100
B2b@8		53.74	0.66	0.42	1.07	5.28	0.14	17.94	0.12	0.02	20.13	0.50	0.00	100
Ca@1	R511C_1	53.77	0.63	0.31	1.01	5.00	0.13	18.51	0.07	0.00	20.10	0.46	0.01	100
Ca@2		53.84	0.70	0.39	1.16	5.01	0.14	18.47	0.07	0.00	19.77	0.45	0.00	100
Ca@3		53.47	0.51	0.35	0.88	5.76	0.10	18.10	0.08	0.00	20.23	0.50	0.01	100
Ca@4		53.97	0.68	0.40	1.10	4.98	0.13	18.13	0.08	0.00	20.03	0.50	0.00	100
Cc1@1	R511C_4B	53.80	0.66	0.48	0.92	5.71	0.14	17.75	0.12	0.00	19.90	0.49	0.02	100
Cc1@2		54.30	0.43	0.29	0.91	5.15	0.15	18.69	0.11	0.03	19.49	0.44	0.01	100
Cc1@3		53.79	0.55	0.32	0.99	5.46	0.16	18.36	0.10	0.00	19.80	0.48	0.00	100
Cc1@4		53.97	0.55	0.37	0.94	5.44	0.15	18.27	0.11	0.01	19.73	0.47	0.01	100
Cc1@5		54.02	0.51	0.33	0.95	5.35	0.15	18.44	0.11	0.01	19.67	0.46	0.01	100
Cc1@6		53.93	0.53	0.34	0.96	5.41	0.15	18.36	0.10	0.01	19.73	0.47	0.01	100
Cc1@7		53.97	0.53	0.34	0.95	5.40	0.15	18.35	0.11	0.01	19.71	0.47	0.01	100
Cc1@8		53.97	0.52	0.34	0.95	5.39	0.15	18.38	0.11	0.01	19.70	0.47	0.01	100

Cc2@1	R511C_4A	53.08	0.57	0.36	0.82	5.40	0.17	18.23	0.06	0.00	20.80	0.50	0.01	100
Cc2@2		53.14	0.66	0.33	1.09	5.12	0.18	18.24	0.08	0.05	20.59	0.51	0.01	100
Cc2@3		55.03	0.61	0.30	1.17	5.34	0.15	16.49	0.08	0.04	20.33	0.44	0.02	100
Cb@1	R511C_2	54.03	0.69	0.47	0.68	5.77	0.20	17.49	0.14	0.00	20.07	0.47	0.00	100
Cb@2		53.62	0.76	0.48	1.01	5.41	0.15	17.82	0.02	0.01	20.21	0.50	0.01	100
Cd@1	R511C_3B	55.60	0.99	0.33	1.03	5.97	0.13	16.64	0.10	0.00	18.84	0.38	0.00	100
Cd@2		52.38	0.72	0.42	1.15	5.37	0.14	18.87	0.06	0.02	20.39	0.49	0.01	100
Cd@3		53.45	0.77	0.32	1.06	4.89	0.15	19.29	0.07	0.02	19.50	0.48	0.00	100
Cd@4		53.82	0.82	0.36	1.08	5.41	0.14	18.26	0.08	0.01	19.57	0.45	0.00	100
Cd@5		53.22	0.77	0.36	1.10	5.22	0.14	18.81	0.07	0.02	19.82	0.47	0.01	100
Cf@1	R511C_5B	54.67	0.68	0.36	1.04	5.14	0.16	17.54	0.09	0.04	19.79	0.47	0.01	100

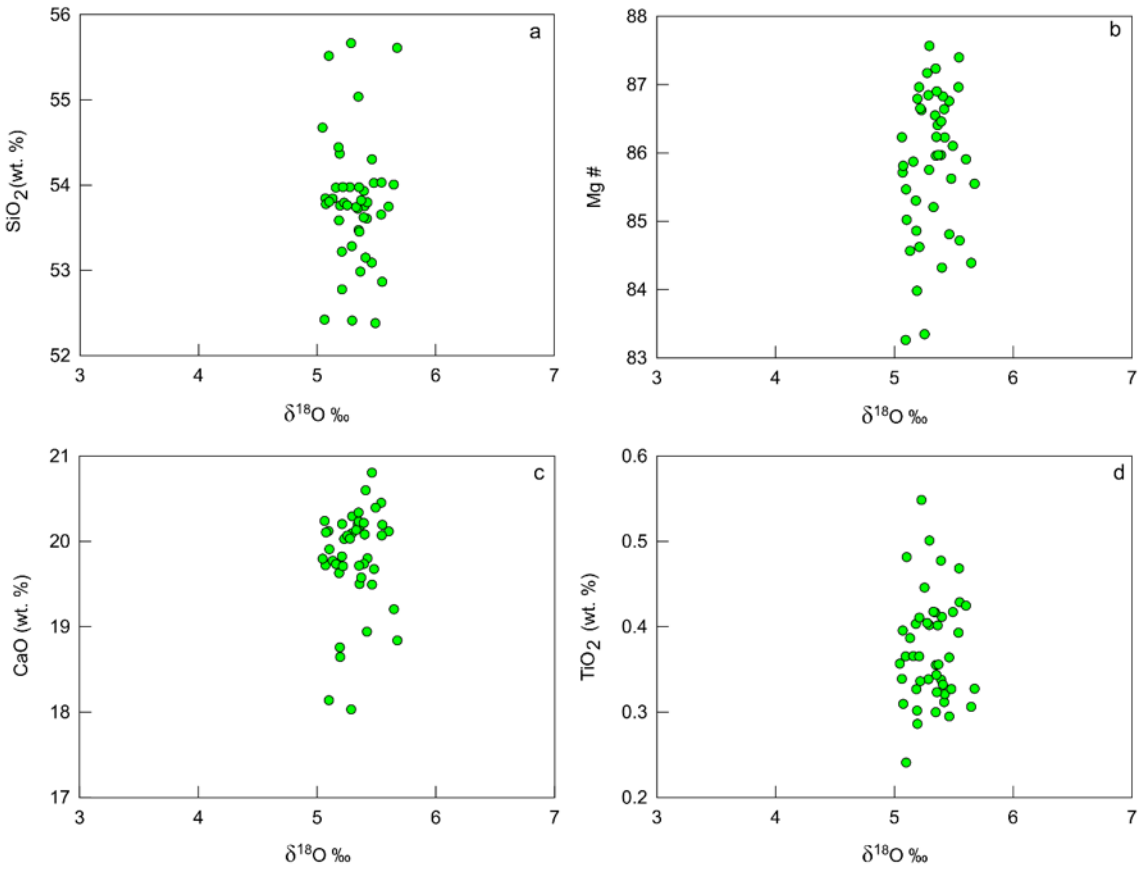

Figure A1. 8 Plot of major element against oxygen isotope compositions of the clinopyroxene grains in the Westonaria komatiites.

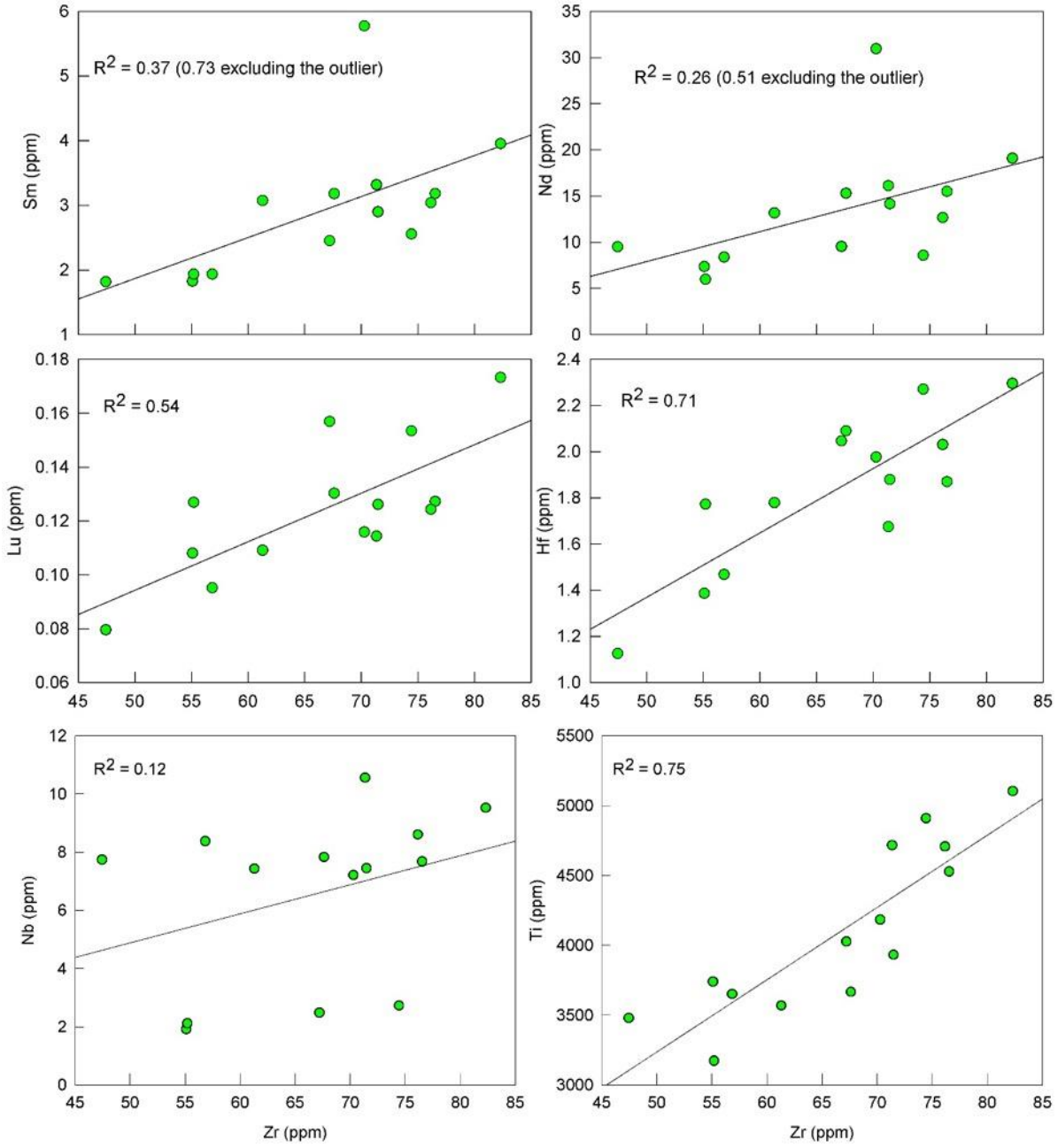

Figure A1. 9 Selected trace elements versus the immobile element to test element mobility. The plots suggests that Lu and Nd may have been mobilised during post-magmatic hydrothermal event, however, the correlation (R2) is moderate indicating that the mobilization was of small degree.

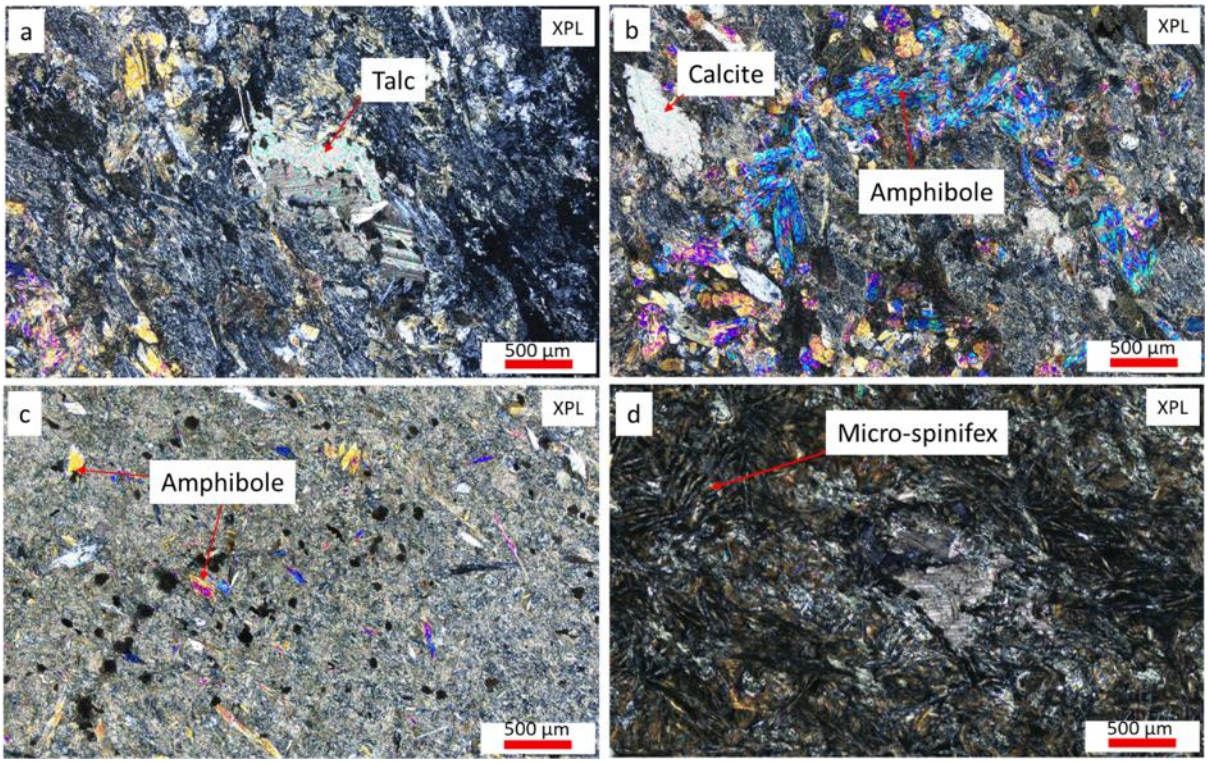

Figure A1. 10 Photomicrographs of samples that show severe alteration and metamorphism. a- c) Metamorphic minerals in the samples are well crystallized (euhedral and coarse grained). d) Micro-spinifex texture similar to the one observed in borehole E5. The sample is more altered than the other spinifex samples and contains coarse calcite and talc grains.

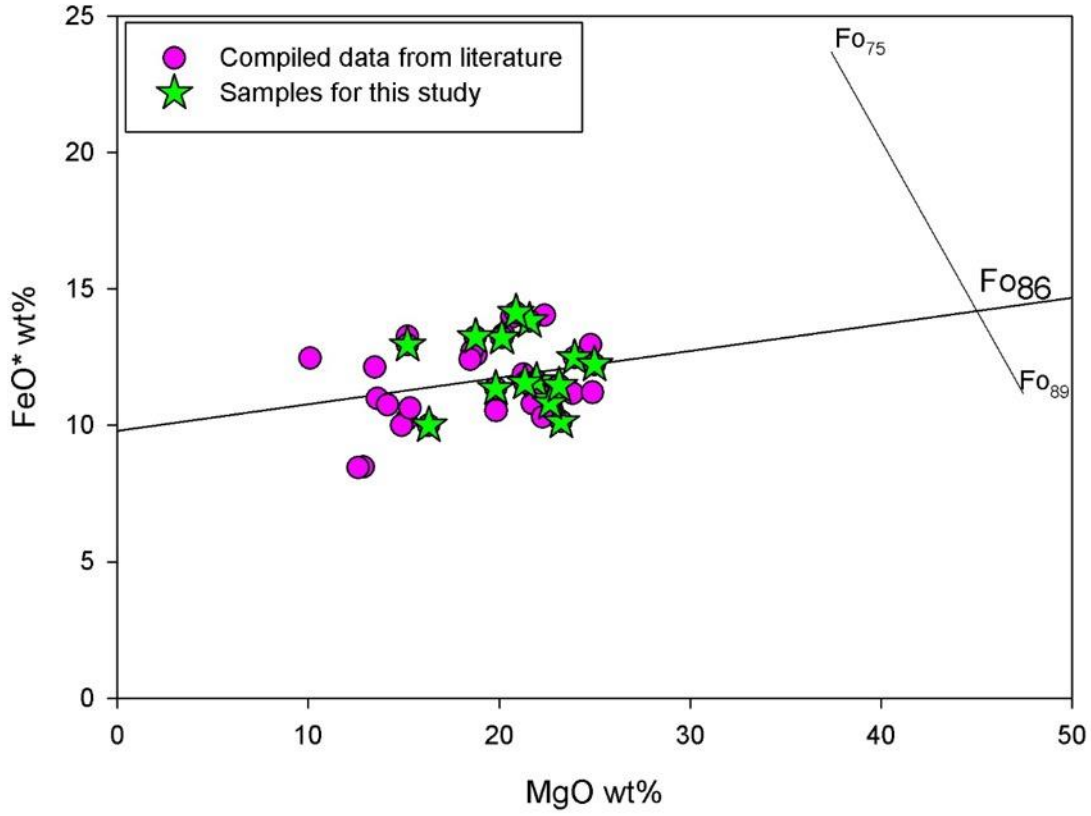

Figure A1. 11 Plot of whole-rock FeO against MgO to determine the equilibrium composition of olivine for the Westonaria lavas. FeO* is the ferrous iron that has been recalculated from total FeO with Fe2+/Fe3+ set at 0.85.*

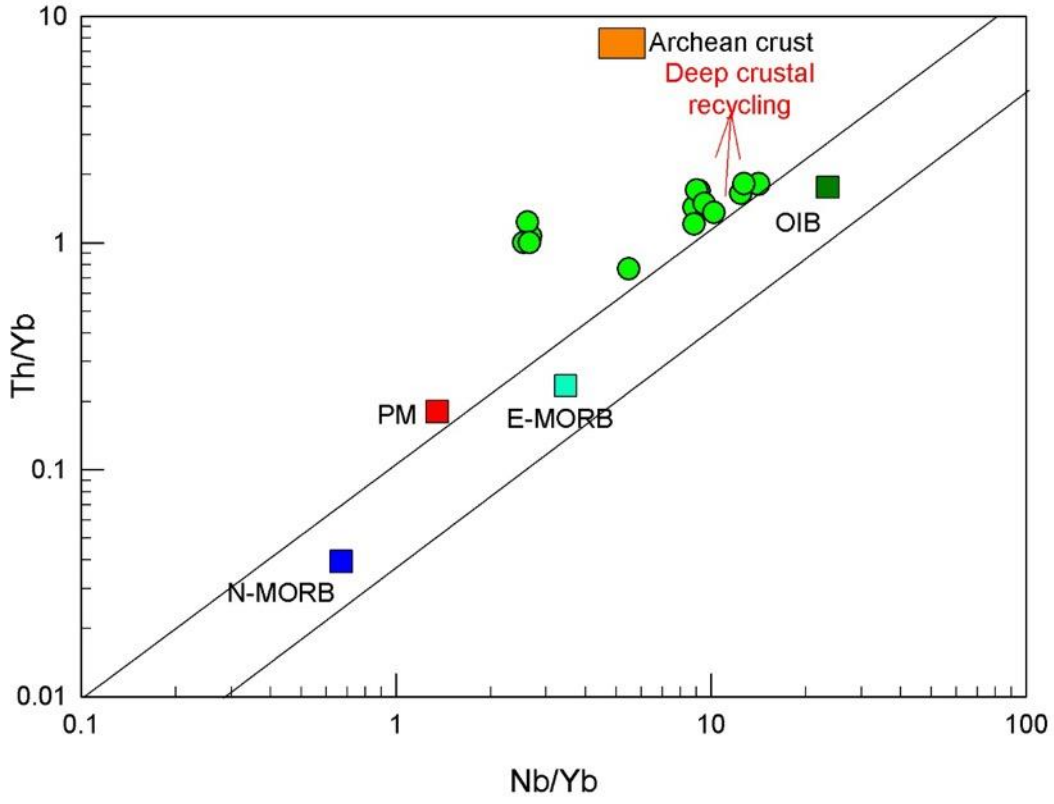

Figure A1. 12 The plot of Th/Yb versus Nb/Yb in Pearce (2008) of the Westonaria komatiite indicating a deep recycling of crustal material that influenced the mantle source. Samples that plot to the left of the main cluster have low Nb because of the mobilization of the Nb during alteration and metamorphism.

Appendix 4

Table A4. 1 Major element compositions of the Ventersdorp Supergroup lavas.

Formation	Sample	SiO2	TiO2	Al2O3	FeO*	Fe2O3*	MnO	MgO	CaO	Na2O	K2O	P2O5	Total	LOI
Westonaria	R048	48.55	0.73	3.59	13.82	2.71	0.21	21.60	8.69	0.00	0.02	0.06	100	11.18
	R141	52.64	1.00	5.73	13.20	2.59	0.17	20.14	4.40	0.00	0.02	0.10	100	6.52
	R359	53.68	1.13	10.16	10.00	1.96	0.22	16.32	6.24	0.10	0.08	0.11	100	5.16
	R360	49.69	0.78	6.71	10.13	1.99	0.19	23.24	7.13	0.02	0.04	0.08	100	6.23
	R362	51.70	0.80	3.82	13.24	2.60	0.20	18.77	8.54	0.06	0.16	0.10	100	2.94
	R434	50.74	0.94	4.70	14.13	2.77	0.21	20.87	5.52	0.00	0.03	0.09	100	5.39
	R432	52.83	1.29	5.35	12.95	2.54	0.24	15.20	9.22	0.11	0.16	0.11	100	6.24
	R502	51.73	0.91	7.19	11.62	2.28	0.18	21.94	4.05	0.00	0.01	0.09	100	5.64
	R503	50.14	0.86	6.27	10.94	2.15	0.16	22.72	6.45	0.18	0.04	0.09	100	5.48
	R505	54.18	0.98	5.85	11.35	2.23	0.14	19.82	5.33	0.01	0.02	0.09	100	4.95
	R506	50.62	0.95	5.58	11.55	2.27	0.17	21.35	7.31	0.07	0.03	0.10	100	4.71
	R507	51.04	0.93	5.81	10.82	2.12	0.17	22.66	6.25	0.09	0.01	0.10	100	5.6
	R508	50.85	1.13	5.16	12.48	2.45	0.14	23.96	3.63	0.09	0.00	0.11	100	5.18
	R509	52.17	1.03	5.05	12.23	2.40	0.15	24.99	1.80	0.06	0.01	0.11	100	5.46
	R511	52.52	0.93	4.83	11.46	2.25	0.18	23.14	4.49	0.06	0.04	0.10	100	5.85
Alberton	LZ41	57.79	1.09	14.51	7.82	1.53	0.13	4.70	5.86	5.46	0.96	0.14	100	1.38
	LZ31	55.05	1.11	15.11	9.19	1.80	0.18	4.88	6.91	3.76	1.87	0.14	100	3.20
	LZ35	55.59	1.15	14.90	8.52	1.67	0.14	4.59	7.83	3.39	2.06	0.16	100	1.98
	R030	54.76	1.30	15.46	9.15	1.79	0.12	5.42	6.44	4.14	1.23	0.18	100	1.52
	R038	55.88	1.30	15.82	8.78	1.72	0.13	4.28	6.30	4.67	0.93	0.18	100	1.73
	R040	54.49	1.34	15.98	8.75	1.72	0.13	4.48	7.13	4.22	1.57	0.20	100	1.30
	R129	56.37	1.21	15.16	8.88	1.74	0.13	5.25	6.58	3.34	1.15	0.18	100	0.66
	R134	55.01	1.33	15.10	9.02	1.77	0.16	4.51	7.16	4.09	1.67	0.18	100	0.89
	R357	55.92	1.23	14.99	8.36	1.64	0.13	4.76	6.89	3.85	2.06	0.17	100	1.53
	R420	56.18	1.08	15.21	8.56	1.68	0.12	4.22	7.49	4.04	1.27	0.16	100	1.78
Orkney	LZ18	56.31	0.97	14.52	9.28	1.82	0.16	4.65	7.47	3.36	1.33	0.11	100	1.72
	LZ23	53.61	1.07	15.04	9.92	1.94	0.15	5.46	7.43	3.07	2.18	0.13	100	2.23
	LZ29	55.38	1.07	14.60	9.23	1.81	0.14	4.45	8.63	3.19	1.38	0.12	100	2.63
	R347	55.84	1.09	14.70	9.89	1.94	0.17	5.11	6.85	3.36	0.93	0.13	100	1.21
	R005	55.61	0.87	12.90	9.28	1.82	0.13	7.88	6.93	2.08	2.38	0.11	100	1.49
	R105	56.46	0.97	13.79	9.37	1.84	0.14	5.03	7.60	2.68	2.00	0.13	100	1.48
	R333	57.25	0.99	14.63	9.38	1.84	0.14	5.32	5.68	4.33	0.32	0.12	100	1.56
	R335	55.73	0.99	14.38	9.38	1.84	0.15	4.54	7.64	3.09	2.12	0.12	100	0.79
Jeannette	R326	55.91	0.73	14.36	8.22	1.61	0.16	5.74	9.04	2.32	1.81	0.08	100	0.54
	LZ17	55.09	0.77	13.55	8.69	1.70	0.16	7.59	8.42	2.44	1.50	0.10	100	1.88
Lora-Eden	KL136	54.01	0.66	13.75	9.14	1.79	0.16	7.35	9.64	2.11	1.31	0.08	100	2.18
	KL141	53.07	0.58	11.99	9.03	1.77	0.18	10.71	9.30	1.60	1.70	0.08	100	2.74
	KL142	51.50	0.64	13.60	9.32	1.83	0.18	8.42	10.66	3.11	0.69	0.06	100	2.69
	KL145	55.05	0.61	13.90	8.85	1.74	0.17	7.73	9.96	0.15	1.77	0.07	100	1.98
	KL147	54.50	0.60	13.20	8.99	1.76	0.24	7.93	7.58	3.52	1.61	0.08	100	0.27
	KL150	52.64	0.68	14.95	9.16	1.80	0.15	7.43	8.63	3.04	1.44	0.08	100	2.79
	KL153	52.79	0.75	15.54	9.35	1.83	0.23	7.18	6.36	3.34	2.52	0.10	100	2.57
	KL155	54.93	0.52	13.12	7.88	1.55	0.16	11.32	6.62	2.35	1.46	0.08	100	3.84
	KL156	54.52	0.41	10.74	8.46	1.66	0.19	13.55	8.31	1.82	0.29	0.05	100	3.88
	KL158	51.33	0.46	11.37	9.31	1.83	0.18	15.04	8.46	1.56	0.40	0.06	100	4.32
Goedgenoeg	PG166	54.04	1.59	14.99	9.02	1.77	0.14	6.26	7.02	3.77	0.66	0.75	100	2.77
	PG168	54.65	1.63	14.83	9.65	1.89	0.18	7.19	5.29	2.82	1.06	0.81	100	3.53
	PG163	56.68	1.64	13.84	8.87	1.74	0.15	6.87	5.93	2.48	0.99	0.80	100	3.67
	PG175	60.63	1.44	14.95	7.09	1.39	0.11	4.25	4.06	3.16	2.25	0.66	100	3.76
Rietgat	PR472	56.66	1.68	17.17	8.46	1.66	0.13	2.99	4.05	4.29	2.26	0.66	100	3.03
	PR487	60.28	1.45	13.75	6.42	1.26	0.13	3.78	7.61	3.53	1.04	0.76	100	2.92
	PR484	55.84	1.48	13.75	8.52	1.67	0.15	6.11	7.74	1.92	2.16	0.66	100	3.10
	PR182	58.02	1.29	13.78	7.59	1.49	0.10	5.84	6.67	3.44	1.18	0.61	100	3.28
	PR185	55.12	1.85	13.81	9.99	1.96	0.18	6.55	6.29	2.68	0.59	0.98	100	3.89
	PR189	56.24	1.66	14.73	8.41	1.65	0.14	5.50	6.61	4.06	0.15	0.85	100	2.92

Allanridge	AR199	57.71	1.16	13.94	8.85	1.74	0.12	4.22	6.51	4.09	1.43	0.23	100	3.32
	AR446	59.42	1.09	14.80	8.21	1.61	0.15	4.06	4.66	4.07	1.70	0.24	100	3.14
	AR451	58.84	0.90	14.47	6.25	1.22	0.14	4.51	7.00	4.08	2.43	0.17	100	3.46
	AR300	62.41	1.23	14.48	7.52	1.47	0.12	3.67	2.82	2.83	3.21	0.22	100	3.52
	AR305	58.70	1.31	14.97	10.87	2.13	0.13	4.84	2.46	2.81	1.60	0.18	100	3.87
	AR345	57.72	1.08	15.06	9.13	1.79	0.15	4.86	5.42	3.97	0.59	0.23	100	3.58
	AR364	57.59	1.14	14.17	7.45	1.46	0.11	4.36	7.11	4.06	2.29	0.25	100	3.52

The compositions are reported in wt. % and are normalized to 100 % volatile free. The data were obtained from Bowen (1984), Myers (1990) and Linton (1992).

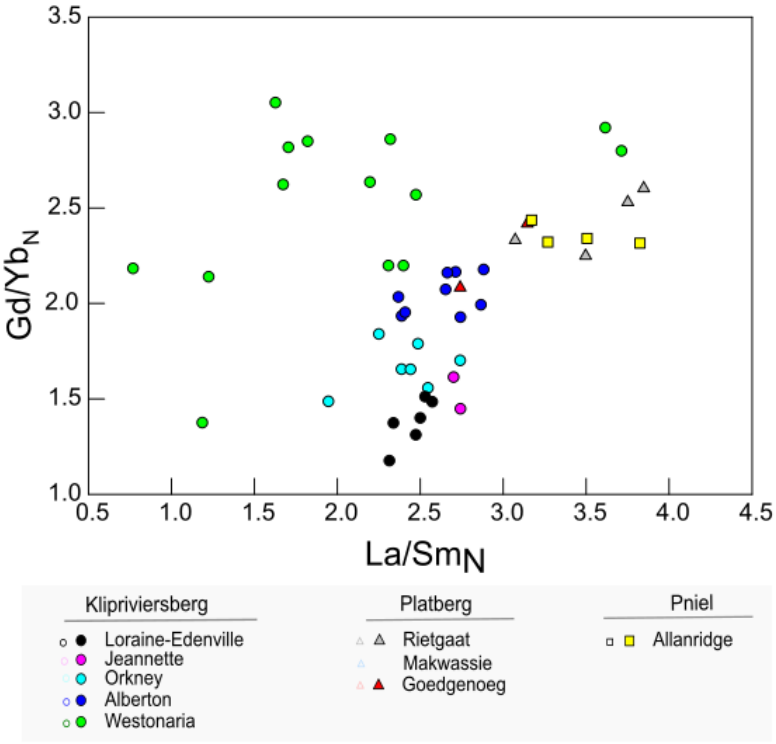

Figure A2. 1 Plot of normalised La/Sm versus Gd/Yb showing the relationship of enrichments of the LREE and HREE. There is greater variation in LREE than in HREE.

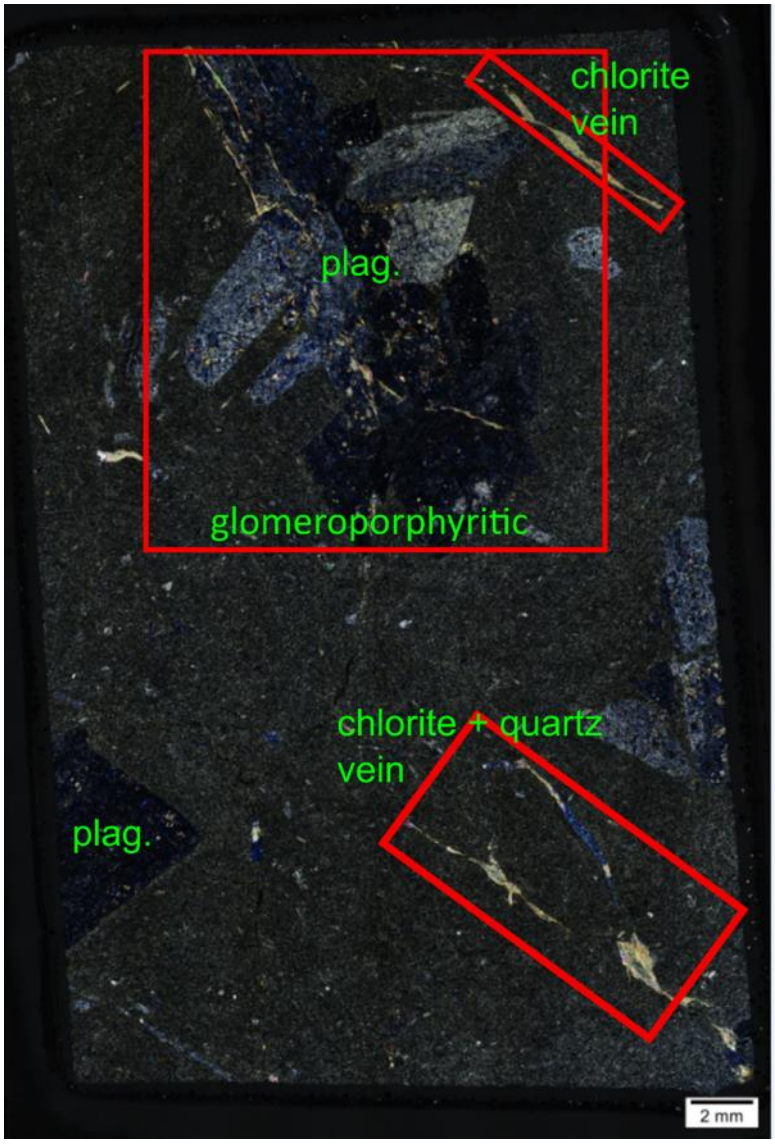

Figure A2. 2 A porphyritic basalt with altered plagioclase phenocrysts. The plagioclase varies from euhedral to anhedral and they are hosted in a fine-grained groundmass. The plagioclase phenocrysts form glomeroporphyritic clusters that are partly silicified. There are chlorite and quartz veins in the basalt.

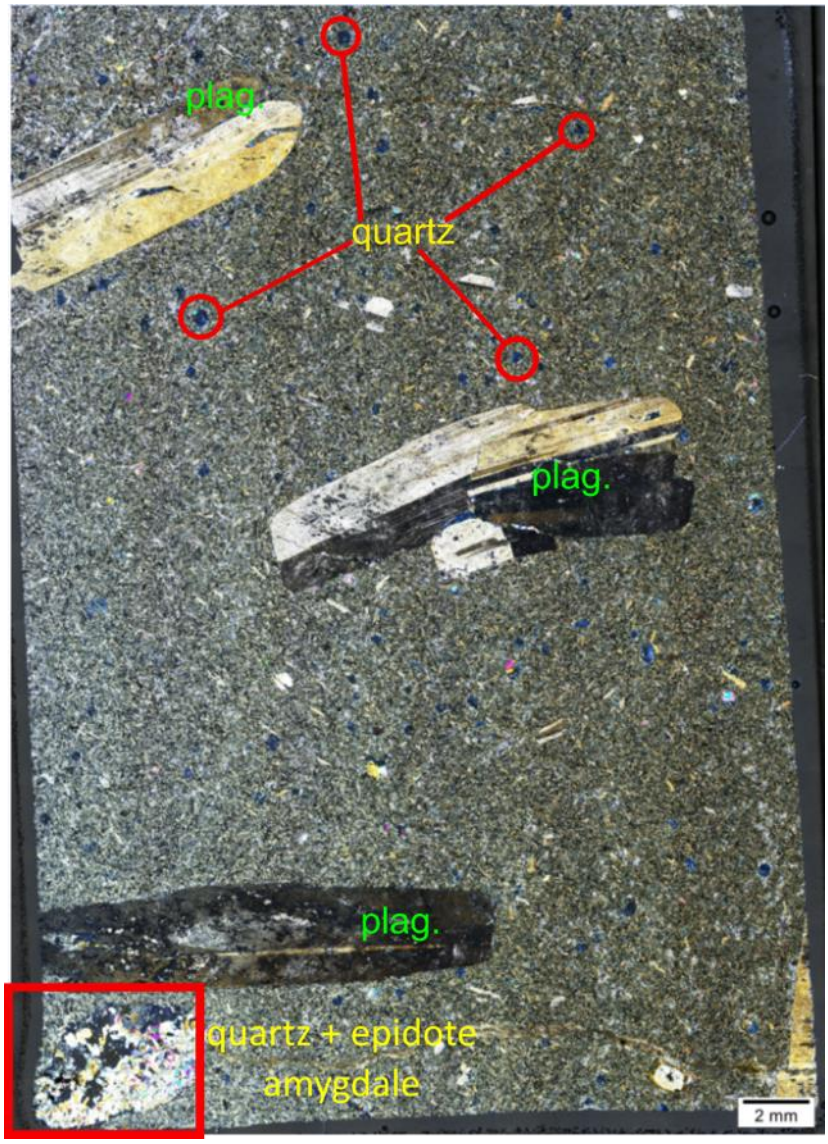

Figure A2. 3 A porphyritic basalt with elongate, subhedral plagioclase phenocrysts that are hosted in a fine-grained to medium-grained (≤0.5mm) groundmass of plagioclase laths. The plagioclase phenocrysts display a preferred orientation and the groundmass laths are randomly orientated. There are quartz-epidote-filled amygdales and quartz amygdales.

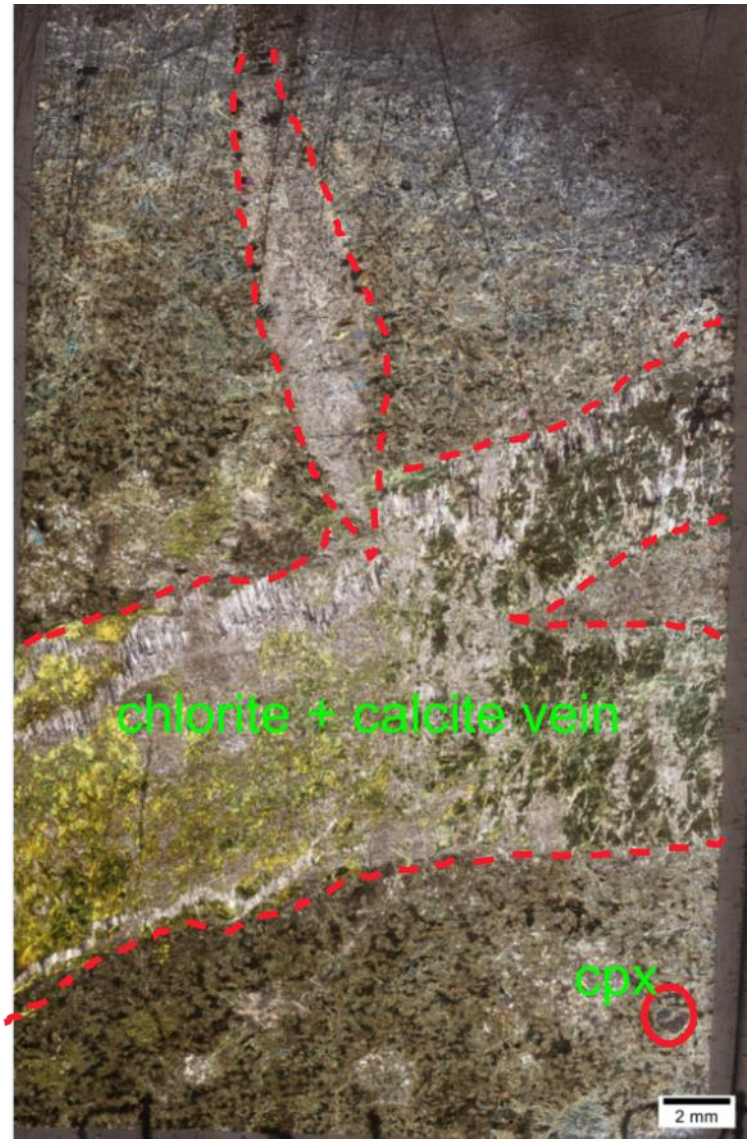

Figure A2. 4 A chlorite-calcite vein across a sample. The sample contains a few clinopyroxene grains that are freshly preserved. The clinopyroxene grains are a few distances (~4 mm) from the vein.